ABSTRACT

KIM, WAN SOO. Influence of Water Infiltration on the Deformation of Mechanically Stabilized Earth (MSE) Walls. (Under the direction of Dr. Roy H. Borden.)

The use of locally available soils, often with significant fines contents, clearly has great economic impact on the cost of mechanically stabilized earth (MSE) wall construction. However, numerous problems associated with large deformations and some failures after surface water infiltration into these “marginal soils” have been documented in the literature (e.g. Soong and Koerner, 1999). The documented problems can be better understood using the framework of unsaturated soil mechanics because compacted soils are typically found in an unsaturated state.

This thesis presents the implementation of infiltration, seepage, volume change, and shear strength modeling of unsaturated conditions appropriate for compacted soils into the FLAC (Fast Lagrangian Analysis of Continua) code to study the behavior of an MSE wall constructed with marginal soils. The effect of matric suction (as well as net normal stress) on the soil properties such as elastic modulus and shear strength was considered in the developed FLAC model.

The stress dependent elastic modulus was determined from the results of the one-dimensional oedometer test. The elastic moduli of specimens prepared under various compaction conditions were investigated for soaked specimens as well as specimens tested at

as-compacted moisture contents while considering both drained and undrained loading conditions. A procedure to estimate the undrained modulus from the constitutive relation for drained loading and the predicted pore pressure due to loading was suggested. The prediction of pore pressure was computed by modifying Hilf's equation.

Comprehensive studies on the prediction on unsaturated shear strength were performed using the three most commonly used empirical procedures (Vanapalli et al.'s 1st and 2nd approaches and the Khalili and Khabbaz method). The influence of the shape of Soil Water Characteristic Curve (SWCC) on the predicted shear strength was investigated through a parametric study. Moreover, shear strength data published in the literature for fifteen soils were examined using these procedures. Comparisons between measured and predicted values of unsaturated shear strength were presented for different soil types. The effect of stress state on the prediction of shear strength was also discussed.

A series of numerical simulations including transient seepage analyses and stress deformation analyses were performed in order to predict the behavior of a MSE wall subjected to surface-water infiltration. In this research, two mechanisms to cause the deformation due to wetting were considered in simulations; (1) the deformation induced by shear strength decreases and (2) the volumetric deformation (swell or collapse) due to wetting. The effect of a low-quality compaction zone behind the wall face and the resulting higher permeability on the wall behavior was investigated. As result of the simulations, the wall deformations (face deflections and settlements) and reinforcement tensions (average and maximum tensions) were presented during construction and after periods of infiltration.

Influence of Water Infiltration on the Deformation of Mechanically Stabilized Earth (MSE) Walls

by

Wan Soo Kim

A dissertation submitted to the Graduate Faculty of
North Carolina State University
in partial fulfillment of the
requirements for the degree of
Doctor of Philosophy

Civil Engineering

Raleigh, North Carolina
November, 2007

Approved by:

Dr. Roy H. Borden Chair of Advisory Committee	Dr. Mohammed A. Gabr
Dr. M. Shamimur Rahman	Dr. R. Wayne Skaggs

DEDICATION

To the memories of my grandmother in Heaven

and

my family for their endless love and unfailing support

이 논문을 사랑하는 나의 가족,

그리고 하늘에 계신 할머니께 바칩니다.

BIOGRAPHY

Wan Soo Kim was born June 20, 1973 in Seoul, Korea, to Youngdae Kim and Kyungja Park. He received his B.S and M.S degrees in Civil Engineering from Kyung Hee University in 1997 and 2000, respectively. After earning a M.S degree, he worked with the Kumho Construction Co. as a project engineer from April 2000 to June 2001. In the fall of 2002, he began his Ph.D. study in the Department of Civil Engineering at North Carolina State University.

ACKNOWLEDGEMENTS

I would like to express my deepest appreciation to my advisor, Dr. Roy H. Borden for his advice and mentorship through my career. None of the work presented in this dissertation would have been possible without his help and encouragement. Any expression would not be enough to him regarding his guidance, mentorship, encouragement, and support. Thank you, Dr. Borden! I was so happy working with you.

I would also like to thank to Dr. Mohammed Gabr., Dr. Shamimur Rahman, and Dr. Wayne Skaggs for serving on my Ph.D. advisory committee. They were always there when I needed clarification and guidance on my research.

I would like to acknowledge Dr. Delwyne G. Fredlund (University of Saskatchewan), Dr. Harianto Rahradjo (Nanyang Technological University), Dr. Wei Lee (Taiwan Construction Research Institute), Dr. Christine Detournay (Itasca Consulting Group), Dr. Sai Vanapalli (University of Ottawa), Dr. Robert Holts (University of Washington), and Dr. Craig Benson (University of Wisconsin) for their willingness to share their achievements and knowledge regarding my questions.

Appreciation is also expressed to the NC State Department of Civil, Construction and Environmental Engineering for giving me the opportunity to study at NC State University and also work as a Teaching Assistant during my stay at NC State. These experiences were invaluable for me.

I would like to express my special thanks to the Subsurface Construction Company, as they provided me the opportunity to work as an intern during the 07' summer and purchased the unsaturated soil database program, SoilVision, necessary for this research.

I would like to express my gratitude to the NCSU geotechnical group members for their kind help and true friendship; Jongkoo Jeon, Hyesun Yuom, Youngjin Park, Sangchul Pyo, Brent Robinson, Nadia Sharmin, Xueliang Zhao, Ben Possiel, Mehmet Ulker, Tanya Kunberger, Rabia Sarica, Dennis Rorie, Joe Godwin, and Gargi anandjiwala. Additional thanks go to Rick Lamy, Bill Dunleavy, Renee Howard, and Lorenzo Watson who made my stay at NC State enjoyable and memorable.

Last, but certainly not least, I am grateful to my wife Hyunsook Moon, my precious daughter Nuri Kim, and my parents, Youngdae Kim and Kyungja Park, for their presence and great support during this long journey.

TABLE OF CONTENTS

LIST OF TABLES

LIST OF FIGURES

Page

CHAPTER 1

INTRODUCTION

1.1 General

The general field of soil mechanics can be subdivided into that portion dealing with saturated soils and that portion dealing with unsaturated soils (Fig. 1.1). The differentiation between saturated soils and unsaturated soil becomes necessary due to basic differences in their nature and engineering behavior (Fredlund and Rahardjo, 1993).

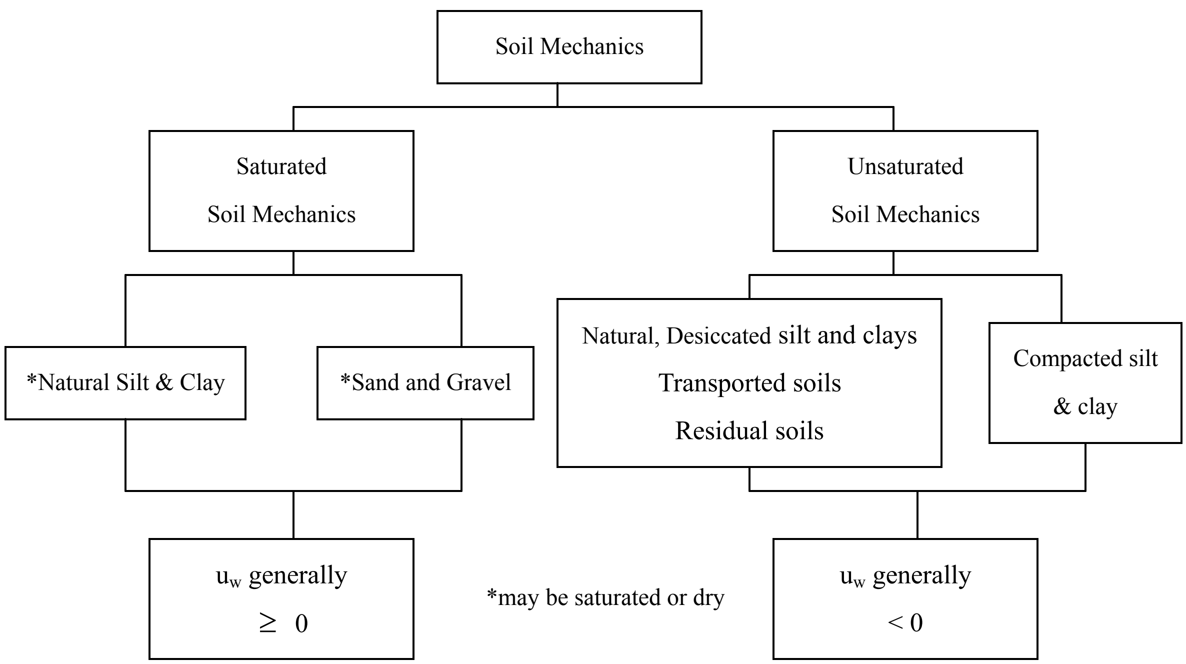

Fig. 1. 1 Categorization of soil mechanics (Fredlund and Rahardjo, 1993)

Many persistent problems associated with earth structures involve the classical soil mechanics problems of shear strength, volume change, and seepage, which are governed by unsaturated soil mechanics principles. The mechanical behavior of unsaturated soil is controlled by two stress state variables, while one stress state variable, the effective stress, (σ-u_w) is associated with saturated soil response (Fredlund and Morgenstern, 1976; Fredlund and Rahardjo, 1993). These two stress state variables are net normal stress, (σ-u_a), and matric suction, (u_a–u_w), where σ is total normal stress, u_a is pore-air pressure and u_w is pore-water pressure. Although a theoretical framework for unsaturated soil mechanics has been established over the past few decades, there is not yet a significant application of unsaturated soil mechanics to the design and analysis of practical problems.

1.2 Problem statement

For the past few decades, mechanically stabilized earth (MSE) has been an alternative to conventional retaining systems. Granular soils are preferred for MSE applications because they are stable, free draining, and relatively non-corrosive to the reinforcing elements. The result has been the development of reinforced earth backfill specifications that provide for granular backfill properties in most construction. However, the main disadvantage to this specification is that such material is often imported and therefore, costly.

It has been proposed that marginal soils (greater than 50% fines) with low plasticity (PI<20) may be used for MSE construction (Collin, 1997). The use of marginal fill clearly has significant impact on the cost of MSE wall construction. However, there are increased risks associated with using marginal soils for MSE walls, as indicated by the reported problems, such as large deformations and failures resulting from water infiltration. Twenty out of 26 case histories on geosynthetic MSE wall failures identified by Soong and Koerner (1999) were for walls constructed with silt and clay soils.

Since compacted soils are used as backfills, unsaturated soil behavior and subsequent infiltration play a dominant role in the behavior of MSE walls. Compacted soils are typically in an unsaturated state, with negative pore-water pressure because the degree of saturation less than 100%. Therefore, flow, volume change, and shear strength of compacted soils must be well understood and quantified to enable better prediction of the performance of MSE walls. The shear strength and unsaturated hydraulic conductivity are commonly determined from the Soil-Water Characteristic Curve (SWCC) which is the relationship between soil water content and matric suction.

Failure of MSE walls during rainfall can be primarily associated with a decrease in the matric suction of the unsaturated soils. With infiltration, the pore-water pressure becomes less negative or even positive. As a result, changes occur in the permeability, volume and shear strength of the soil. Decreasing suctions generally result in low resistance to flow, volume change (swelling or collapsing) and significant loss of shear strength.

The effect of soil structure on unsaturated properties and behavior of unsaturated soils can be of great significance, particularly for compacted soils (Toll, 1990). The structure and fabric of compacted soils is highly dependent on the compaction conditions (i.e. compaction effort, water content and dry density).

As mentioned above, prediction of MSE wall behavior due to infiltration is a very complicated problem which includes seepage, shear strength, and volume change based on the principle of unsaturated soil mechanics. In addition, the effect of soil structure on compacted soil properties must also be understood and incorporated into the unsaturated soil response model.

1.3 Thesis objectives

A 5.4 m high MSE wall constructed with marginal fills in the Research Triangle Park of North Carolina experienced a localized collapse during rainfall in the spring of 2001 (Fig. 1.2). The main objective of this study is to provide better understanding of the behavior of MSE walls subjected to surface-water infiltration based on an unsaturated soil mechanics framework. A series of numerical simulations using the developed FLAC models are developed in order to implement infiltration, seepage, volume change, and shear strength modeling of unsaturated conditions appropriate for compacted soils. The reinforced soil mass deformations (face deflections and soil settlements) and reinforcement tensions (average and maximum tensions) are investigated for both the end of the construction and after infiltration conditions.

In the process of developing the FLAC model, this research also attempted to fulfill two secondary objectives: (1) to investigate the effects of various compaction conditions on the volume change behavior of compacted soils (for soaked and as-compacted conditions, and for drained and undrained loadings); and, (2) to investigate the influence of the shape of the SWCC (or soil type) and stress state on the shear strength envelope predicted using three prediction methods (Vanapalli et al.'s 1st and 2nd approaches and the Khalili and Khabbaz method).

Fig. 1. 2 MSE wall collapse during rainfall (the Research Triangle Park of North Carolina, 2001)

1.4 Thesis organization

This thesis has six chapters. In the first chapter, the problem of the MSE wall constructed with marginal soils is stated and objectives of this research are explained. Then, volume change behavior in compacted soils for both drained and undrained loading are discussed in the second chapter. Chapter three discusses the predictions of unsaturated shear strength based on SWCC, which includes parametric studies and comparisons between measured and predicted values of unsaturated shear strength. Chapter four describes the developed FLAC model that accounts for unsaturated soil properties, and presents predicted wall behavior during and at the end of construction. In Chapter five, an analysis method to predict wall behavior due to rainfall or irrigation infiltration is suggested and the simulation results are discussed. Finally, Chapter six presents a thesis summary and conclusions with future research recommendations.

1.5 References

Collin, J. G. (1997). Design manual for segmental retaining walls, Edition 2, National Concrete Masonry Association, NCMA.

Fredlund, D. G.., and Morgenstern, N. R. (1976). Constitutive relations for volume change in unsaturated soils, Canadian Geotechnical Journal, 13, pp. 261-276.

Fredlund, D. G., and Rahardjo, H. (1993). Soil mechanics for unsaturated soils, New York: Wiley.

Soong, T. and Koerner, R. M. (1999). Geosynthetic reinforced and geocomposite drained retaining walls utilizing low permeability backfill soils, GRI Report #24, Geosynthetic Research Institute, Folsom, PA, 140p.

Toll, D. G. (1990). A framework for Unsaturated Soil Behavior, Geotechnique, Vol. 40, No. 1, pp. 31-44.

CHAPTER 2

Volume changes in compacted soils for drained and undrained loading

2.1 INTRODUCTION

Volume change prediction of unsaturated soils still remains a challenging problem for geotechnical engineers because of its complexities of analysis utilizing the concepts of unsaturated soil mechanics and the increased difficulties in performing experimental studies on unsaturated soils compared to saturated soils. The mechanical behavior of unsaturated soil is controlled by two stress state variables, while one stress state variable, the effective stress, (σ-u_w) is associated with saturated soil response (Fredlund and Morgenstern, 1976; Fredlund and Rahardjo, 1993). These two stress state variables are net normal stress, (σ-u_a), and matric suction, (u_a–u_w), where σ is total normal stress, u_a is pore-air pressure and u_w is pore-water pressure. The effects of net normal stress and matric suction changes must be dealt with independently for unsaturated soil. Changes in matric suction as well as changes in net normal stress contribute to volume change in unsaturated soil. As an example, the collapse or expansive behavior of soils due to wetting can be analyzed by changes in matric suction of soils (Hung and Fredlund, 2000; 2003; 2004; Fredlund and Hung, 2001; Rao and Revanasiddappa, 2000; Rodrigues and Vilar, 2006).

The modified oedometer or modified triaxial device, which can control pore-water pressure and pore-air pressure separately, have been used to determine stress state variables (net normal stress or matric suction) -strain relationships for unsaturated soils. However, these experimental studies are generally expensive, time-consuming, and difficult to perform.

Therefore a simple method to estimate volume change behavior of unsaturated soil is needed.

In this paper, a procedure to estimate the elastic modulus of compacted soils using the stress-strain relations obtained from the conventional oedometer test is presented. The elastic modulus is evaluated for soaked specimens as well as specimens at as-compacted moisture contents while considering both drained and undrained loading conditions. The undrained modulus is determined from the constitutive relation for drained loading and the predicted pore pressure due to loading. The prediction of pore pressure is accomplished by modifying Hilf's equation (1948). The effects of various compaction conditions (dry density and as-compacted water content) on the volume change behavior of compacted soils are discussed. The computed pore pressure parameters (tangent- and secant-type parameters) for each compaction condition are also presented.

2.2 VOLUME CHANGE THEORY

2.2.1 Elastic modulus during drained loading

Volume change in an unsaturated soil is described using two stress state variables; net normal stress, (σ-u_a) and matric suction (u_a-u_w). Assuming the soil behaves as an incrementally isotropic and linear-elastic material, Fredlund and Rahardjo (1993) presented the total volumetric deformation of an unsaturated soil, $d\varepsilon_v$, in an elasticity form for general three-dimensional loading (Eq. 2.1). This formulation (Eq. 2.1) can be applied to various loading conditions such as uniaxial, K_o, plane strain, plane stress, and triaxial loading conditions.

$$d\varepsilon_v = 3\left(\frac{1-2\mu}{E}\right)d(\sigma_{mean} - u_a) + \frac{3}{H}d(u_a - u_w) \tag{2.1}$$

where E = elastic modulus for the soil structure with respect to a changes in net normal stress;

H = elastic modulus for the soil structure with respect to a changes in matric suction;

σ_{mean} = average total normal stress (= $(\sigma_x+\sigma_y+\sigma_z)/3$); and,

μ = Poisson's ratio

The volume change for the soil structure can also be presented in compressibility form, as shown in Eq. 2.2, and can be presented graphically in the form of a constitutive surface (Fig. 2.1). The coefficient of volume change, m_1^s is commonly called m_v when the soil matric suction is equal to 0 kPa (saturated soil).

$$d\varepsilon_v = \frac{\Delta V_v}{V_0} = m_1^s d(\sigma_{mean} - u_a) + m_2^s d(u_a - u_w) \tag{2.2}$$

where m_1^s = coefficient of volume change with respect to a change in net normal stress; and,

m_2^s = coefficient of volume change with respect to a change in matric suction.

The semi-logarithmic plot of the void ratio constitutive surface can be plotted as shown in Fig.2.2. The volume change indices, C_t and C_m, are compressive indices with respect to net normal stress and matric suction, respectively. The indices with a subscripted "s", such as C_{ts} and C_{ms}, are for the unloading surface.

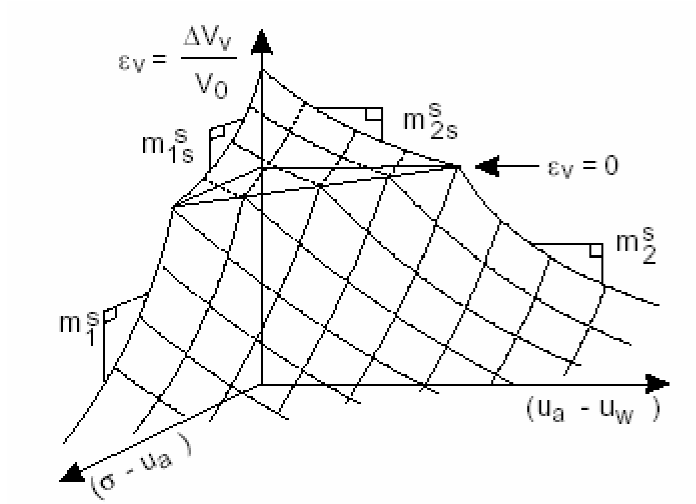

Fig. 2. 1 Three-dimensional constitutive surface for soil structure of an unsaturated soil (Fredlund and Rahardjo, 1993)

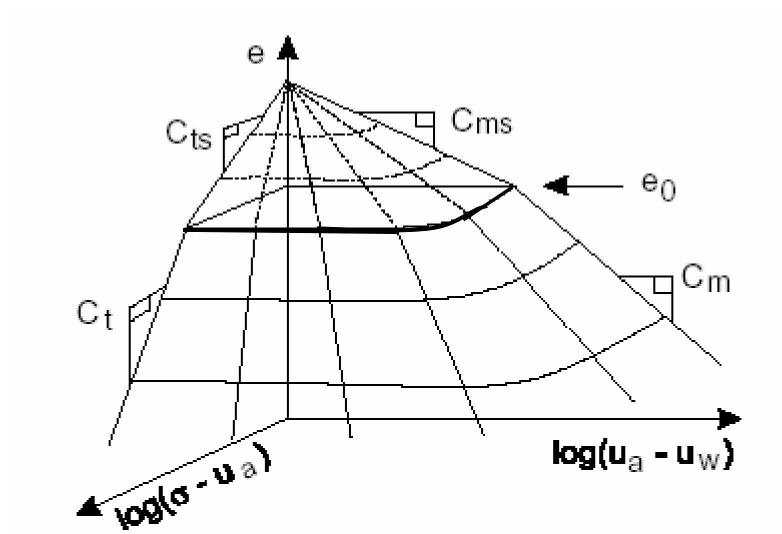

Fig. 2. 2 The semi-logarithmic plot of the void ratio constitutive surface (Fredlund and Rahardjo, 1993)

The elasticity parameters, E and H, can be calculated from the constitutive surface by computing the coefficients of volume change, m_1^s and m_2^s, which are obtained by differentiating the constitutive surface for soil structure (Fig. 2.1). The relationships between the coefficients of volume change and the elastic moduli for various testing conditions are presented in Table 2.1. For K_o loading, the constrained modulus, M, is calculated from the coefficient of volume change from a one-dimensional compression test. The Elastic modulus is then computed from the relation with M as follows:

$$E = M\frac{(1+\mu)(1-2\mu)}{(1-\mu)} \tag{2.3}$$

where M is equal to $1/m_1^s$.

Table 2. 1 Relationship between the fundamental elasticity parameters and the coefficients of volume change (Hung and Fredlund, 2000)

Loading	Stress state variables	Coefficient of volume change functions	Elasticity parameter functions
Three-dimensional (3D)	$d(\sigma_{mean} - u_a)$ $d(u_a - u_w)_{3D}$	$m_1^s = \frac{d\varepsilon_v}{d(\sigma_{mean} - u_a)} = \frac{0.434}{(1+e_0)}\frac{C_s}{(\sigma_{mean} - u_a)}$ $m_2^s = \frac{d\varepsilon_v}{d(u_a - u_w)_{3D}} = \frac{0.434}{(1+e_0)}\frac{C_m}{(u_a - u_w)_{3D}}$	$E = 3\frac{(1-2\mu)}{m_1^s}$ $H = \frac{3}{m_2^s}$
K_0-loading (1D)	$d(\sigma_y - u_a)$ $d(u_a - u_w)_{1D}$	$m_{1-1D}^s = \frac{d\varepsilon_y}{d(\sigma_y - u_a)} = \frac{0.434}{(1+e_0)}\frac{C_s}{(\sigma_y - u_a)}$ $m_{2-1D}^s = \frac{d\varepsilon_y}{d(u_a - u_w)_{1D}} = \frac{0.434}{(1+e_0)}\frac{C_m}{(u_a - u_w)_{1D}}$	$E = \frac{(1+\mu)(1-2\mu)}{(1-\mu)m_{1-1D}^s}$ $H = \frac{(1+\mu)}{(1-\mu)m_{2-1D}^s}$
Plane strain (2D)	$d(\sigma_{ave} - u_a)$ $d(u_a - u_w)_{2D}$	$m_{1-2D}^s = \frac{d(\varepsilon_x + \varepsilon_y)}{d(\sigma_{ave} - u_a)} = \frac{0.434}{(1+e_0)}\frac{C_s}{(\sigma_{ave} - u_a)}$ $m_{2-2D}^s = \frac{d(\varepsilon_x + \varepsilon_y)}{d(u_a - u_w)_{2D}} = \frac{0.434}{(1+e_0)}\frac{C_m}{(u_a - u_w)_{2D}}$	$E = \frac{2(1+\mu)(1-2\mu)}{m_{1-2D}^s}$ $H = \frac{2(1+\mu)}{m_{2-2D}^s}$

Note: $\sigma_{mean} = (\sigma_x + \sigma_y + \sigma_z)/3$; $\sigma_{ave} = (\sigma_x + \sigma_y)/2$
$d\varepsilon_y = d\varepsilon_v$ for K_0-loading; $d(\varepsilon_x + \varepsilon_y) = d\varepsilon_v$ for plane strain loading

*Note: $C_s = C_t$

Hung and Fredlund (2000) calculated the elasticity parameter functions, E and H, of expansive soils from volume change indices (Table 2.1). The elastic modulus, E, can be expressed as a function of volume change indices, C_t (or C_{ts}), initial void ratio, e_0, and Poisson's ratio, μ. The elastic modulus, H, can be expressed as a function of the volume change index with respect to matric suction, C_m (or C_{ms}), initial void ratio and Poisson's ratio. The elastic parameter functions with respect to C_t and C_m can be written for K_o-loading conditions as follows:

$$E = \frac{2.304(1+\mu)(1-2\mu)(1+e_0)}{(1-\mu)C_t}(\sigma_y - u_a) \tag{2.4}$$

$$H = \frac{2.304(1+\mu)(1+e_0)}{(1-\mu)C_m}(u_a - u_w) \tag{2.5}$$

Figure 2.3 and Figure 2.4 illustrate the relationships between elastic moduli and stress state variables for various values of volume change index. The moduli are seen to increase with increases in stress state variables and also with decreases in volume change indices (C_t or C_m).

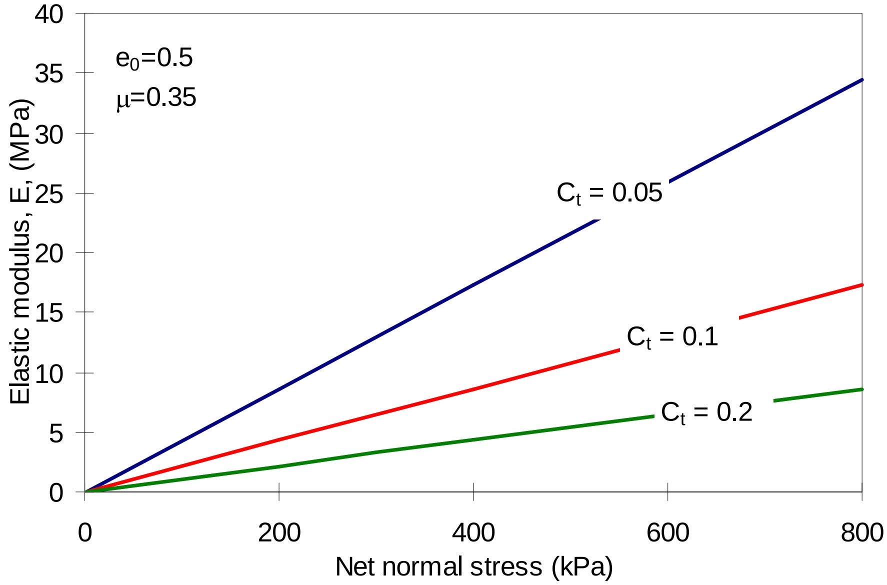

Fig. 2. 3 Relationship between elasticity parameter, E, and net normal stress for $C_t = 0.05$, 0.1, and 0.2 (from K_0-loading)

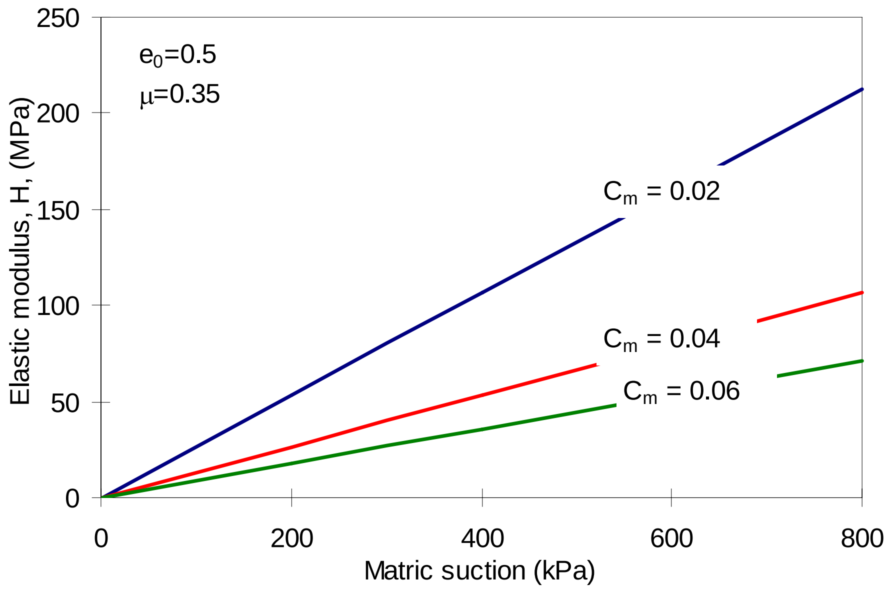

Fig. 2. 4 Relationship between elasticity parameter, E, and net normal stress for $C_m = 0.02$, 0.04, and 0.06 (from K_0-loading)

2.2.2 Elastic modulus during undrained loading

Fredlund and Rahardjo (1993) explained how the constitutive relationships obtained from drained loading apply to undrained loading (Fig. 2.5). Drained loading allows air and water are to drain from the soil subsequent to the application of a total stress increment whereas the air and water are not allowed to drain from the soil during undrained loading. Either drained loading or undrained loading can cause a change in volume of an unsaturated soil. During drained loading, matric suction is not altered but net normal stress is changed because of changed in total normal stress. The volume change due to a change in net normal stress can be computed from the stress state variable changes in accordance with the constitutive relationship for the soil structure. During undrained compression, the pore-air and pore-water pressures are increased by the total stress increase. The excess pore pressures compress the pore fluids and consequently change soil volume.

The volume change equivalent to the pore fluid compression, dV_v, can be computed from the compressibility of the air-water mixture, C_{aw} as follows (Fredlund and Rahardjo, 1993).

$$(\frac{dV_V}{V_0})_0 = C_{aw} n d\sigma \qquad (2.6)$$

where $(\frac{dV_V}{V_0})_0$ = volume change during undrained compression; and,

n = porosity.

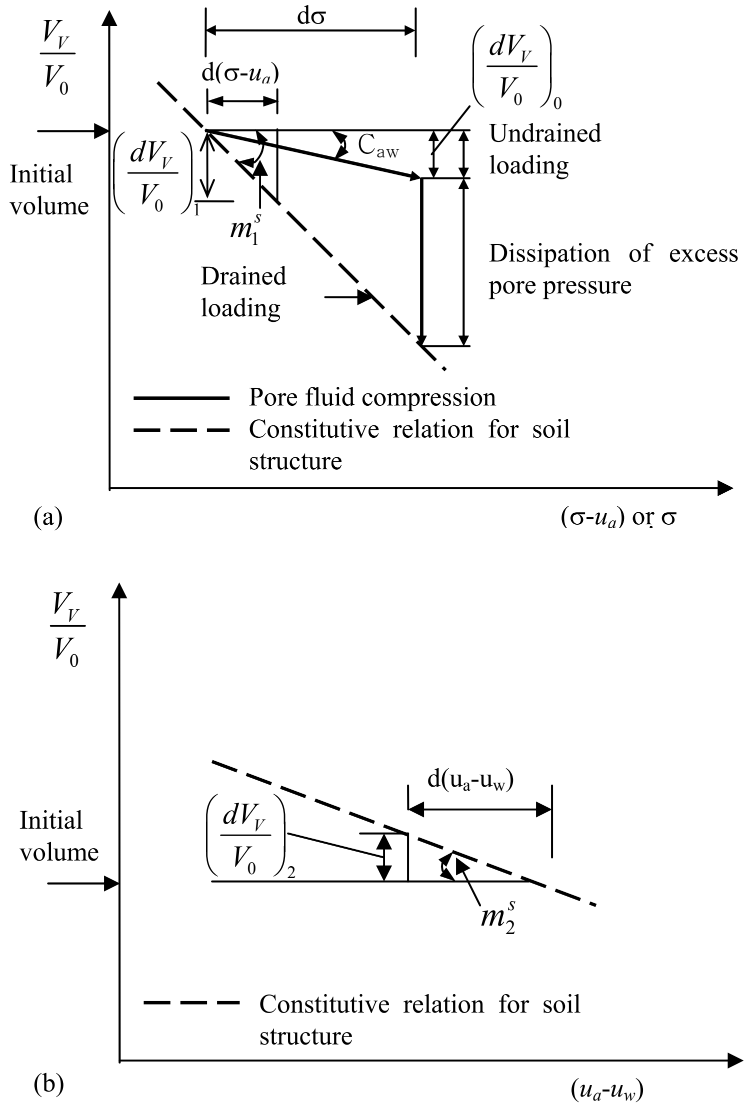

Fig. 2. 5 Volume changes in an unsaturated soil during loading. (a) volume change with respect to a change in (σ-u_a) or σ and (b) volume change with respect to a change in (u_a-u_w) (Fredlund and Rahardjo, 1993)

The volume change during undrained loading also can be expressed as the sum of volume changes due to the changes in net normal stress and matric suction (Fredlund and

Rahardjo, 1993).

$$(\frac{dV_V}{V_0})_0 = (\frac{dV_V}{V_0})_1 + (\frac{dV_V}{V_0})_2 \quad (2.7)$$

where $(\frac{dV_V}{V_0})_1$ = volume change due to the change in net normal stress; and,

$(\frac{dV_V}{V_0})_2$ = volume change due to the change in matric suction.

The terms in the right side of Eq. 2.7 can be rewritten in terms of stress state changes and coefficients of volume change in accordance with the constitutive relationship for the soil structure as follows.

$$(\frac{dV_V}{V_0})_1 = m_1^s d(\sigma - u_a) \quad (2.8)$$

$$(\frac{dV_V}{V_0})_2 = m_2^s d(u_a - u_w) \quad (2.9)$$

Under undrained loading, the volume change of unsaturated soil is highly dependent on degree of saturation. As an example, the soil volume change is very small for saturated soils because a total stress increase is first transmitted to the water phase which is rarely compressed (Fig. 2.6). In contrast, a relatively larger volume change is produced in a dry soil since a total stress increment is entirely transmitted to the soil structure (Fig. 2.7).

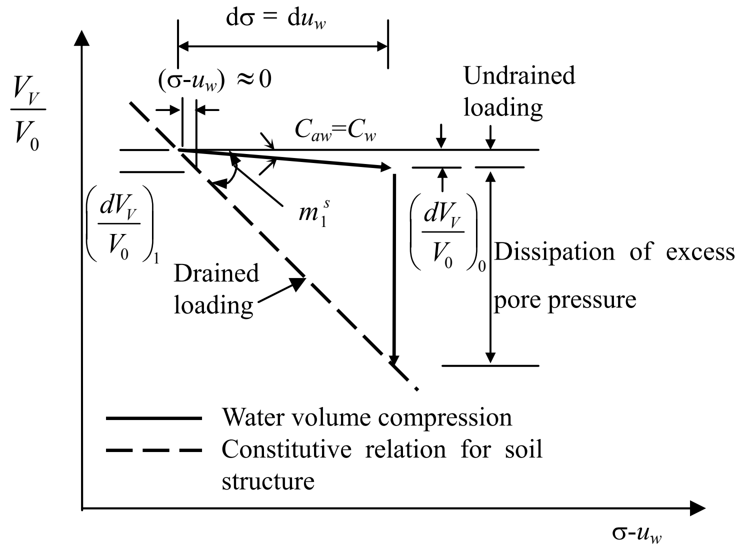

Fig. 2. 6 Volume change in a saturated soil during loading (Fredlund and Rahardjo, 1993)

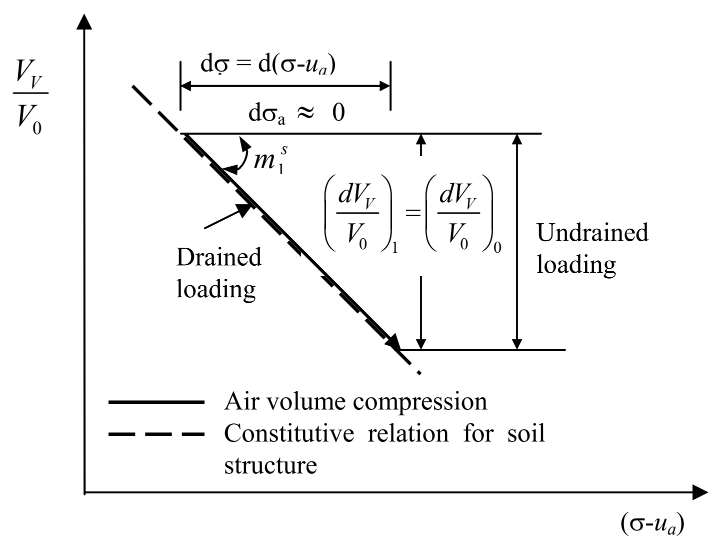

Fig. 2. 7 Volume change in a dry soil during loading (Fredlund and Rahardjo, 1993)

2.2.3 Pore pressure parameters

The pore pressure parameters for an unsaturated soil can be defined either as a tangent- or secant-type parameter. Figure 2.8 shows the developed pore-air and pore-water pressures during isotropic, undrained compression and the corresponding tangent and secant pore parameters for air and water phases.

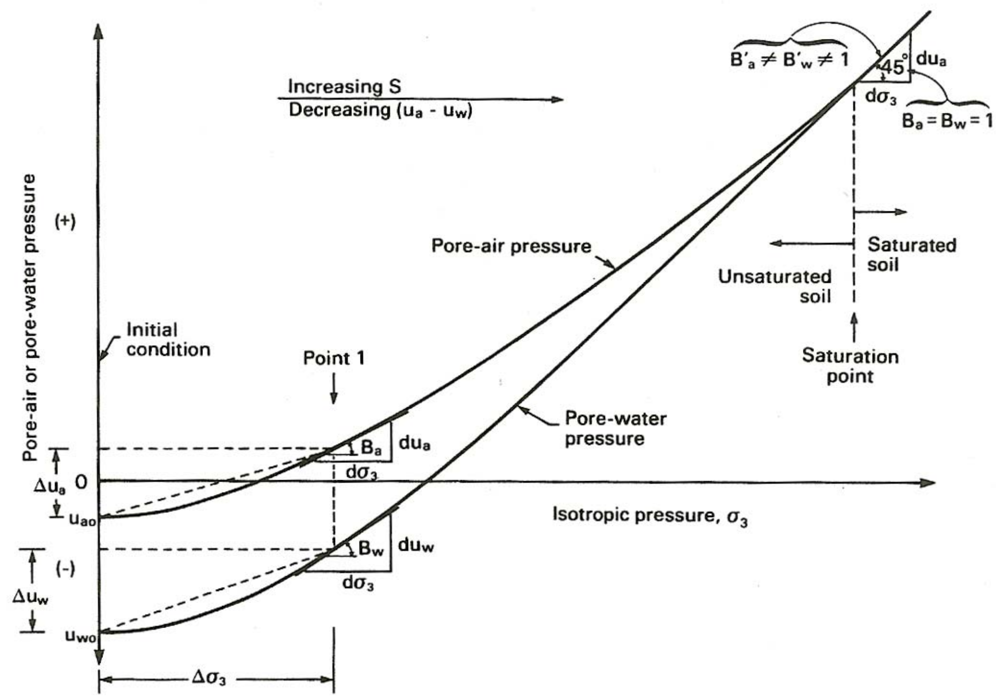

Fig. 2. 8   Tangent and secant pore pressure parameters (Fredlund and Rahardjo, 1993)

The secant *B'* pore pressure parameters for the air and water phases can be expressed as

$$B_a^{'} = \frac{\Delta u_a}{\Delta \sigma_3} \qquad (2.10)$$

$$B_w^{'} = \frac{\Delta u_w}{\Delta \sigma_3} \qquad (2.11)$$

where $B_a^{'}$ = secant pore pressure parameter for the air phase during isotropic, undrained compression;

$B_w^{'}$ = secant pore pressure parameter for the water phase during isotropic, undrained compression;

$\Delta\sigma_3$ = increase in isotropic pressure from the initial condition;

Δu_a = increase in pore-air pressure due to an increase in isotropic pressure, $\Delta\sigma_3$; and,

Δu_w = increase in pore-water pressure due to an increase in isotropic pressure, $\Delta\sigma_3$.

The equations for tangent B pore pressure parameters can be written as follows:

$$B_a = \frac{du_a}{d\sigma_3} \tag{2.12}$$

$$B_w = \frac{du_w}{d\sigma_3} \tag{2.13}$$

where B_a = tangent pore pressure parameter for the air phase during isotropic, undrained compression;

B_w = tangent pore pressure parameter for the water phase during isotropic, undrained compression;

$d\sigma_3$ = infinitesimal increase in isotropic pressure;

du_a = increase in pore-air pressure due to an infinitesimal increase in isotropic pressure, $d\sigma_3$; and,

du_w = increase in pore-water pressure due to an infinitesimal increase in isotropic pressure, $d\sigma_3$.

Hilf (1948) presented a procedure to calculate the change in pore pressure in compacted earth fills induced by an applied total stress, σ_y, using the results of a one-dimensional oedometer test, Boyle's law, and Henry's law. In his analysis, he assumed that the change in pore-water pressure was equal to the change in pore-air pressure, so that the volume change due to a change in matric suction was negligible. He also assumed that the constitutive relation for the soil structure under a given matric suction could be determined by measuring the volume change of the soil structure due to increased loading of saturated soil. In other words, it was assumed that the compressibility of unsaturated soil, m_1^s, is equal to the coefficient of volume change, m_v, measured under saturated condition. Based on these assumptions, Hilf derived the following expression to predict an increase in pore-air pressure.

$$\Delta u_a = \left[\frac{1}{1 + \dfrac{(1 - S_0 + hS_0)n_0}{(u_{a0} + \Delta u_a)m_v}} \right] \Delta\sigma_y \qquad (2.14)$$

where, Δu_a = change in pore pressure;

u_{a0} = initial absolute air pressure (= initial gauge pressure + atmospheric pressure);

S_0 = initial degree of saturation;

h = the volumetric coefficient of solubility;

n_0 = initial porosity;

$\Delta \sigma_y$ = increase in overburden pressure; and,

m_v = coefficient of volume change measured on a saturated soil in a one-dimensional oedometer test.

The secant pore-air pressure parameter is obtained by dividing the pore-air pressure increase by the total stress increase. The secant pore-air pressure parameter from Hilf's analysis can be written as

$$B'_{ah} = \left[\frac{1}{1 + \dfrac{(1 - S_0 + hS_0)n_0}{(u_{a0} + \Delta u_a)m_v}} \right] \tag{2.15}$$

Equation 2.15 suggests that the coefficient of volume change (m_v) and the initial degree of saturation (S_0) are both important variables affecting the pore pressure response. A higher degree of saturation and increased soil compressibility result in a greater pore pressure response as a result of an increase in total stress.

2.3 EXPERIMENTAL DATA USED IN THE ANALYSIS

In order to investigate soil suction in a silty sand compacted at various water contents and with varying compactive efforts, Rorie (2006) performed collapse potential tests (ASTM D 5333-03), filter paper tests (ASTM D 5298-03), and Pressure Plate tests (ASTM D 6836-02). The liquid and plastic limits of the material tested are 29% and 19%, respectively. The clay content (% < 2μ) and specific gravity of the soil are 12 % and 2.64, respectively. The index properties of the residual soil tested are presented in Table 2.2 and the grain size distribution curve is shown in Fig. 2.9. The soil was compacted using three different energies: 10%, 30% and 100% of the standard energy (600 kN-m/m^3). Table 2.3 presents the combinations of hammer fall height and blows per layer with resulting Proctor Energy. The compaction curves developed with the three different energies are shown in Figure 2.10.

Table 2. 2   Index properties and grain sizes of residual soil

Liquid limit, LL (%)	29
Plastic limit, PL (%)	19
Plasticity index, I_p (%)	10
Sand (%)	39
Silt (%)	46
Clay (%)	12
Specified gravity, *Gs*	2.64
USCS classification	CL
Maximum dry density (g/cm3)	1.90
Optimum Moisture Content (%)	11.7

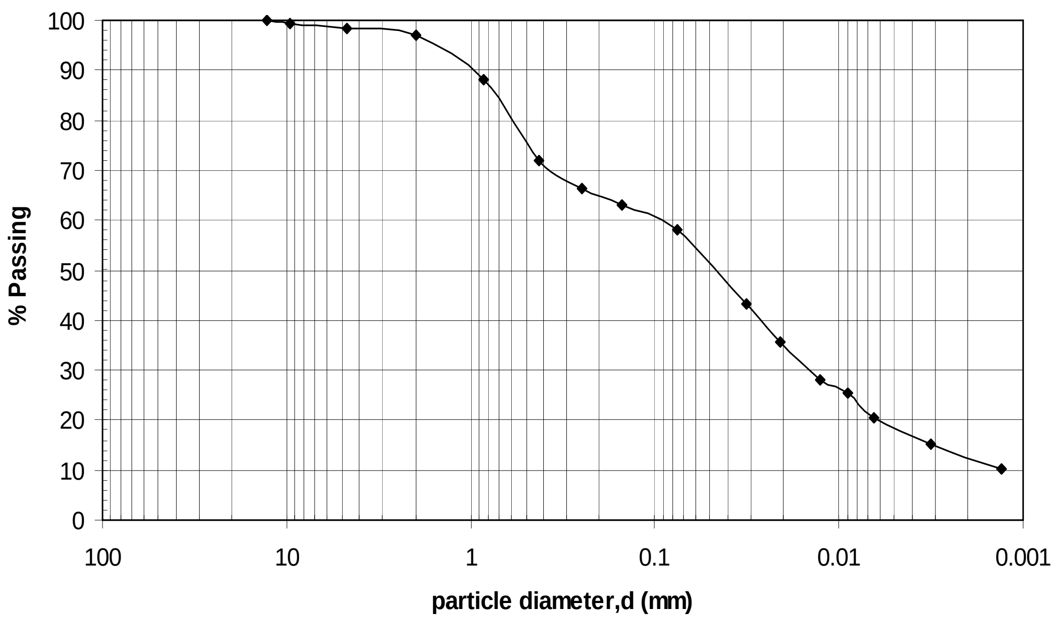

Fig. 2. 9   Grain size distribution curve (Rorie, 2006)

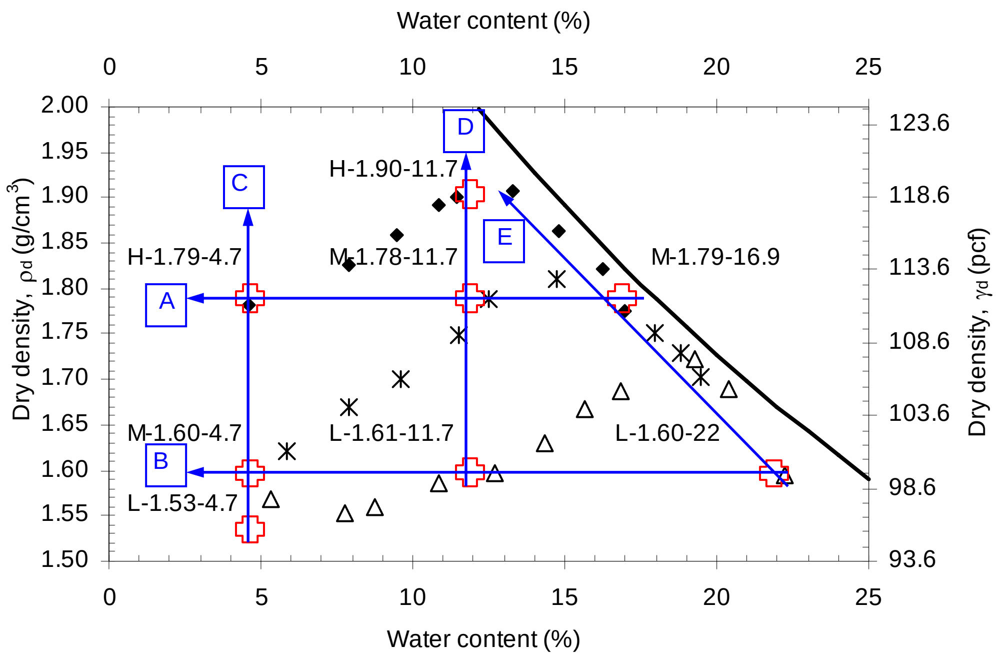

Fig. 2. 10 Compaction curve for three different energies (after Rorie, 2006)

Table 2. 3 Compaction methodology (After Rorie, 2006)

No. of Layers	Hammer wt. (Newton)	Drop Height (mm)	Blows/Layer	Energy (kN-m/m^3)	%SP
3	24.4	305	25	600	100
3	24.4	152	15	180	30
3	24.4	76	10	60	10

In this research, the results of double oedometer tests (Rorie, 2006) were used to estimate elastic modulus of compacted soils. Typical results of a double oedometer test are shown in Fig. 2.11. The method requires testing two of nominally identical samples (Lawton et al., 1991). One sample was initially inundated with water under a small seating load (5kPa) and allowed to swell until primary swelling or collapse was completed. The sample was then loaded with incrementally increasing overburden pressures (25, 50, 100, 200, 400, and 800kPa). The other sample was tested at the as-compacted moisture content using the same incremental loading procedure. The vertical strain difference between soaked (or inundated) and unsoaked (as-compacted) samples was assumed to be the collapse or swell potential. In this research, the relationships of volumetric strain versus overburden pressure for soaked and as-compacted specimens were used to determine the elastic modulus of soaked specimens and as-compacted specimens, respectively.

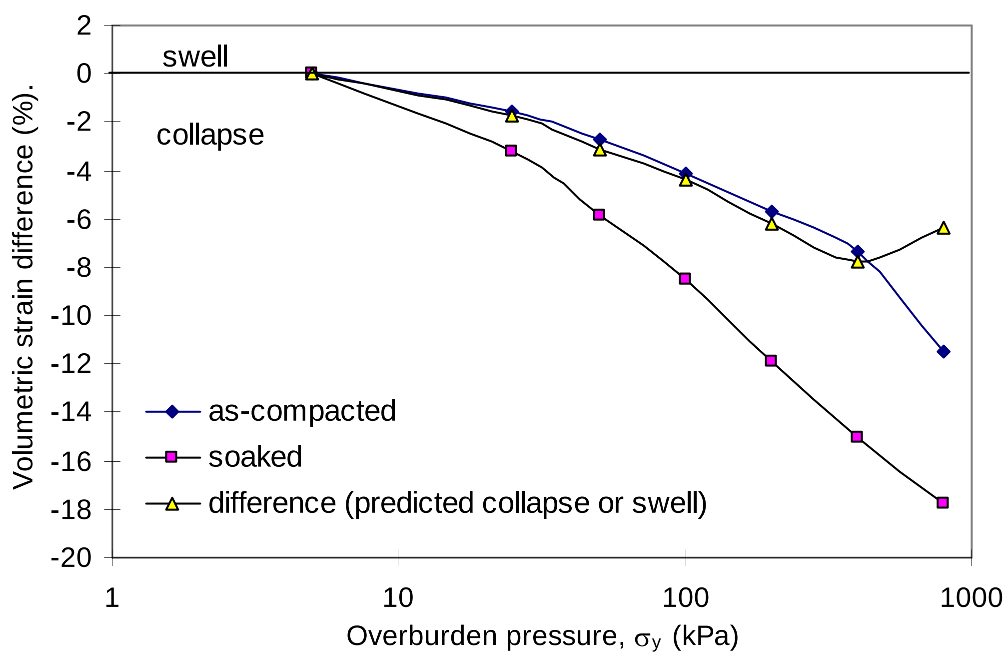

Fig. 2. 11 Typical result of double oedometer test for the specimen (after Rorie, 2006)

A total of eight specimens (noted in Fig. 2.10) prepared under various compaction conditions were used to develop data from which the elastic modulus could be determined.

Each specimen was designated using a code to enable easy identification. The first letter in the symbol, H, M, or L indicates either High, Medium, or Low compaction energy. The following two numbers indicates the dry density (g/cm^3) and the initial as-compacted water content (%). Therefore, H-1.79-4.7 stands for a specimen compacted with the highest energy to a dry density of 1.79g/cm^3 at a moisture content of 4.7%. In order to observe the influence of initial moisture content and dry density on the elastic modulus of compacted soil, five different groups (A through E) were selected, as shown in Fig. 2.10. The effect of initial water content on elastic modulus was investigated from the results of specimens in rows A and B, which were compacted at as-compacted dry densities of approximately 1.79 g/cm^3 and 1.60 g/cm^3, respectively. Also the effect of the density on elastic modulus of the specimens compacted at different water contents was investigated from the results of columns C, D, and E. Table 2.4 presents the specimens which belong to the various groups.

Table 2. 4 Groups and corresponding specimens

Groups	**Specimens**
A	H-1.79-4.7, M-1.78-11.7, M-1.79-16.9
B	M-1.60-4.7, L-1.61-11.7, L-1.60-22
C	H-1.79-4.7, M-1.60-4.7, L-1.53-4.7
D	H-1.90-11.7, M-1.78-11.7, L-1.61-11.7
E	H-1.90-11.7, M-1.79-16.9, L-1.60-22

2.4 ANALYSIS OF DATA

2.4.1 Elastic modulus during drained loading

The as-compacted and soaked stress versus volumetric strain curves from the oedometer tests were used to determine the elastic modulus of the as-compacted and soaked specimens, respectively. As water and air were allowed to drain through the top and bottom of the specimens during testing and sufficient time was allowed for 100% consolidation (according to the Taylor's construction), the elastic modulus estimated from the measured curves was a drained elastic modulus. The as-compacted and soaked specimens under the seating load (5kPa) were assumed to be "identical" even though there was a small difference in density. The reasonableness of this assumption is supported by small differences in strain (on the order of +/- 2%) between the as-compacted and soaked specimens. Table 2.5 shows the difference in volume change for the as-compacted and soaked specimens under the seating load of 5 kPa.

Table 2. 5 Volume change due to wetting under seating load

Sample ID	Volume change difference (%)
H-1.79-4.7	0.41
M-1.60-4.7	0.05
L-1.53-4.7	-2.73
H-1.90-11.7	0.64
M-1.78-11.7	-0.31
L-1.61-11.7	-0.99
M-1.79-16.9	-1.17
L-1.60-22	-1.55

In this research, the elastic modulus under overburden pressures ranging from 25kPa to 200kPa is determined. Figures 2.12 and 2.13 show the data and the best fit log-linear relationship between overburden pressure and measured volumetric strain for the soaked and unsoaked specimens, respectively. It can be seen that in this range the measured volumetric strain increases linearly with increasing overburden pressure in the semi-logarithm scale. The coefficient of volume change was obtained by differentiating the log-linear constitutive relation and the tangent elasticity parameter, E, was then calculated using Eq. 2.3 with the computed coefficient of volume change and the assumed Poisson's ratio. The assumed values of Poisson's ratios for the specimens used in this research are presented in Fig. 2.14. The different values of Poisson's ratio were considered based on the as-compacted conditions (Kulhawy et al., 1969). For example, a higher Poisson's ratio of 0.35 was selected based on the specimen with high degree of saturation and a lower Poisson's ratio of 0.25 was assigned for dry soils. In this research, the same values of Poisson's ratio were assumed for drained and undrained loading. As shown in Figures 2.12 and 2.13, the slopes of constitutive curves for the soaked specimens are steeper than those for the as-compacted specimens, which implies that the elastic modulus of soil decreases if the soil is inundated (or saturated).

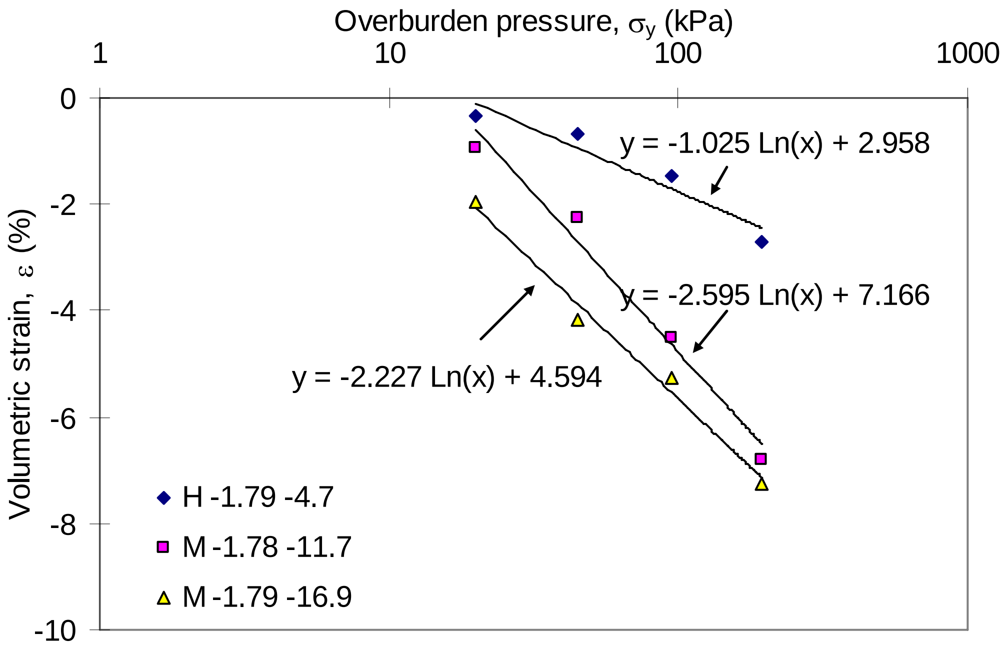

Fig. 2. 12 Volumetric strain vs. overburden pressure for unsoaked specimens (Group A)

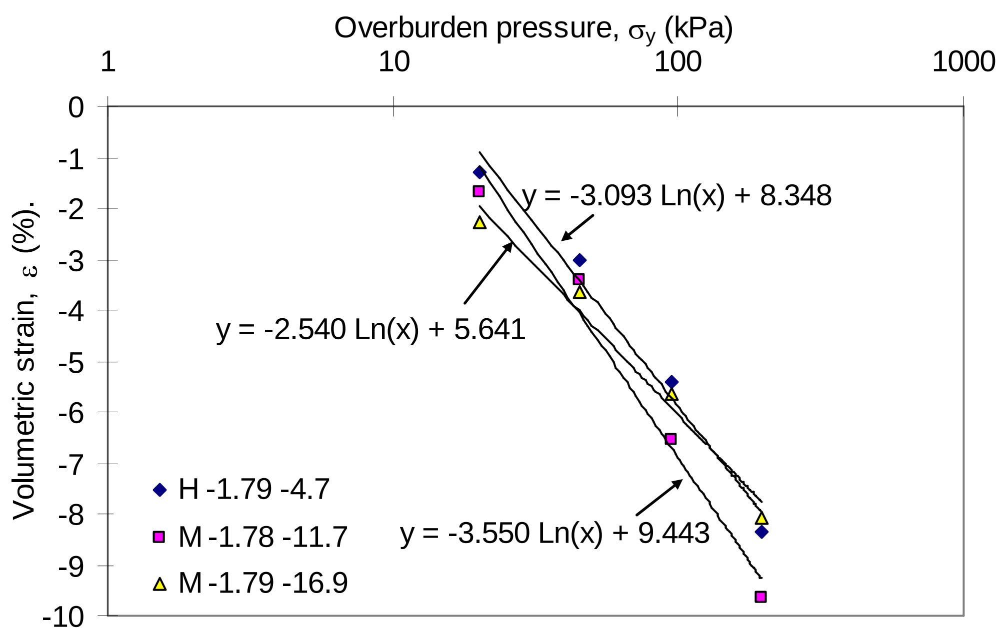

Fig. 2. 13 Volumetric strain vs. overburden pressure for soaked specimens (Group A)

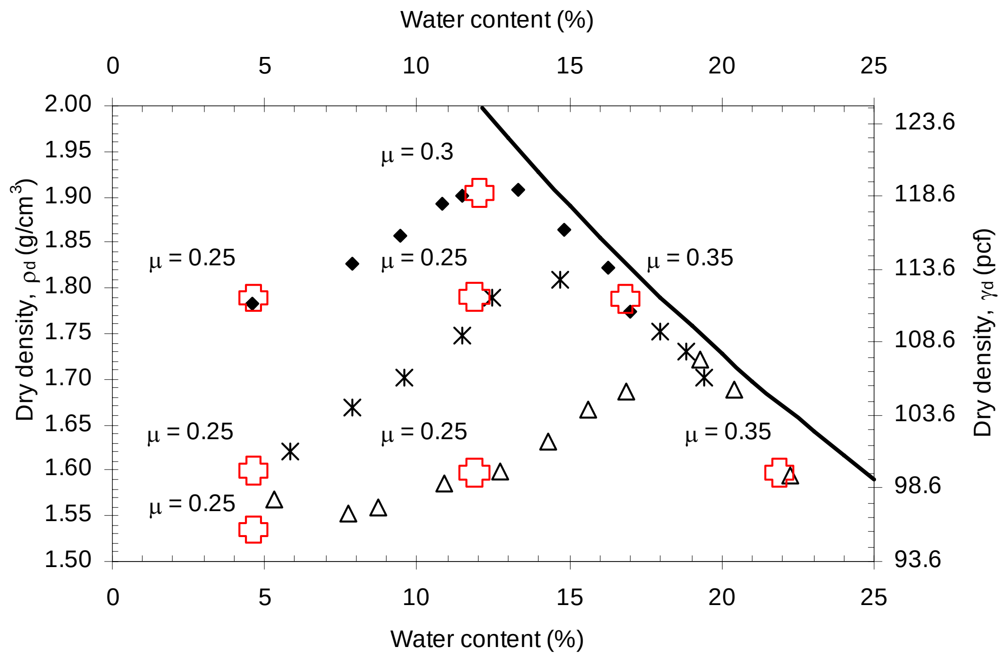

Fig. 2. 14 Assumed Poisson's ratios of specimens at different compaction conditions

The elastic moduli of the eight specimens, shown in Fig. 2.10, were calculated following the procedures described above. Figures 2.15-2.19 show the elastic modulus of unsoaked and soaked specimens for each group of specimens (i.e. A-E) over the range of overburden pressure, from 25 to 200 kPa. It should be noted that markers in the elastic modulus plots are used only to better distinguish the lines not to imply measured points.

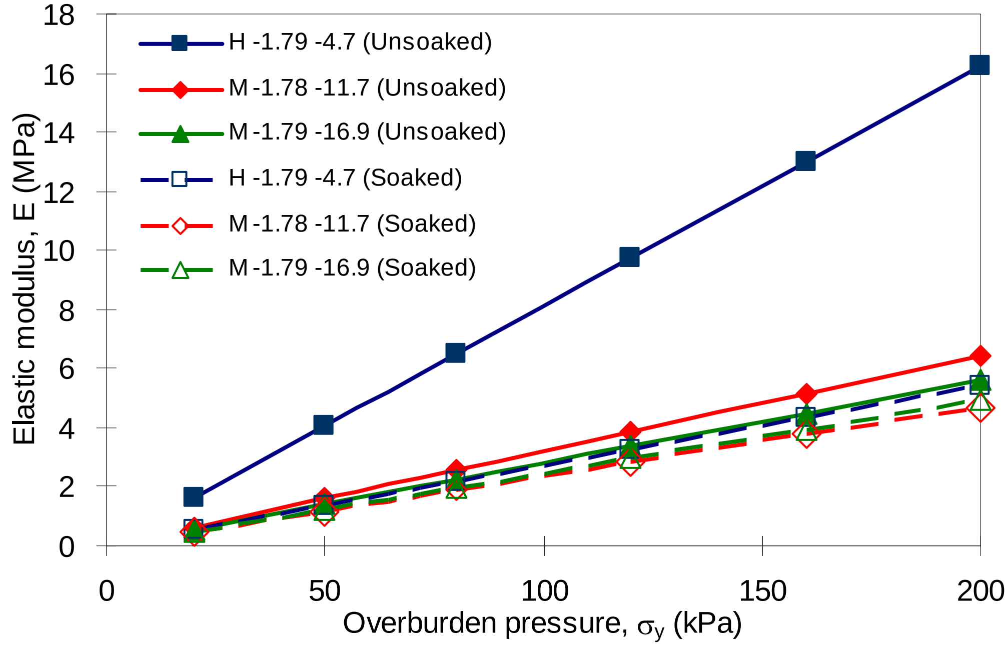

Fig. 2. 15 Elastic modulus of soaked and unsoaked specimens (Group A)

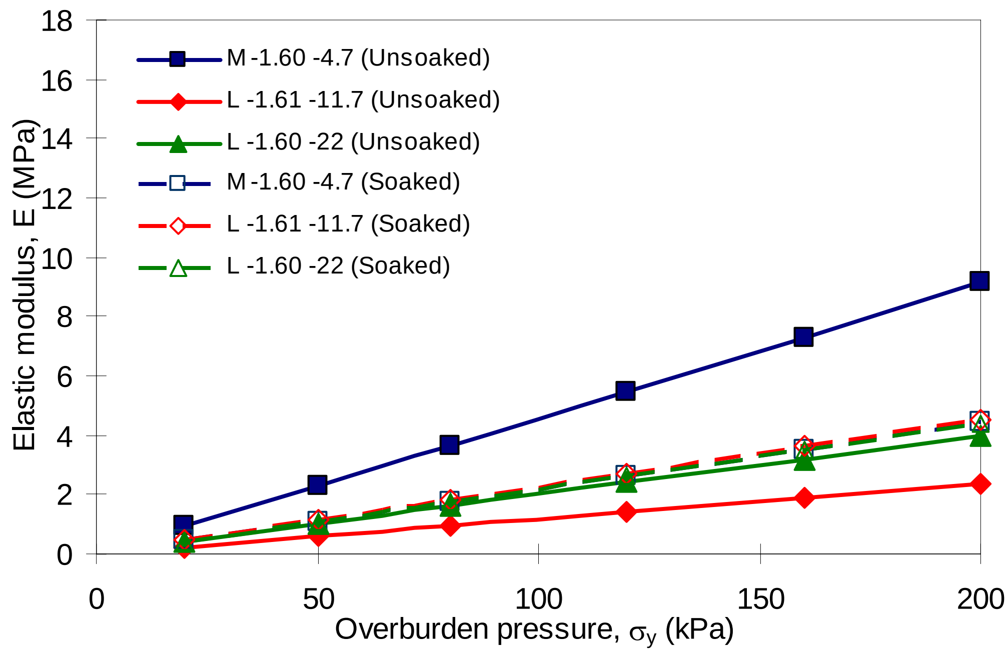

Fig. 2. 16 Elastic modulus of soaked and unsoaked specimens (Group B)

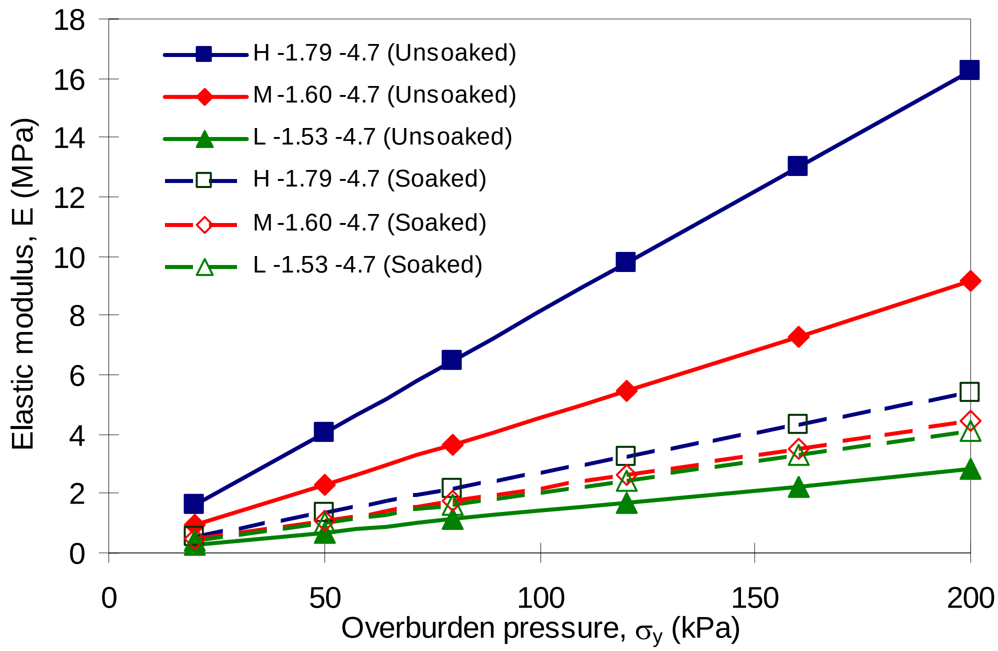

Fig. 2. 17 Elastic modulus of soaked and unsoaked specimens (Group C)

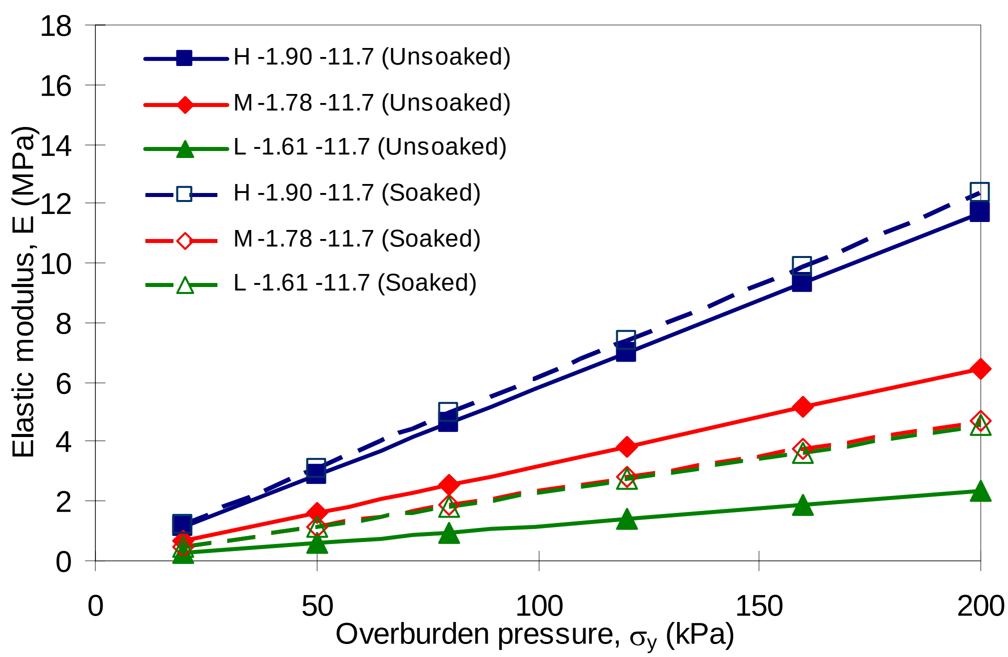

Fig. 2. 18 Elastic modulus of soaked and unsoaked specimens (Group D)

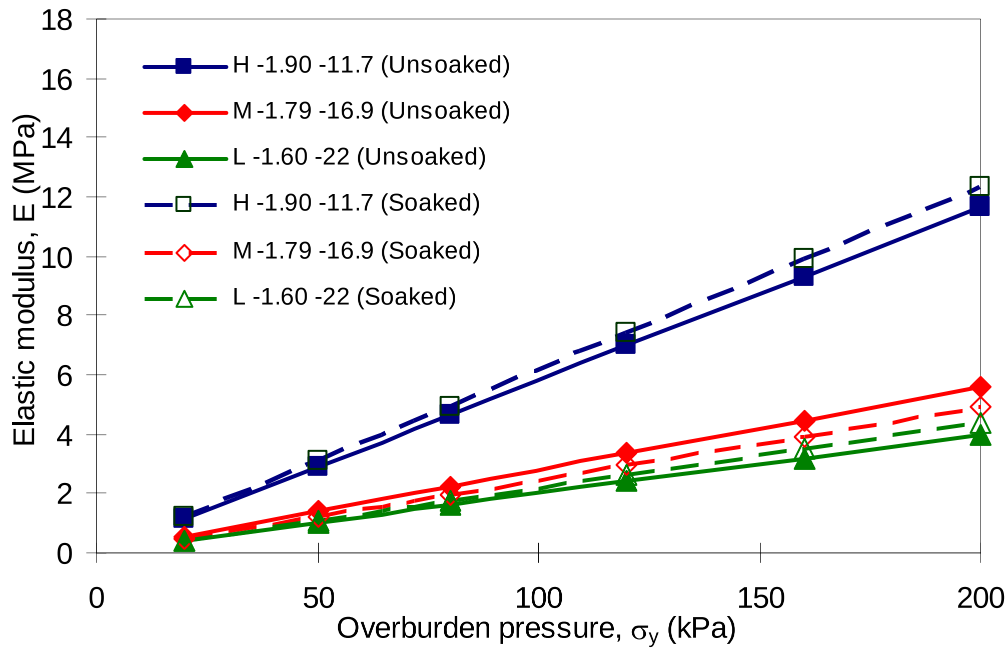

Fig. 2. 19 Elastic modulus of soaked and unsoaked specimens (Group E)

Figures 2.20–2.24 present the elastic moduli of specimens at an overburden pressure of 200 kPa for each group. For the specimens compacted at a dry density of 1.79 g/cm^3 (Fig. 2.20), it can be clearly seen that for unsoaked specimens, the elastic modulus increases as the as-compacted water content decreases from 16.9% to 4.7%. A similar trend is displayed upon examination of Figure 2.21 for the specimens compacted at 1.60 g/cm^3. However, the elastic modulus of soaked specimens, which were compacted at the same dry densities (1.79 g/cm^3 or 1.60 g/cm^3), were not sensitive to the magnitudes of as-compacted water content showing almost same elastic modulus. The large differences in moduli between soaked and unsoaked specimens, shown in Figs. 2.20 and 2.21, imply that there would be significant decreases in the elastic modulus of compacted soils when the soils are compacted very dry of optimum and then wetted by rain infiltration.

Figure 2.22 shows the values of elastic moduli for both soaked and unsoaked specimens with as-compacted water contents of 4.7% and three different dry densities (1.79 g/cm^3, 1.60 g/cm^3, and 1.53 g/cm^3). As dry density increases from 1.53 g/cm^3 to 1.79 g/cm^3, the elastic modulus of unsoaked specimen increases from 2.8 MPa to 16.3 MPa while that of the soaked specimen increases very little (from 4.1 MPa to 5.3 MPa). For the specimens compacted at the lowest dry density (1.53 g/cm^3), there was not a significant difference in the elastic moduli of soaked and unsoaked specimens. Therefore, it can be concluded that at low as-compacted water contents (w = 4.7%), the difference between elastic moduli of soaked and unsoaked specimens increases significantly with increasing dry density but the difference may be negligible if the dry density of the specimen is relatively very low (i.e. 1.53 g/cm^3). Figure 2.24 shows moduli for specimens which have as-compacted water contents on the wet side of optimum (Group E). There was little difference in soaked and unsoaked moduli for the specimens in this group because of the initial high degrees of saturation in the as-compacted state.

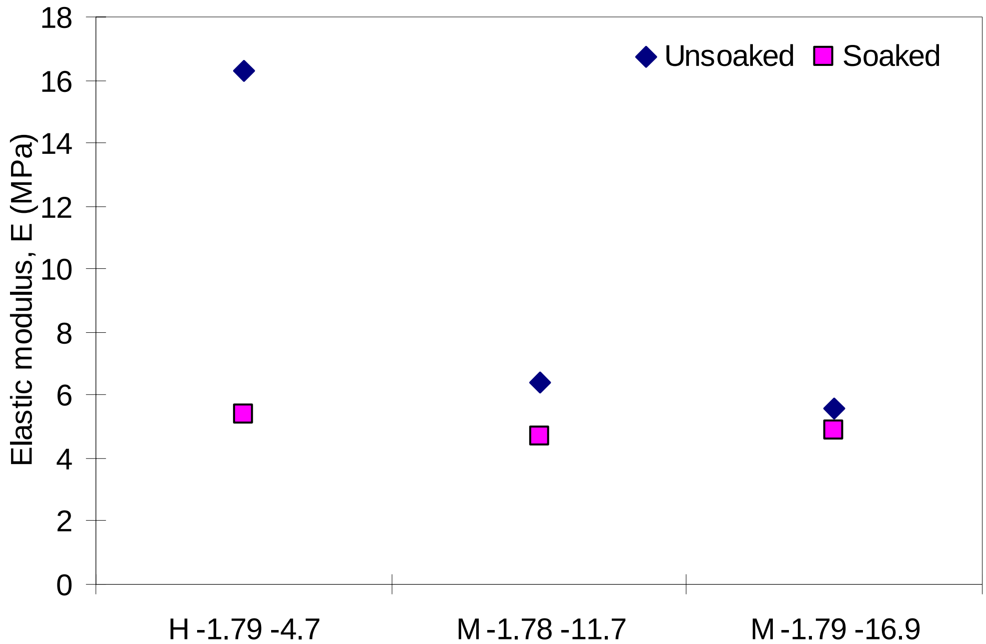

Fig. 2. 20 Elastic modulus of soaked and unsoaked specimens at σ_y = 200 kPa (Group A)

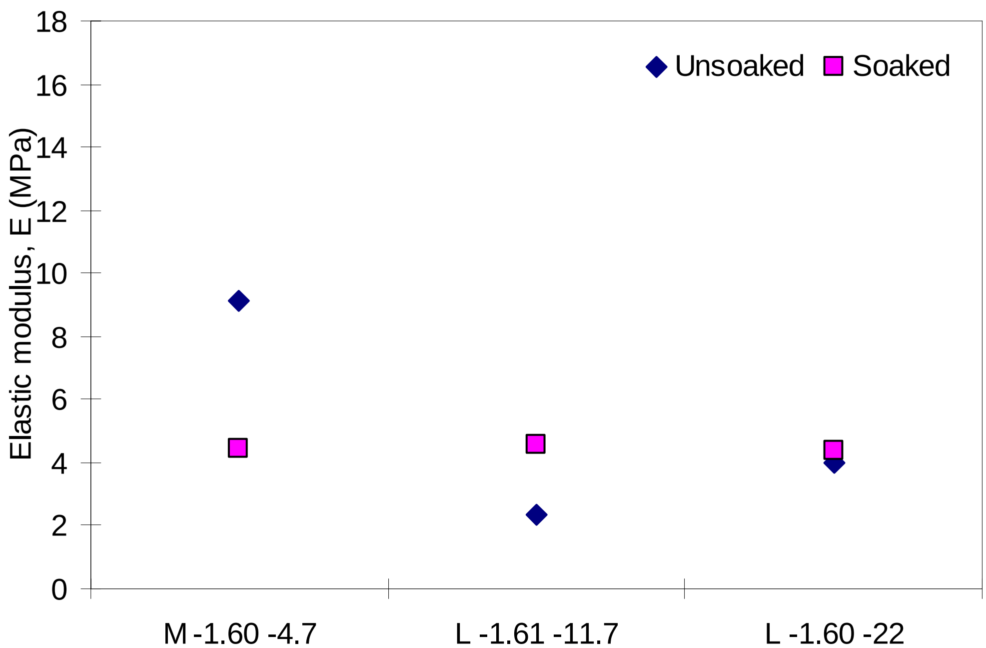

Fig. 2. 21 Elastic modulus of soaked and unsoaked specimens at σ_y = 200 kPa (Group B)

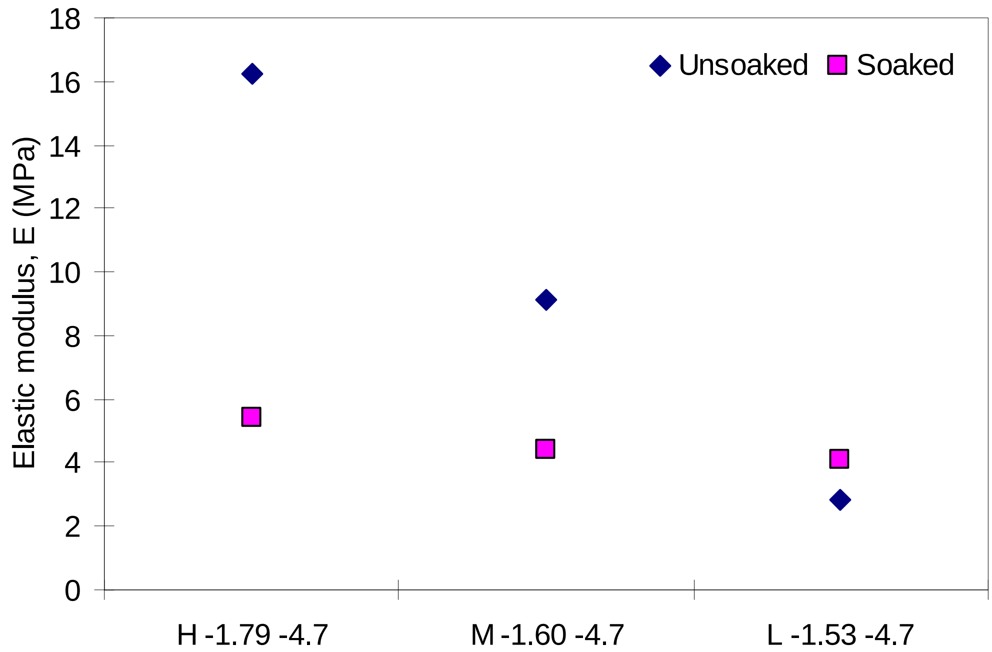

Fig. 2. 22 Elastic modulus of soaked and unsoaked specimens at σ_y = 200 kPa (Group C)

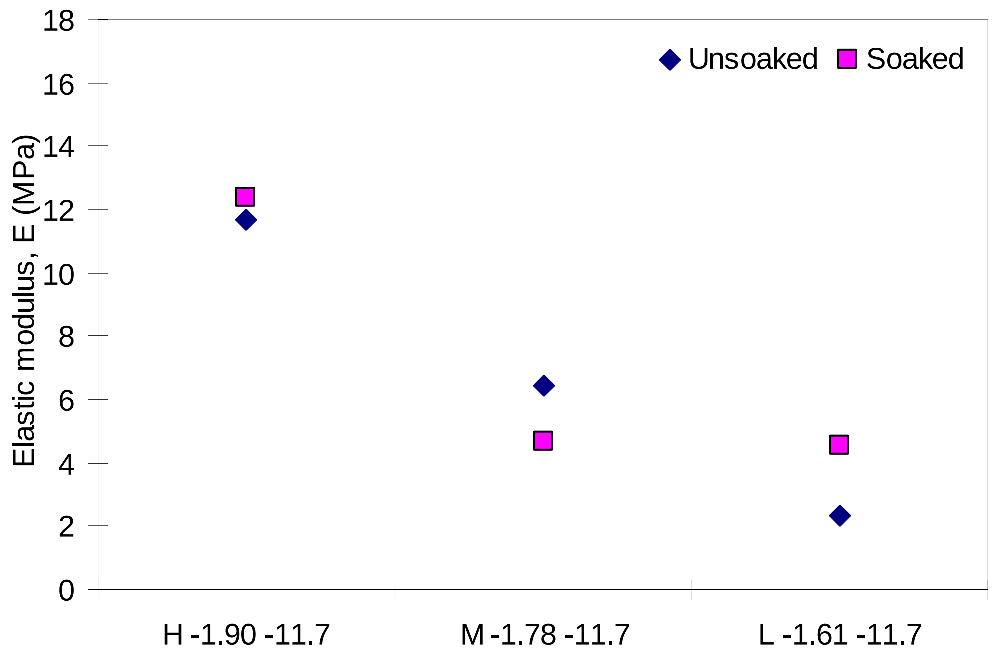

Fig. 2. 23 Elastic modulus of soaked and unsoaked specimens at σ_y = 200 kPa (Group D)

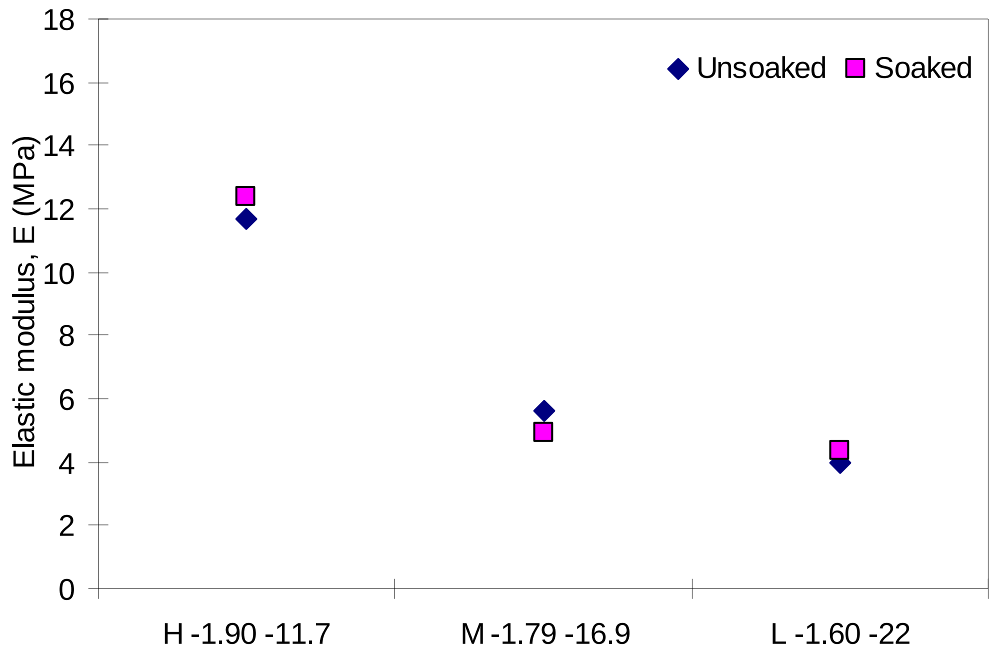

Fig. 2. 24 Elastic modulus of soaked and unsoaked specimens at σ_y = 200 kPa (Group E)

The stress dependent modulus, which increases linearly with increasing overburden pressure, can be defined using a modulus number, *K*, as following:

$$E = K \cdot \sigma_y \tag{2.16}$$

where *K* = dimensionless modulus number.

The modulus numbers for the specimens tested in this research were computed from the slope of the relation between *E* and σ_y shown in Figs. 2.15-2.19 (the range of overburden pressure, from 25 to 200 kPa). Figures 2.25 and 2.26 show the computed modulus numbers, K_{DU} and K_{DS}, of unsoaked and soaked specimens respectively. The modulus number for unsoaked specimens varies from 12 to 81 and is highly dependent on the as-compacted water content and dry density. However, the modulus number for soaked specimens is seen to be relatively insensitive to both initial water content and dry density, with majority of values fall within the 20 to 30 range (from 21 to 27). The one exception was the specimen compacted at the optimum water content (11.7%) to the maximum dry density (1.90 g/cm^3) which had a modulus number of 62, higher than the other saturated specimens tested. However, this value (62) is quite close to that measured for the similar unsoaked specimen (58), as shown in Fig. 2.25. As both of these specimens are at relatively high degrees of saturation, it appears logical that the values would be similar.

In general, the modulus number (or modulus) of unsoaked specimens should be equal to or greater than those of soaked specimens, because we know that the soil matric suction contributes to the stiffness of unsaturated soils (i.e. unsoaked specimens) (Rahardjo et al., 2004; Thu et al., 2006). However, four pairs of specimens tested in this research (L-1.61-11.7, L-1.60-22, L-1.53-4.7, and H-1.90-11.7) show somewhat conflicting results, in that the modulus number of the unsoaked specimen is lower than that of the corresponding soaked specimen (Figs. 2.25 and 2.26). Among these values of modulus numbers, those of specimens, L-1.60-22 and H-1.90-11.7, which show small differences between the values of K_{DU} and K_{DS} (6% and 9%, respectively), could be considered acceptable, as those values are quite close. Furthermore, theses specimens were compacted to high degrees of saturation, therefore the values of modulus numbers would be expected to be similar. However, it can not be explained as to why the large differences (48% and 50%) exist for the specimens compacted at 1.61 g/cm^3 (w = 11.7%) and 1.53 g/cm^3 (w = 4.7%), respectively. Logic would suggest that

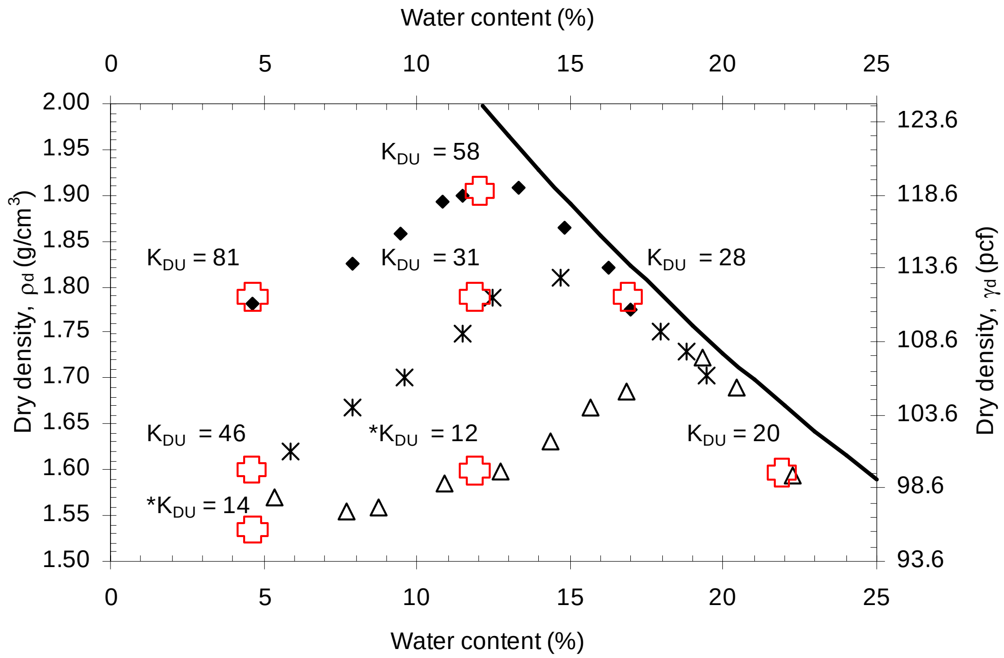

Fig. 2. 25 Modulus number, K_{DU}, for drained loading - unsoaked specimen (*computed from the measured stress-volumetric strain data in question)

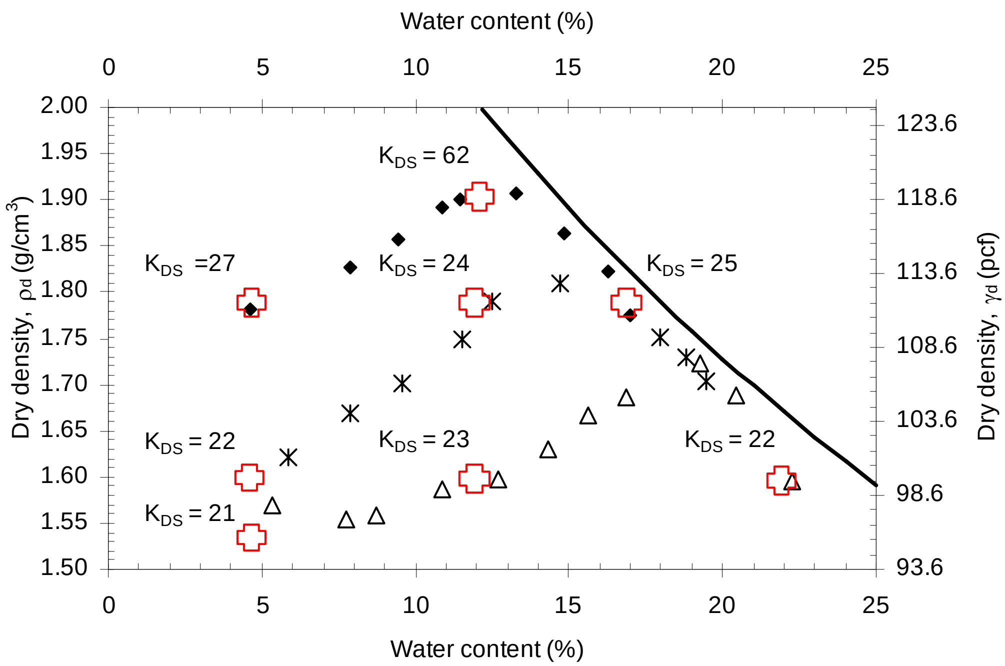

Fig. 2. 26 Modulus number, K_{DS}, for drained loading - soaked specimen

the modulus values for the soaked specimens (K_{DS}) at similar as-compacted densities should be similar, and the data support this thought with values of 22, 23, and 22 at as-compacted water contents of 4.7, 11.7, and 22%, respectively. Therefore, as the unsoaked specimens should be stiffer, logic suggests that the values of K_{DU} of 12 and 14 are probably too low but there is no conclusive explanation.

2.4.2 Elastic Modulus during undrained loading

The volume change of soils due to undrained loading can be estimated from changes in both net normal stress and matric suction, as explained in section 2.2.2. In this research, the volume change due to change in net normal stress ($=(\frac{dV_V}{V_0})_1$), as shown in Fig. 2.5 (a), was only regarded as the volume change of unsaturated soils due to undrained loading assuming that the volume change due to change in matric suction ($=(\frac{dV_V}{V_0})_2$), as shown in Fig. 2.5 (b) was negligible. This assumption is similar to that used by Hilf (1948) in his analysis. In order to compute the change in net normal stress, it was necessary to estimate the change in pore air pressure induced by the change in total stress. The following section describes how to compute the excess pore air pressures induced within the specimens due to loading.

Determination of pore pressures due to loading

Hilf's equation (Eq. 2.14) was used in order to estimate pore pressure increments due to loading. In this study, the compressibility of as-compacted soils obtained from the oedometer test was used instead of the coefficient of volume change of saturated soil, m_v, which is required for use in the original Hilf's equation. This modification on the Hilf's equation was made based on the results from the double oedometer test that showed the compressibilities of the as-compacted specimens were smaller than those of the saturated specimens, especially when the specimens were compacted at high density and at low water content. Therefore, using the compressibility of saturated soil, m_v, could produce erratic values of pore pressure increments. Using the compressibility of as-compacted soil, Hilf's equation (Eq. 2.14) can be rewritten as follows:

$$\Delta u_a = \left[\frac{1}{1 + \frac{(1 - S_0 + hS_0)n_0}{(u_{a0} + \Delta u_a)m_{as}}} \right] \Delta \sigma_y \qquad (2.17)$$

where m_{as} = compressibility of as-compacted specimen measured from an oedometer test.

Figures 2.27-2.31 show the pore air pressure increments at the selected total overburden pressures (1, 40, 80, 120, 160, and 200 kPa) computed from Eq. 2.17 using the average compressibility for the overburden pressure range from 0 to 200 kPa. Also, the average secant pore pressure parameter, B'_{avg}, was determined for each of the specimens from the slopes of the linear trend lines shown in the figures. It can be clearly seen that the pore pressure parameter increases with increasing as-compacted water content (Figs. 2.27 and 2.28) or with decreasing soil density (Figs. 2.29 and 2.30). For example, the average secant pore pressure parameters of the specimens with as-compacted water contents of 4.7% (B'_{avg} = 0.06, 0.10, 0.25) are determined for the specimens of dry density from 1.53, 1.60, and 1.79 g/cm^3, respectively. In contrast, the average secant pore pressure parameters of the specimens compacted on the wet side of optimum are 0.71, 0.77 and 0.30 for the specimens of dry densities 1.60, 1.79 and 1.90 g/cm^3, respectively (Fig. 2.31). It should be noted that the specimen with dry density of 1.90 g/cm^3 and an as-compacted water content of 11.7% has a relatively small secant pore pressure parameter (B'_{avg} = 0.3) compared to the other specimens. It is believed that this is due to the higher stiffness of the specimen. The B'_{avg} values for all the specimens are shown in Table 2.6, as well as on Fig. 2.32 with the compaction curves. Also, the average compressibility and degree of saturation are presented in Table 2.6.

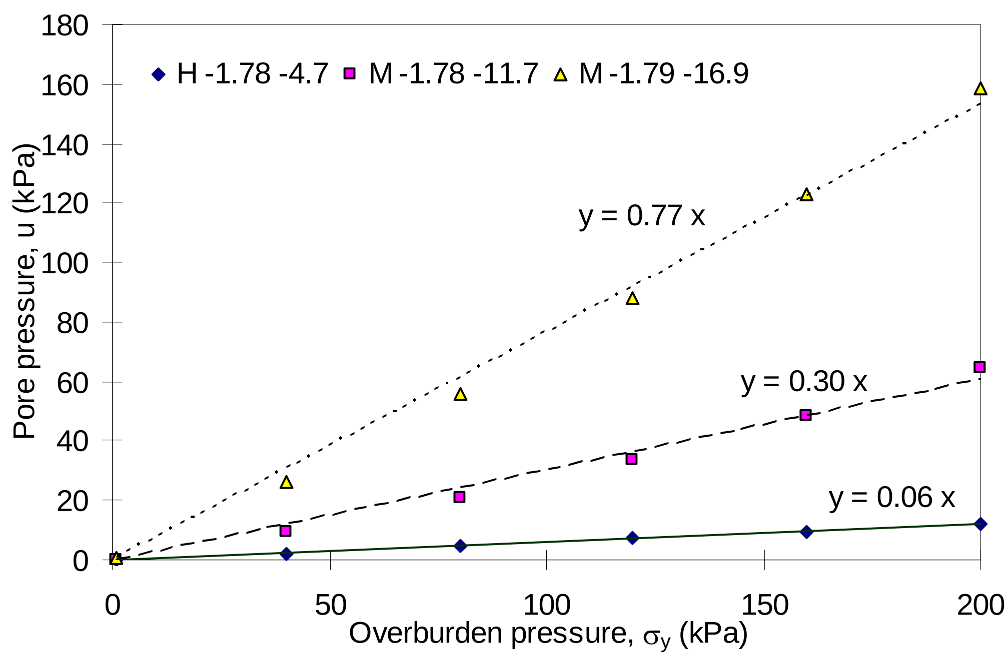

Fig. 2. 27 Computed pore-air pressures (Group A)

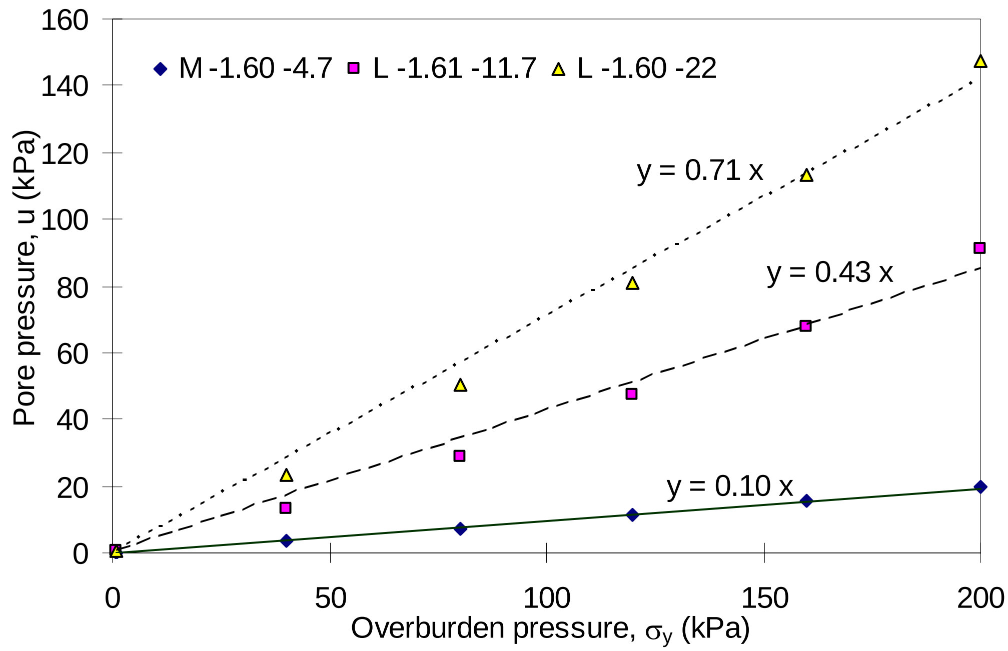

Fig. 2. 28 Computed pore-air pressures (Group B)

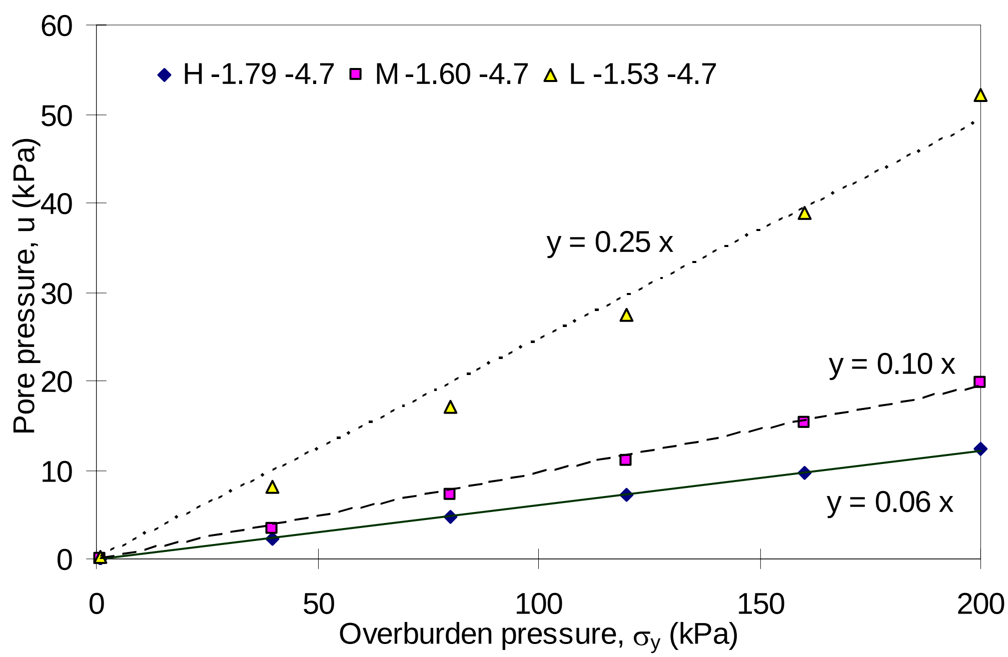

Fig. 2. 29 Computed pore-air pressures (Group C)

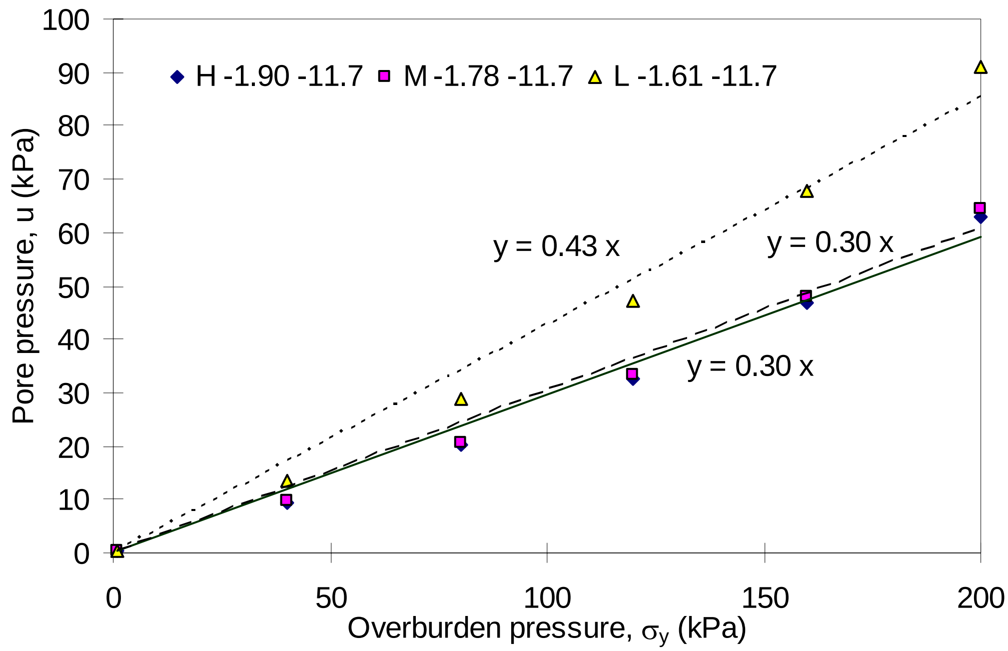

Fig. 2. 30 Computed pore-air pressures (Group D)

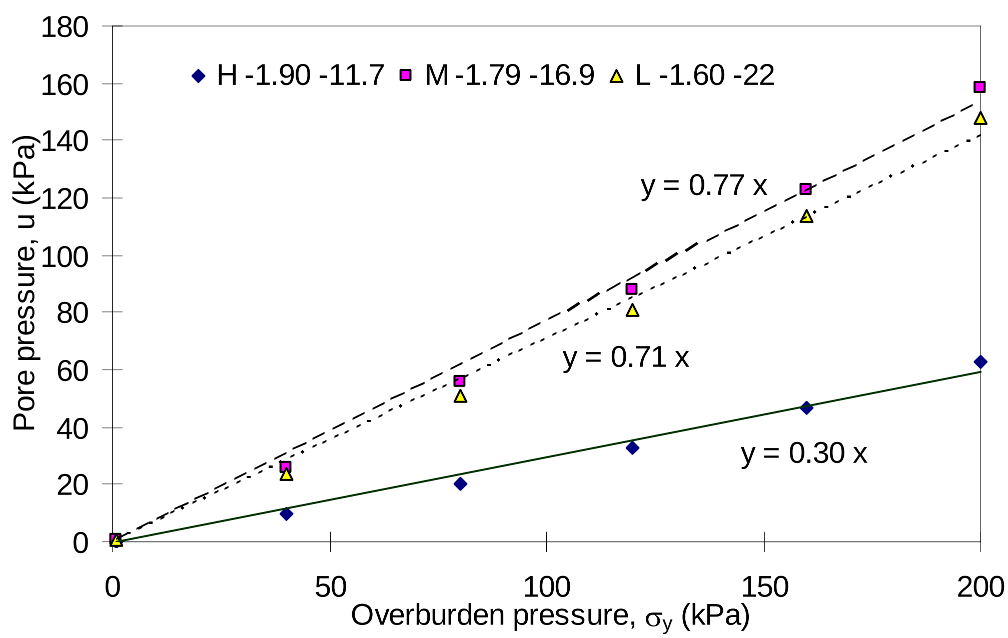

Fig. 2. 31 Computed pore-air pressures (Group E)

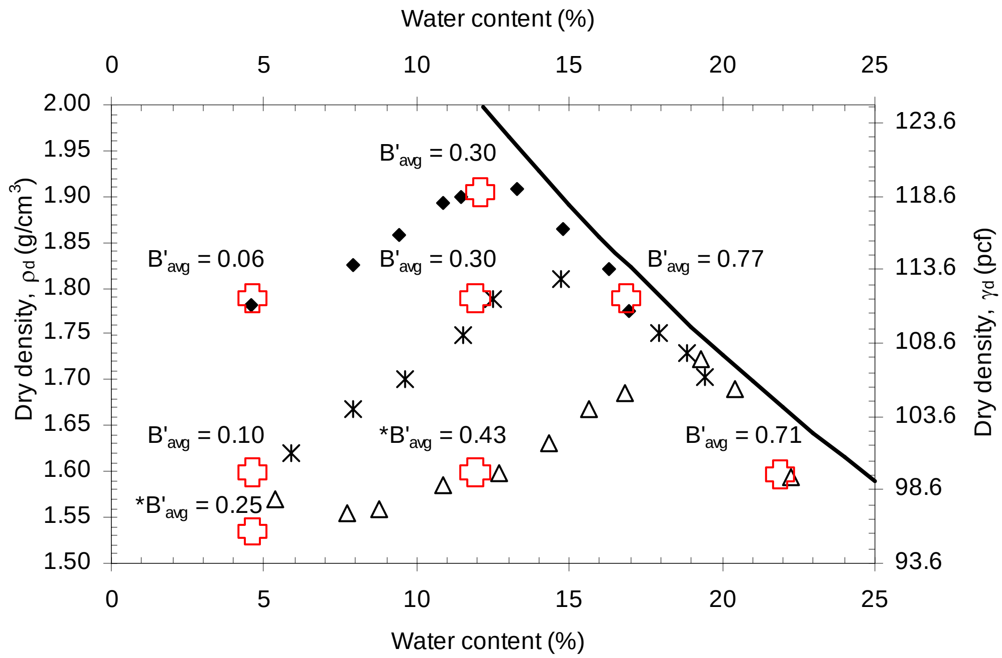

Fig. 2. 32 Averaged secant pore pressure parameter for all the specimens (*computed from the measured stress-volumetric strain data in question)

Table 2. 6 Compressibility, degree of saturation, and average secant pore pressure parameter

Sample ID	**Compressibility, m_{oed} (1 / kPa)**	**Degree of saturation, S (%)**	**Ave. secant pore pressure parameter, B'_{avg}**
H-1.79-4.7	1.38E-4	26.1	0.06
M-1.60-4.7	2.91E-4	19.1	0.10
L-1.53-4.7	8.06E-4	17.1	0.25*
H-1.90-11.7	1.75E-4	79.3	0.30
M-1.78-11.7	3.58E-4	63.9	0.30
L-1.61-11.7	8.99E-4	48.3	0.43*
M-1.79-16.9	3.71E-4	94.0	0.77
L-1.60-22	5.55E-4	89.4	0.71

*computed from the measured stress-volumetric strain data in question

In order to estimate the tangent pore pressure parameter, *B*, the computed pore pressures were first fitted with quadratic functions, as shown in Fig. 2.33. The tangent pore pressure parameter was then computed by differentiating the quadratic fit. Figures 2.34-2.38 present the tangent pore pressure parameter, *B*, with the secant pore pressure parameter, B' up to an overburden pressure of 200 kPa by passing a function thru the values which were computed at the overburden pressures of 1, 40, 80, 120, 160, and 200 kPa. The figures show that the tangent pore pressure parameter, *B*, is greater than the secant pore pressure parameter, *B'*. Comparing the *B* pore pressure parameters determined for the specimens (H-1.78-4.7, M-1.78-11.7, and M-1.79-16.9 from Fig 34; M-1.60-4.7, M-1.60-11.7, and L-1.60-22 from Fig 35), one can see that the rate of increase of *B* with overburden pressure is faster for the specimens with higher water content. It also can be seen that the rate of increase of *B* with overburden pressure is faster for the low density specimens (more compressible) from the *B* pore pressure parameters determined for the specimens (H-1.79-4.7, M-1.60-4.7 and L-1.53-4.7 from Fig 36; H-1.90-11.7, H-1.78-11.7, and H-1.61-11.7 from Fig 37).

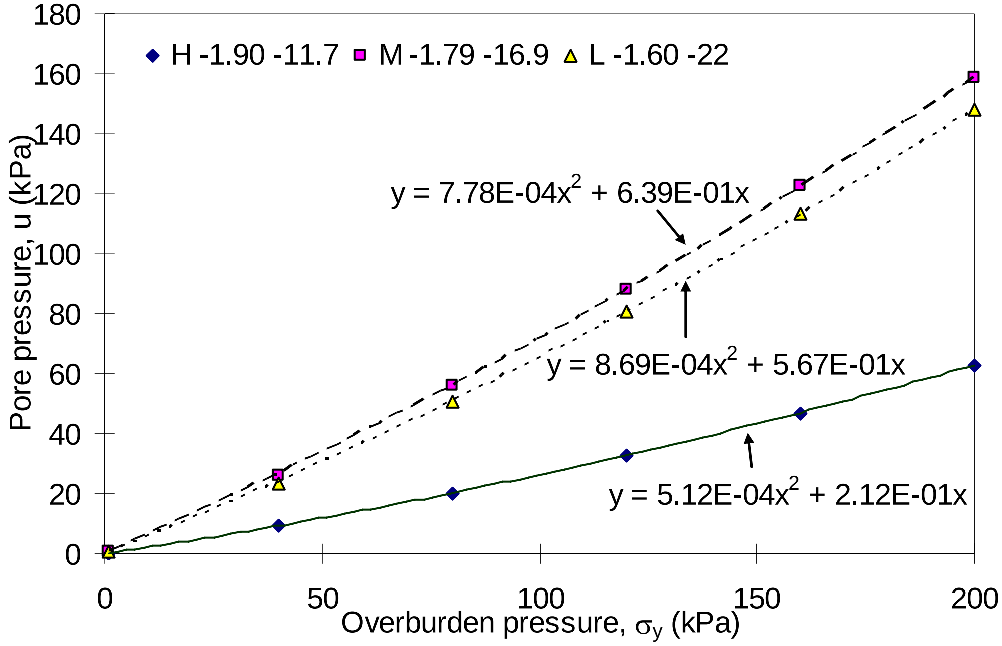

Fig. 2. 33 Predicted pore pressures fitted by quadratic functions

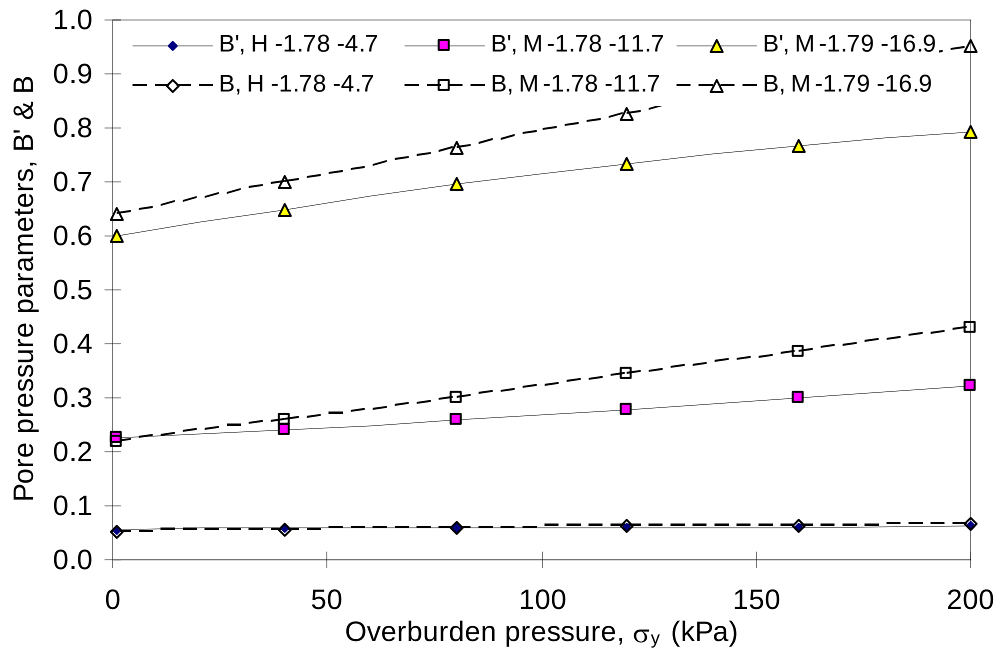

Fig. 2. 34 Secant (*B'*) and tangent (*B*) pore pressure parameters (Group A)

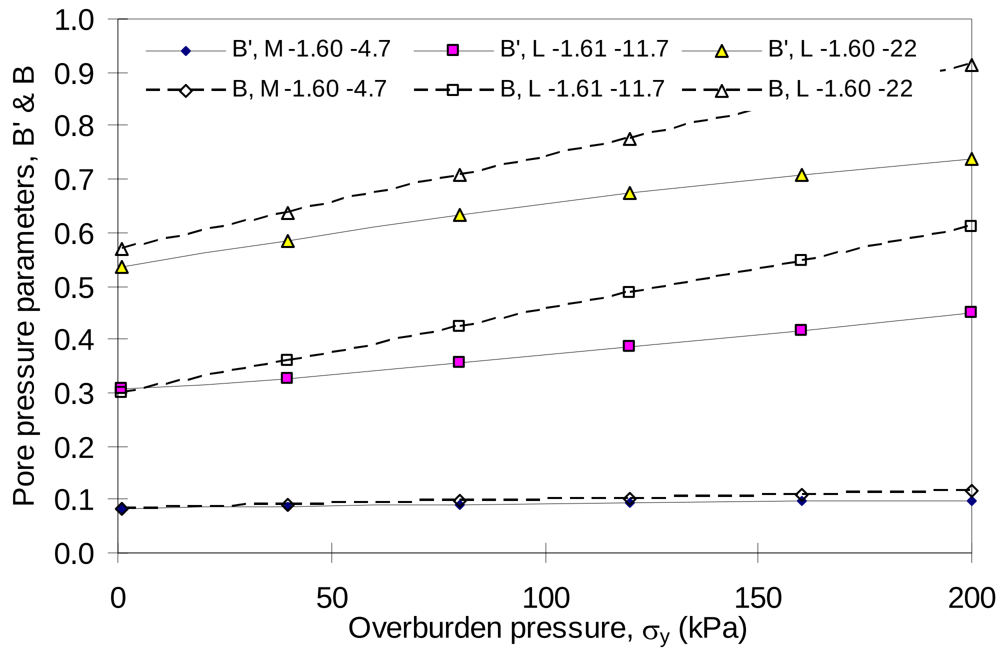

Fig. 2. 35 Secant (*B'*) and tangent (*B*) pore pressure parameters (Group B)

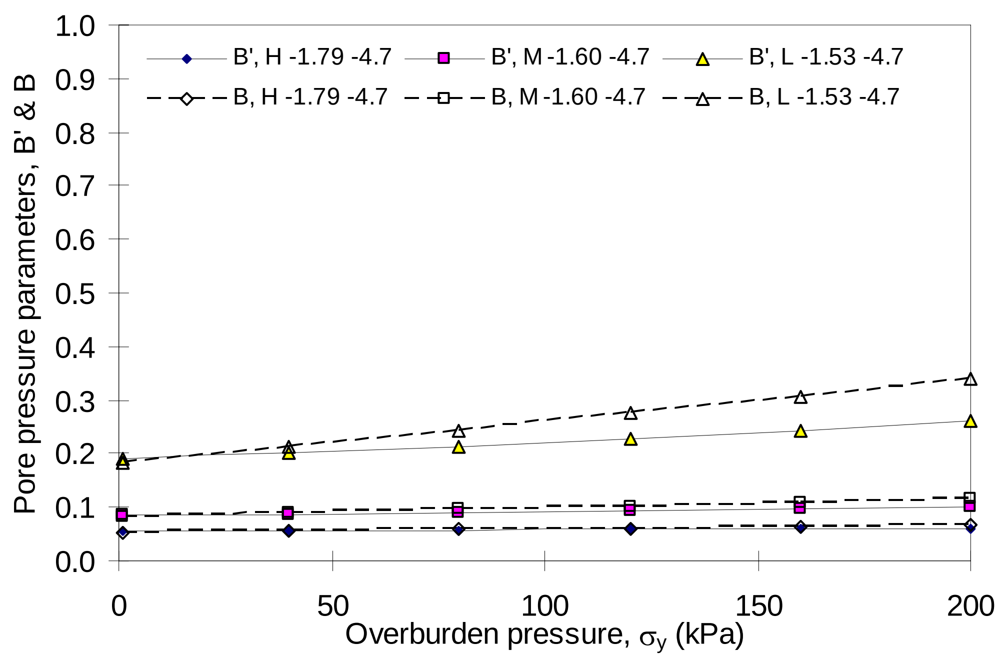

Fig. 2. 36 Secant (*B'*) and tangent (*B*) pore pressure parameters (Group C)

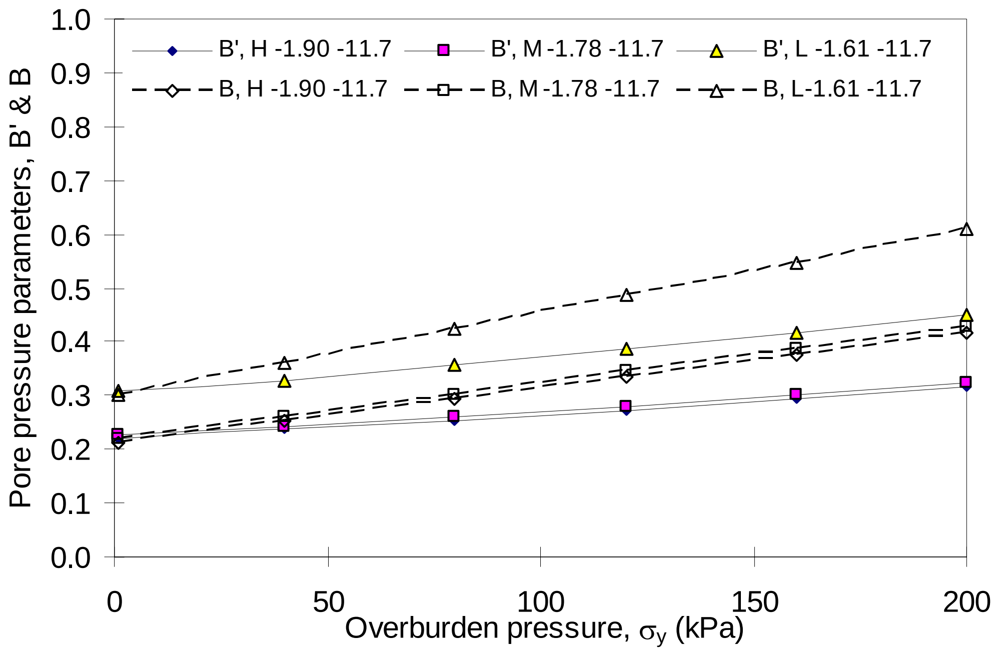

Fig. 2. 37 Secant (*B'*) and tangent (*B*) pore pressure parameters (Group D)

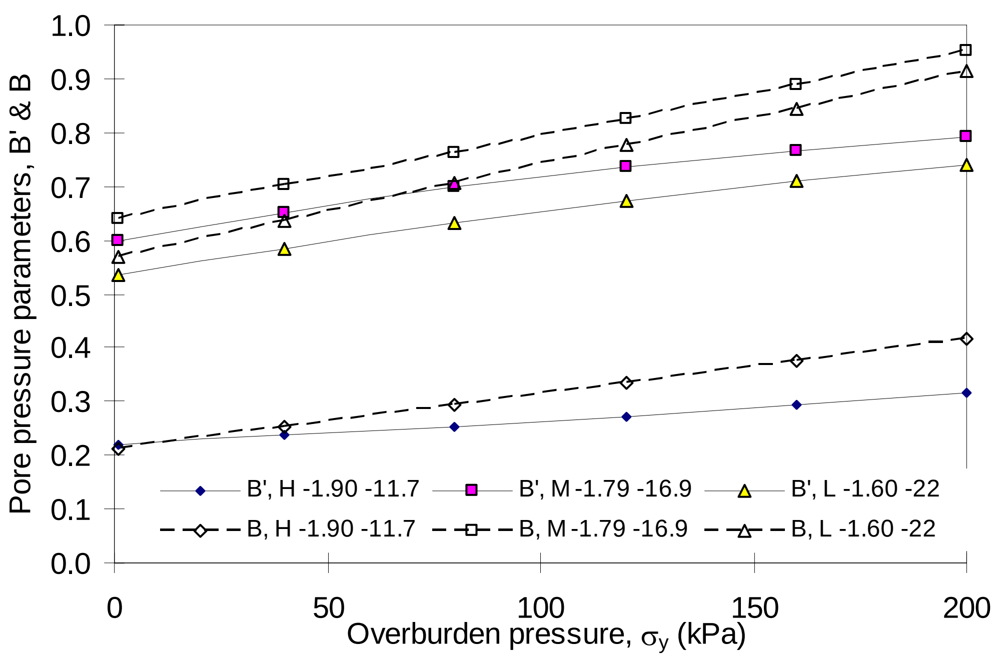

Fig. 2. 38 Secant (*B'*) and tangent (*B*) pore pressure parameters (Group E)

Determination of constitutive relation for undrained loading

Figure 2.39 presents the procedures used in this research for determining the constitutive relation for undrained loading from that for drained loading. Once the constitutive relation for undrained loading was determined (the log-linear constitutive relation was adopted in this research), the undrained modulus could be estimated by computing the slope at any point of interest. In this research, the volume change due to changes in matric suction (resulting from the change in degree of saturation produced by the strain during loading) was ignored based on the assumption that it is relatively small compared to the volume change due to changes in net normal stress. Details of the procedure can be described as follows (numbers shown in Fig. 2.39 represent each of the steps):

1) The stress-volumetric strain relationship of as-compacted soil, obtained from a oedometer test, is assumed to be representative of the constitutive relationship under drained loading for the soil structure (which actually exists during loading with constant matric suction).
2) During undrained loading, pore-air pressures would be generated, and these are calculated from Eq. 2.17. Now, with these values of u_a, values of $\Delta(\sigma - u_a)$ can be determined for any values of σ_y. On Fig. 2.39 (b), the value of $\Delta(\sigma - u_a)$ for the specimen at an overburden pressure of 200 kPa is shown.
3) The volume change corresponding to this change in net normal stress is determined from the constitutive relation of the soil structure (i.e. moving along this line as shown by the arrow)
4) This volume change is then re-plotted in terms of total normal stress, σ_y (shown as point 4).
5) Steps 2, 3, and 4 are repeated for the volumetric strains measured at any other overburden

pressure (i.e. 25, 50, 100 kPa…).

6) The constitutive relation for undrained loading is drawn based on the predicted volume changes in terms of total normal stress, σ_y.

7) Finally, the undrained elastic modulus is then computed from the slope of the constitutive relation for undrained loading in terms of total stress, $\sigma_{y.}$

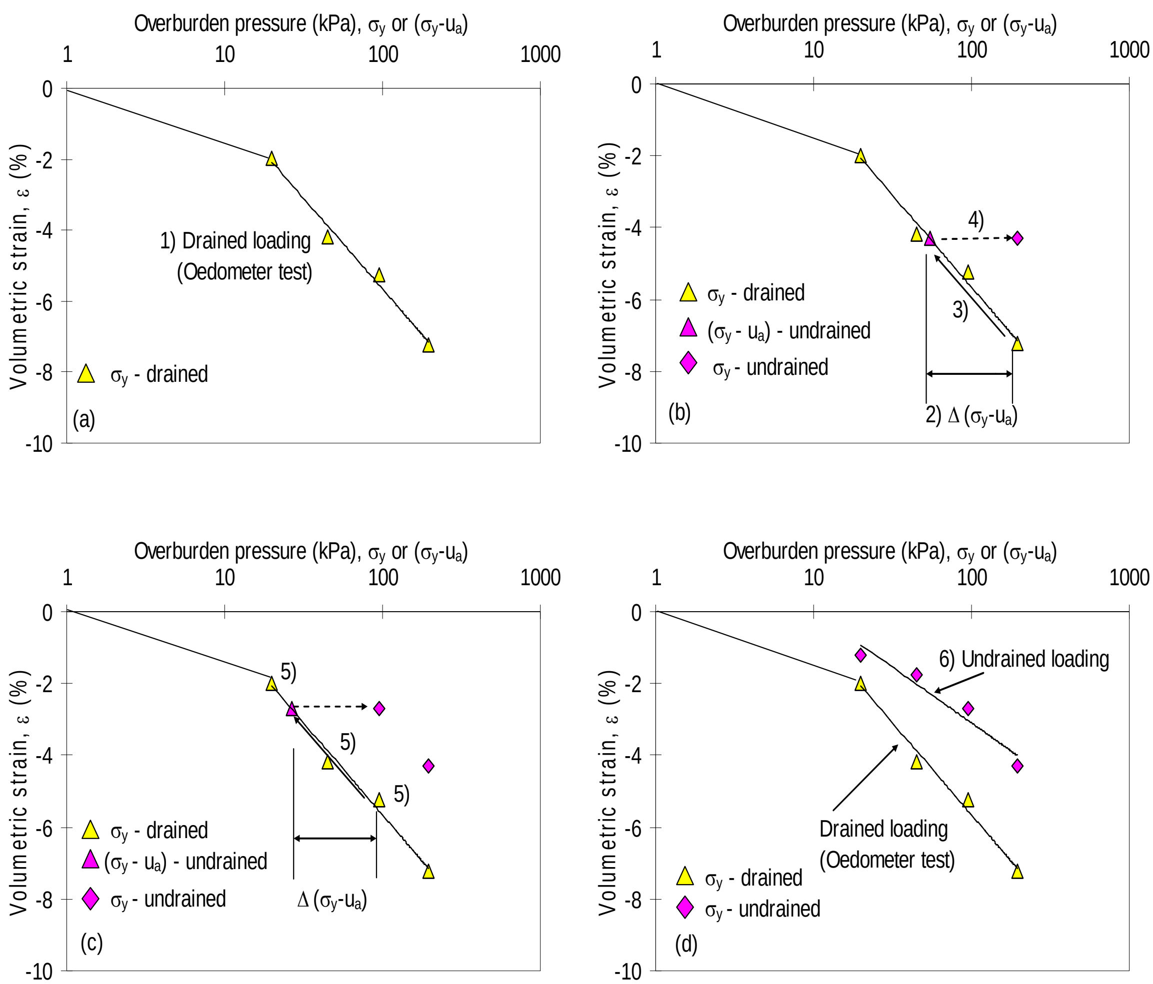

Fig. 2. 39 Determination of constitutive relation for undraind loading from drained loading

Figure 2.40 shows two potentially different volume change behaviors of unsaturated soil subjected to undrained loading. If a soil experiences a very small change in pore pressure, the volume change for undrained loading could be very similar to that of drained loading, as illustrated in Fig. 2.40(a). As an example, a high stiffness soil with low water content would tend to show this type of volume change behavior. On the other hand, if a soil develops a high pore pressure increment, the difference in volume change between the undrained and drained loading conditions would be more significant, as shown in Fig. 2.40 (b). A low stiffness soil with high degree of saturation would produce this response. The reader can note the conceptual similarity of these figures to those of Fredlund and Rahardjo (1993).

The undrained modulus values, determined by the procedure described above, for each of the test specimens are shown in Figs. 2.41-2.45. Again, in these plots, the points are only shown for clarification and do not represent data or analysis results. Both the drained and undrained modulus values are presented for the purpose of comparison. Figures 2.46-2.50 show the elastic moduli for both drained and undrained loading conditions under an overburden pressure of 200kPa. From the results shown in the figures (2.41-2.50), it can be seen that there are substantial differences between the drained modulus and undrained modulus values for the specimens compacted at high degree of saturation (H-1.90-11.7, M-1.79-16.9, L-1.60-22), whereas the differences are very small for the specimens with the lowest water content of 4.7% (H1.79-4.7, M1.60-4.7, L1.53-4.7). The results also show the trend that undrained modulus increases with decreasing as-compacted water content (Figs. 2.46 and 2.47) or increasing the density (Figs. 2.48 and 2.49). The values of modulus number, K_{UN}, for undrained loading condition are presented in Fig. 2.51 with the compaction curves.

The values of K_{UN} determined range from the smallest value of 15 to the largest value of 83.

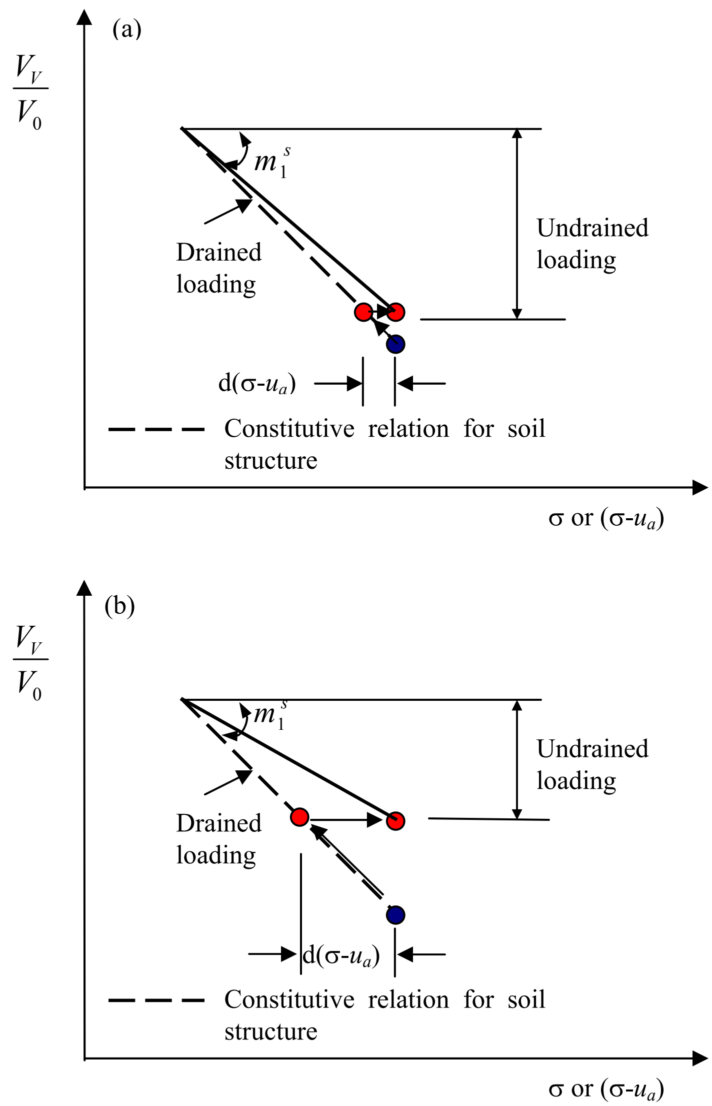

Fig. 2. 40 Volume changes due to drained and undrained loading (a) with a small induced pore pressure and (b) with a larger induced pore pressure.

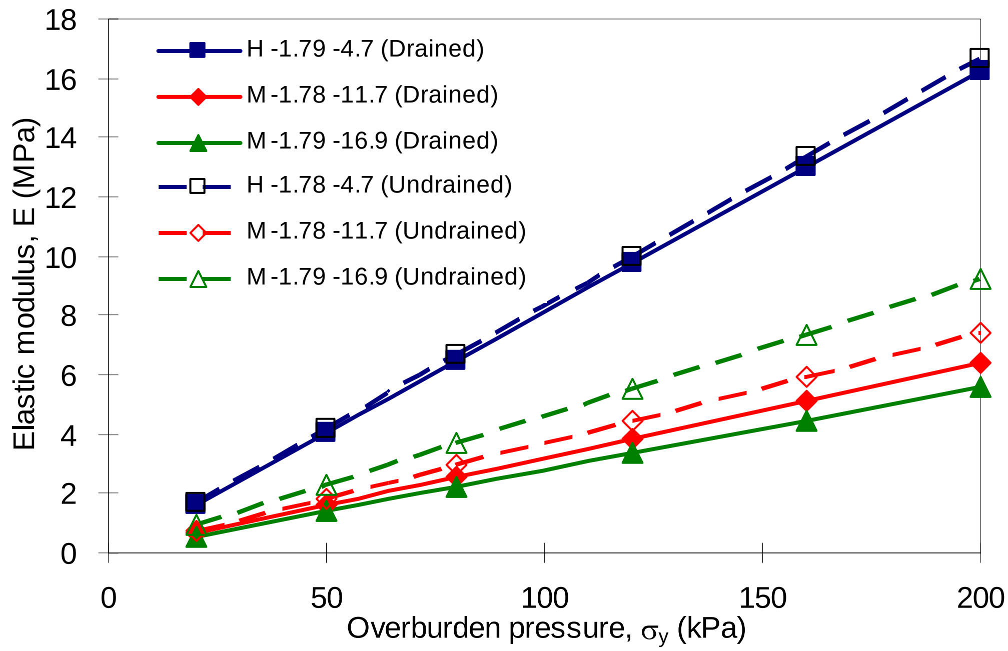

Fig. 2. 41 Drained and undrained elastic modulus (Group A)

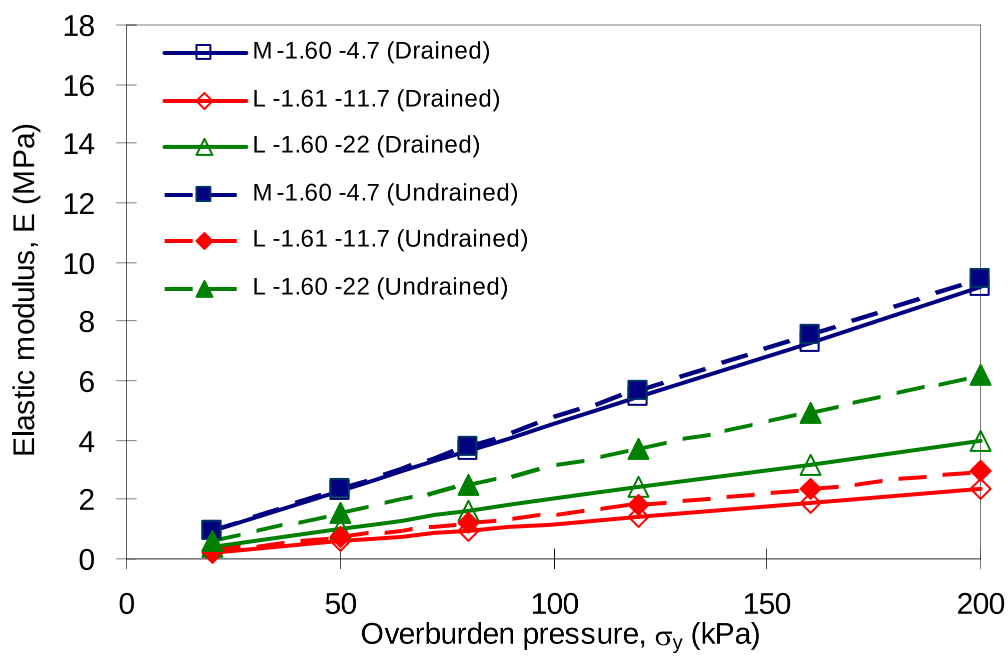

Fig. 2. 42 Drained and undrained elastic modulus (Group B)

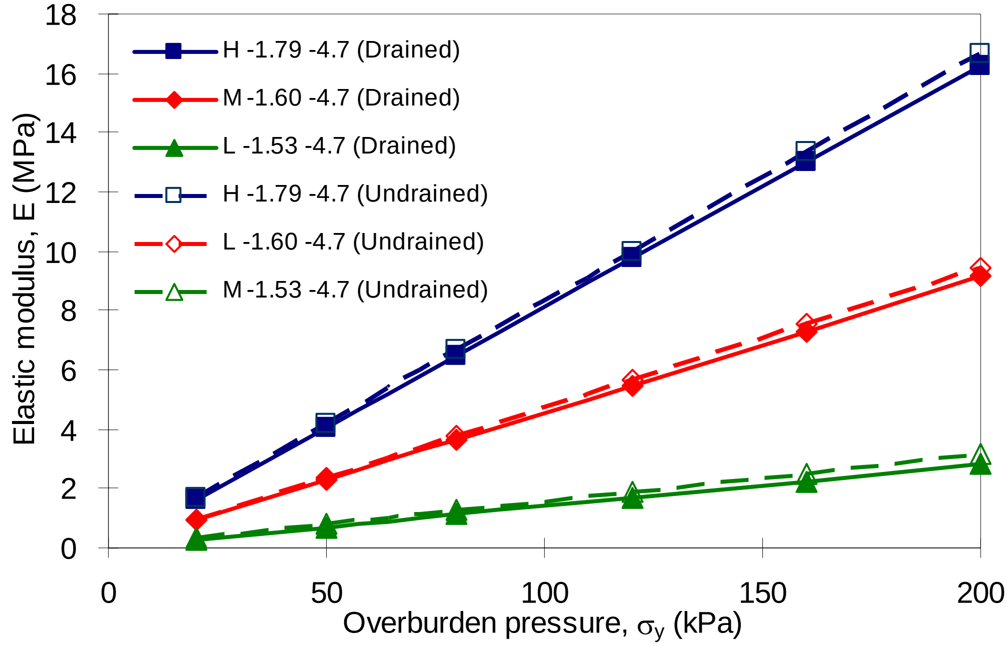

Fig. 2. 43 Drained and undrained elastic modulus (Group C)

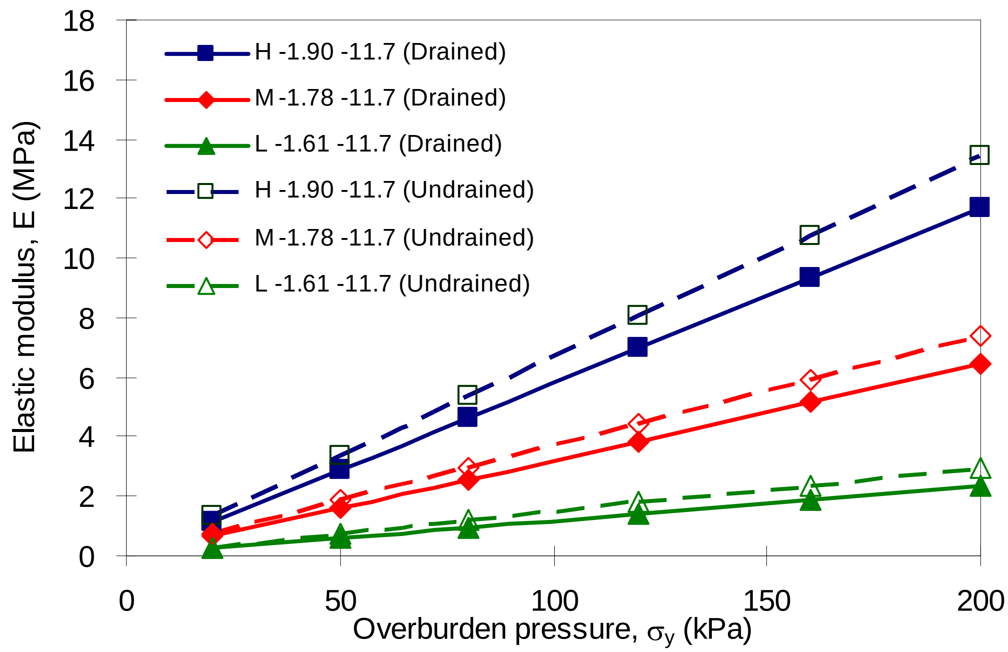

Fig. 2. 44 Drained and undrained elastic modulus (Group D)

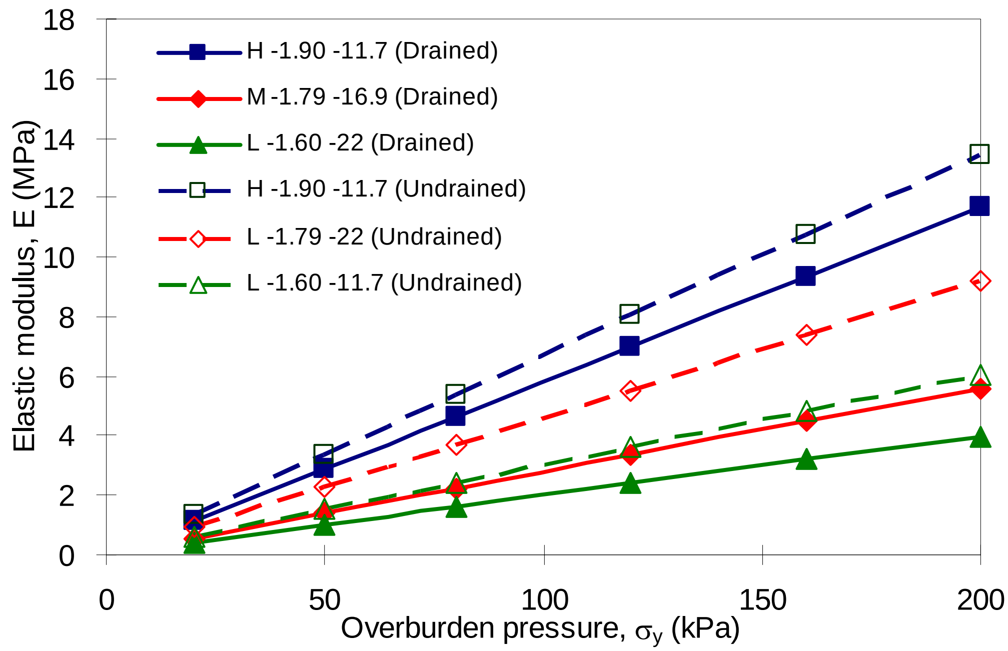

Fig. 2. 45 Drained and undrained elastic modulus (Group E)

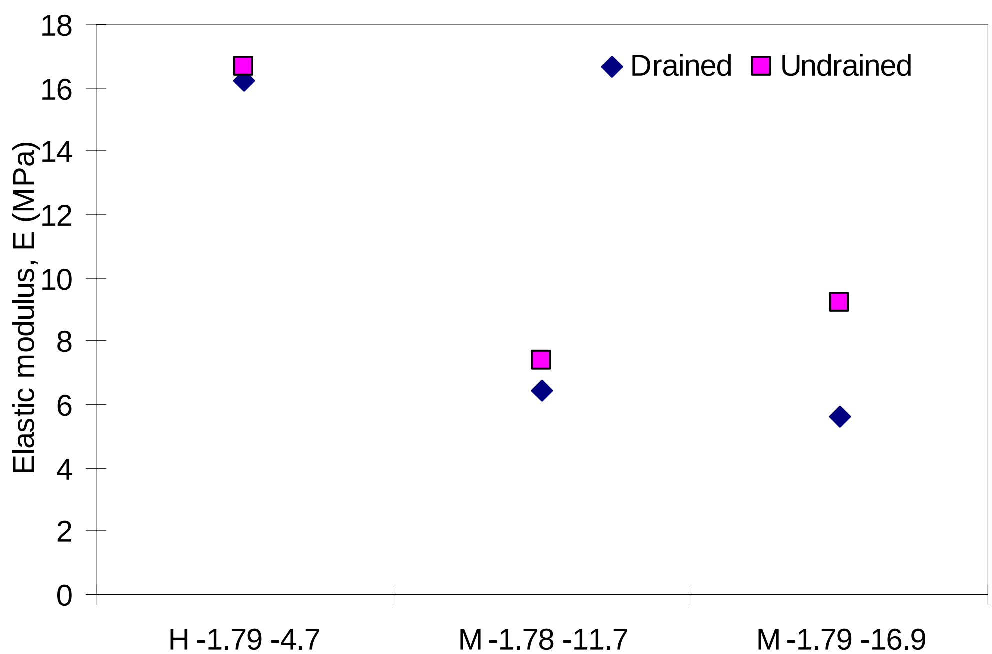

Fig. 2. 46 Drained and undrained elastic modulus at σ_y = 200 kPa (Group A)

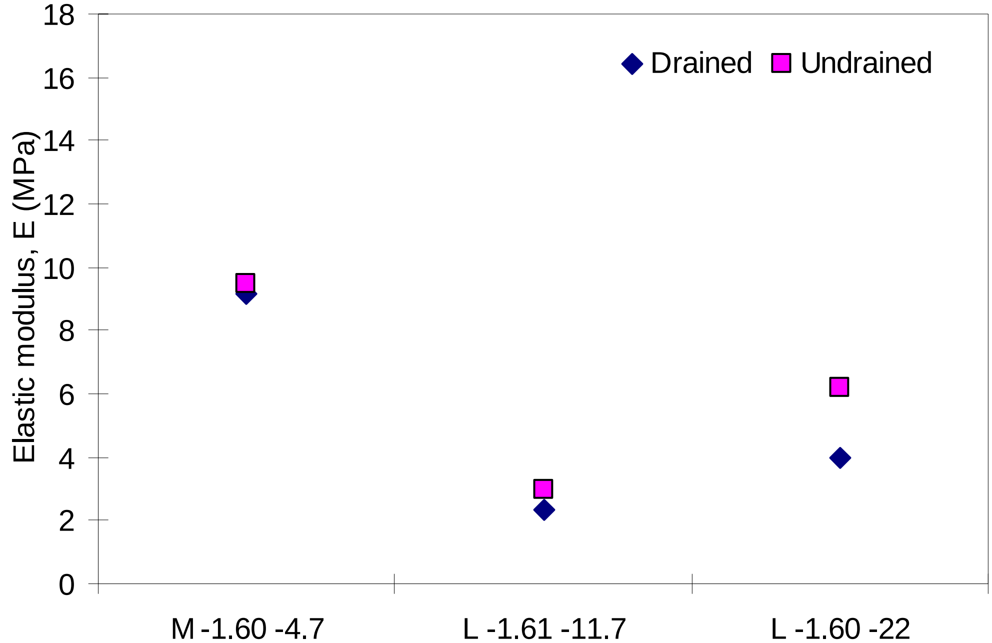

Fig. 2. 47 Drained and undrained elastic modulus at σ_y = 200 kPa (Group B)

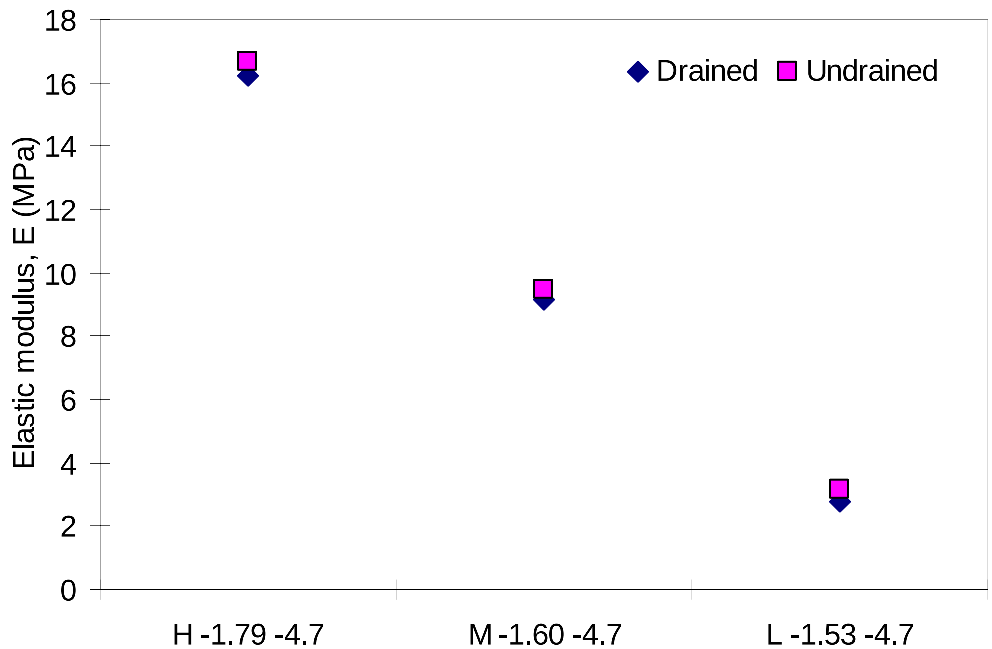

Fig. 2. 48 Drained and undrained elastic modulus at σ_y = 200 kPa (Group C)

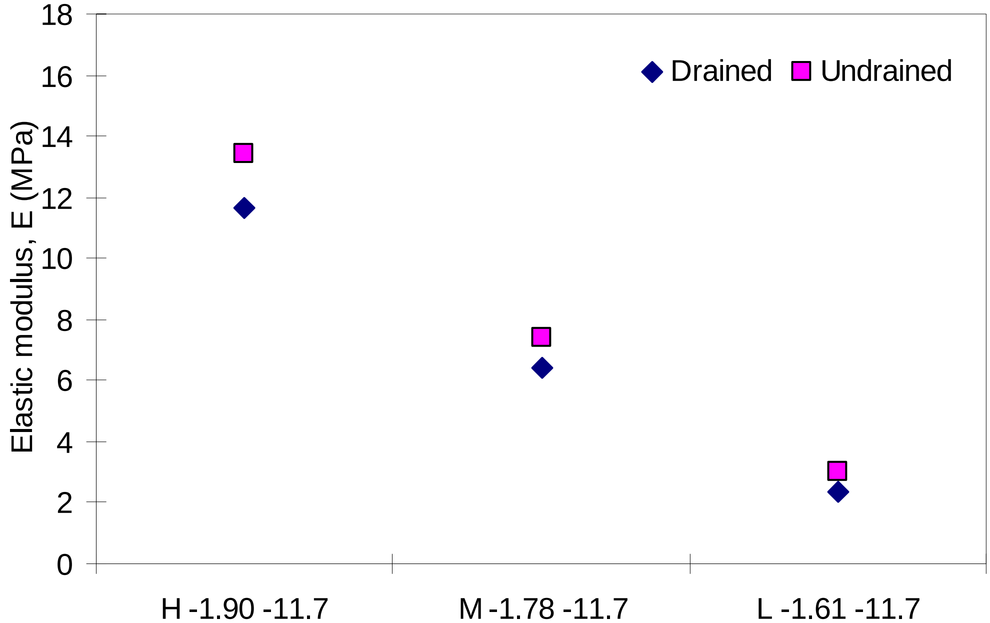

Fig. 2. 49 Drained and undrained elastic modulus at σ_y = 200 kPa (Group D)

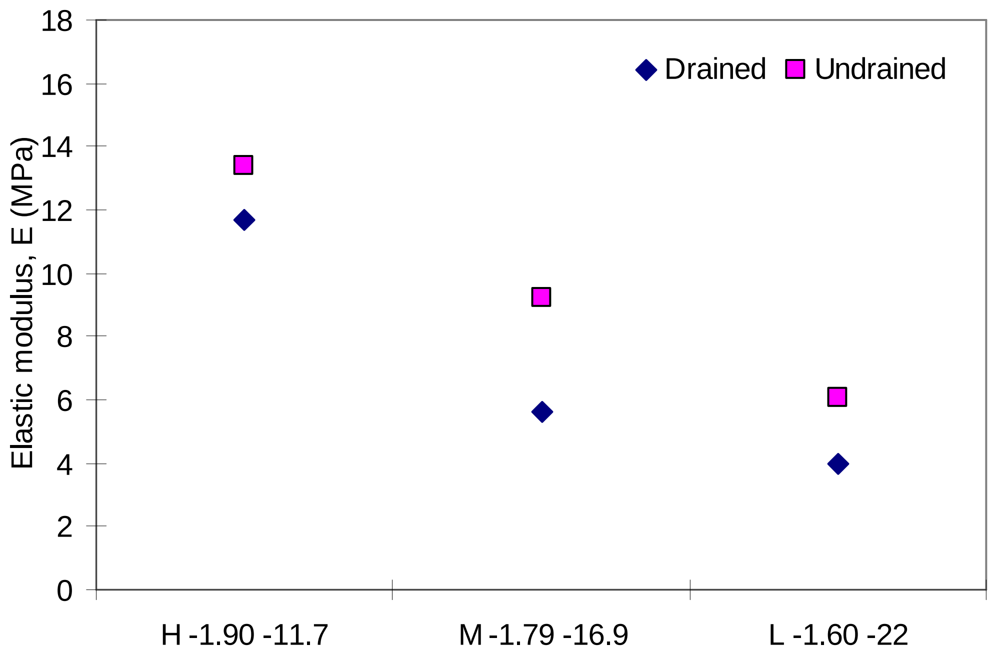

Fig. 2. 50 Drained and undrained elastic modulus at σ_y = 200 kPa (Group E)

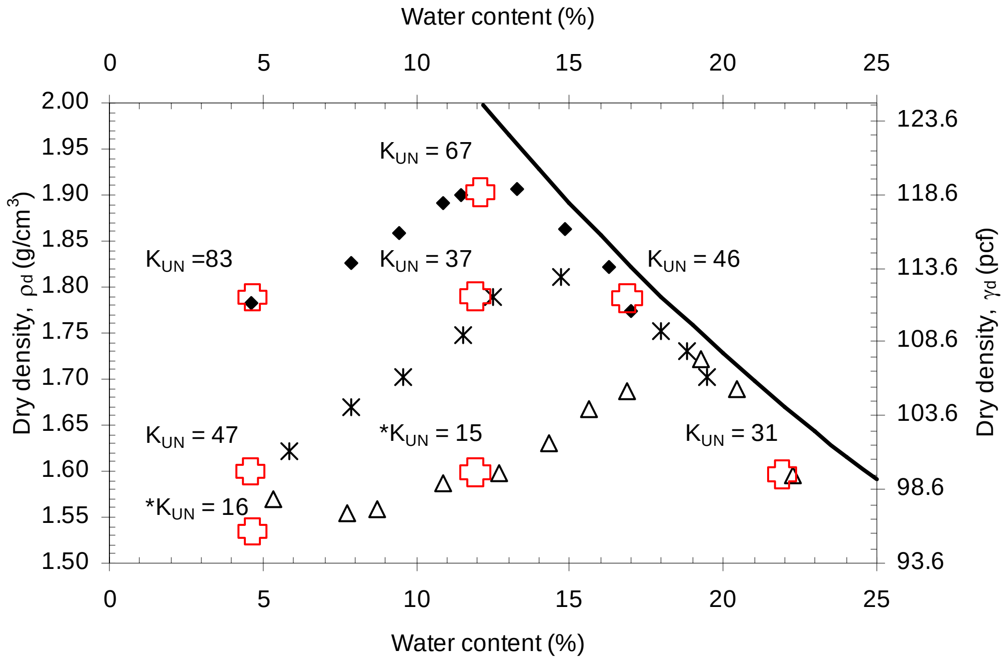

Fig. 2. 51 Modulus constant, K_{UN}, for undrained loading (*computed from the measured stress-volumetric strain data in question)

Theoretically, the undrained modulus should be greater than the drained modulus, or at least of equal magnitude. From undrained triaxial tests on compacted soils with varying compaction conditions, Kulhawy et al. (1969) showed that the undrained elastic modulus increased with decreasing as-compacted water content at a given density and with increasing dry density at a given water content. However, some results in this research showed the undrained elastic modulus of specimens with higher as-compacted water contents to be greater than those of specimens with lower water contents (i.e. M-1.78-11.7 and M-1.79-16.9 from Fig. 46, and L-1.61-11.7 and L-1.60-22 from Fig. 47). It is suggested that this result may be due to the influence of matric suction on the soil volume change not having been negligible, as assumed, especially for the specimens compacted at a water content of 11.7%.

Figure 52 shows the volume changes measured by Rodrigues and Vilar (2006) in soil as the matric suction was reduced from its initial value of 200 kPa to 0 kPa. It was clearly observed that most of the volume change occurred in the lower suction ranges. Based on these results, the volume change due to changes in matric suction would be expected to be very small for all specimens compacted at a water content of 4.7% since the matric suction changes due to loading (0-200 kPa) may occurs in high suction ranges. The specimens compacted at a 4.7% as-compacted water content had average value of matric suction of 783 kPa (Rorie, 2006). For the specimens compacted at high degrees of saturation, the magnitudes of volume change potential (swelling or collapse) due to changes in matric suction may be negligible due to the specimen's stability. Additionally, the pore-air pressure approached the pore-water pressure which also caused only small changes in matric suction. Another possible explanation is that the assumed Poisson's ratios of the specimens in various compaction conditions, used to compute the elastic moduli, were in error. For example, if a Poisson's ratio of 0.4 is used instead of a value of 0.35 for a specimen with a high degree of saturation (M-1.79-16.9 and L-1.60-22) it would cause the calculated elastic modulus to be 25% smaller.

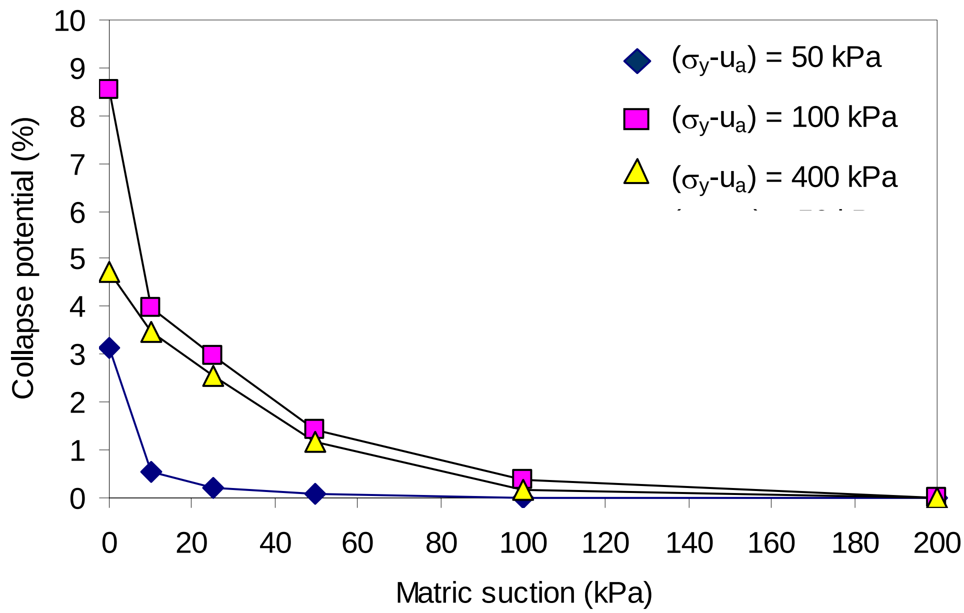

Fig. 2. 52 Volume change (%) under gradual suction reduction (Rodirigues and Vilar, 2006).

The modulus numbers for both drained (soaked and unsoaked) and undrained loading conditions are summarized in Table 2.7. The ratio K_{DU}/K_{DS} varies from about 1 for the specimens compacted at high degrees of saturation up to 3 for the specimen compacted at the lowest water content (4.7%) and high density (1.79 g/cm^3) excluding those of two specimens (L-1.53-4.7 and L-1.61-11.7), which showed the questionable results on their stress- strain relations. The similar range (1.2 -3.1) is shown for the ratio K_{UN}/K_{DS}.

Table 2. 7 Modulus numbers for drained and undrained loading conditions

Sample ID	K_{DS}	K_{DU} **(times** K_{DS}**)**	K_{UN} **(times** K_{DS}**)**
H-1.79-4.7	27	81 (3.0 K_{DS})	83 (3.1 K_{DS})
M-1.60-4.7	22	46 (2.1 K_{DS})	47 (2.1 K_{DS})
L-1.53-4.7	21	*14 (0.7 K_{DS})	*16 (0.8 K_{DS})
H-1.90-11.7	62	58 (0.9 K_{DS})	67 (1.2 K_{DS})
M-1.78-11.7	24	31 (1.3 K_{DS})	37 (1.5 K_{DS})
L-1.61-11.7	23	*12 (0.5 K_{DS})	*15 (0.7 K_{DS})
M-1.79-16.9	25	28 (1.1 K_{DS})	46 (1.8 K_{DS})
L-1.60-22	22	20 (0.9 K_{DS})	31 (1.4 K_{DS})

*computed from the measured stress-volumetric strain data in question

2.5 SUMMARY AND CONCLUSIONS

The drained moduli of as-compacted and soaked specimens prepared under various initial conditions were estimated based on assumed Poisson's ratios and the relationships between volumetric stress and strain, which were measured from as-compacted and soaked specimens in double oedometer tests. The undrained modulus was also able to be computed from the constitutive relation for undrained loading, which was determined using the procedures suggested in this paper. Determination of the constitutive relation for undrained loading was accomplished by using Hilf's equation (1948) along with the compressibility of as-compacted soil to compute changes in pore pressure. The secant and tangent pore pressure parameters were then determined from the computed pore pressures. From the analyses of computed modulus and pore pressure presented in this paper, the following conclusions can be drawn:

1. At the dry densities studied (1.6 g/cm^3 or 1.79 g/cm^3), the drained elastic modulus of a series of as-compacted specimens increased significantly (over 130% and 190%, respectively) as the as-compacted water content decreased to 4.7% while the drained elastic modulus of soaked specimens remained almost constant.
2. For specimens with water contents of 4.7% and tested in their as-compacted state, the drained elastic modulus at 200 kPa overburden pressure increased from 2.8 MPa to 16.3 MPa as dry density increased from 1.53 g/cm^3 to 1.79 g/cm^3. The elastic drained modulus of soaked specimens increased very little, from 4.1 MPa to 5.3 MPa. The influence of soaking on the drained elastic modulus for specimens compacted at a dry density of 1.53 g/cm^3 was seen to be insignificant.
3. Specimens compacted at high degrees of saturation and tested in either soaked or unsoaked conditions showed little difference in the drained elastic moduli.
4. The induced pore pressures due to loading increased with increasing as-compacted water content and decreasing dry density. The averaged secant pore pressure parameter, B'_{avg} , in the range of 0-200 kPa overburden pressure was as low as 0.06 for the specimen compacted at 1.79 g/cm^3 (w = 4.7%) and as high as 0.77 for the specimen compacted at 1.79 g/cm^3 (w = 16.9%).
5. The specimens compacted at the lowest water content of w = 4.7% showed no significant difference in drained and undrained moduli (2%, 2%, and 14% for specimen compacted at 1.79g/cm^3, 1.60g/cm^3, and 1.53g/cm^3, respectively). However, there was an increasing difference in these moduli for specimens with increasing as-compacted water content. The differences determined were 16%, 64%, and 55% for

specimens compacted at 1.90g/cm^3 (w = 11.7%), 1.79g/cm^3 (w = 16.9%), and 1.60g/cm^3 (w = 22%), respectively.

6. The linearly increasing elastic modulus was defined using a modulus number, K (Eq. 2.16). For drained and undrained loading conditions, the computed modulus numbers of all the specimens tested were presented in Table 2.7. The ratios, K_{DU}/K_{DS} and K_{UN}/K_{DS}, were seen to vary from about 1 to 3. The maximum values for these ratios were observed for the specimen compacted at the lowest water content (4.7%) and high density (1.79 g/cm^3).

2.6 REFERENCES

Fredlund, D. G.., and Hung, V. Q. (2001). Prediction of volume change in an expansive soil as a result of vegetation and environmental changes, Expansive Clay Soils and Vegetative Influences on Shallow Foundations, Geotechnical Special Publication, No. 115, pp. 24-43.

Fredlund, D. G.., and Morgenstern, N. R. (1976). Constitutive relations for volume change in unsaturated soils, Canadian Geotechnical Journal, 13, pp. 261-276.

Fredlund, D. G., and Rahardjo, H. (1993). Soil mechanics for unsaturated soils, New York: Wiley.

Hilf, J. W. (1948). Estimating construction pore pressures in rolled earth dams, Pro. 2nd Int. Conf. Soil Mech. Found. Eng. Rotterdam, The Netherlands, vol. 3, pp. 234-240.

Hung, V. Q., and Fredlund, D. G. (2000). Volume change predictions in expansive soils using a two-dimensional finite element method, Proceedings of Asian Conference on Unsaturated Soils, Singapore, pp. 231-236.

Hung, V.Q., and Fredlund, D.G. (2003). Uncoupled and coupled solutions of two-dimensional swelling in expansive soils, Proceedings of the 2nd Asian Conference on Unsaturated Soils (UNSAT-ASIA 2003), Osaka, Japan, 10-12 November 2003, Edited by D. Karubu, A. Iizuka, S. Kato, K. Kawai, and K. Tateyama, The organizing committee on UNSAT-ASIA, The Japanese Geotechnical Society, Tokyo, Japan, pp. 53-58.

Hung, V. Q., and Fredlund, D. G. (2004). The prediction of one-, and two-, and three-dimensional heave in expansive soils, Canadian Geotechnical Journal , 41, pp. 713-737.

Kulhawy, F. H., Duncan, J. M., and Seed, H. B. (1969). Finite element analyses of stresses and movements in embankment during construction: Report TE-69-4, Department of Civil Engineering, University of California at Berkeley

Lawton, E. C., Fragaszy, R. J., and Hetherington, M. D. (1991). View of wetting-induced collapse in compacted soil, Journal of Geotechnical Engineering, 118(9), pp. 1376-1394.

Rahardjo, H., Heng, O. M., and Leong, E. C. (2004). Shear strength of a compacted residual soil from consolidated drained and constant water content triaxial tests, Canadian Geotechnical Journal, 41, pp 421-436.

Rao, S. M., and Revanasiddappa, K. (2000). Role of matric suction in collapse of compacted clay soil, Journal of Geotechnical and Geoenvironmental Engineering, 126(1), pp. 85-90.

Rodrigues, R. A. and Vilar, O. M. (2006) Relationship between collapse and soil-water retention curve of a sandy soil, Proceedings of the fourth international conference on unsaturated soils, Geotechnical Special Publication, No. 147, Vol.1, pp. 1025-1036.

Rorie, D. (2006). Investigation of soil suction in low density silty sands, MS thesis, North Carolina State University, Raleigh

Thu, T. M., Rahardjo, H., and Leong, E. C. (2006). Shear strength and pore-water pressure characteristics during constant water content triaxial tests. Journal of Geotechnical and Geoenvironmental Engineering, 132(3), pp. 411-419.

CHAPTER 3

Influence of soil type and stress state on predicting the shear strength of unsaturated soils using the soil-water characteristic curve

3.1 INTRODUCTION

The experimental determination of the shear strength of unsaturated soils is generally difficult, time-consuming, and relatively expensive. For this reason, several semi-empirical procedures have been proposed to predict shear strength of unsaturated soils (Fredlund et al., 1996; Vanaplli et al., 1996; Oberg and Sallfours, 1997; Khalili and Khabbaz, 1998; Bao et al., 1998). In these procedures, the relationship between the water content and soil suction is used as a tool along with the saturated shear strength parameters in the prediction of the shear strength of an unsaturated soil. The relationship between the water content and soil suction is referred as the soil-water characteristic curve (SWCC).

The soil-water characteristic curve is conventionally measured by means of a pressure plate extractor, with the application of only a nominal normal stress or without the application of any applied vertical stress. For this reason, the shear strength of soil under a chosen stress is commonly estimated using the SWCC performed at zero or very small net normal stress. However, it has been shown from experimental studies that the SWCCs for some soils are significantly influenced by the magnitude of net normal stress (Vanapalli et al, 1999; Ng and Pang, 2000; Lee et al., 2005; Rorie, 2006). Accordingly, different magnitudes of shear strength are estimated if the SWCC that has been determined taking into account the influence of the stress state is used.

In this paper, the shear strength of unsaturated soil is predicted from the three most commonly used procedures, which are namely the 1st and 2nd approaches of Vanapalli et al.(Vanapalli et al. 1996), and the Khalili and Khabbaz model (Khalili and Khabbaz, 1998). Each of these procedures was originally developed based on limited experimental data obtained from a few soils. For this reason, each method could predict inconsistent values of shear strength depending on the types of soil. Garven and Vanapalli (2006) evaluated six empirical procedures for predicting the shear strength of unsaturated soils using shear strength data from twenty soils. It was shown from their finding that each procedure provides "the successful prediction" of shear strength of only a few of the twenty soils tested. Different soils could be represented by the different shapes of SWCC (i.e. air entry value, slope of SWCC, residual water content). Therefore, in this work, a parametric study is performed by varying the a and n values of the Fredlund and Xing SWCC model (Fredlund and Xing, 1994) in order to study the influence of the shape of SWCC on the shear strength envelopes predicted using three prediction procedures. In addition, shear strength data from fifteen soils published in the literature is examined using these procedures. Comparisons between measured and predicted values of unsaturated shear strength are presented dividing the fifteen soils into four different groups; 1) all soils used in this study; 2) low plasticity clay; 3) sandy soils; and 4) soils that desaturate relatively fast as soil suction increases (the Fredlund and Xing SWCC model fitting parameter, n, > 2).

The effect of net normal stress on the prediction of shear strength is also discussed in this paper. First, comparisons between the measured and predicted shear strengths are presented both for low and high net normal stress ranges. Secondly, comparisons are presented between the measured values of shear strength and the values of shear strength predicted using the SWCCs performed at different net normal stresses.

3.2 SHEAR STRENGTH THEORY FOR UNSAUTRATED SOILS

Bishop (1959) suggested an effective stress for unsaturated soils. The Bishop's effective stress can be used to evaluate the shear strength of unsaturated soils by extending Terzaghi's principle of effective stress for saturated soils. The shear strength equation based on Bishop's effective stress can be expressed as follows:

$$\tau_f = c' + \left[(\sigma_n - u_a)_f + \chi (u_a - u_w)_f \right] \tan\phi' \qquad (3.1)$$

where $\sigma' = (\sigma_n - u_a)_f + \chi (u_a - u_w)_f$ is Bishop's effective stress;

c' is the effective cohesion of saturated soil;

ϕ' is the effective friction angle with respect to net normal stress for a saturated soil;

χ is a parameter dependent on the degree of saturation;

$(\sigma_n - u_a)_f$ is the net normal stress on the failure plane at failure; and

$(u_a - u_w)_f$ is the matric suction of the soil on the failure plane at failure.

The magnitude of the χ parameter is unity for a saturated soil and zero for a dry soil. Figure 3.1 demonstrates the relationship between χ and the degree of saturation, S, for various soils.

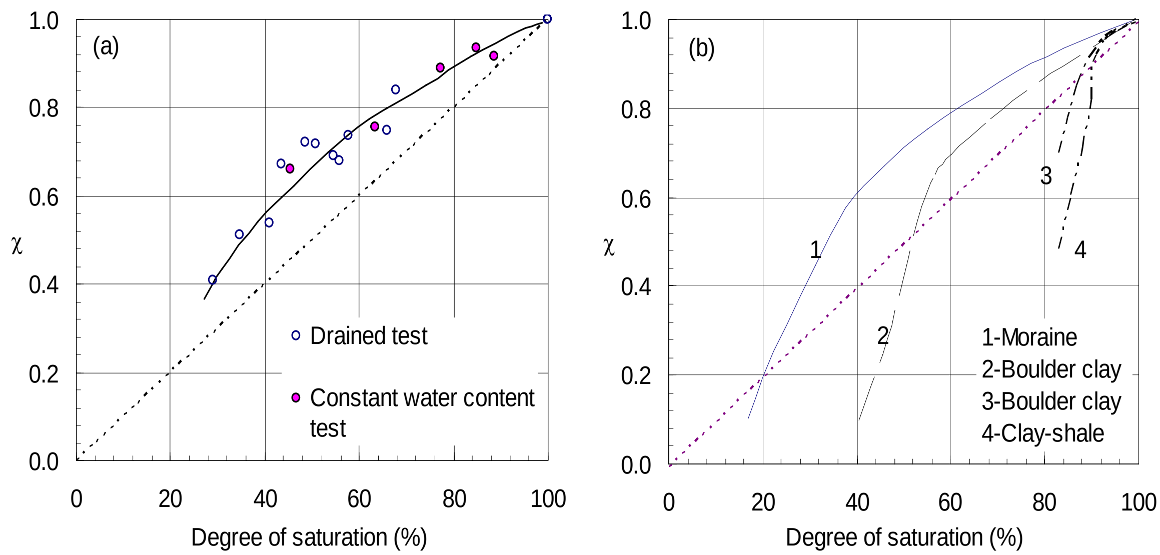

Fig. 3. 1 The relationship between the χ parameter and the degree of saturation, S. (a) χ values for cohesionless silt (after Donalds, 1961); (b) χ values for compacted soils (after Blight, 1961)

Fredlund et al. (1978) have evaluated the shear strength of unsaturated soils in terms of two independent stress state variables as follows:

$$\tau_f = c' + (\sigma_n - u_a)_f \tan\phi' + (u_a - u_w)_f \tan\phi^b \qquad (3.2)$$

where ϕ^b is the angle of shearing resistance with respect to matric suction.

Figure 3.2 shows the extended Mohr-Coulomb failure envelope assuming a planar failure envelope that intersects the shear stress axis, giving a cohesion intercept, *c'*. The envelope has slope angles of ϕ' and ϕ^b with respect to the (σ-u_a) and (u_a-u_w) axes, respectively. The cohesion intercept, *c'*, and the slope angles, ϕ' and ϕ^b, are the strength parameters used to relate to the stress state variables to the shear strength. Experimental studies (Gan et al., 1988; Ecario and Juca, 1989) showed a curved failure envelope, thus decreasing ϕ^b with increase of matric suction.

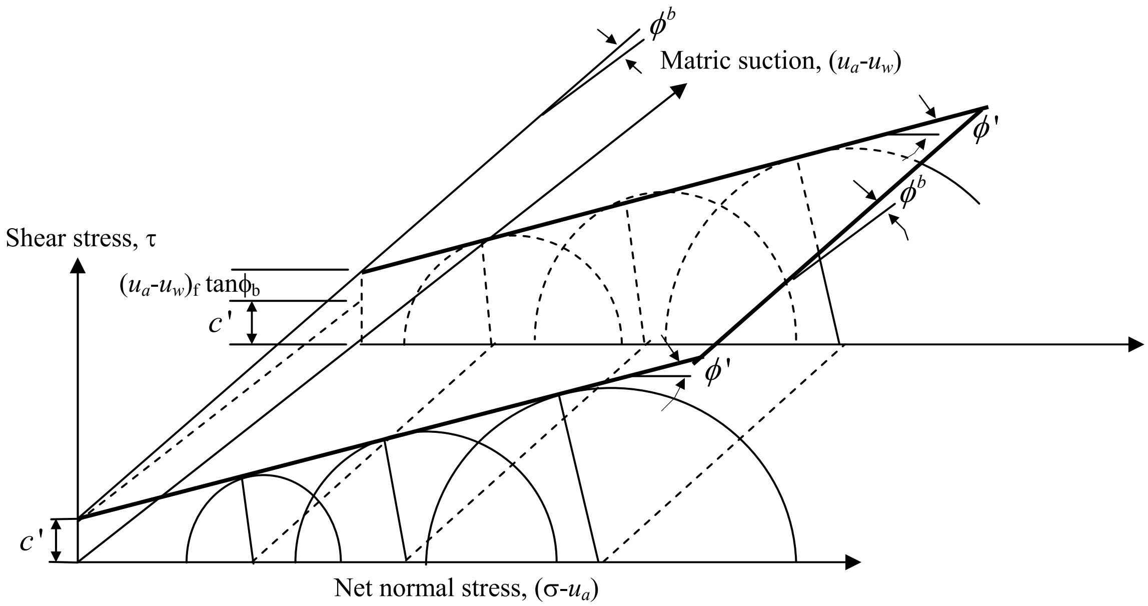

Fig. 3. 2 Extended Mohr-Coulomb failure envelope for unsaturated soil (Fredlund and Rahardjo, 1993)

The modified direct shear device (Gan and Fredlund, 1988; Gan et al., 1988) and the modified triaxial device (Ho and Fredlund, 1982), which can control pore-water pressure and pore-air pressure separately, have been used to determine shear strength of unsaturated soil. However, the experimental studies on unsaturated soils are generally expensive, time-consuming, and difficult to perform. For this reason, several investigators have proposed semi-empirical procedures for predicting the shear strength of unsaturated soils using the relationship between the water content and soil suction, which is called a soil-water characteristic curve (SWCC). The following sections (3.2.1, 3.2.2, and 3.2.3) describe the SWCC, the relationship between the SWCC and the shear strength of unsaturated soils, and different procedures for predicting shear strength of unsaturated soils using the SWCC, respectively.

3.2.1 Soil-Water Characteristic Curve (SWCC)

The SWCC defines the relationship between soil suction and water content (gravimetric or volumetric) or degree of saturation. A typical soil- water characteristic is shown in Fig. 3.3. Vanapalli (1994) suggested there are three identifiable stages of desaturation: the boundary effect stage, the transition stage, and the residual stage of unsaturation. In the boundary effect stage almost all the soil pores are filled with water. The soil is essentially saturated at this stage, and there is no reduction in the area of water in this stage. The soil starts to desaturate at the air-entry value in the transition stage. The air-entry value identifies the point at which air enters the largest pores of the soil. The water content in the soil reduces significantly with increasing suction in this stage. Eventually large increases in suction produce only relative small changes in water content. This stage is referred to as the residual stage of unsaturation. The degree of saturation in the soil at the commencement of this stage is generally referred to as the residual degree of saturation, S_r.

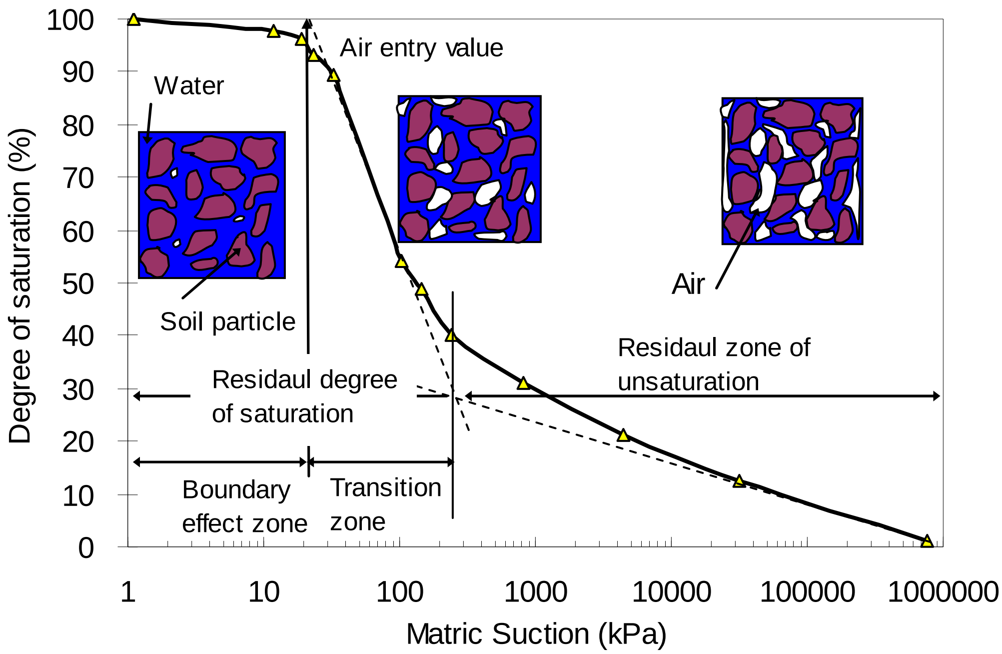

Fig. 3. 3 Typical soil-water characteristic showing zones of desaturation (Vanapalli, 1994)

Vanapalli et al. (1999) presented a graphical procedure that defines the air entry value and the residual state when the entire suction range is used (Fig. 3.3). The procedure involves first drawing a line tangent to the curve through the point of maximum slope (inflection point) on the straight line potion of the SWCC. The air entry value can be defined at the point where the tangent line intersects the horizontal line through maximum degree of saturation (S = 1). The residual degree of saturation can be defined at the intersection of the tangent line and the extended line from 1,000,000 kPa along the SWCC.

Various equations have been proposed to represent the SWCC. The two most common equations are the van Genuchten equation (1980), and the Fredlund and Xing equation (1994).

The van Genuchten equation is expressed as:

$$\frac{\theta_w - \theta_r}{\theta_s - \theta_r} = \left[\frac{1}{1 + (\alpha\psi)^n} \right]^m \quad m = 1 - \frac{1}{n} \tag{3.3}$$

where α, and n are curve fitting parameters.

The Fredlund and Xing equation is expressed as :

$$\theta_w = C(\psi) \frac{\theta_S}{\{\ln[e + (\psi / a)^n]\}^m} \tag{3.4}$$

where a, n, and m are curve fitting parameters; and

$C(\psi)$ is a correction factor function defined as :

$$C(\psi) = \frac{\ln(1 + \psi / \psi_r)}{\ln[(1 + (1000000 / \psi_r)]}$$

where ψ_r is the suction corresponding to the residual water content θ_r.

The Fredlund and Xing (1994) equation provides the SWCC over the entire suction range from 0 to 10^6 kPa. As shown in Fig. 3.4, the fitting parameter, a, is the matric suction at the inflection point. This value is closely related to the air-entry value of the soil. The fitting parameter, n, is the slope of the SWCC at the inflection point. Finally, m is a fitting parameter related to residual water content.

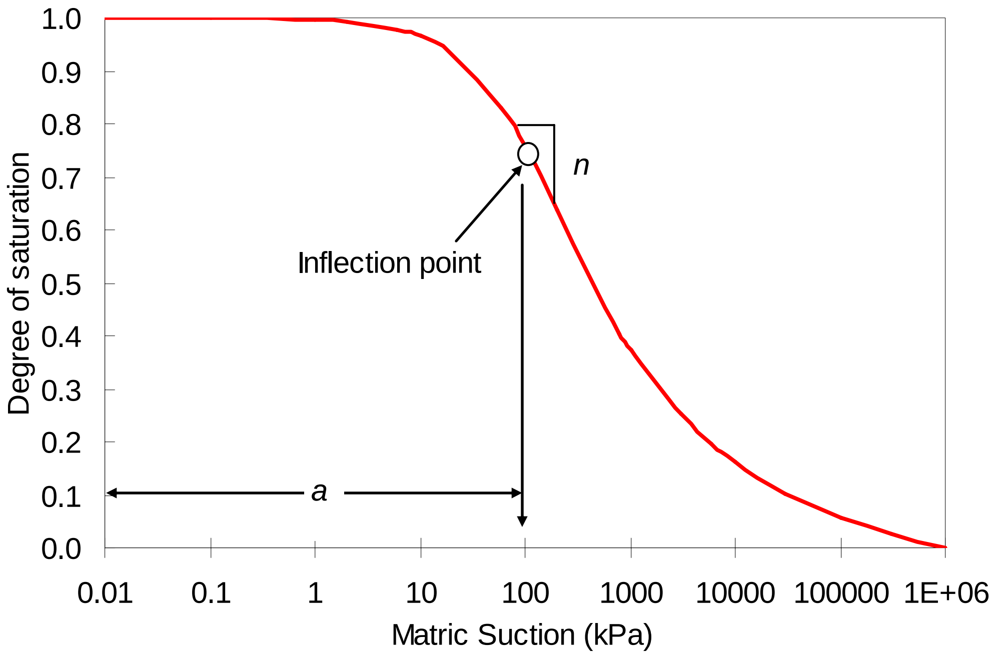

Fig. 3. 4 Fredlund and Xing SWCC model fitting parameters

3.2.2 The relationship between the SWCC and the shear strength of unsaturated soils

The relationship between soil water content and matric suction is one of the fundamental relationships used to describe unsaturated soil behavior. Figure 3.3 also shows that the wetted area of contact between soil particles decreases with an increase in soil suction. The shear strength of an unsaturated soil is strongly related to the amount of water in the voids of the soil, and therefore to matric suction. Thus it is apparent that there should be a relationship between the SWCC and the shear strength of an unsaturated soil.

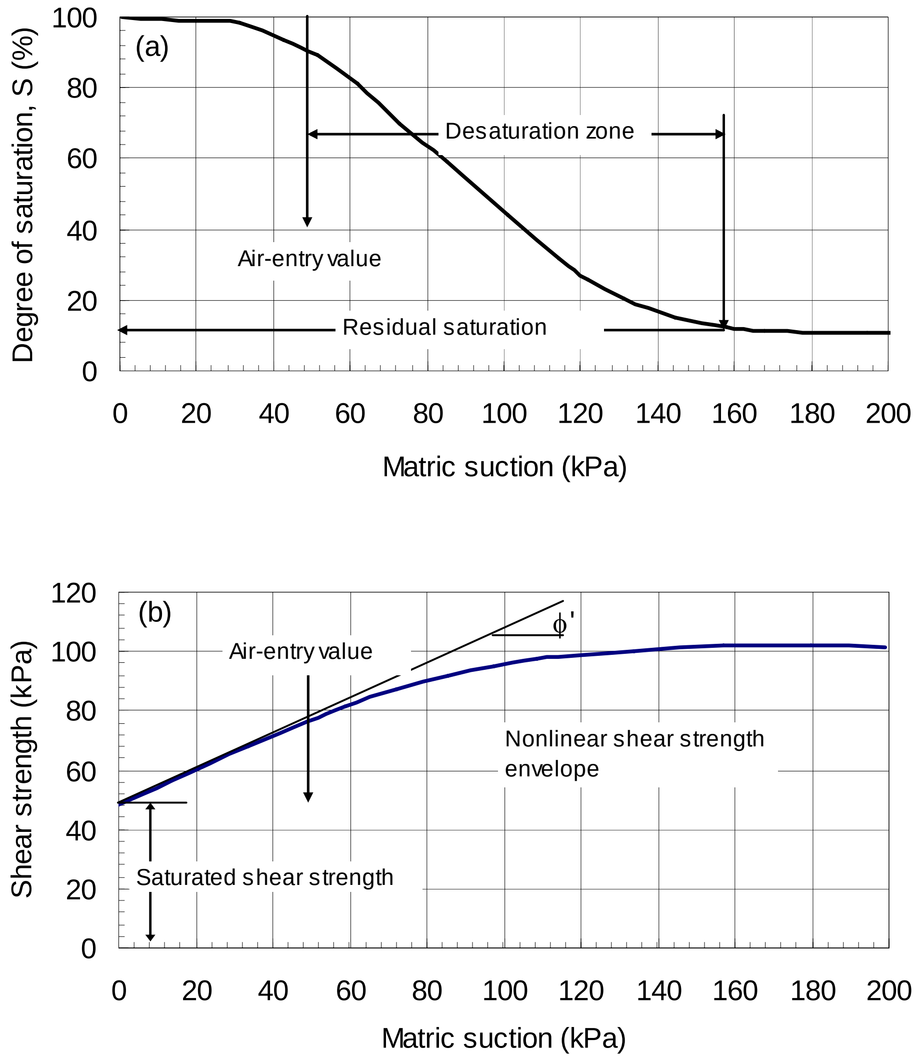

Fig. 3. 5 Shear strength behavior of soil as it relates to SWCC (Vanapalli et al., 1996)

Vanapalli et al. (1996) explained the typical relationship between the SWCC and the shear strength using Fig. 3.5. Shear strength increases linearly up to the air-entry value and then increases nonlinearly between the air-entry value and the residual suction. The shear strength of an unsaturated soil beyond the residual suction conditions may increase, decrease, or remain relatively constant during further desaturation. In their paper, they described the effect of soil type on shear strength over a wide range of suction using the SWCC as follows: "…In some case, particularly in soils that desaturate relatively fast (e. g., sands and silt), it can be expected that shear strength will decrease. It can be expected that there is little water left in soil pores when the soil reaches the residual state. The water content in sands and silts at the residual suction condition can be quite low and may not transmit suction effectively to the soil particles or aggregate contact points. Thus, even large increases in suction will not result in a significant increase in shear strength. In contrast, clays may not have a well-defined residual state. Even at high values of suction there could still be considerable water available to transmit suction along the soil particle or aggregate contacts, which would contribute toward increases in shear strength."

3.2.3 Different procedures for predicting the shear strength of an unsaturated soil

Vanapalli et al. model (1996)

Fredlund et al. (1996) and Vanapalli et al. (1996) presented the contribution of matric suction to shear strength of an unsaturated soil in terms the normalized area of water, a_w. This can be mathematically expressed as:

$$\tau_f = a_w(u_a - u_w)(\tan\phi') \qquad (3.5)$$

where $a_w = A_{dw}/A_{tw}$; A_{dw} is the area of water corresponding to any degree of saturation; and the A_{tw} is the total area of water at saturation.

The normalized area of water, a_w varies from unity at saturation to 0 when the soil is dry. It is noted that the contribution of matric suction to shear strength, τ_f, would decrease with increasing matric suction if the reduction rate of the normalized area exceeds the increase rate of the matric suction. Vanapalli et al. (1996) have proposed two approaches (1st and 2nd approaches) for predicting the shear strength of an unsaturated soil defining the normalized area of water in two different ways.

Vanapalli et al.'s 1st approach

Assuming that the normalized area of water can be related to the normalized volumetric water content, θ, Vanapalli et al. (1996) have proposed the shear strength of an unsaturated soil at any given value of suction (i.e., 0 to 1,000,000 kPa) as follows:

$$\tau_f = c' + (\sigma_n - u_a)\tan\phi' + (u_a - u_w)[\left(\theta^{\kappa}\right)(\tan\phi')] \tag{3.6}$$

where θ is the normalized water content (θ_w / θ_s); and the κ value is a fitting parameter used for obtaining a best-fit between the measured and predicted values.

Vanapalli and Fredlund (2000) proposed the fitting parameter, κ, may be influenced by several parameters including plasticity index and soil structure. Fig.3.6 shows the relationship between the fitting parameter, κ, and plasticity index, I_p, obtained from the shear strength data of five statically compacted soils reported in the literature (Ecario and Juca, 1989; Vanapalli et al. 1996; Wulfsohn et al., 1996).

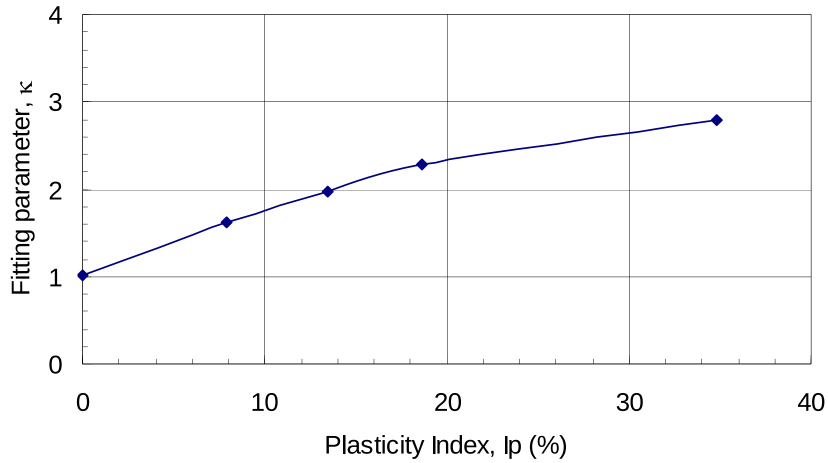

Fig. 3. 6 The relationship between the fitting parameter, κ, and Plasticity Index, I_p (Vanapalli and Fredlund, 2000)

Garven and Vanapalli (2006) verified this relationship using ten data sets of statically compacted soils. In their paper, the relationship they found was mathematically expressed by the equation below:

$$\kappa = -0.0016 \cdot I_P^2 + 0.0975 \cdot I_P + 1 \qquad (3.7)$$

where I_p = plasticity index (%).

Vanapalli et al.'s 2nd approach

Vanapalli et al. (1996) presented another equation for predicting the shear strength of unsaturated soils (Eqs. 3.8 or 3.9). In these equations, the residual volumetric water content, θ_r, (or the residual degree of saturation, S_r) is used to define the normalized area of water instead of using the fitting parameter, κ.

$$\tau_f = c' + (\sigma_n - u_a)\tan\phi' + (u_a - u_w)[(\tan\phi')\left(\frac{\theta_w - \theta_r}{\theta_s - \theta_r}\right)] \quad \text{or,} \tag{3.8}$$

$$\tau_f = c' + (\sigma_n - u_a)\tan\phi' + (u_a - u_w)[(\tan\phi')\left(\frac{S - S_r}{100 - S_r}\right)] \tag{3.9}$$

where θ_w = volumetric water content;

θ_s = saturated volumetric water content;

θ_r = residual volumetric water content;

S = degree of saturation; and

S_r = residual degree of saturation.

Khalili and Khabbaz model

Khalili and Khabbaz (1998) have extended the Bishop's effective stress equation (1959) for predicting the shear strength of an unsaturated soil. They suggested χ is a parameter strongly related to the soil structure and therefore no direct correlation is found between it and a volumetric parameter, such as the degree of saturation. In fact, they proposed a form of χ as the ratio of matric suction to air entry value (suction ratio). A unique relationship was found for most soils, as shown in Fig. 3.7. Using this empirical effective stress parameter, χ, they proposed the following equation for predicting the shear strength of unsaturated soils:

$$\tau_f = c' + (\sigma_n - u_a)\tan\phi' + (u_a - u_w)_f[\chi(\tan\phi')] \tag{3.10}$$

where, $\chi = \left(\frac{(u_a - u_w)_f}{(u_a - u_w)_b} \right)^{-0.55} \quad for\ (u_a - u_w) > (u_a - u_w)_b$

$\chi = 1 \quad for\ (u_a - u_w) < (u_a - u_w)_b$

$(u_a\text{-}u_w)_f$ = matric suction in the specimens at failure conditions, and

$(u_a\text{-}u_w)_b$ = air entry value for drying curve or expulsion curve for wetting curve.

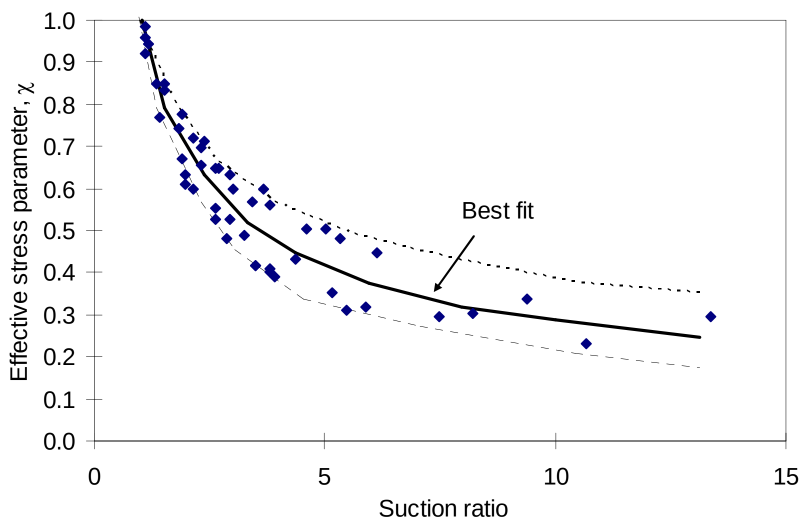

Fig. 3. 7 Effective stress parameter, χ, versus suction ratio (Khalili and Khabbaz, 1998)

3.3 PARAMETRIC STUDY

In order to study the influence of the SWCC on the shear strength predicted using three different procedures (Vanapalli et al.'s 1st and 2nd approaches, and the Khalili and Khabbaz method), the parametric study was performed by varying the fitting parameters *a* and *n* of the Fredlund and Xing SWCC model (Eq. 3.4). The same saturated shear strength parameters (c'= 0 kPa and ϕ'=30°) and m value (m = 1) were used in this parametric study. The residual suction of 3000 kPa was used for Vanapalli et al.'s 2nd approach. Fredlund et al.

(1996) and Vanapalli et al. (1996) predicted the shear strength of unsaturated soil successfully using the residual suction of 3000 kPa. The significance of the residual suction on the prediction of shear strength will be discussed later in section 3.4.1. The predicted shear strength values are presented over the range of suction values of practical interest, 0 to 1500 kPa.

3.3.1 Results for Vanapalli et al.'s 1st approach

The results obtained from Vanapalli et al.'s 1st approach (Eq. 3.6) were not directly comparable to those obtained from Vanapalli et al.'s 2nd approach (Eq. 3.9) and the Khalili and Khabbaz method (Eq. 3.10) since Eq. 3.6 requires knowing the parameter, κ, as well as the SWCC and saturated shear strength parameters (c' and ϕ'). In contrast, the shear strength can be estimated using Eq. 3.9 and Eq. 3.10 with only the SWCC (a, n, m, air entry value, and residual suction) and saturated shear strength parameters. Figures 3.8(a) and 3.8(b) shows the four SWCC for the assumed values of a (100 and 200) and n (1 and 2).The shear strength failure envelopes predicted from Eq. 3.6 are shown in Figs. 3.8(c), (d), (e), and (f) for soils with various values of κ (1, 2, 3, and 4). It is clearly shown that the shear strength increase as the a value increases. Also, the higher shear strength failure envelope is evaluated for soils with the lower n and κ values. This is because these soils have greater normalized area of water, a_w, at a given matric suction. It is observed that the shear strength envelope of soil with higher values of κ and n (soil that desaturates fast) has a peak point and drop off. This peak point appears at lower suction when either the n value or the κ value is higher. The decrease in shear strength after the peak point occurs because the reduction rate of the normalized area ($=\theta^{\kappa}$) exceeds the increase rate of the matric suction.

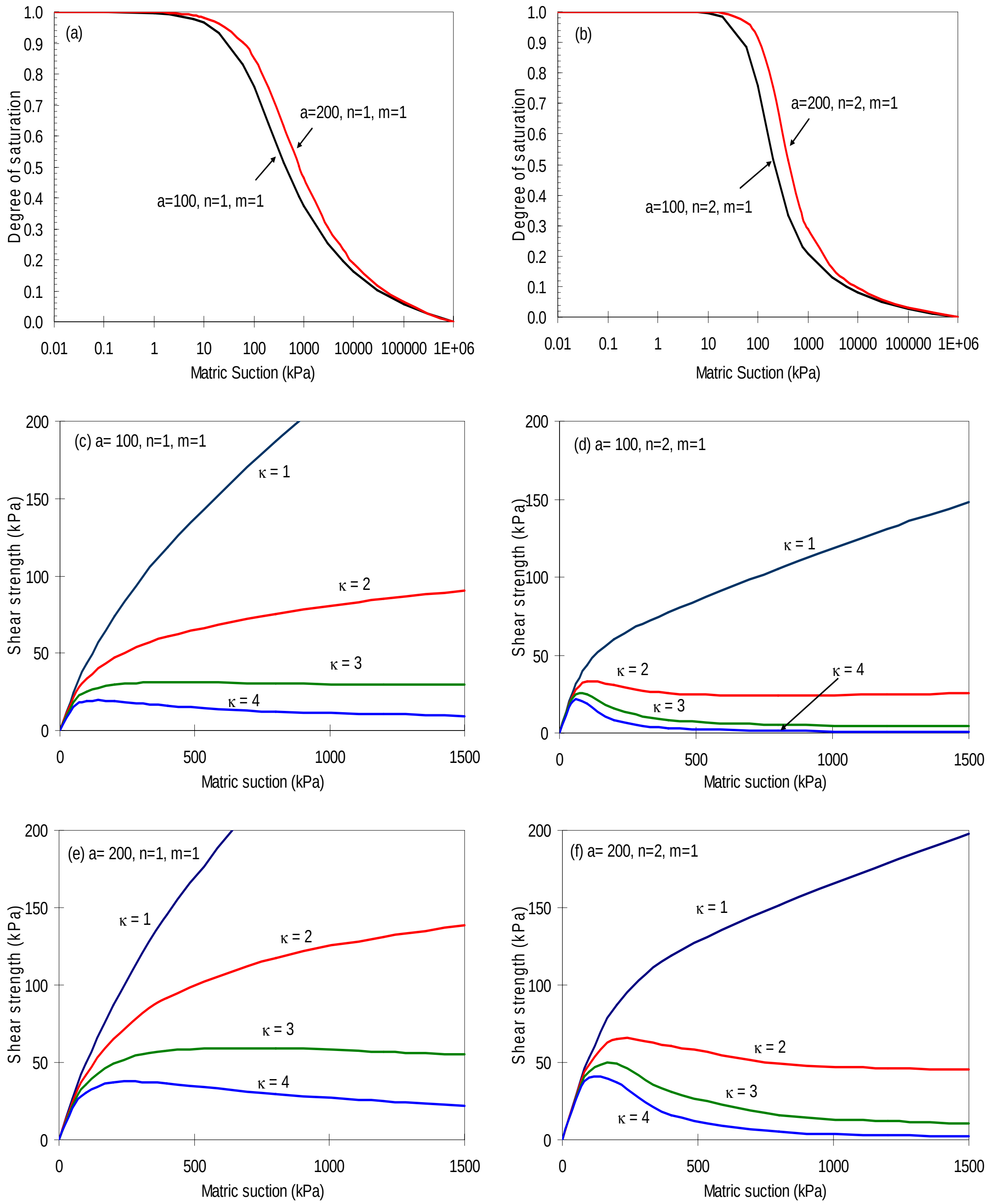

Fig. 3. 8 Shear strength envelopes for soils from Vanapalli et al.'s 1st approach with various values of a, n, and κ (c'= 0 kPa and ϕ'=30°)

3.3.2 Results for Vanapalli et al.'s 2nd approach and Khalili and Khabbaz model

Soils with various a values (10, 50, 100, and 200) were studied in order to investigate the effect of air entry values on the shear strength predicted from Vanapalli et al.'s 2nd approach (Eq. 3.9) and the Khalili and Khabbaz model (Eq. 3.10). The analyses were performed for two different slopes of SWCC (n = 1 and 2). The SWCCs and corresponding shear strength envelopes for the soils with various a values and n = 1 are shown in Figs. 3.9(a), (c), and (e). The air entry values determined by the construction method (Vanapalli, 1999) are 2.2, 11, 22, and 42 kPa for the soils with the a values of 10, 50, 100, and 200, respectively. Figures 3.9(b), (d), and (f) show the SWCCs and corresponding shear strength for the soils with various a values and n = 2. The air entry values of 4.2, 21, 42, and 80 kPa were determined for the soils with the a values of 10, 50, 100, and 200, respectively. It is clearly shown from Figs. 3.9(c) thru (f) that the shear strengths predicted from both methods increase with increasing a value (or air entry value) regardless of the slopes of SWCC. However, there is a distinction in the shapes of shear strength envelopes predicted from the two methods. The Khalili and Khabbaz model always shows increasing shear strength with increasing suction, with the greatest rate of increase in shear strength up to the air-entry value (Fig. 3.9e and Fig. 3.9f). On the other hand, Vanapalli et al.'s 2nd approach shows a linear increase in shear strength up to the air-entry value and then the strength may either increase nonlinearly up to 1500 kPa, or have a peak point and drop off, depending on the shape of SWCC (Fig. 3.9c and Fig.3.9d).

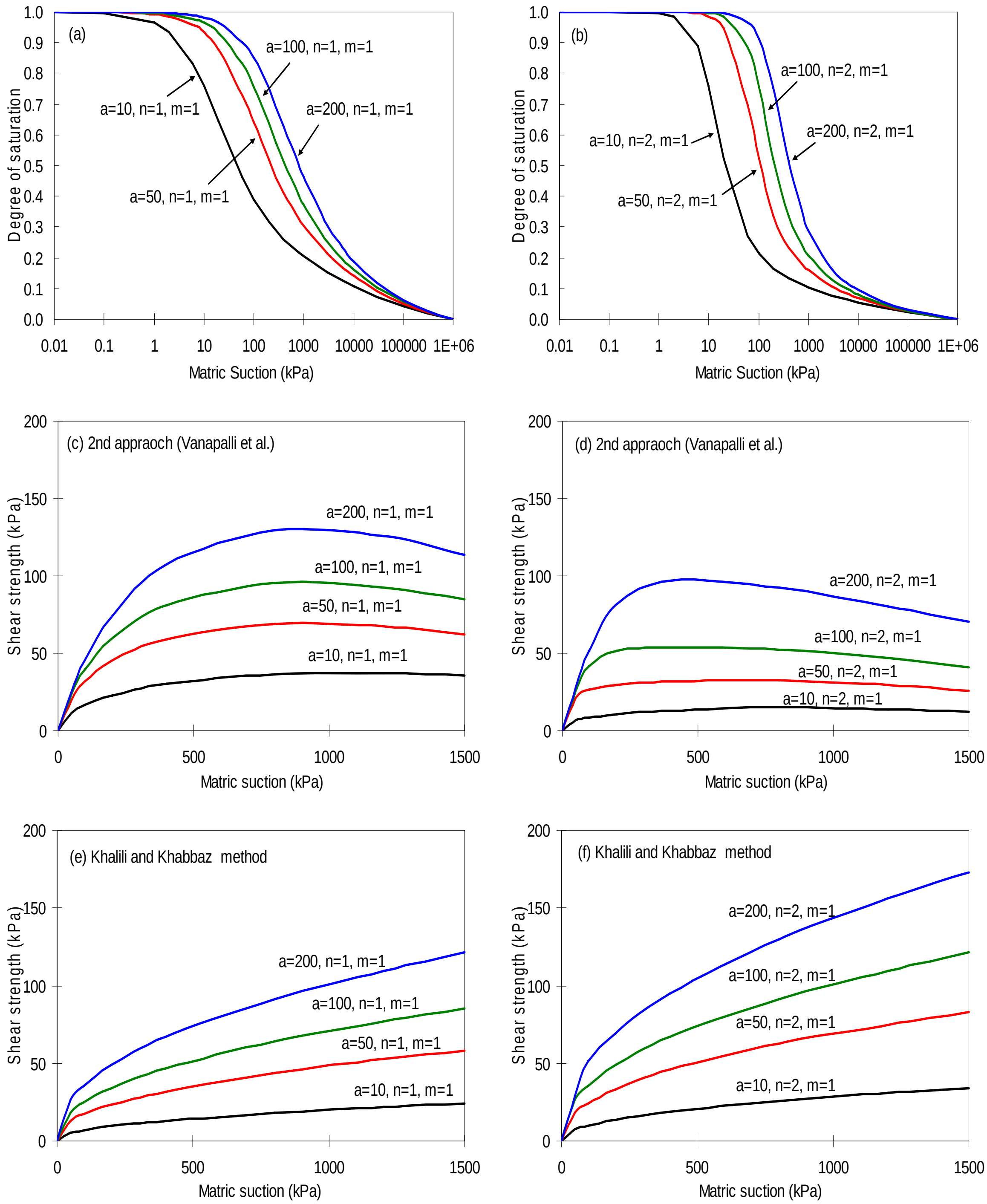

Fig. 3. 9 SWCCs and corresponding shear strength envelopes from Vanapalli et al.'s 1st approach and the Khalili and Khabbaz method with various a values (n = 1 and 2)

For the shear strength envelopes predicted from Vanapalli et al.'s 2nd approach, it is shown that at the given value of a (10, 50, 100, or 200) the shear strength for soils with the n value of 2 are lower than that for soils with the n value of 1 throughout most of the range of suction presented (0-1500 kPa), although the soils with the n value of 2 have higher air entry values. The peak strength is observed at a lower suction for soils with the higher n value (n = 2). In contrast, the shear strength predicted from the Khalili and Khabbaz model is only function of air entry value irrespective of the slope of SWCC. The shear strength for soil with the n value of 2 is higher than that for soil with the n value of 1 because of higher air entry values.

Figure 3.10 shows comparisons of the results from Figs. 3.8 and 3.9. For the range of a values used in this analysis (10-200), the shear strength envelopes for Vanapalli et al.'s 2nd approach plot above those for the Khalili and Khabbaz model over most of the ranges of suction presented (0-1500 kPa) when the n value is 1 (Figs. 3.10a and 3.10c). However, the shear strength predicted from Khalili and Khabbaz becomes greater than that from Vanapalli et al.'s 2nd approach over much of the range of suction when the n value is increased to 2 (Figs. 3.10b and 3.10d).

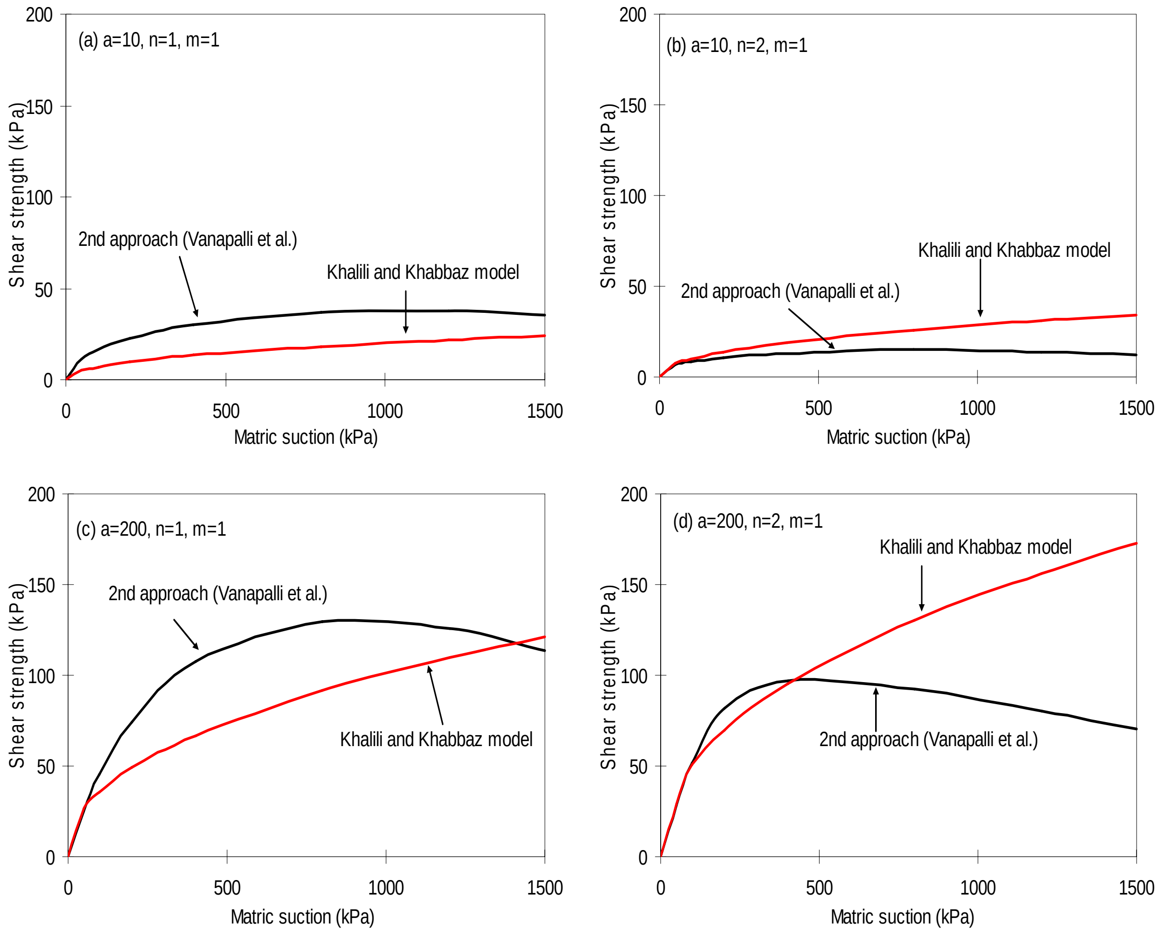

Fig. 3. 10 Comparison between shear strength predicted from Vanapalli et al.'s 2nd approach and the Khalili and Khabbaz model (a = 10 and 200; n = 1 and 2)

In order to better see the effect of the slope of SWCC on shear strength, the parametric study was extended by investigating n value from 0.5 to 3 (n = 0.5, 1, 2, and 3). The results are presented for two different a values (a = 10 and 100). For the n values of 0.5, 1, 2, and 3, the air entry values determined are 0.6, 2.2, 4.2, and 5.9 kPa, respectively, when the a value is 10, and 6, 22, 42, and 59 kPa, respectively, when the a value is 100. From Figs. 3.11(c) and (d) it is shown that the shear strength predicted from Vanapalli et al.'s 2nd

approach decreases significantly as the *n* value increases. In contrast, it is observed that the shear strength predicted from the Khalili and Khabbaz model increases remarkably as the *n* value increases, since higher air-entry values are determined for the soils with higher *n* values and the same *a* value.

Among the SWCCs presented in Figs. 3.11 (a) and (b), four soil-water characteristic curves (a = 10, n = 0.5; a = 10, n = 3; a = 100, n = 0.5; a = 100, n = 3) are used to compare the shear strength predicted from Vanapalli et al.'s 2nd approach and Khalili and Khabbaz model. Figures 3.12 (a) and (b) show that Vanapalli et al.'s 2nd approach predicts higher shear strength than the Khalili and Khabbaz method irrespective of the a values for the soils with the *n* of 0.5. For the soils with the *n* value of 3, however, the shear strengths predicted from Khalili and Khabbaz method are greater than those predicted from Vanapalli et al.'s 2nd approach (Figs. 3.12b and 3.12d).

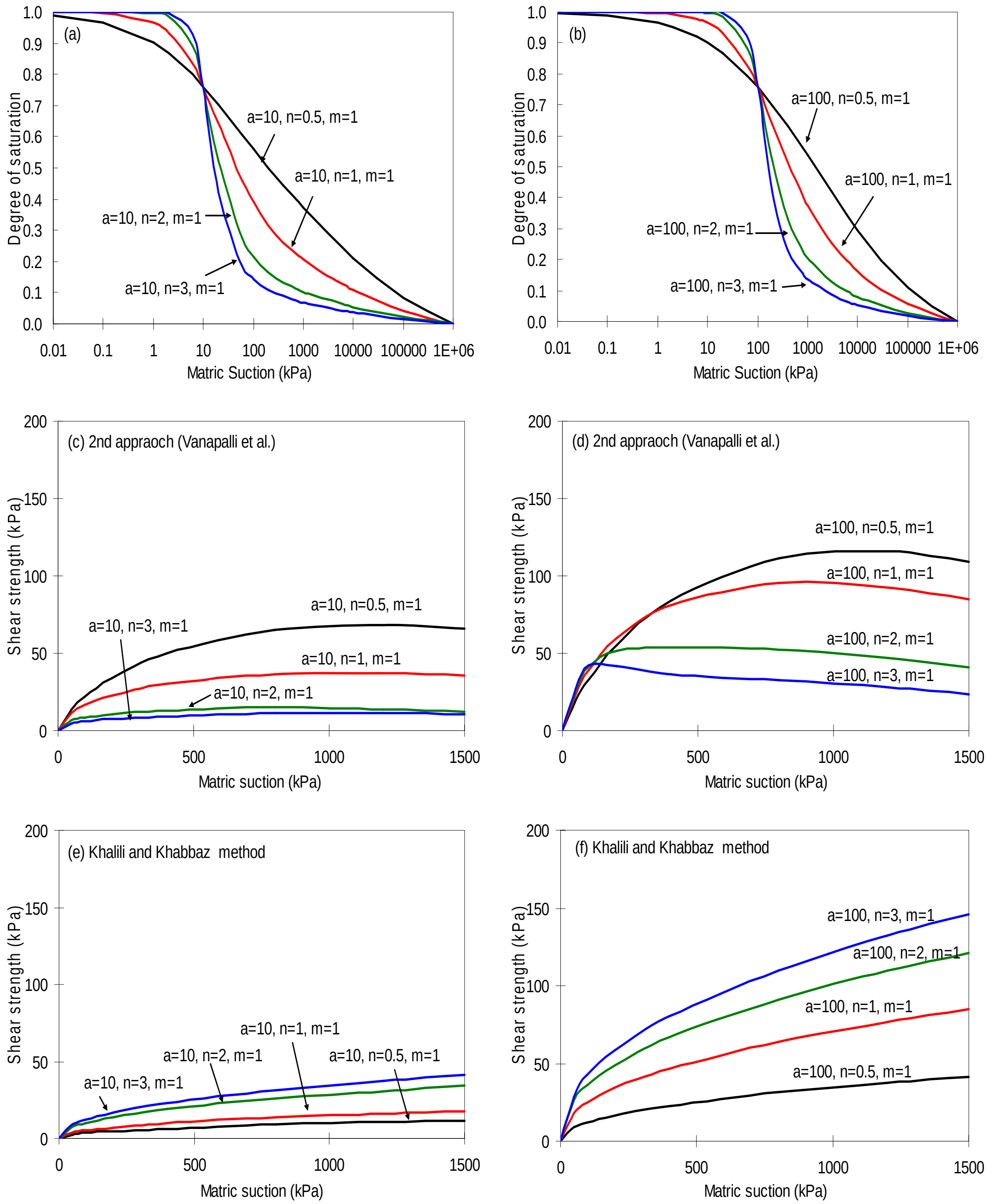

Fig. 3. 11 SWCCs and corresponding shear strength envelopes from Vanapalli et al.'s 1st approach and the Khalili and Khabbaz method with various n values (a = 10 and 100)

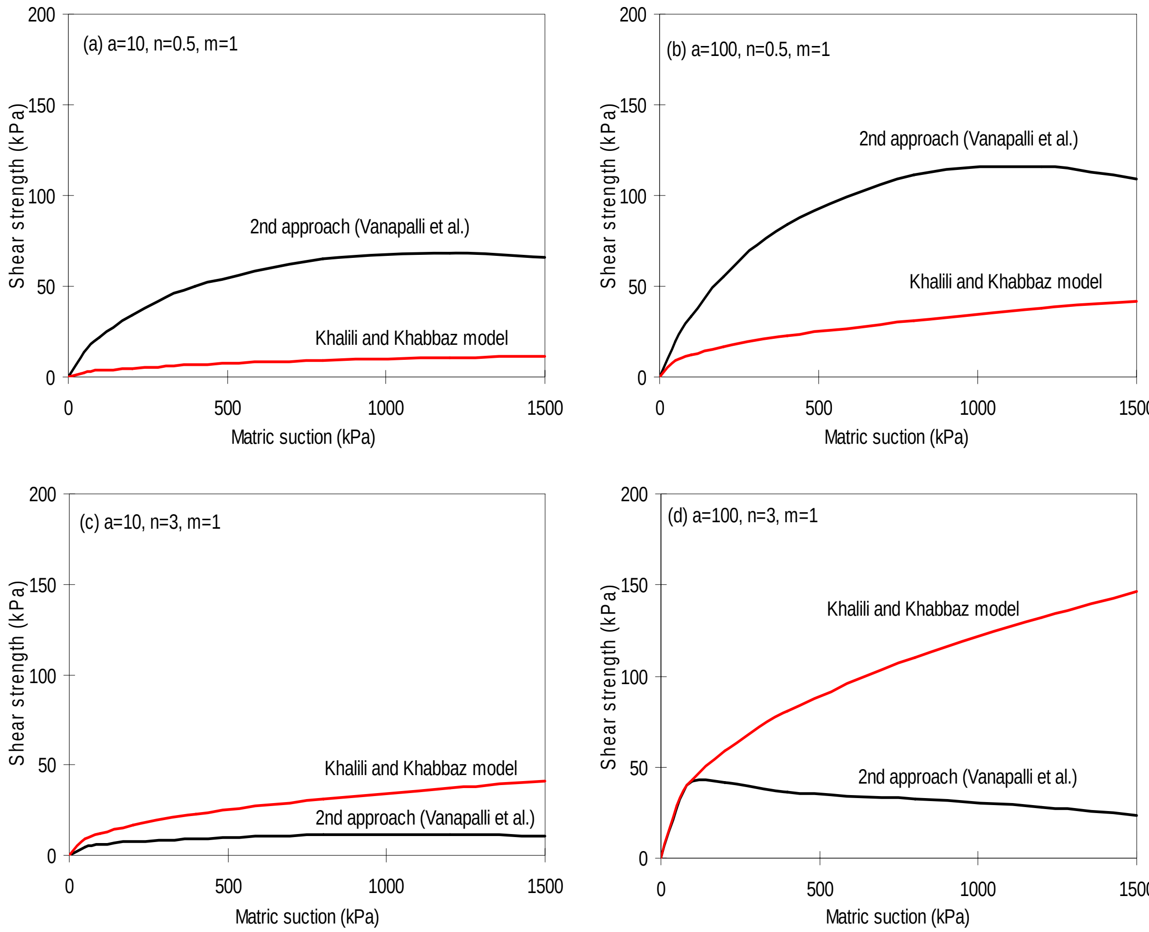

Fig. 3. 12 Comparison between shear strength predicted from Vanapalli et al.'s 2nd approach and the Khalili and Khabbaz model (a = 10 and 100; n = 0.5 and 3)

3.3.3 Effect of soil types

The SWCCs for three different soil types were selected from the literature in order to investigate the effect of soil type on the shear strength values predicted from the three prediction methods. The SWCCs over the entire range of suction were estimated by the best fit from the fitting parameters of Fredlund and Xing SWCC model (Fig. 3.13). The gradation, plasticity index, and shear strength parameters of the soils are provided in Table 3.1. A coarse grained soil such as soil A has large interconnected pores and shows a tendency to desaturate quickly as matric suction increases. However, fine grained soils such as soils B and C have generally small interconnected pores and therefore desaturate slowly with increasing suction. The air entry values determined were 2.4, 12, and 121 kPa for soils A, B, and C, respectively. It is shown that the air-entry value increases with an increase of fines.

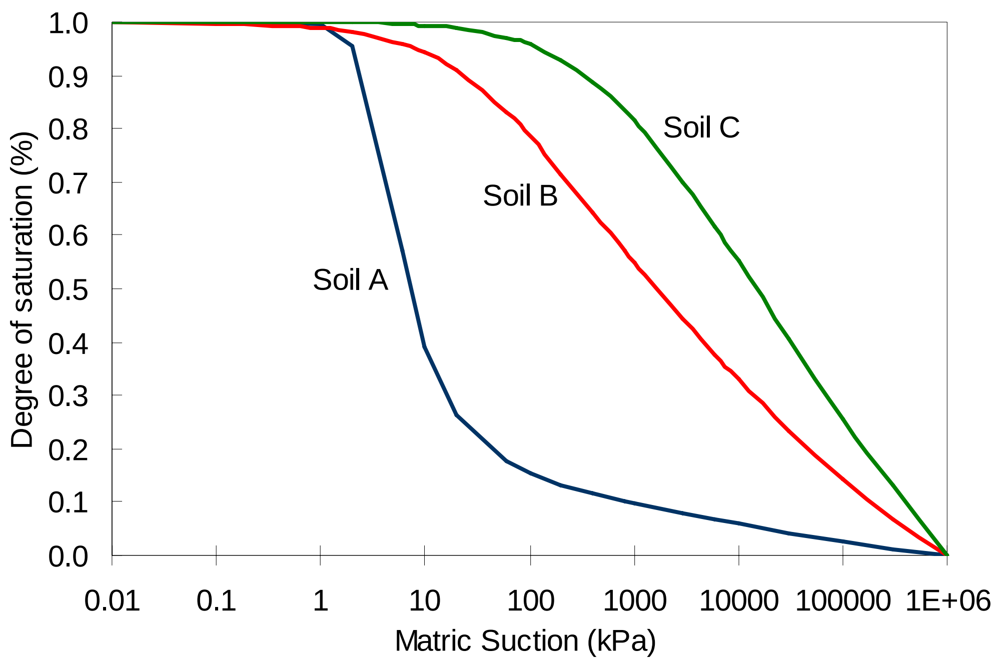

Fig. 3. 13 Soil-water characteristic curves for different soil types shown in the literature (after Rassam and William, 1999; Han et al., 1995; and Khalili et al, 2005)

Table 3. 1 Summary of soil properties for different types of soil

Soil type	**Sand: %**	**Silt: %**	**Clay: %**	I_p	c'	ϕ'	**Ref.**
A	79	13	1	-	0	41.7	Rassam and William (1999)
B	49	25	26	18	0	33	Han et al. (1995)
C	33	67 (silt +clay)		21	5	29	Khalili et al. (2004)

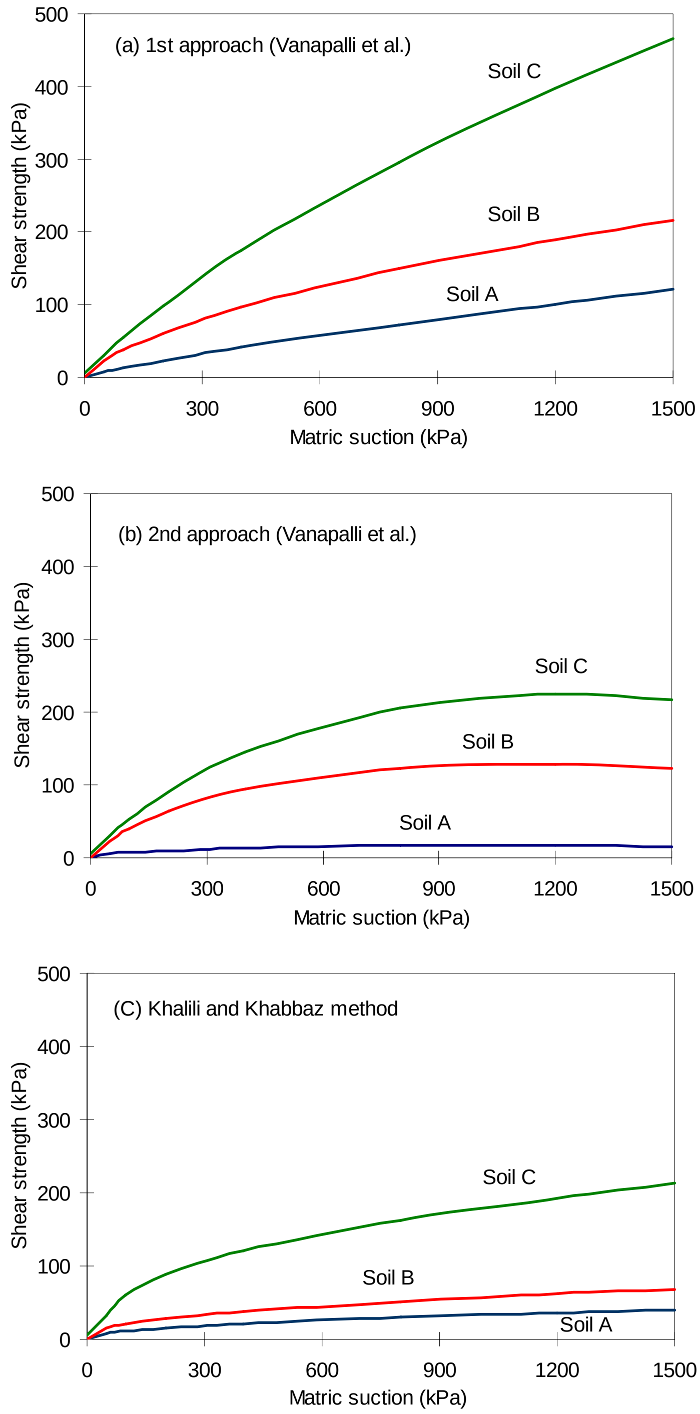

Fig. 3. 14 Predicted shear strength envelopes for different soil types using (a)Vanapalli et al.'s 1st approach; (b) Vanapalli et al.'s 2nd approach; and (c) the Khalili and Khabbaz method.

Figure 3.14 shows the shear strength envelopes predicted from Vanapalli et al.'s 1st approach, 2nd approach, and the Khalili and Khabbaz method. For all prediction methods, it can be seen that the soil suction tends to contribute more to the shear strength as both amount of fines and the plasticity index of the soil increase. However, the magnitude of these contributions to shear strength determined by each method could be very different. As an example, the greatest shear strength of 465 kPa at matric suction of 1500 kPa was predicted from Vanapalli et al.'s 1st approach whereas the shear strengths of 218 and 213 kPa were predicted from Vanapalli et al.'s 2nd and the Khalili and Khabbaz method, respectively.

3.4 COMPARISON OF PREDICTION METHODS USING THE MEASURED DATA

Each of these three prediction methods was originally developed based on limited experimental data obtained from a few soils. For this reason, each method could predict very different values of shear strength depending on the types of soil (or the shape of SWCC) as shown in the results of the parametric study. Therefore, it is very important for engineers to know which method predicts more reasonable values compared to the measured values of shear strength for each type of soil. This section provides comparisons between measured and predicted values of unsaturated shear strength using three methods described in the previous section. The measured shear strengths of 15 cases with the SWCCs were extracted from the literature. The shear strengths measured within the range of matric suction from 0 to 1500kPa and under the net normal stress from 0 to 250 kPa were selected for this study. Table 3.2 provides details of the cases and the relevant soil properties. Also, the information of SWCC (the range of suction measured, the Fredlund and Xing parameters for SWCC, and air entry value) and the type of apparatus used for measuring shear strength are shown in

Table 3.2. The soil types used in this research are mostly clays (10 out of 15), two silts, and three sands. The shear strength and the SWCC were extracted from the plots of the original publications using digitizing software, Grab It (Datatrend Software, Inc.). The Fredlund and Xing equation (Eq. 3.4) was fit to the SWCC for obtaining the parameters (a, n, and m). The ranges of Fredlund and Xing parameters and air-entry values estimated for fifteen soils are given in Table 3.3. The values of shear strength were then estimated from the air entry value and the SWCC defined by the Fredlund and Xing parameters using three prediction methods. For example, Fig. 3.15 shows measured values of shear strength extracted from the literature and the values of shear strength predicted using the three methods for Kaolin samples, referenced as Soil I in Table 3.2.

Table 3. 2 Details of soils data used for analysis

ID	Reference	USCS	Soil type and properties*	Saturated shear strength parameters	Info. of SWCC (Measured suction range, Fredlund and Xing fitting parameters, Air entry value)	Apparatus (Net normal stress**)
A	Rahardjo et al. (2004)	CL	Jurong sedimentary formation; compacted, ρ_{dmax}=1.86g/cm^3, OMC= 14.2%, sand=34%, silt=24%, clay=42% , Gs=2.72, LL=36.4%, I_p=10%, ρ_d=1.71g/cm^3, RC=92%, w=15.6%	c'= 0 kPa ϕ'= 31.5°	0 - 200 kPa a=105.5, n=2.02, m=1.17 AEV=50 kPa	MTD (σ_3-u_a)=0 kPa
B	Thu et al. (2006)	MH	Kaolin; compacted, ρ_{dmax}=1.35g/cm^3, OMC=22%, silt=85%, clay=15% , Gs=2.65, LL=51%, I_p=15%, ρ_d=1.35g/cm^3, RC=100%, w=22%	c'= 0 kPa ϕ'= 32°	0 - 700 kPa a= 66.3, n=4.19, m=0.59 AEV = 48 kPa	MTD (σ_3-u_a)=0 kPa
C	Han et al. (1995)	ML	Granite residual soil; compacted, ρ_{dmax}=1.61g/cm^3, OMC=16%, sand=49%, silt=25%, clay=26% , Gs=2.66, LL=47%, I_p=18%, ρ_d=1.74g/cm^3, RC=108%, w=14.5%	c'= 0 kPa ϕ'= 33°	0 - 700 kPa a=46.1, n=0.77, m=0.58 AEV =12 kPa	MDS (σ_y-u_a)=200kPa
D	Khalili et al. (2004)	CL	Sample SJ10a (11.5m-11.8m); undisturbed, sand=33%, silt + clay=67%, LL=39%, I_p=21%, ρ_d=1.82g/cm^3, w=17%	c'= 5 kPa ϕ'= 29°	0 - 1400 kPa a= 234.0, n= 0.86, m=0.25 AEV =121 kPa	MTD (σ_3-u_a)=200kPa
E	Khalili et al. (2004)	CL	Sample SJ10b (20.5m-20.8m); undisturbed, sand=25%, silt + clay=75%, LL=33%, I_p=11%, ρ_d=1.69g/cm^3, w=18%	c'= 19 kPa ϕ'= 29°	0 - 1400 kPa a= 336.9, n= 0.68, m= 0.47 AEV = 144 kPa	MTD (σ_3-u_a)=200kPa

Table 3.2 (Continued).

F	Khalili et al. (2004)	CL	Sample SJ11 (23.5m-23.8m); undisturbed, sand=36%, silt + clay=64%, LL=25%, I_p=6%, ρ_d=1.91g/cm^3, w=13%	c'= 5 kPa ϕ'= 30°	0 - 1400 kPa a= 705.5, n= 0.69, m= 0.84 AEV = 129 kPa	MTD (σ_3-u_a)=200kPa
G	Ecario and Juca (1989)	CL	Guadalix red clay; Compacted, ρ_{dmax}=1.80g/cm^3, OMC=17%, sand=14%, silt + clay=86%, LL=33%, I_p=13.6%, ρ_d=1.80g/cm^3, RC=100%, w=13.6%	c'= 26.3 kPa ϕ'= 32.5°	0-15000 kPa a=2500, n= 0.58, m= 1.85) AEV = 152 kPa	MDS (σ_y-u_a)=120kPa
H	Ecario and Juca (1989)	SC	Madrid clayey sand; Compacted, ρ_{dmax}=1.91g/cm^3, OMC= 11.5%, sand= 83%, silt + clay= 17%, LL= 32%, I_p= 15%, ρ_d= 1.91g/cm^3, RC= 100%, w= 9.2%	c'= 41.5 kPa ϕ'= 39.5°	0-4000 kPa a= 148.2, n= 1.75, m= 0.52 AEV = 79 kPa	MDS (σ_y-u_a)=120kPa
I	Gallage and Uchimura (2006)	SM or SC	Edosaki Sand; Compacted, ρ_{dmax}=1.725g/cm^3, OMC=16.5%, sand=83.6%, silt + clay=16.4% , Gs=2.75, LL & I_p=NP, ρ_d=1.5g/cm^3, RC=87%, w=10%	c'= 0 kPa ϕ'= 46°	0 - 200 kPa a= 4.4, n= 17.0, m= 0.29 AEV = 3.4 kPa	MTD (σ_3-u_a)=0 kPa
J	Vanapalli et al. (1998)	CL	Botkin silt; Compacted, sand=27.5%, silt=48.5%, clay=24% LL=25%, I_p=8%, ρ_d=1.85g/cm^3	c'= 14.2 kPa ϕ'= 36.5°	Whole range a= 110.9, n= 0.95, m=0.70 AEV = 37 kPa	Unconfined Compression Test
K	Oloo and Fredlund (1996)	CL	Indian Head Till; Compacted, ρ_{dmax}=1.804g/cm^3, OMC=16.3%, sand=28%, silt=42%, clay=30% , Gs=2.73, LL=36%, I_p=19%, ρ_d=1.733g/cm^3, RC=96%	c'= 7 kPa ϕ'= 22°	0 - 200 kPa a=47.5, n=4.33, m=0.31 AEV = 36 kPa	MDS (σ_y-u_a)=50, 100, 150 kPa

Table 3.2 (Continued).

L	Oloo and Fredlund (1996)	SM	Botkin Pin Silt; Compacted, ρ_{dmax}=1.876g/cm^3, OMC=14.2%, sand=52.5%, silt=37.5%, clay=10%, Gs=2.68, LL=22%, I_p=6%, ρ_d=1.784g/cm^3, RC=95%	c'= 2.5 kPa ϕ'= 28°	0 - 130 kPa a=46.4, n=4.76, m=0.17 AEV = 35 kPa	MDS $(\sigma_y$-$u_a)$=50, 100, 150 kPa
M	Vanapalli et al. (1996)	CL	Indian head till (dry of optimum); Compacted, ρ_{dmax}=1.8g/cm^3, OMC=16.3%, sand=28%, silt=42%, clay=30%, LL=35.5%, I_p=18.7%, ρ_d=1.73g/cm^3, RC=96.1%, w=13%	c'= 0 kPa ϕ'= 23°	0 - 30000 kPa - $(\sigma_y$-$u_a)$=25 kPa a=34.1, n=0.80, m=0.57 AEV = 11.63 kPa -$(\sigma_y$-$u_a)$=100 kPa a=71.4, n=0.66, m=0.54 AEV = 34.84 kPa -$(\sigma_y$-$u_a)$=200 kPa a=125.2.1, n=0.8, m=0.45 AEV = 75.19 kPa	MDS $(\sigma_y$-$u_a)$=25, 100, 200 kPa
N	Vanapalli et al. (1996)	CL	Indian head till (Optimum); Compacted, ρ_{dmax}=1.8g/cm^3, OMC=16.3%, sand=28%, silt=42%, clay=30%, LL=35.5%, I_p=18.7%, ρ_d=1.8g/cm^3, RC=100%, w=13%	c'= 0 kPa ϕ'= 23°	0 - 30000 kPa -$(\sigma_y$-$u_a)$=25 kPa a=140.3, n=0.77, m=0.57 AEV = 57.1 kPa -$(\sigma_y$-$u_a)$=75 kPa a=406.7, n=0.81, m=0.60 AEV = 155.71 kPa -$(\sigma_y$-$u_a)$=200 kPa a=812.7, n=0.84, m=0.61 AEV = 289.69 kPa	MDS $(\sigma_y$-$u_a)$=25, 75, 200 kPa

Table 3.2 (Continued).

O	Vanapalli et al. (1996)	CL	Indian head till (wet of Optimum); Compacted, ρ_{dmax}=1.8g/cm^3, OMC=16.3%, sand=28%, silt=42%, clay=30%, LL=35.5%, I_p=18.7%, ρ_d=1.77g/cm^3, RC=98%, w=19.2%	c'= 0 kPa ϕ'= 23°	0 - 30000 kPa -(σ_y-u_a)=25 a=482.8, n=0.88, m=0.71 AEV = 154.54 kPa -(σ_y-u_a)=100 a=473.1, n=0.91, m=0.59 AEV = 180.2 kPa -(σ_y-u_a)=200 a=239.5, n=1.15, m=0.40 AEV = 132.6 kPa	MDS (σ_y-u_a)=25, 100, 200 kPa

* LL = Liquid Limit; I_p = Plasticity Index; ρ_{dmax} = Maximum Dry Density; OMC = Optimum Moisture Content; ρ_d = Dry Density at testing, RC = Relative Compaction, w = as-compacted or natural water content, AEV = air entry value

** MTD = Modified Triaxial Device, MDS = Modified Direct Shear device

Table 3. 3 Measured ranges of *a*, *n*, and air-entry values for the soils used

Estimated value	Ranges
Fitting parameter, *a*	4.4 – 2500
Fitting parameter, *n*	0.58 – 17.0
Air-entry value (kPa)	3.4 – 290

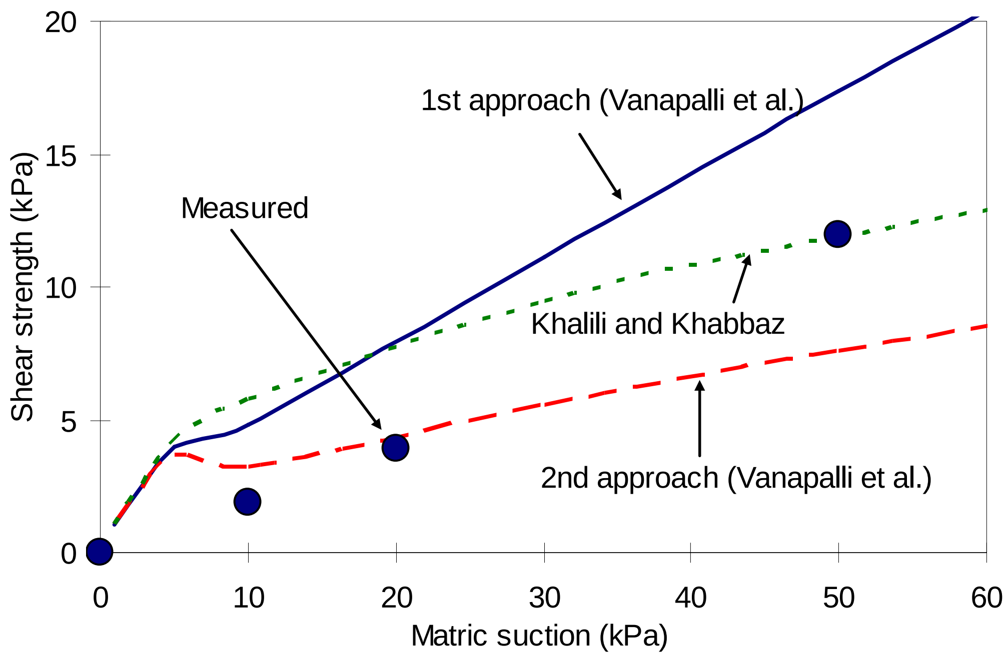

Fig. 3. 15 Comparison of predicted and measured shear strength values using three different procedures for Kaolin (Soil I).

3.4.1 Limitations and difficulties in the use of the prediction methods

Several limitations and difficulties for using each of the prediction methods were experienced. In this section, these limitations and difficulties found for applying each method are described.

Vanapalli et al.'s 1st method

The κ value in Eq. 3.6 was originally a fitting parameter used for obtaining a best-fit between the measured and predicted values. Therefore, the κ value for the soil must be estimated in order to predict the shear strength using this equation. Vanapalli and Fredlund (2000) proposed the relationship between the fitting parameter, κ, and plasticity index, Ip, based on five shear strength data sets from statically compacted soils (Fig. 3.6). Garven and Vanapalli (2006) verified this relationship using ten shear strength data sets from statically compacted soils and suggested the mathematical equation shown as Eq. 3.7. However, the suitability of this equation should be evaluated for soils existing under different conditions (i.e. natural soils, dynamically compacted soils). In addition, the κ value may be influenced by not only plasticity index but other parameters such as the amount of clay, stress history, soil structure, etc. (Vanapalli and Fredlund, 2000). The relationship between the fitting parameter, κ, and other parameters, however, is still unknown.

Vanapalli et al.'s 2nd method

In order to predict the shear strength using this model (Eqs. 3.8 or 3.9), it is necessary to identify a residual water content of the soil. Figure 3.16 shows the predicted shear strength using four different values of residual suction, ψ_r (500, 1500, 3000, and 5000kPa). It is clearly shown that the shear strength predicted from this equation is highly dependent on the residual suction.

The main limitation of using this method is that the residual water content and the corresponding residual suction are defined in different ways by several researchers. Brooks and Corey (1996) defined the residual water content as the water content at which suction reaches infinity. According to van Genuchten (1980) the residual water content is defined as the water content at a soil suction of 1500kPa, which is similar to the wilting point of many plants. van Genuchten et al. (1991) suggested that residual water content is defined as the water content at which the slope of the SWCC goes to zero. Also, residual water content is often treated as a fitting parameter with no real physical significance. More discussions of this residual state of soils can be found in Vanapalli et al. (1998).

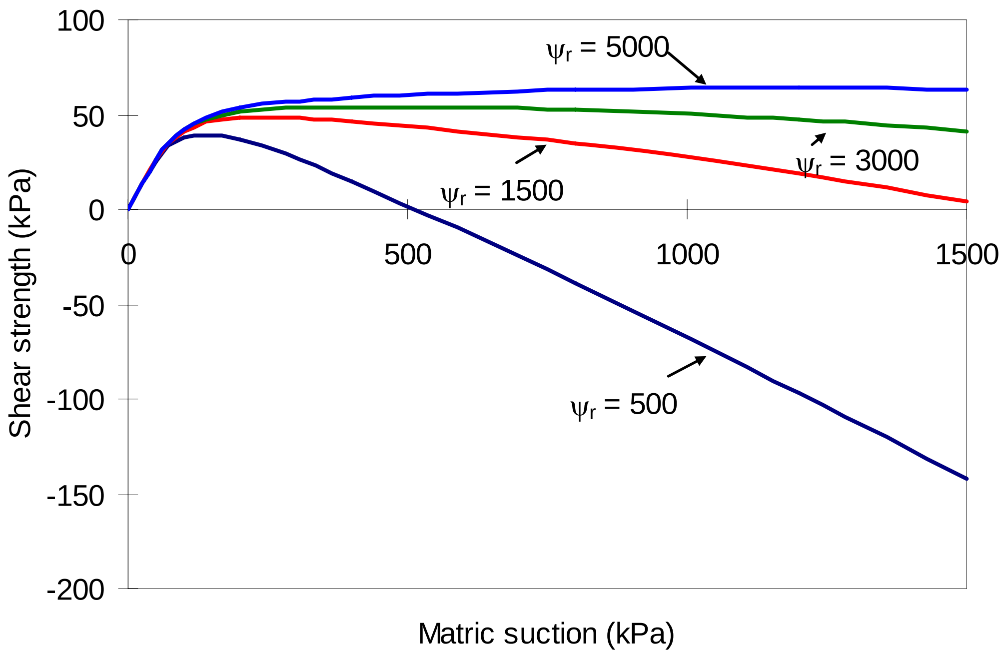

Fig. 3. 16 Effect of residual suction on the predicted shear strength envelope using Vanaplli et al.'s 2nd approach (a = 100, n = 2, and m = 1)

A graphical construction method is often used as an alternative method of determining the residual water content. Vanapalli et al. (1996) suggested graphical procedures to be used to define both air-entry value and the residual state when the entire suction range is used for the SWCC (Fig.3.3). Best-fit parameters for Eq. 3.4 are found in order to describe the soil-water characteristic curve over the entire range of suction. The SoilVision^{TM} database (SoilVision System Ltd.) provides a computational technique for estimating the air entry value and residual state. Figure 3.17(a) shows the results of the air entry and residual suction values applied to soil B using this technique. More details of the procedural steps involved in this computational technique are found in the SoilVision^{TM} manual (2006).

The values of residual suction determined by the construction method are often smaller than 1500 kPa. Using a residual suction lower than 1500 kPa, however, could provide unreasonable results in estimating shear strength for the suction range of 0-1500 kPa as Eq. 3. 10 forces the shear strength to drop to zero when the value of suction approaches the residual suction. As an example, Fig. 3.17(b) shows the measured shear strengths and the shear strength envelope predicted from the low residual suction of 212 kPa from Fig. 3.17(a). It is observed that there are remarkable differences between the measured and predicted values of shear strength. The negative predicted values of shear strength beyond the residual suction are not meaningful. The same trend is shown for soils A, G, I, and J for which the residual suctions determined by the construction method are lower than 1500 kPa.

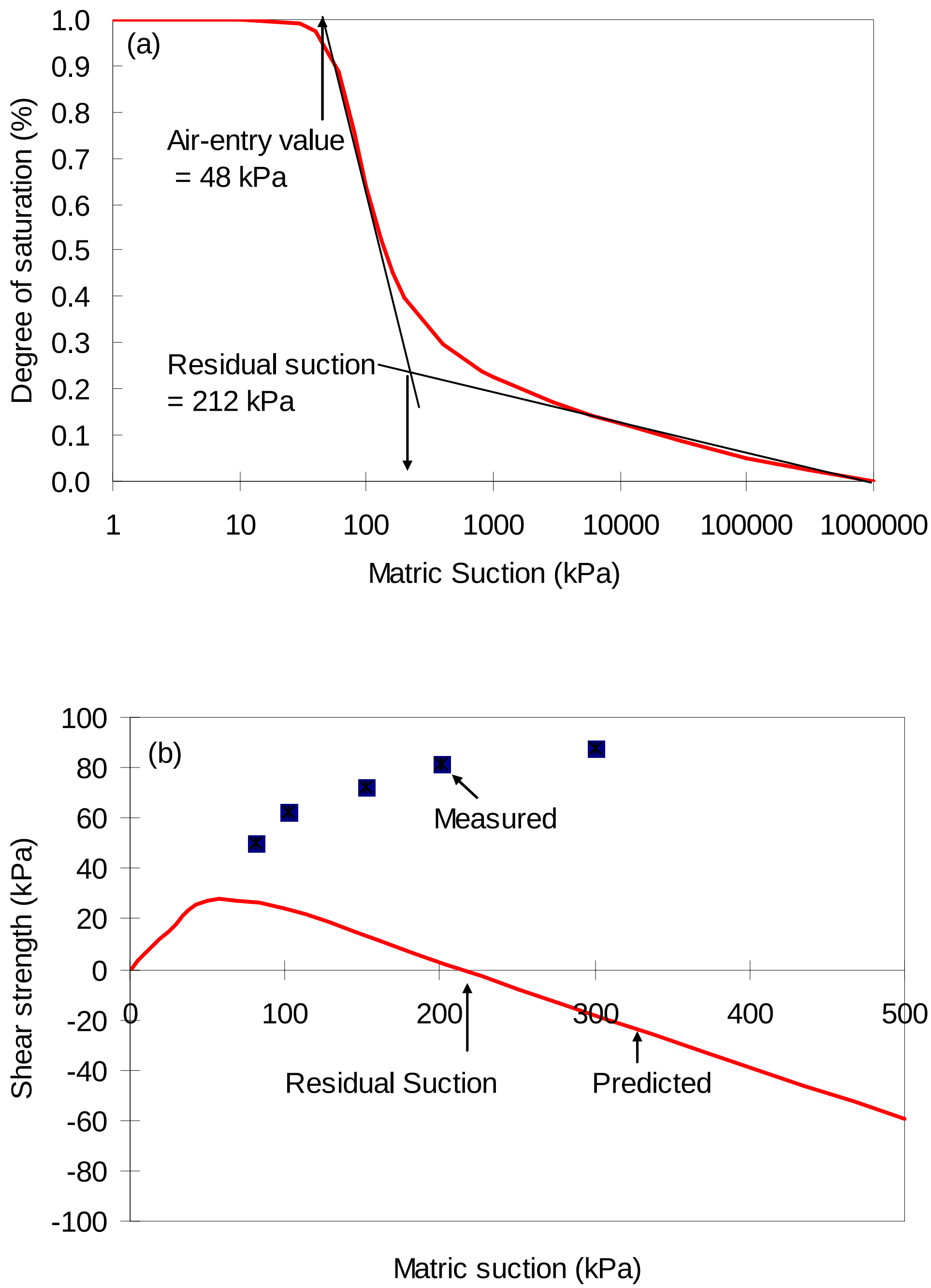

Fig. 3. 17 Result of the construction technique and comparison of the predicted shear strength curve with the experimental shear strength data (Soil B)

Khalili and Khabbaz (1998)

Eq. 3.10 was developed using the measured value of shear strength for 14 fine grained soils. The air entry values of these soils range from 35 kPa to 153 kPa. Therefore, this equation would not be used for coarse grained soils and soils which have air entry values out of that range.

The only required parameters for predicting the shear strength of unsaturated soils using this method are the air entry value of the soil and saturated shear strength parameters. Therefore, determining reliable air entry values in a consistent way is very important. Different air entry values, however, could be estimated from the same SWCC by either human error or the use of different interpretation procedures. This variance of determined air-entry values could be great, as it is usually determined from a semi-logarithm plot. Figure 3.18 presents the method for determining the air entry value shown in Khalili et al. (2004). This method uses a sloping line in contrast to the construction method suggested by Vanapalli et al. (1999), which uses a horizontal line extended through the maximum volumetric water content. An air entry value of 200 kPa was determined from the Khalili et al.'s procedure, whereas a much smaller air entry value of 121 kPa was determined from Vanapalli's construction method. A 30% greater value of shear strength is estimated if the air entry value of 200 kPa is used instead of that of 121 kPa (when the matric suction of soil is larger than 200kPa).

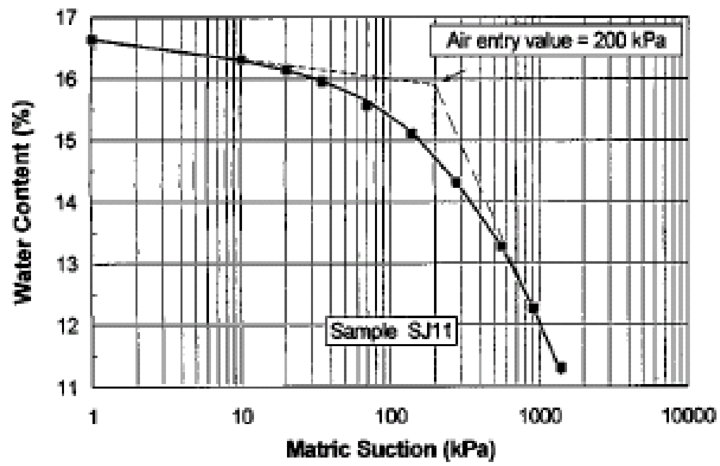

Fig. 3. 18 Determination of air entry value shown in Khalili et al. (2004)

3.4.2 Analysis of data

As described in the previous chapter, each prediction method has its own limitations and application difficulties. Therefore, several assumptions were made in using the prediction methods and the suitability of these assumptions will be reviewed later in conjunction with the results of analysis. The assumptions made in this study are:

1. The κ value was determined from the relationship to plasticity index irrespective of soil condition (natural soils and statically compacted soils).
2. A residual suction of 3000 kPa was used for all soil types (sand, silt, and clay).
3. The Khalili and Khabbaz equation was used for all types of soil irrespective of the magnitude of air entry value estimated.

The air entry values for the fifteen soils used in this research were determined using the computational technique incorporated in the SoilVision^{TM} program, although different air entry values for some of these soils have been presented the literature. This decision was made in order to estimate air entry values in a consistent way, and minimize the variance of air entry values determined which might occur by human error and by using different procedures.

For each of the soils included in this study, the predicted shear strength is plotted in Fig. 3.19 against the measured shear strength. The linear regression line, with the intercept set to the origin, was then generated. The slope of linear regression line (S_L) and R-squared value (R^2) were determined. In general, a prediction method tends to give a good agreement with the measured data if both the slope of regression line and the R-squared value are close to 1. The prediction method tends to underestimate the shear strength when the slope is less than one and overestimate the strength when the slope is more than one. Also, it should be noted that the prediction method with a very low value of R^2 may result in poor predictions although the slope of regression line (S_L) is close to one.

The percentage of overestimation (PO), which indicates by what percentage the predicted shear strengths are greater than the measured shear strengths, is defined as:

$$PO(\%) = \frac{No.\ of\ \ data\ \ (predicted\ \ shear\ \ strength > measured\ \ shear\ \ sthrength)}{No.\ of\ \ total\ \ data} \times 100 \quad (3.11)$$

The measured vs. predicted shear strength for fifteen sets of shear strength data are shown in Fig. 3.19. Most of the shear strengths extracted from the literature are within the range of 0 – 200 kPa. Only a few data are shown above a strength of 200 kPa. Since the amount of data is not sufficient to determine the trend of shear strength above 200 kPa, it was decided to use only shear strength values within 0-200 kPa for subsequent analysis.

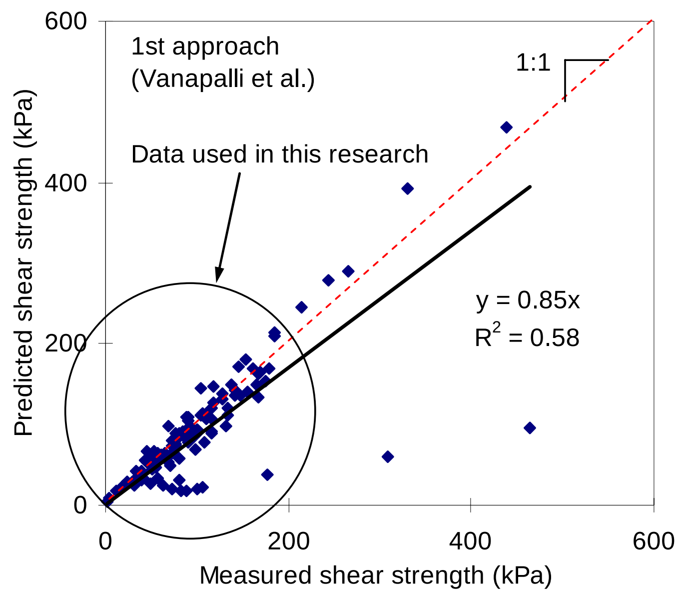

Fig. 3. 19 Selected shear strength data sets for analysis

The SWCC of a soil is conventionally measured by means of a pressure plate extractor with only the application of a nominal normal stress or without the application of any applied vertical stress. In the field, the soil is usually subjected to a certain stress. Although the stress state has been shown to have some influence on the SWCC for some types of soils, few experimental results can be found in the literature (Vanapalli et al, 1996; Ng and Pang, 2000; Rorie, 2006). For this reason, the shear strength of soil under a certain stress is commonly estimated using the SWCC performed at zero net normal stress. Figure

3.20(a) shows the shear strength failure surface determined from the SWCC obtained at zero net normal stress. This failure surface is defined by the constant friction angle, ϕ', with matric suction.

If the SWCCs are measured taking into account the influence of the stress state, the shear strength failure surface is determined as shown in Fig .3.20(b). It is shown from the shear strength failure surface that the internal friction angle would be different with respect to matric suction.

In this research, the analyses are performed taking into account the effect of net normal stress on the prediction of shear strength. Comparisons between the measured and predicted shear strengths are presented for the shear strength at low net normal stress range (0-50 kPa) and high net normal stress range (50-200 kPa) when the shear strengths are predicted using the SWCC performed at zero net normal stress. Comparison between measured and predicted values of shear strengths using SWCCs performed at different stresses is also presented.

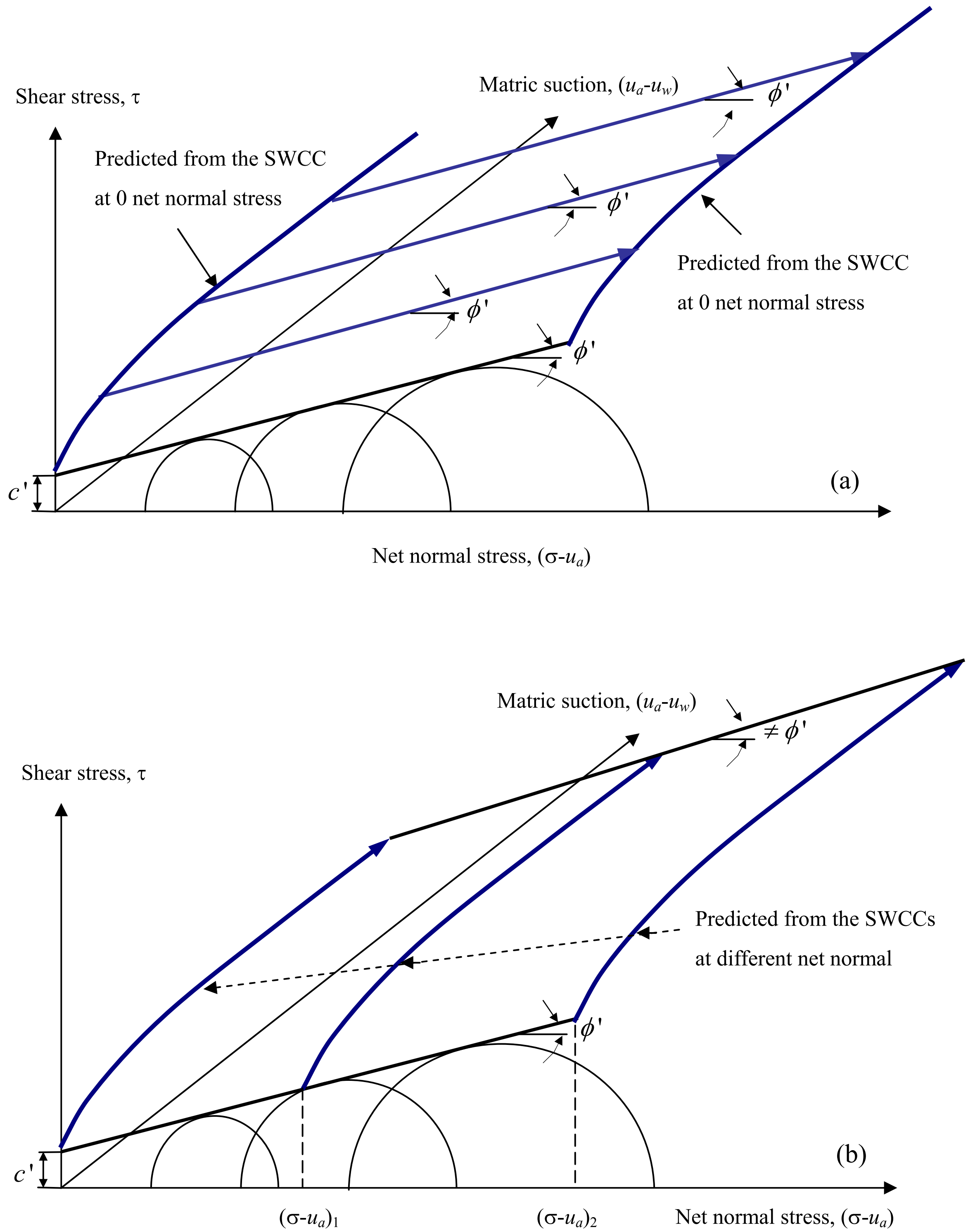

Fig. 3. 20 Predicted shear strength surface using (a) the SWCC at 0 kPa net normal stress and (b) the SWCCs at different net normal stresses.

Comparison between measured and predicted shear strengths for low net normal stress range (0-50kPa)

In this section, comparison is made between measured and predicted shear strengths for the 15 soils for the low net normal stress range (0-50kPa). The reported shear strengths at a net normal stress of 0 kPa (total cohesion or apparent cohesion) were used for soils A, thru J. If the shear strength data were presented at only one single normal stress in the literature, and this value was higher than 50 kPa, the shear strength at zero net normal stress was computed from the shear strength at that net normal stress and the reported value of internal friction angle (as for soils C thru F). The reported shear strengths measured under net normal stress of 25 kPa and 50 kPa were used for soils (M, N, and O) and soils (K and L), respectively.

The results of the analyses preformed are presented for the following four groupings of soils: 1) all soils used in the analysis, 2) low plasticity clays, 3) sandy soils, and 4) the soils that desaturate relatively fast (the fitting parameter, n >2). Figures 3.21 – 3.24 show the measured vs. predicted shear strengths for each soil group. The slopes of regression lines (S_L), R-squared values (R^2), and percentages of overestimation (PO) for three prediction methods are summarized in Table 3.4.

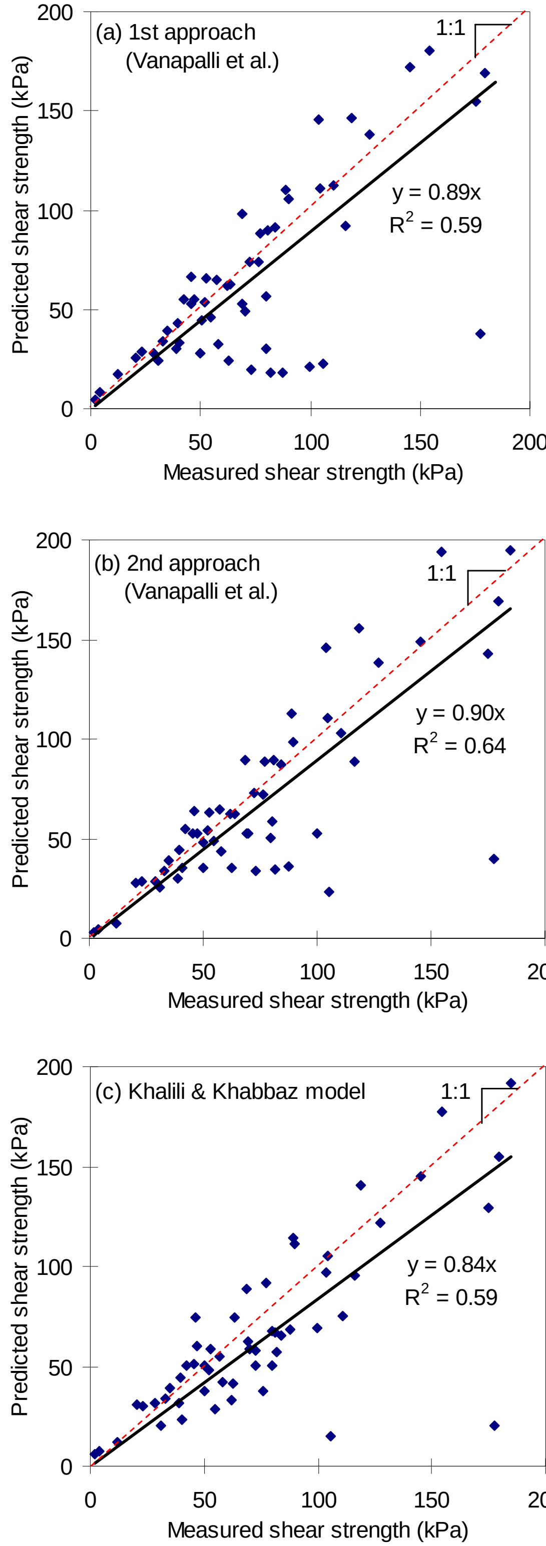

Fig. 3. 21 Measured vs. predicted shear strength for all soils used

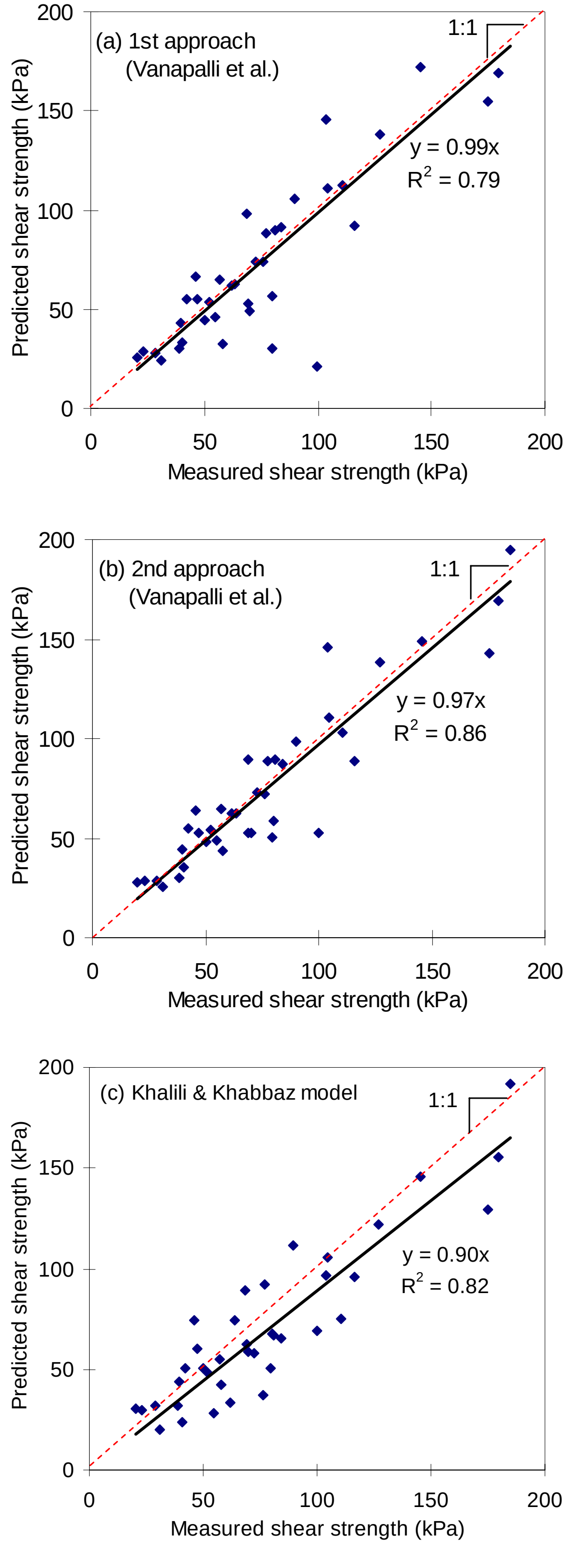

Fig. 3. 22 Measured vs. predicted shear strength for low plasticity clays

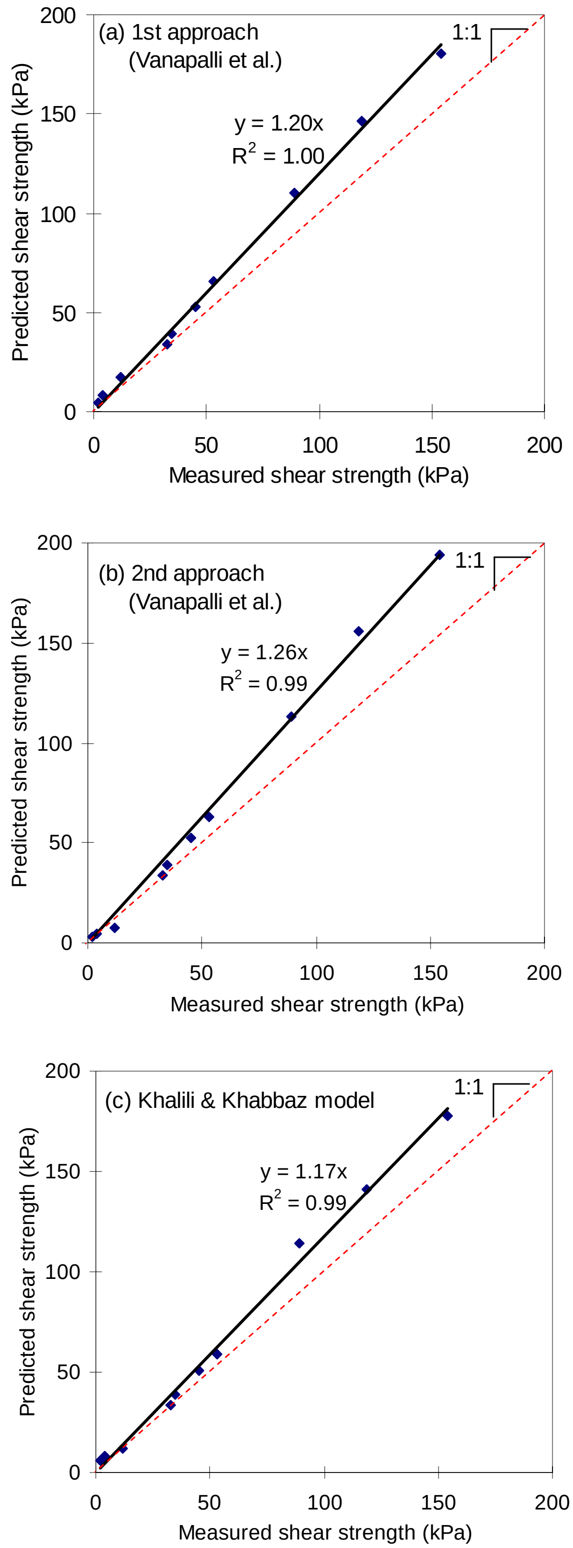

Fig. 3. 23 Measured vs. predicted shear strength for sandy soils

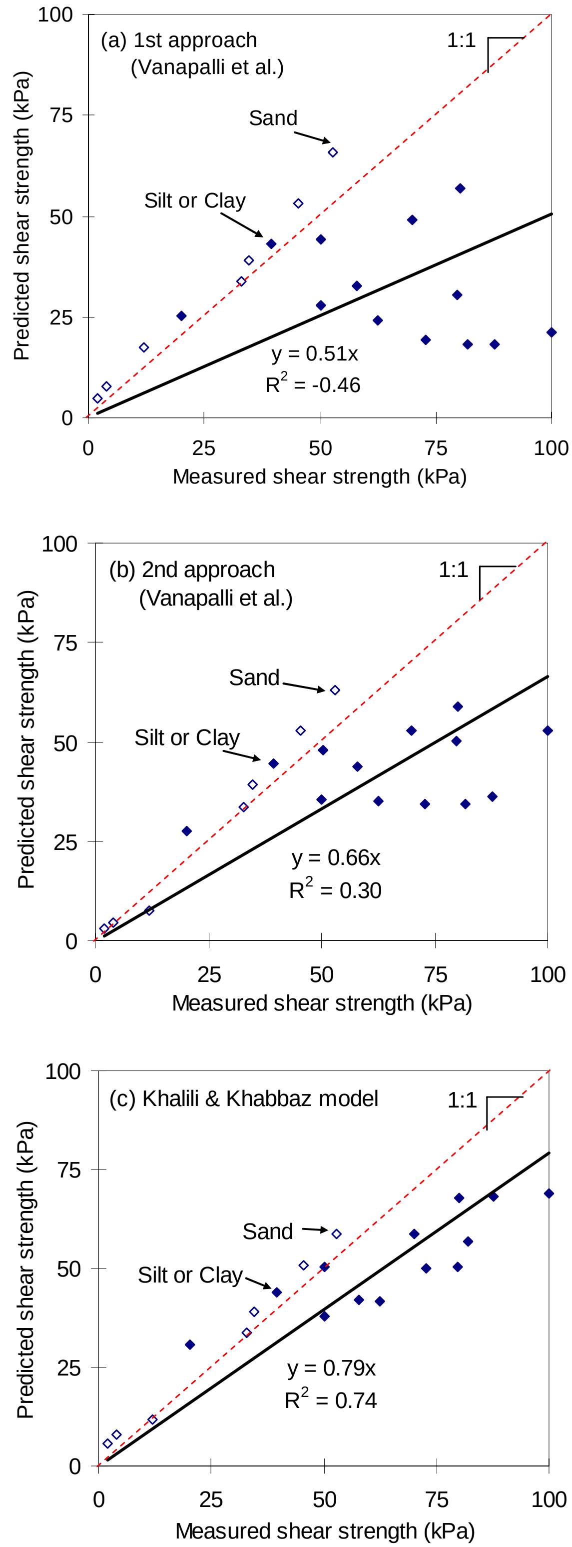

Fig. 3. 24 Measured vs. predicted shear strength for soils that desaturate relatively fast (n >2)

Table 3. 4 Summary of results for the net normal stress range of 0-50 kPa

Soil type	Vanapalli et al.'s 1st approach			Vanapalli et al.'s 2nd approach			Khalili & Khabbaz model			No. of data (No. of soil)
	S_L	R^2	PO (%)	S_L	R^2	PO (%)	S_L	R^2	PO (%)	
All soils	0.89	0.59	55	0.90	0.64	53	0.84	0.59	40	55 (15)
CL	0.99	0.79	53	0.97	0.86	53	0.90	0.82	34	38 (10)
Sand	1.20	1.00	100	1.26	0.99	90	1.17	0.99	90	10 (3)
$n > 2$	0.51	-0.46	45	0.66	0.30	40	0.79	0.74	40	20 (5)

* S_L = slope of linear regression line, *PO* = percentage of overestimation

For all soil used for analysis, the slopes of the regression lines were all less than one, with values of 0.89, 0.90, and 0.84 for Vanapalli et al.'s 1st approach, Vanapalli et al.'s 2nd approach and the Khalili and Khabbaz model, respectively, as shown in Table 3.4. That is, the predicted values tended to be smaller than those measured. The R-squared values estimated were 0.59, 0.64 and 0.59 respectively.

If only the low plasticity clays were used for analysis, the prediction methods are shown to produce better results. The slopes of regression line determined were 0.99, 0.97, and 0.90 and the values of R^2 were 0.79, 0.86, and 0.82 for Vanapalli et al.'s 1st approach, Vanapalli et al.'s 2nd approach, and the Khalili and Khabbaz model, respectively. Among the prediction methods, the slope of 0.99, which was closest to one, was found for Vanapalli et al.'s 1st approach and the highest R-squared value (0.86) was found for Vanapalli et al.'s 2nd approach.

For sandy soils used for analysis, most of the predicted shear strengths were greater than the measured shear strength (S_L > 1). The percentages of overestimation determined were 100%, 90%, and 90% for Vanapalli et al.'s 1st approach, Vanapalli et al.'s 2nd approach, and the Khalili and Khabbaz model, respectively. Very high R-squared values were observed for these data, but it should be noted that these results were determined from a very limited number of soils (N = 3) and shear strength data points (N = 10).

For the soils with n values higher than 2, there are very poor comparisons between measured and predicted shear strengths using Vanapalli et al.'s 1st and 2nd approaches, whereas the Khalili and Khabbaz model provided more meaningful results (S_L = 0.79, R^2 =0.74). From Fig. 3.24 it can be observed that the trend of predicted values of shear strength is different depending on soil type. The shear strengths of silt and clay are highly underestimated by the prediction methods, whereas those of sand are slightly overestimated. It is also of interest to note that the magnitude of the slope for the Khalili and Khabbaz model is greater than those for Vanapalli et al.'s 1st and 2nd approaches. For the other soil groups analyzed, the lowest values of slope were found for the Khalili and Khabbaz model. This finding is consistent with the results of the parametric study in section 3.2.2, which showed that the shear strength predicted from the Khalili and Khabbaz method tended to become larger than that predicted from Vanapalli et al.'s 2nd approach as the n value increases.

It should be noted that the results for silty soils (soils classified as MH or ML in the

USCS; soils B and C), although they were not presented in this paper, showed the poorest comparison between measured and predicted shear strengths, providing very small values of slopes ($S_L < 0.35$) and negative R-squared values for all the prediction methods.

Figure 3.25 shows the results for the natural soils used in this study (soils D, E, and F) using Vanapalli et al.'s 1st approach. As previously described, the κ value was estimated from the relationship to plasticity index (Eq. 3.7), even though the relationship was developed based on the shear strength data set from statically compacted soils. For the limited data available, the results show reasonably good comparison between the measured and predicted shear strengths.

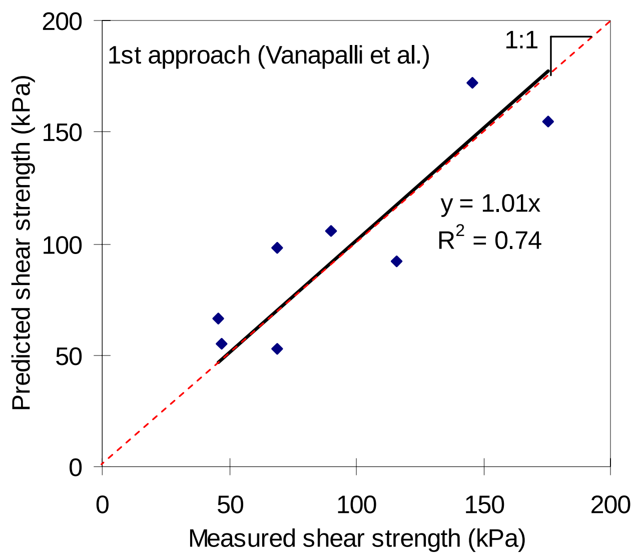

Fig. 3. 25 Measured vs. predicted shear strength for natural soils (Vanapalli et al.'s 1st approach)

The residual suction of 3000 kPa could reasonably be used for predicting shear strength of unsaturated soils in Vanapalli et al.'s 2nd approach (Eq. 3.9). As shown in Table 3.4, the very similar results of both Vanapalli et al.'s 1st and 2nd approaches are shown for all types of soil tested in this paper. For soil groups evaluated in this paper, there is very good comparison between the experimental results and the predicted values for the low plasticity soils using a residual suction of 3000 kPa. Also, this value of residual suction enables realistic shear strengths to be predicted for soils for which low residual suctions are estimated by the construction method, since Equation 3.9 would otherwise forces the shear strength to be a negative value beyond the residual suction. Therefore, the meaningful results (S_L = 1.01 and R^2 = 0.74) were able to be obtained for sandy soils which possibly have low residual suction values.

The Khalili and Khabbaz model (Eq. 3.10) was developed based on experimental shear strength data on 14 soils, in which air entry values ranges from 35 kPa to 153 kPa. However, the Khalili and Khabbaz model was used to predict the sear strength of soils having air entry values less than 35 kPa (soils C, I, and M) and the results of these comparisons are shown in Fig. 3.26. For the very limited shear strength data used, it can be seen that the predicted shear strengths are much lower than those measured.

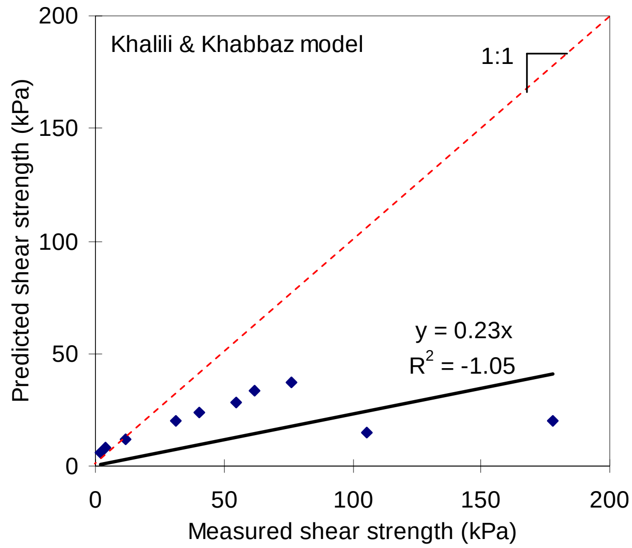

Fig. 3. 26 Measured vs. predicted shear strength for soils with air entry values < 35kPa (Khalili & Khabbaz model)

Comparison between the measured and predicted shear strength for high net normal stress range (50-200kPa)

The effect of stress state on the values of shear strength predicted using SWCCs developed under zero net normal stress (or small net normal stress) was investigated. The shear strength data for soils K thru O (Indian Head Till) were used for this study since the shear strengths under various net normal stresses were provided in the literature (50, 100, and 150 kPa for soils K and L; 25, 100 (or 75), and 200 kPa for soils M, N, and O). Comparisons between measured and predicted values of shear strength are presented both for low (0 -50 kPa) and high (50-200 kPa) net normal stress ranges. The measured vs. predicted shear strength determined from Vanapalli et al.'s 1st and 2nd approaches, and the Khalili and Khabbaz method are presented in Figs. 3.27 (a) and (b), (c) and (d), and (e) and (f), respectively .

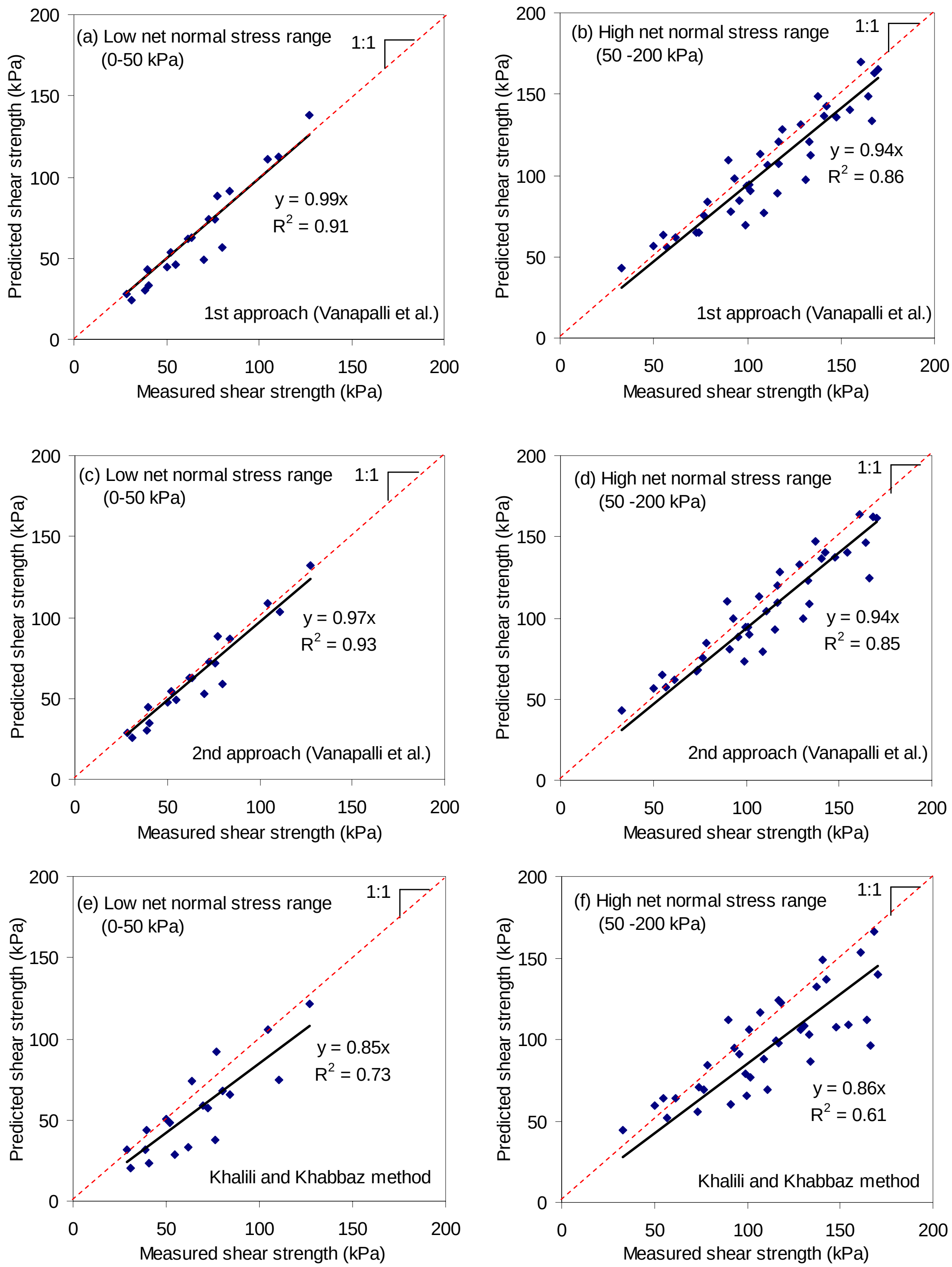

Fig. 3. 27 Measured vs. Predicted shear strength for low and high net normal stress ranges (Indian Head Till; soils K thru O)

Table 3.5 summarizes the values of slope (S_L), and the R^2 values determined from each method. For most of the procedures, the values of S_L and R^2 for high net normal stress decrease slightly when compared with those for low net normal stress (the Khalili and Khabbaz model showed little change in the S_L value). In other words, for the soils used in this analysis (Indian Head Till), the predicted values of shear strength in the higher net normal stress range have a slight tendency to more underestimate those measured with larger variation. This result can be explained by the variation of friction angle (ϕ') with matric suction. The shear strength failure surface, shown in Fig. 3.20(a), is defined by a constant friction angle, ϕ', with increasing matric suction, when it is determined from the SWCC performed at zero net normal stress. Therefore, there would be significant differences between the S_L values determined for high and low net normal stress ranges if the actual friction angle of soil changes as matric suction increases.

Table 3. 5 Summary of results for the net normal stress range of 50-200 kPa

Net normal stress range	**Vanapalli et al.'s 1st approach**		**Vanapalli et al.'s 2nd approach**		**Khalili & Khabbaz model**	
	S_L	R^2	S_L	R^2	S_L	R^2
0-50 kPa	0.99	0.91	0.97	0.93	0.85	0.73
50-200 kPa	0.94	0.86	0.94	0.86	0.86	0.61

A constant friction angle with increasing matric suction has been found for many soils reported in the literature (Fredlund et al., 1993; Gallage and Uchimura, 2006; Rahardjo et al., 2004; Nishimura et al., 1999; Rahardjo et al., 1995; Melinda et al., 2004). However, it also has been reported that the friction angle is influenced by matric suction for some soils

(Escario and Juca, 1989; Lee et al., 2005; Feuerharmel, 2006). Figure 3.28 shows the relationship between the friction angle and matric suction for several soils. The Madrid clayey sand (soil H) shows the friction angle is independent of matric suction. The data from the Indian Head Till (soils M and O) shows a slight increase in the friction angle (from 23° to 26°) as the matric suction increases up to 500 kPa. Therefore, one would expect there to be a slight decrease in the S_L value under higher net normal stresses. In contrast, the Botucatu silty clay shows very significant increase in the friction angle as matric suction increases. For soils showing this behavior, the predicted values of shear strength at high matric suction range would tend to become significantly underestimated as the net normal stress increases, when there is a good agreement between the measured and predicted shear strengths at low net normal stresses.

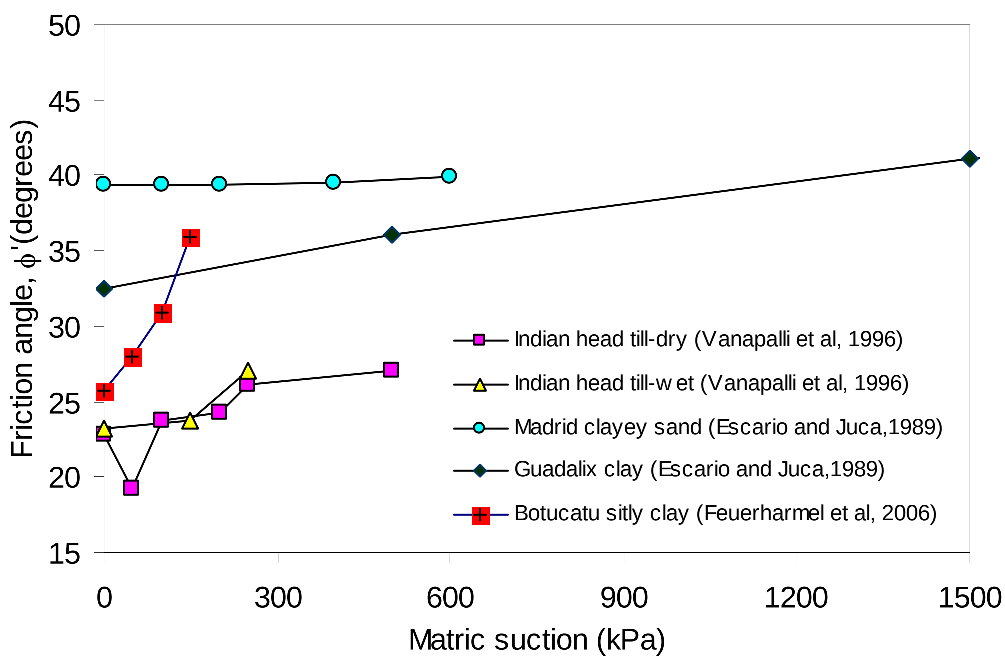

Fig. 3. 28 Internal friction angle, ϕ', vs. matric suction for several types of soils

Effect of soil-water characteristic curve on the predicted shear strength

SWCCs are conventionally determined in the laboratory only with the application of a nominal normal stress or without the application of any applied vertical stress. However, experimental results show that the SWCCs of some soil types are significantly affected by the change of net normal stress (Vanapalli et al., 1999; Ng and Pang, 2000; Lee et al., 2005; Rorie, 2006). For this reason, it has been suggested by several researchers that the shear strength envelope of unsaturated soil would be more precisely described using SWCCs that have been determined under different stress states.

Soils M and O (Indian Head Till) were used in order to demonstrate the effect of stress state (at which the SWCCs were measured) on the prediction of shear strength. These soils were selected since both the SWCCs and shear strength data were measured at different net normal stresses. Soil M is compacted dry of optimum and Soil O is compacted wet of optimum. Figure 3.29 shows the SWCCs developed for these compacted soils at equivalent pressures of 25, 100 and 200 kPa. For the soil compacted dry of optimum the soil-water characteristics appear to be highly dependent on the stress condition which might be expected because of the predominant macrostructure (pores) in the soil developed during the compaction. Meanwhile, the soil-water characteristics of soils compacted wet of optimum appear to be the same in spite of the different stress conditions because of the micro-structures in the soil (Vanapalli et al., 1999)

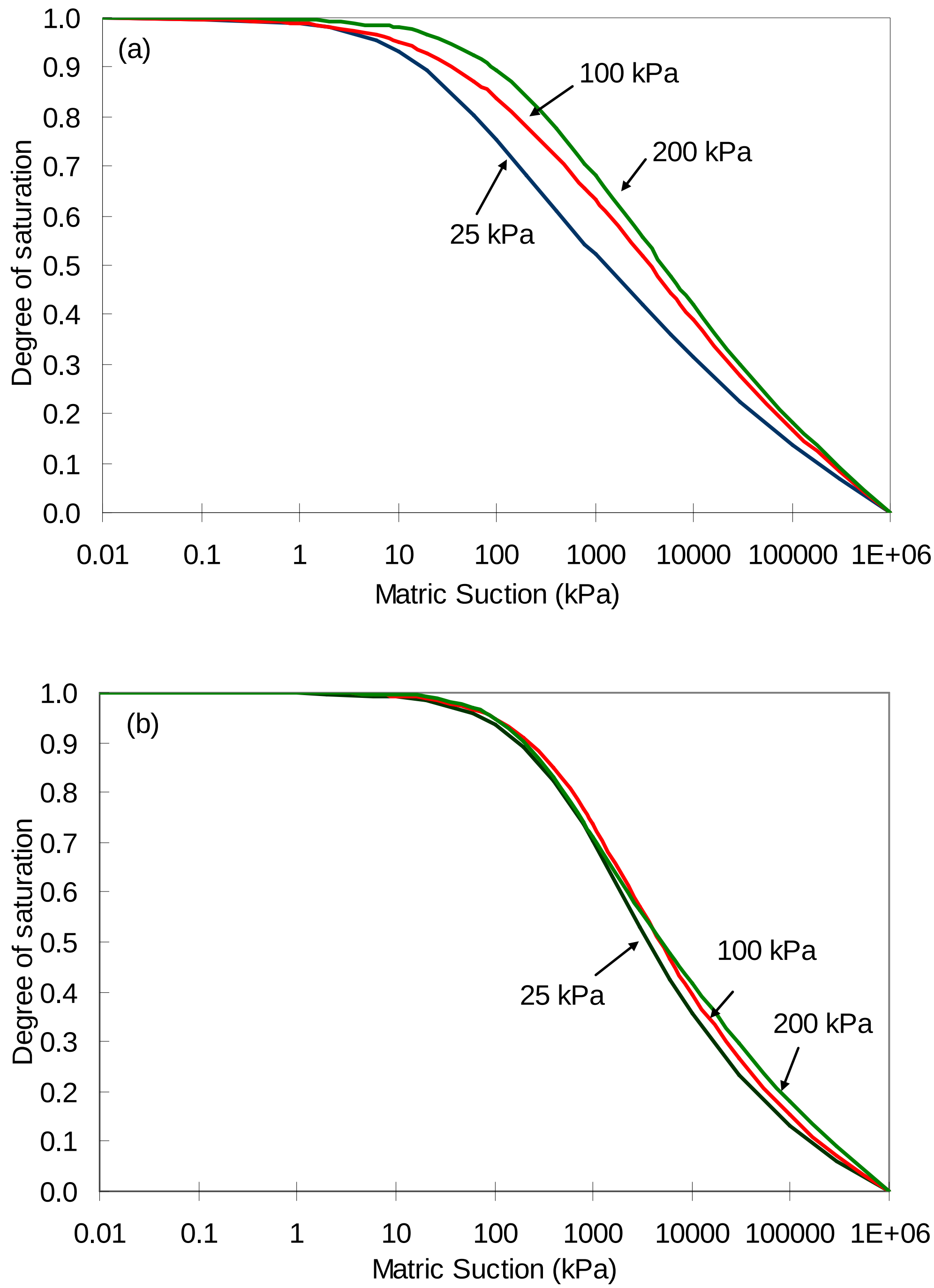

Fig. 3. 29 SWCCs performed at different net normal stresses; (a) soil compacted dry of optimum - soil M and (b) soil compacted wet of optimum - soil O (after Vanapalli et al., 1996)

In this paper, the results of analyses are presented based on two different approaches predicting the shear strength of unsaturated soils. One approach uses one SWCC performed at a net normal stress of 25 kPa to predict shear strengths at different net normal stresses (Fig. 3.20a). The other approach uses the SWCCs performed at different net normal stresses in predicting shear strengths under the different net normal stresses (Fig. 3.20b). The results of both approaches are shown in Fig. 3.30. Figures 3.30 (a) and (b), (c) and (d), and (e) and (f) present the measured vs. predicted shear strengths determined from Vanapalli et al.'s 1^{st} and 2^{nd} approaches, and the Khalili &.Khabbaz method, respectively. The solid lines in the figures represent the regression lines determined from the former approach and the broken lines represent those determined by the latter approach. A significant increase in the regression line slope is observed for the soil compacted dry of optimum (soil M) when using the SWCCs developed at different normal stresses. Therefore, Vanapalli et al.'s 1^{st} and 2^{nd} approaches tend to slightly overestimate the shear strength using the SWCCs at different stresses (S_L = 1.13 and 1.10, respectively). For the Khalili & Khabbaz model, the shear strength was somewhat more reliably predicted from the SWCCs at different stresses. Table 6 summarizes the values of slope (S_L) and the R^2. However, caution is warranted in interpreting the significance of these findings, i.e. as to whether or not the shear strength contribution due to suction can be more accurately estimated using SWCCs that were determined under different stress states due to the limited number of soils and shear strength data used.

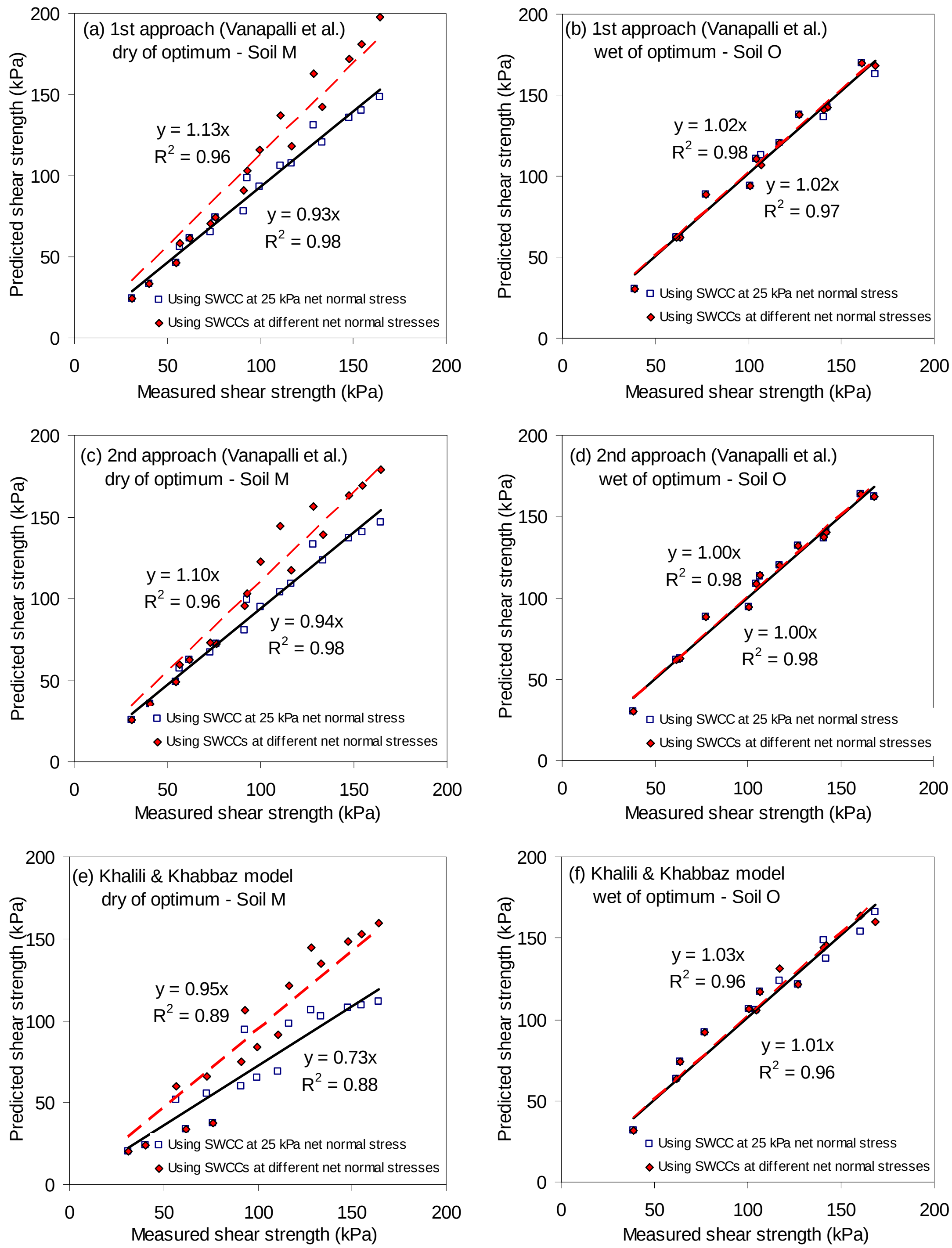

Fig. 3. 30 Measured vs. predicted shear strength using the SWCC at 25 kPa net normal stress and the SWCCs at different net normal stresses (soils M and O)

Table 3. 6   Summary of results (using the SWCCs at different net normal stresses)

Soil	**Net normal stress**	**Vanapalli et al.'s 1st approach**		**Vanapalli et al.'s 2nd approach**		**Khalili & Khabbaz model**	
		S_L	R^2	S_L	R^2	S_L	R^2
Dry of optimum	25 kPa	0.93	0.98	0.94	0.98	0.73	0.88
	Diff. stresses	1.13	0.96	1.10	0.96	0.95	0.89
Wet of optimum	25 kPa	1.02	0.97	1.00	0.98	1.03	0.96
	Diff. stresses	1.02	0.98	1.00	0.98	1.01	0.96

3.5 SUMMARY AND CONCLUSIONS

In this research, comparisons among the shear strengths predicted from three empirical procedures (1st and 2nd approaches of Vanapalli et al., and Khalili and Khabbaz model) that use SWCCs were presented. In order to study the influence of the SWCC on the predicted shear strength for these procedures a parametric study was performed by varying the *a* and *n* values of the Fredlund and Xing SWCC model. A comprehensive analysis was undertaken to examine shear strength data of fifteen soils published in the literature using these procedures. Comparisons are presented between measured and predicted shear strengths taking into account soil type, net normal stress range, and stress state under which the SWCCs were measured.

From the results of the parametric study, the following conclusions can be drawn:

1) For 1st and 2nd approaches of Vanapalli et al., the predicted shear strength increases as the *a* value (related to air entry value) increases or the *n* value (related to slope of SWCC) decreases.
2) For the Khalili and Khabbaz model, the predicted shear strength for a given net

normal stress increases as the *a* value increases. However, the predicted shear strength is independent of the *n* value (rate of desaturation). For example, the same value of shear strength would be predicted irrespective of the slope of the SWCC, if the air entry values of two soils are the same.

3) There is a difference in the shear strengths predicted using the three procedures although the same SWCC is used for the prediction. This difference was shown to be either insignificant or significant depending on the shape of SWCC. For example, at a given values of *a* (10 or 100), Vanapalli et al.'s 2nd approach predicted much higher shear strength than that of the Khalili and Khabbaz model, for soils with an *n* value of 0.5. However, the shear strengths predicted from the Khalili and Khabbaz method are greater than that predicted from Vanapalli et al.'s 2nd approach for soils with an *n* value of 3.

From the comparisons between the measured and predicted shear strengths, the following conclusion can be summarized:

1) For low plasticity clays, all prediction methods provide relatively good comparisons between measured and predicted shear strengths with the predicted values slightly smaller than those measured (underpredicted by a maximum of 10% based on the computed slopes of regression lines). In contrast, for sandy soils the predicted shear strengths are greater than the measured shear strengths (overpredicted by a maximum of 26%). The Khalili and Khabbaz model generally provides the smallest value of shear strength for the low plasticity clays and sandy soils.
2) For soils that desaturate relatively fast ($n > 2$), the 1st and 2nd approaches of Vanapalli

et al. provide very poor comparison between the measured and predicted shear strengths, predicting significantly smaller values of shear strength (on average, 49% and 55 % smaller than the measured shear strength, respectively) with high variation of data. More meaningful results are found using the Khalili and Khabbaz model, with the predicted values being, on average, only 21% smaller than those measured. Among soil types with n values higher than 2, the predicted shear strengths are highly underestimated for fine grained soils (clay or silt), while the predicted shear strengths are slightly overestimated for sandy soils.

3) For the purpose of this research, several assumptions were made to enable the use of the three procedures. First, the relationship between the κ value and plasticity index (Eq. 3.7), which was developed from shear strength data on statically compacted soils, was applied to the natural soils (Vanapalli et al.'s 1st approach). Secondly, the residual suction was assumed to be 3000 kPa irrespective soil types (from Vanapalli et al.'s 2nd approach). Lastly, the Khalili and Khabbaz method was applied irrespective of the magnitude of air entry value. From the results of analysis for the limited amount of data, it could be suggested that the relationship can be used for natural soils as well as compacted soils and that a residual suction of 3000 kPa can be reasonably used to predict shear strength for the sandy soils and low plasticity clays. The Khalili and Khabbaz model predicts values of shear strength much smaller than those measured (on average 77% smaller) for soils in which the air entry value is small (< 35 kPa).

4) The effect of net normal stress state on the predicted shear strength would be significant if the friction angle of the soil increases significantly with increasing matric suction. For the soils showing this behavior, the predicted values of shear

strength at high matric suction tended to be significantly underestimated with increasing net normal stress, if there was a good agreement between the measured and predicted shear strengths at low net normal stresses.

5) The shear strengths predicted using the SWCCs performed at different net normal stresses would be significantly higher than that predicted using the one SWCC performed at zero or nominal net normal stress, if the SWCCs are highly dependent on stress state.

3.6 REFERENCES

Bao, C., Gong, B., and Zhan, L. (1998). Properties of unsaturated soils and slope stability of expansive soils, Proceeding of the 2nd International Conference on Unsaturated Soils (UNSAT 98). Beijing, China, 1, pp. 71-98.

Bishop, A. W. (1959). The principle of effective stress, Tecknish Ukebland, 106 (39), pp. 859-863.

Blight, G.E. (1961). Strength and consolidation characteristics of compacted soils, Ph.D. dissertation, Univ. of London, London, England, p217.

Donald, I. B. (1961). The mechanical properties of saturated and partly saturated soils with special reference to negative pore water pressure, Ph.D. dissertation, Univ. of London, London, England.

Ecario, V., and Juca, J. F. T. (1989). Strength and deformation of partly saturated soils, Proc. of the 12th International Conference on Soil Mechanics and Foundation Engineering, Rio de Janerio, 2.

Feuerharnel, C., Pereira, A., Gehling, W. Y. Y., and Bica, A. V. D. (2006). Determination of the shear strength parameters of two unsaturated colluvium soils using the direct shear test, Proceedings of the Fourth International Conference on Unsaturated Soils, Geotechnical Special Publication, No. 147, Vol.2, pp. 2570-2581.

Fredlund D. G., and Morgenstern, N. R., and Widger, R. A. (1978). The shear strength of unsaturated soils. Canadian Geotechnical Journal, 15, pp. 313-321.

Fredlund, D. G. and Rahardjo, H. (1993). Soil Mechanics for unsaturated soils, New York: Wiley.

Fredlund, D. G., and Xing, Anqing. (1994). Equations for the soil-water characteristic curve, Canadian Geotechnical Journal, 31, pp. 521-532.

Fredlund, D. G.., Xing, A. X., Fredlund, M. D. and Barbour, M. D. (1995). The relationship of the unsaturated soil shear strength to the soil-water characteristic curve, Canadian Geotechnical Journal, 32, pp. 440-448.

Gallage C. P. K., and Uchimura T. (2006). Effect of wetting and drying on the unsaturated shear strength of a silty sand under low suction, Proceedings of the Fourth International Conference on Unsaturated Soils, Geotechnical Special Publication, No. 147, Vol.1, pp. 1247-1258.

Gan, J. K. M., and Fredlund, D.G. (1986). Multi-stage direct shear testing of unsaturated soils, Geotechnical Testing Journal, ASTM, 11(2), pp. 132-138.

Gan, J.K.M., Fredlund, D.G., and Rahardjo (1988). Determination of shear strength parameters of an unsaturated soil using the direct shear test, Canadian Geotechnical Journal, 25, pp. 500-510.

Garven, E. A. and Vanapalli, S. K. (2006). Evaluation of empirical procedures for predicting the shear strength of unsaturated soils, Proceeding of the Fourth International Conference on Unsaturated Soils, Geotechnical Special Publication No. 147, Vol.2, pp. 2570-2581.

Han, K. K., Rahardjo, H., and Broms, B. B. (1995). Effect of hysteresis on the shear strength of a residual soil, Proceedings of the First International Conference on Unsaturated soil (UNSAT 95), Paris, France, 3, pp. 499-504.

Ho, D. Y. F., and Fredlund, D. G. (1982). Multi-stage triaxial tests for unsaturated soils. Geotechnical Testing Journal, ASTM, 5, pp. 18-25.

Khalili, N., Geiser, F., and Blight, G. E. (2004). Effective stress in unsaturated soils: Review with new evidence, International Journal of Geomechanics, 4(2), pp.15-26.

Khalili, N., and Khabbaz, M. H. (1998). A unique relationship for χ for the determination of the shear strength of unsaturated soils, Geotechnique 48. No. 5, pp. 681-687.

Lee, I., Sung, S., and Cho, G. (2005). Effect of stress state on the unsaturated shear strength of a weathered granite, Canadian Geotechnical Journal, 42, pp. 624-631.

Melinda, F., Rahardjo, H., Han, K. K., and Leong E. C. (2004). Shear strength of compacted soil under infiltration condition, Journal of Geotechnical and Geoenvironmental Engineering, 130(8), pp. 807-817.

Nishimura, T., Hirabayashi, Y., Fredlund, D.G., and Gan J.K.-M. (1999). Influence of stress history on the strength parameters of an unsaturated statically compacted soil, Canadian Geotechnical Journal, 36, pp. 251-261.

Ng, Charles, W. W., and Pang, Y. W. (2000). Influence of stress state soil-water characteristics and slope stability, Journal of Geotechnical and Geoenvironmental Engineering, Vol. 126, No. 2, pp. 156- 166.

Oberg, A., and Sallfours, G. (1997). Determination of shear strength parameters of unsaturated silts and sands based on the water retention curve, Geotechnical Testing Journal, 20, pp. 40-48.

Oloo, S. Y. and Fredlund D. G. (1996). A method for determination of ϕ^b for statically compacted soils, Canadian Geotechnical Journal, 33, pp. 272-280.

Rahardjo, H., Lim, T. T., Chang, M. F., and Fredlund, D. G. (1995). Shear-strength characteristics of a residual soil, Canadian Geotechnical Journal, 32, pp. 60-70.

Rahardjo, H., Heng, O. M., and Leong, E. C. (2004). Shear strength of a compacted residual soil from consolidated drained and constant water content triaxail tests, Canadian Geotechnical Journal, 41, pp. 421-436.

Rassam, D. W., and Williams, D. J. (1999). A relationship describing the shear strength of unsaturated soils, Canadian Geotechnical Journal, 32, pp. 60-77.

Rorie, D. (2006). Investigation of soil suction in low density silty sands, MS thesis, North Carolina State University, Raleigh

Thu, T. M., Rahardjo, H., and Leong, E. C., (2006). Shear strength and pore-water pressure characteristics during constant water content triaxial tests. Journal of Geotechnical and Geoenvironmental Engineering, 132(3), pp. 411-419.

Tinjum, J. M. and Benson, C. H. and Blotz, L. R. (1997). Soil-water characteristic curves for compacted clays, Journal of Geotechnical and Geoenvironmental Engineering, Vol. 123, No. 11, pp. 1060-1069.

Vanapalli, S. K. (1994). Simple test procedures and their interpretation in evaluating the shear strength of unsaturated soils. Ph.D. thesis, University of Saskatchewan, Saskatoon.

Vanapalli, S. K., and Fredlund, D. G., (2000). Comparison of different procedures to predict unsaturated soil shear strength, Geotechnical Special Publication, 99, pp.195-209.

Vanapalli, S. K., Fredlund, D. G., and Pudahl, D. E., and Clifton, A. W. (1996). Model for the prediction of shear strength with respect to soil suction, Canadian Geotechnical Journal, 33, pp. 379–392.

Vanapalli, S. K., Sillers, W. S., and Fredlund, M. D. (1998). The meaning and relevance of residual water content to unsaturated soils, Proceedings of the 51st Canadian Geotechnical Conference, Edmonton, pp.101-108.

Vanapalli, S. K., Fredlund, D. G., and Pufahl, D. E. (1999). The influence of soil structure and stress history on the soil-water characteristic of a compacted till, Geotechnique, 49(2), pp. 143-159.

Vanapalli, S.K., Wright, A., and Fredlund, D.G., (2000). Shear strength of two unsaturated silty soils over the suction range from 0 to 1,000,000 kPa, Proceedings of the 53rd Canadian Geotechnical Conference, Montreal, pp. 1161-1169

van Genuchten, M. Th. (1980). A closed-form equation for predicting the hydraulic conductivity of unsaturated soils, Soil Science Society of America Journal, 44, pp. 892-898.

Wulfsohn, D., Adams, B. A., Fredlund, D. G.. (1996). Application of unsaturated soil mechanics for agricultural conditions, Canadian Agricultural Engineering, Vol. 38 (3), pp. 173-181.

CHAPTER 4

Numerical simulation of MSE wall behavior during construction based on unsaturated soil properties

4.1 INTRODUCTION

Limit equilibrium analyses have been typically used for the design of internal stability of geosynthetic reinforced soil (GRS) retaining structures. However, there are several disadvantages of limit equilibrium analyses such as the inability to provide deformation information (i.e. face deflection) and the internal stress distributions within GRS retaining structures (i.e. reinforcement tension). Also, a recent study of performance of instrumented fill-scale geosynthetic reinforced soil walls (Allen et al., 2002) showed this current design method to overpredict stress levels inside the GRS retaining structures. Several working stress analyses of GRS walls using numerical simulations have been successfully performed to improve the internal stability design as well as provide deformation predictions of GRS walls (Lee, 2000; Hatami and Bathurst, 2001 and 2003).

It has been proposed that marginal soils (greater than 50% fines) with low plasticity (PI<20) may be used for MSE construction (Collin, 1997). The use of marginal fill clearly has significant impact on the cost of MSE wall construction. However, there are increased risks associated with using marginal soils for MSE walls, as indicated by the reported problems such as large deformations and failures resulting from water infiltration. Twenty out of 26 case histories on geosynthetic MSE wall failures identified by Soong and Koerner (1999) were for walls constructed with silt and clay soils.

A 5.4-m high MSE wall constructed with marginal fills in the Research Triangle Park (RTP) of North Carolina collapsed in March, 2001 during a rainy period shortly after completion of wall construction. Since compacted soils are used as backfills, unsaturated soil mechanics plays a dominant role in the behavior of MSE walls. In this study, numerical simulations with unsaturated soil properties (elastic modulus and shear strength) were performed to provide better understanding of the behavior of failed MSE wall at the end of construction and during rainfall. The finite difference code, FLAC (Fast Lagrangian Analysis of Continua), was used for this simulation because of its excellent capability for modeling geotechnical related stability problems and its options for extended programming. The site investigation at the MSE wall showed that the backfill was possibly compacted very dry of optimum and the backfill within a 1.2m to 1.8m wide zone behind the wall face was not properly compacted. Therefore, the effects of the low as-compacted water content and poorly compacted zone on the behavior of wall are highlighted. In this chapter, MSE wall behavior at the end of construction is presented, and the deformation of wall due to rainfall will be described in the following chapter (Chapter 5).

4.2 PREVIOUS NUMERICAL APPROACHES

In order to predict the response of reinforced-soil retaining walls during construction, numerical models have been developed based on the measured responses of instrumented, full scale GRS walls (constructed with granular fill). The developed models were shown to be able to predict the behavior of the GRS walls successfully, with a good agreement between the measured and computed wall responses. The following sections provide brief summaries of the numerical models reported in previous research.

4.2.1 Lee (2000)

Lee (2000) developed a FLAC numerical model that is able to predict the behavior of a geosynthetic reinforced retaining wall at the end of construction. In his research, material properties such as plane strain soil properties, low confining pressure, soil dilation angle, and in-soil and slow strain rate geosynthetic reinforcement properties were investigated. An extensive parametric study was performed using the developed model and suggested material properties. Through this parametric study, the influence of design factors relevant to GRS walls, such as soil properties, reinforcement stiffness, and reinforcement spacing on the performance, were investigated.

4.2.2 Hatami & Bathurst (2001)

Hatami & Bathurst (2001) modeled the measured response of an instrumented, full-scale segmental retaining wall during construction. The model adopted Mohr- Coulomb failure criterion and a dilation angle in the FLAC program. The stress-dependent hyperbolic model proposed by Duncan et al. (1980) was used to represent non-linear elastic response of the backfill during construction. The response parameters for the wall, such as the facing lateral displacement, toe reaction loads, and reinforcement strain distribution, were examined. In addition, three different dilation angles (0°, 10°, and 26°) were included to examine the influence of backfill dilation angle on segmental wall response.

4.2.3 Hatami & Bathurst (2003)

Hatami & Bathurst (2003) accounted for the backfill stress-dependent stiffness properties and the nonlinear reinforcement strain-dependent axial stiffness in their numerical model. They compared the measured response of GRS wall with the responses of GRS wall that were simulated using two different soil constitutive models: the linear elastic model and the stress dependent model (Hyperbolic model). The measured and numerical results of both models for the construction stage of the walls showed satisfactory agreement for different response parameters including displacements, reinforcement strain and history of toe forces. The reinforcement strain distributions obtained from a hyperbolic soil model were found to be in better agreement with the measured data than those obtained from the linear elastic model.

4.3 PROJECT DESCRIPTION

A 5.4-m high MSE wall in the Research Triangle Park (RTP) of North Carolina experienced a local collapse in 2001 during a period of rainfall shortly after completion of wall construction. The MSE wall geometry and cross section are shown in Fig. 4.1. The wall was built with 11 layers of 4.75m long polyester geogrid reinforcement (Fortrac 35/20-20 Geogrid, Huesker Inc.). Vertical spacings of reinforcements varied from 0.2m to 0.6m throughout the wall height as shown in Fig. 4.1. Commercially available Rockwood blocks (Classic 8, Rockwood retaining walls Inc.) were used as the facing system unit. The blocks were 300mm deep, 200mm high, and 450mm wide, and had a mass of 35 kg per unit. The facing batter of the wall was approximately 7 degrees from vertical, and the 2m-high back-slope portion (18 degrees) extended from the wall face. Crushed gravel (No. 57 stone) was used to infill the spaces between adjoining modular block units and to create a 300-mm thick drainage layer behind the wall facing. The connection between blocks relied on the friction between the contact block material and gravel material filled in the blocks.

The locally available low plasticity silty soil (I_P=10) was used as backfills for the wall. According to the Unified Soil Classification System (USCS), the soil was classified as CL. The standard proctor test yielded a maximum dry unit weight of 1.90g/cm^3 with an optimum water content of 11.7%. More details of backfill material properties are described in Chapter 2.

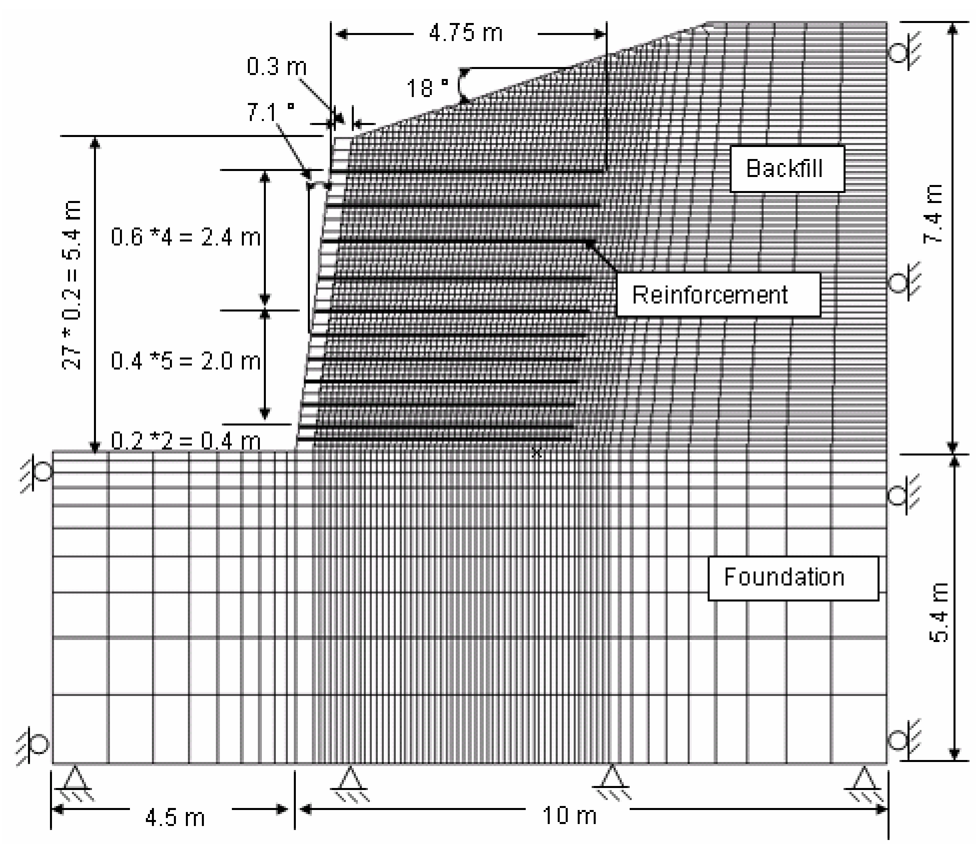

Fig. 4. 1 MSE wall geometry and numerical model used in FLAC

4.4 NUNERICAL ANALYSIS

4.4.1 General

Previous researchers have showed that failures of slopes or MSE walls during rainfall were primarily associated with the decrease in matric suction of the unsaturated soils (Ng and Pang, 2000; Cho and Lee, 2001; Yoo and Jung, 2006). For this reason, efforts in this study were made to investigate the behavior of the MSE wall using unsaturated soil properties (elastic modulus and shear strength) as a function of soil suction. The site investigation of the RTP MSE wall showed that the backfill was compacted very dry of optimum, and the backfill within a 1.2m to 1.8m wide zone behind the wall face was not properly compacted. This poorly compacted zone could occur because the backfills are generally hand-compacted in the zone behind wall face, and sometimes small compaction efforts are intentionally applied in order to avoid wall movements at the face. It was believed that the MSE wall failure was primarily caused by these factors, among others, discovered during the post-failure site investigation. Therefore, this research focused on the behavior of the MSE wall assuming it was constructed with backfill compacted very dry side optimum (w = 4.8%, -7 % of OMC). Also, the effect of a poorly compacted zone behind the wall face (case 2) on the wall behavior was compared to a situation in which the entire mass was adequately compacted (case 1), as shown in Fig. 4.2. The properties of soils compacted to dry densities of 1.79 g/cm^3 (R.C.= 94%) and 1.60 g/cm^3 (R.C.= 84%) were used to simulate well and poorly compacted backfills, respectively. These well and poorly compacted backfills were designated as soil H and soil L. In this chapter, only MSE wall behavior at the end of construction is described, while the wall deformation due to rainfall will be investigated in Chapter 5.

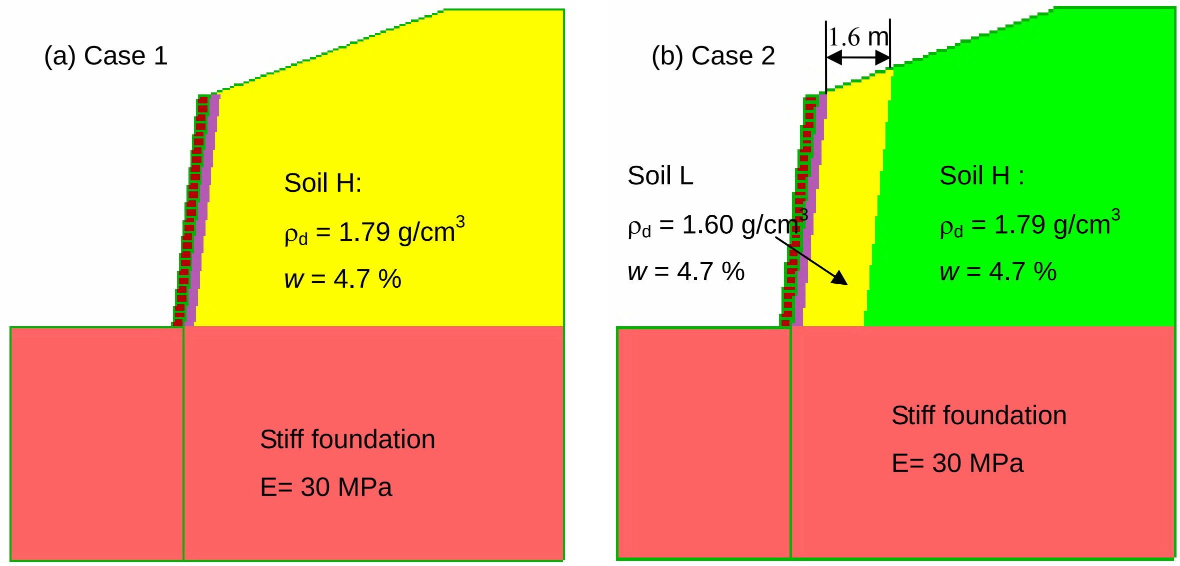

Fig. 4. 2 MSE wall with (a) uniform compaction and (b) low density zone behind the wall face.

4.4.2 FLAC model

The finite difference code, FLAC (Itasca, 2000), was used to simulate the response of the reinforced wall during wall construction. The FLAC program has an excellent capability of modeling geotechnical engineering related stability problems and an extended programming ability providing a FISH programming code to allow users to define their own constitutive material model.

Figure 4.1 shows the numerical grids used for the MSE wall. The simulation modeled the sequential bottom-up construction of the wall facing, soil and reinforcement. The backfill and facing units of the wall model were elevated in lifts of 0.2 m, which was the same as the height of the modular block units, and the reinforcement layers were placed in the model as each reinforcement elevation was reached. To eliminate boundary effects, the unreinforced backfill (right boundary) and the foundation soil in front of the wall (left boundary) were extended a distance equal to at least the length of the reinforced zone, and the foundation soil of the MSE wall models was extended to a depth at least the height of the MSE wall (Lee, 2000). The FLAC mesh boundary conditions were set using horizontal restraints for the left and right boundaries and total restraints for the bottom boundary.

Figure 4.3 shows a cross section of a MSE wall model developed in FLAC. Elastic material elements were used to represent modular blocks, and Mohr-Coulomb material elements were used to represent the gravel column and the MSE wall backfill. The behavior of the geosynthetic reinforcements was simulated using the cable element. Interface elements were used to describe the interaction between backfill soil and modular block and interfaces between modular blocks.

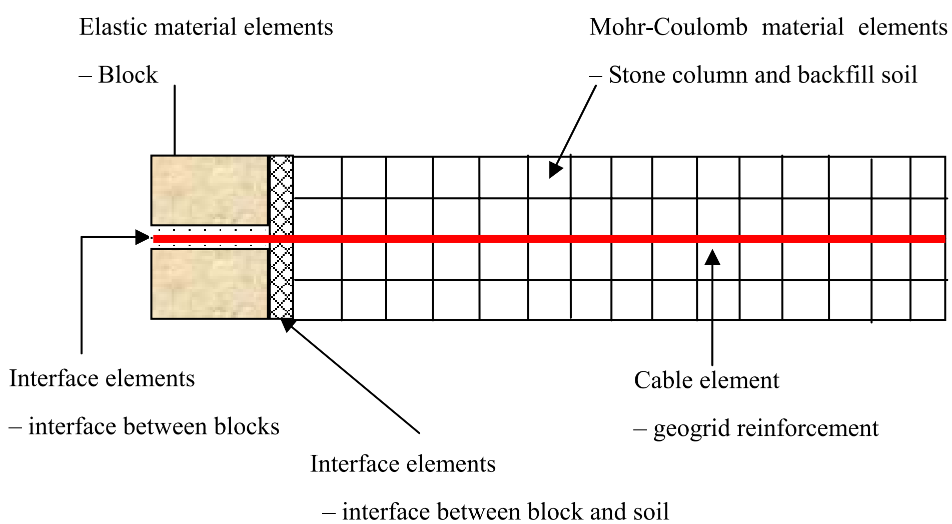

Fig. 4. 3 MSE wall modeled using FLAC (after Lee, 2000)

4.4.3 Material properties

In this section, input material properties for the numerical models are described. Most of these input material properties, such as stiffness and shear strength behavior of construction materials (backfill soil, gravel column, and geosynthetic reinforcement), vary as a function of stress state (normal stress or matric suction). Accordingly, stress dependent models were considered for these material properties, and they were updated based on changes in stress states variables during construction (lift of the backfill) by the programmed FISH subroutine.

Modulus of backfills

The loading condition during wall construction can be characterized as the constant water content condition (CW), in which the pore-air pressure remains constant (drained) and the pore-water pressure increases due to compression (undrained) during incremental backfill loadings (Fredlund and Rahardjo, 1993; Thu et al., 2006). The elastic modulus for CW loading condition could be estimated as somewhere between those for drained loading (drained for both air and water) and undrained loading (undrained for both air and water). However, since the specimens compacted at very low water content (w = 4.7%) showed no significant difference in drained and undrained moduli, as described in Chapter 2, either undrained or drained moduli can be used in order to investigate the volume change behavior of backfills during wall construction. Therefore, the undrained modulus was adopted in this study.

The stress dependent moduli of backfill materials were estimated from the results of conventional oedometer tests by the procedures described in Chapter 2. Figure 4.4 shows the estimated constitutive relations for undrained loading over the relevant range of overburden pressure, from 25 to 200 kPa. In order to develop a smooth continuous constitutive curve from the origin, the stress-strain relations at low stress range were redrawn as shown in Fig. 4.4 (the dotted lines). This procedure was accomplished by drawing the linear line from the origin to a point on the constitutive curve where that linear line was tangent to the constitutive curve. The undrained moduli were then computed from the slopes of constitutive curves (coefficient of volume change, m_1^s). Figure 4.5 shows the determined undrained modulus functions with respect to mean stress for soils H and L. The modulus was constant in low mean stress range (E_{min}) and then increased linearly as the mean stress increased.

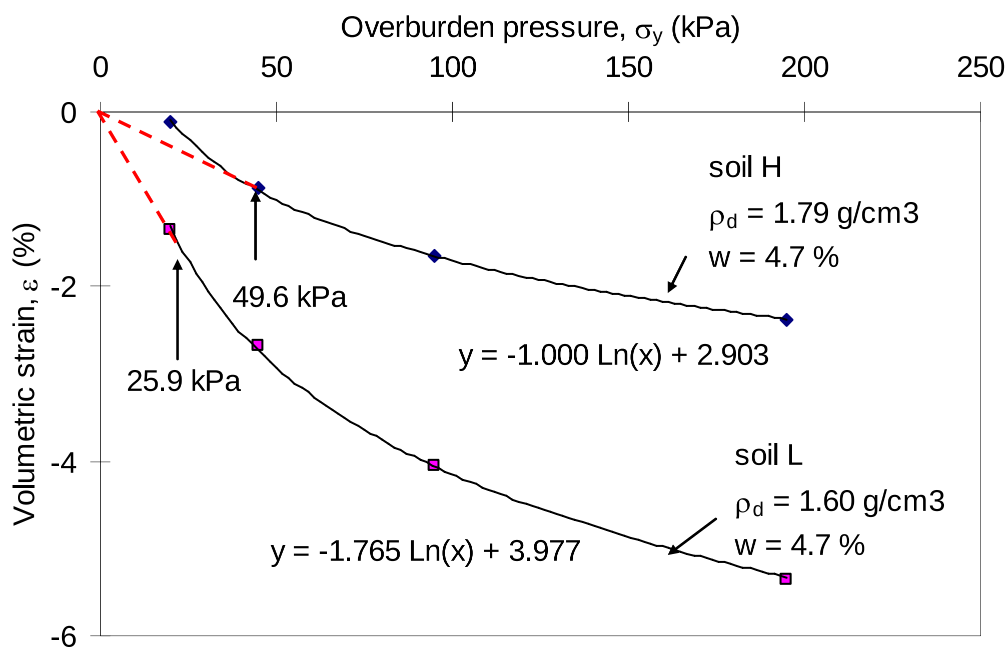

Fig. 4. 4 Estimated constitutive relations for undrained loading (Soils L and H)

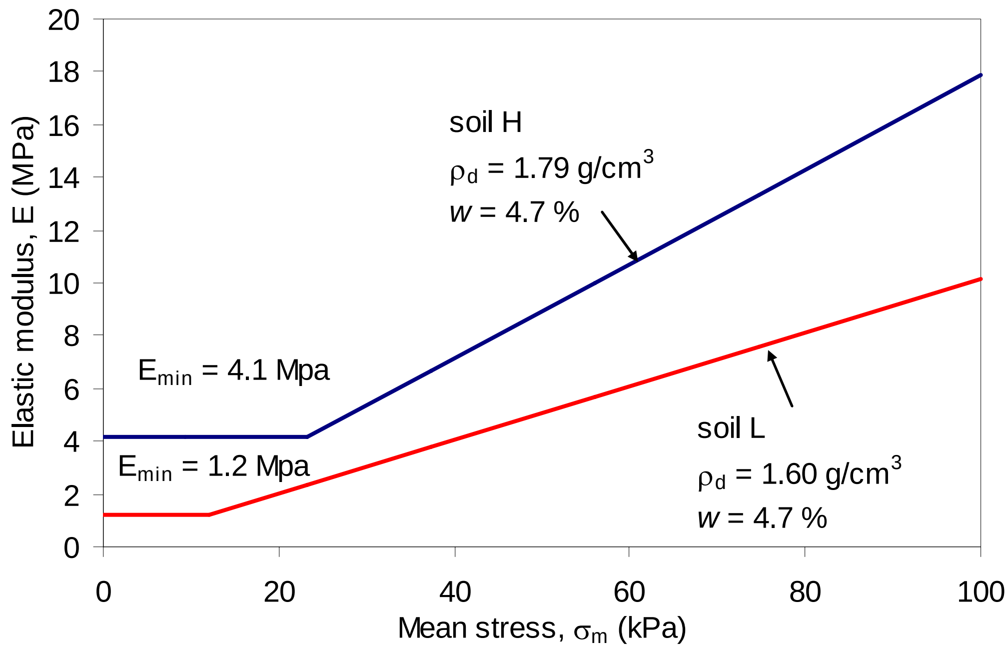

Fig. 4. 5 Undrained modulus functions with respect to mean stress, σ_m (Soils L and H)

Modulus of gravel column

The hyperbolic model (Duncan et al., 1980) with plain strain soil properties was used to simulate the gravel column response. Details for determination of the plain strain soil properties such as friction angle and hyperbolic parameters are found in Lee (2000). The plain strain properties of the gravel column used for this study are extracted from Lee (2000) and summarized in Table 4.1.

Table 4. 1 Input properties for gravel column (extracted from Lee, 2000)

Properties	Values
Friction angle (ϕ)	55°
Dilation angle (ψ)	20°
Modulus number, K	4000
Failure ratio, R_f	0.73
Modulus exponent, n	0.5

Shear strength of backfill soil

Shear strength of unsaturated soil can be predicted using the soil-water characteristic curve (SWCC) and saturated shear strength properties. In Chapter 3, three most common prediction methods using SWCC (the 1st and 2nd approaches of Vanapalli et al. and the Khalili and Khabbaz model) were introduced, and comparisons between measured and predicted values of unsaturated shear strength using these three methods were presented for different soil types. The results showed that Vanapalli et al.'s 2nd approach with a fixed residual suction value of 3000 kPa provided relatively good comparisons between predicted and measured values of shear strength for low plasticity soils. Therefore, this approach was adopted in order to predict the shear strength of the backfill soils in the MSE wall under investigation.

Rorie (2006) performed the pressure plate tests (ASTM D6836-02) at two different overburden pressures, 0 kPa and 100 kPa, under various compaction conditions on the backfill material used to construct the MSE wall in question. Figure 4.6 shows the measured SWCCs for the specimens compacted to dry densities of 1.79 g/cm^3 (w = 4.8 % for 0 kPa overburden pressure and 11.6 % for both 0 kpa and 100 kPa overburden pressures) and 1.60

g/cm^3 (w = 4.8% for 0 kPa overburden pressure). The results show that the specimens compacted at an as-compacted water content of 4.8% terminated below zero degree of saturation. The source of this error was not able to be determined. Regardless of this error, general trends were observed in the measured SWCCs. For the SWCCs measured at zero overburden pressure, the specimen compacted at optimum moisture content (w = 11.6%) showed higher air entry value and slower desaturation rate than those compacted dry of optimum (w = 4.8%). It is also shown in Fig. 4.6 that the SWCCs for each specimen appear to become closer when the overburden pressure increased from 0 kPa to 100 kPa. The SWCCs measured at overburden pressures of 0 kPa and 100 kPa showed quite different behavior for the specimens compacted dry of optimum but nearly the same for the specimens compacted at optimum. These findings are consistent with those reported by Tinjum et al. (1997), Vanapalli et al. (1999), and Ng and Pang (2000).

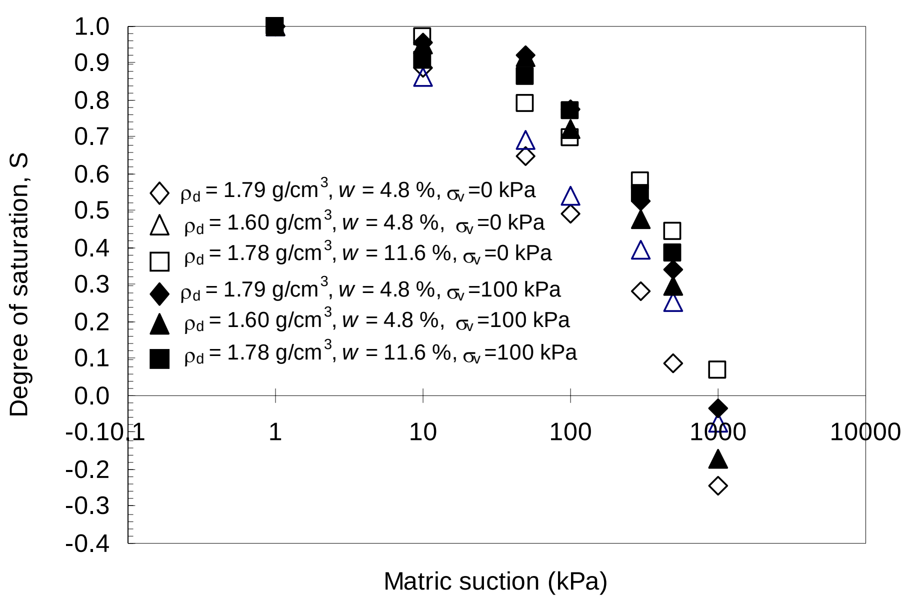

Fig. 4. 6 Measured SWCCs (after Rorie, 2006)

An effort was made to correct the measured SWCCs while preserving the general trends shown in the measured SWCCs in the corrected SWCCs. Cantata et al. (2006) developed a relationship between the slope of SWCC and the liquid limit coupled with the clay fraction, β, as shown in Fig. 4.7. The suction capacity, C, was defined as the amount of moisture gain or loss per log cycle change of suction. With the properties of backfill material (LL = 29% and Clay fraction = 12%), a C value of 4.9% was determined from this relationship. This C value was then compared to that of the measured SWCC for the specimen compacted at optimum (w = 11.6%), as most of SWCCs used for development of the relationship were measured on soils compacted near the optimum moisture content (i.e. +/-3% of OMC). A C value of 7.8% was obtained from the measured SWCC, and this value is significantly higher than that estimated from the relationship (C = 4.9%).

Therefore, the ratio of measured to estimated C values was used to correct the SWCCs. This was accomplished by lifting the measured data points up by that ratio. Details of this procedure are shown in Fig. 4.8 and described as follows (numbers shown in Fig. represent each of the steps):

1) The amount of moisture loss at any given matric suction is found from the measured SWCC. On Fig. 4.8, the amount of moisture loss at matric suction of 1000 kPa is shown.

2) The amount of moisture loss is corrected by multiplying by the ratio

3) Water content at a given matric suction is re-determined from the corrected amount of moisture loss.

4) Steps 1, 2, and 3 are repeated for the measured water content at any other soil suction.

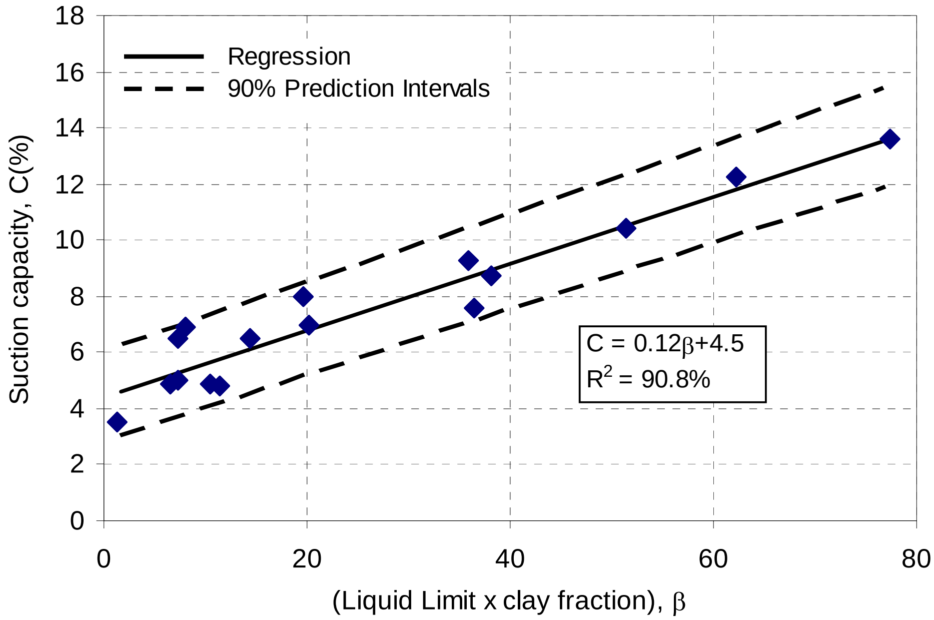

Fig. 4. 7 Suction capacity, C versus liquid limit × clay fraction), β (Catana et al. 2006)

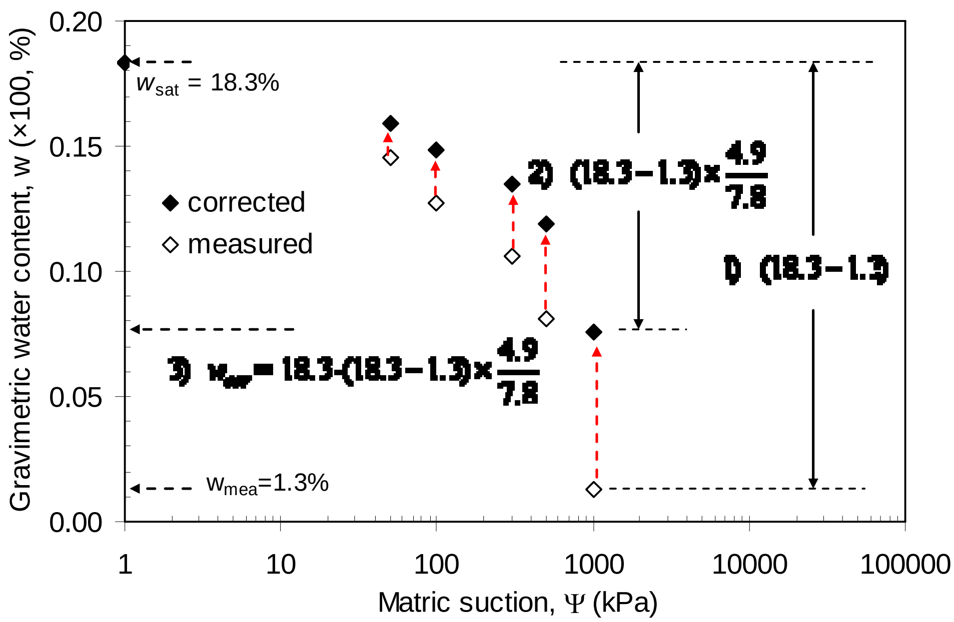

Fig. 4. 8 Procedures of correcting the SWCC (ρ_d = 1.78 g/cm3, w = 11.6%) based on the value of suction capacity

Figure 4.9 shows the corrected SWCCs for zero overburden pressure. In this study, the shear strengths of the backfills were predicted using the SWCCs at 0 kPa overburden pressure. The influence of stress state on predicted shear strength was described in Chapter 3. In order to get more accurate SWCCs in the higher suction range, three air-dry specimens were prepared. The suctions were then measured using the Dewpoint PotentiaMeter (model WP 4, Decagon Device), which uses the chilled-mirror dew point technique to measure soil suction. The average water content and average suction of specimens were 2.7% and 74 MPa, respectively. Since it is believed that the soil-water characteristic behavior appears to be similar in the high suction range regardless as-compacted water content (Vanapalli et al., 1999), the suction of 74MPa at a water content of 2.7% was used in constructing each of the SWCCs. Figure 4.10 shows the data from both pressure plate extractor (after correction) and the Dewpoint PotentiaMeter for the specimen with dry density of 1.78 g/cm^3 and as-compacted water content of 11.6%. The fitted SWCC using the Fredlund and Xing model (1994) is also shown.

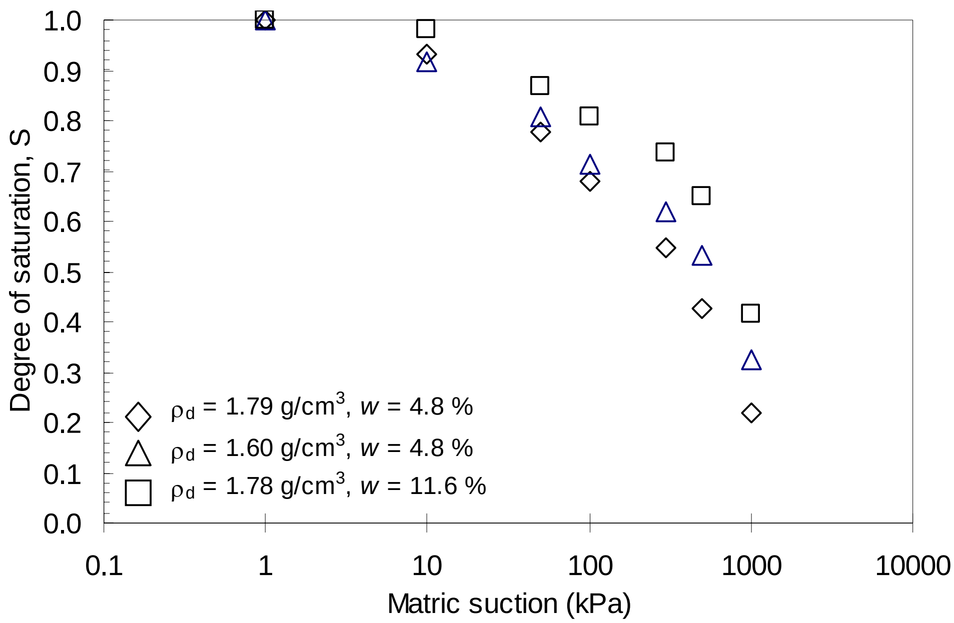

Fig. 4. 9 SWCCs at 0 kPa overburden pressure (after correction)

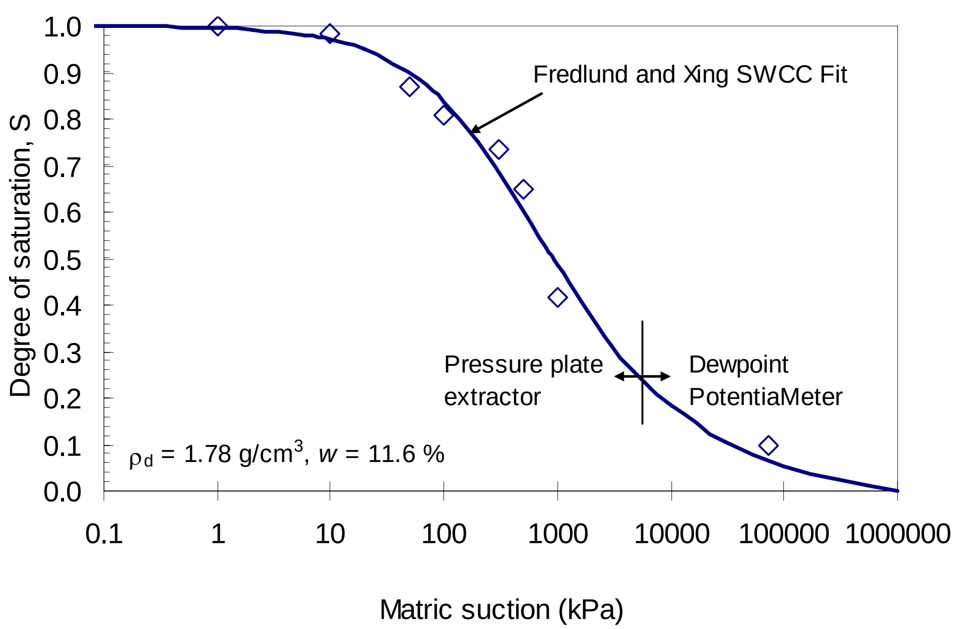

Fig. 4. 10 SWCC fit (after correction) for the entire suction range using the Fredlund and Xing model (specimen with ρ_d= 1.78 g/cm3 and *w* =11.6%)

A number of methods (Arya and Paris, 1981; Fredlund et al., 2000) have previously been proposed for the estimation of the SWCC based on grain size distribution. Therefore, another trial was made in order to estimate the SWCC using grain size distribution for the specimen with a dry density of 1.78 g/cm^3 and an as-compacted water content of 11.6%. In this research, the SWCC was estimated using the Fredlund and Wilson model (2000) incorporated into the Soilvision^{TM} program (SoilVision System Ltd.). Figure 4.11 shows the SWCC from Fig. 4.10, and the SWCC estimated from grain size distribution. It is shown that they are fairly closed to each other. Therefore, it could be concluded that the SWCC corrected based on the relationship between the values of C and β was reasonable.

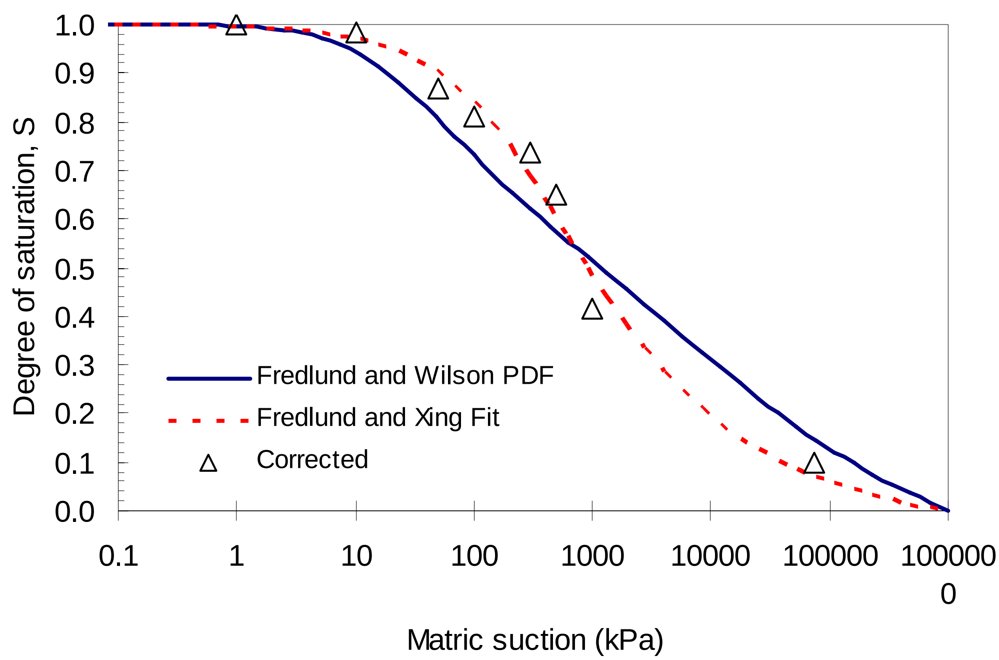

Fig. 4. 11 Corrected and estimated SWCCs for the specimen with ρ_d= 1.79 g/cm3 and *w* =11.6%

Figure 4.12 shows the developed SWCCs for soils H (ρ_d = 1.79 g/cm^3 , w = 4.8%) and soil L ((ρ_d = 1.60 g/cm^3 , w = 4.8%) for the entire suction range. The corresponding Fredlund and Xing SWCC parameters are shown in Table 4.2. The matric suctions of the specimens under various initial conditions were also measured by filter paper method (Rorie, 2006). The specimens compacted at a 4.7% as-compacted water content had average value of matric suction of 783kPa. The initial matric suction values for soils H and L are also shown in Fig. 4.12 with the SWCCs. It is observed that there are differences between the filter paper determined matric suction values of as-compacted specimens and that determined from the SWCCs. This finding is consistent with that of Tripathy et al. (2000). In the determination of the SWCCs, the compacted specimens are generally wetted prior to the pressure plate tests and then incrementally dried during the test. These pre-wetting and drying processes might have an influence on the measured matric suction (or SWCC) of the specimen when it is returned to the as-compacted moisture content. Prediction of unsaturated shear strength in consideration of this hysteretic behavior is not known. In this research, the shear strengths of compacted backfills were predicted using the drying SWCCs.

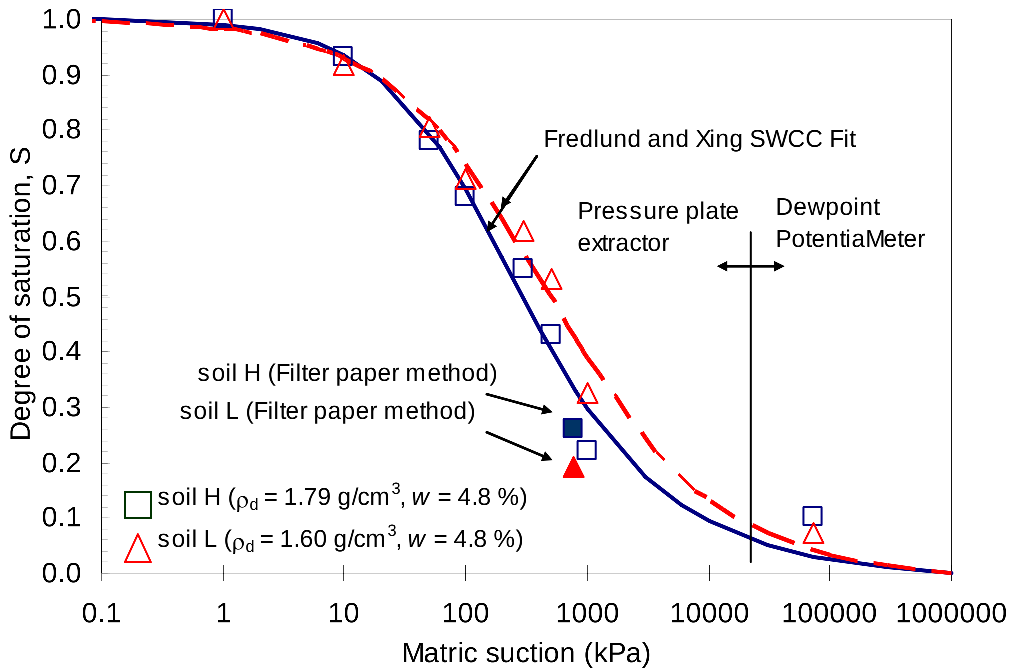

Fig. 4. 12 SWCC fits (after correction) for the entire suction range using the Fredlund and Xing model (soils H and L)

Table 4. 2 Fredlund and Xing SWCC model parameters for soils H and L

	Soil H	**Soil L**
a	138.9	248.4
n	0.81	0.66
m	1.64	1.77
ψ_r (kPa)	3000	3000
A.E.V (kPa)	19.5	21.0

Based on the SWCCs and saturated shear strength parameters (Table 4.3), shear strengths for soil H and L were predicted as shown in Fig. 4.13. In the FLAC model, the shear strength of soils was updated based on changes in matric suction as well as normal stress during construction. The matric suction changes can be computed if the changes of pore air pressure and pore water pressure are known. In this study, it was assumed that there was no increase in pore air pressure (Δu_a) during construction (atmospheric pressure). The increased pore water pressure (Δu_w) was computed from the average secant pore pressure parameter, B'_{avg}. The estimated values of B'_{avg} for soils H and L are 0.06, and 0.10, respectively. Details related to the estimation of B'_{avg} are shown in Chapter 2. The initial values of matric suction and B'_{avg} for soils H and L are presented in Table 4.4.

Table 4. 3 Shear strength parameters for soils H and L

	Soil H	**Soil L**
Cohesion, c' (kPa)	3	0
Friction angle, ϕ' (degrees)	30	26
Dilation angle (degrees)	10	10

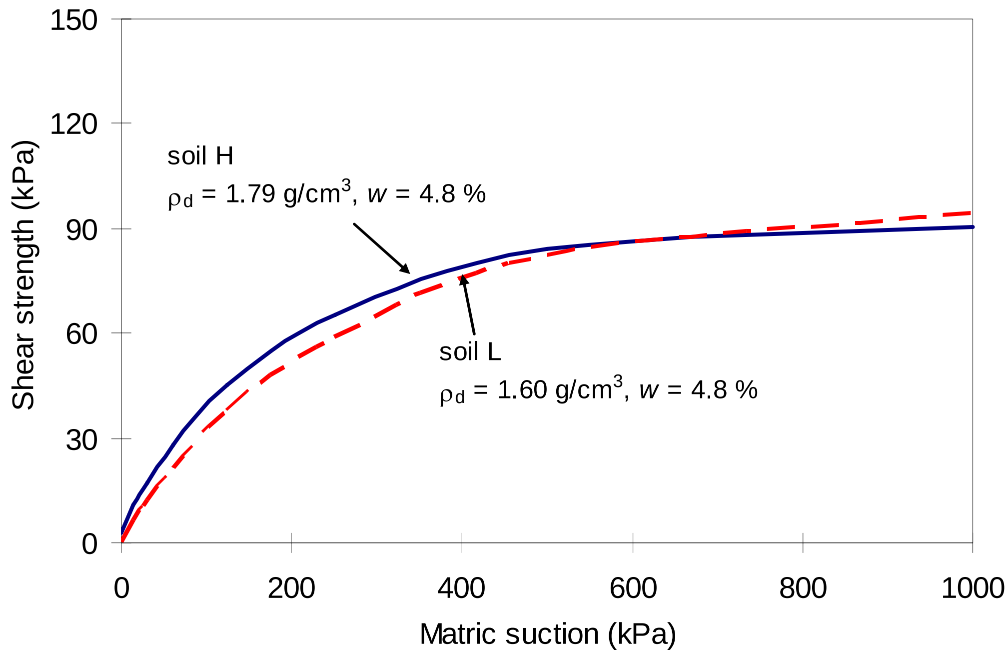

Fig. 4. 13 Predicted shear strength envelopes for soils H and L using Vanapalli et al.'s 2nd approach

Table 4. 4 Initial matric suction and B'_{avg} for soils H and L

	Soil H	**Soil L**
Initial matric suction (kPa)	783	783
B'_{avg}	0.06	0.1

Reinforcement

The geosynthetic reinforcements were simulated using the FLAC Cable element. A cable element is characterized by an axial elastic material element with interface elements around it. Figures 4.14 and 4.15 show the input properties for the cable element and related interface elements, respectively. Input properties for cable element include Young's modulus

(E), tensile yield strength (*yield*), and compressive yield strength (*comp*), and those for interface element include cohesion (*sbond*), friction angle (*sfriction*), and shear stiffness (*kbond*).

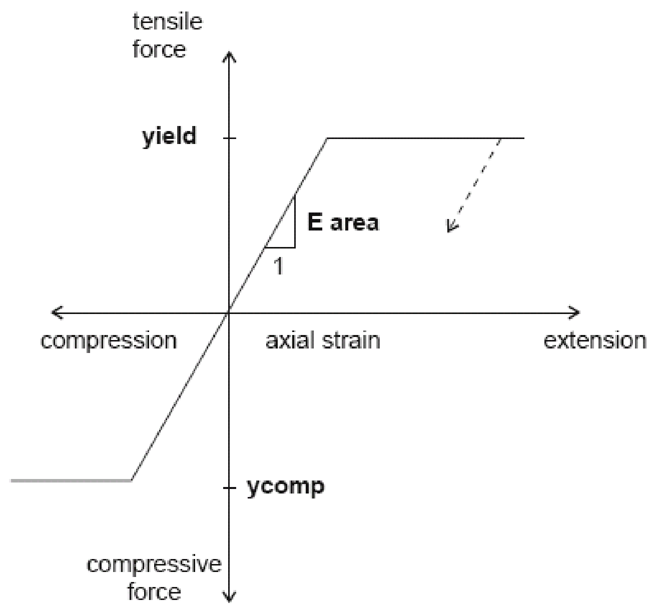

Fig. 4. 14 Cable material behavior model (FLAC, 2000)

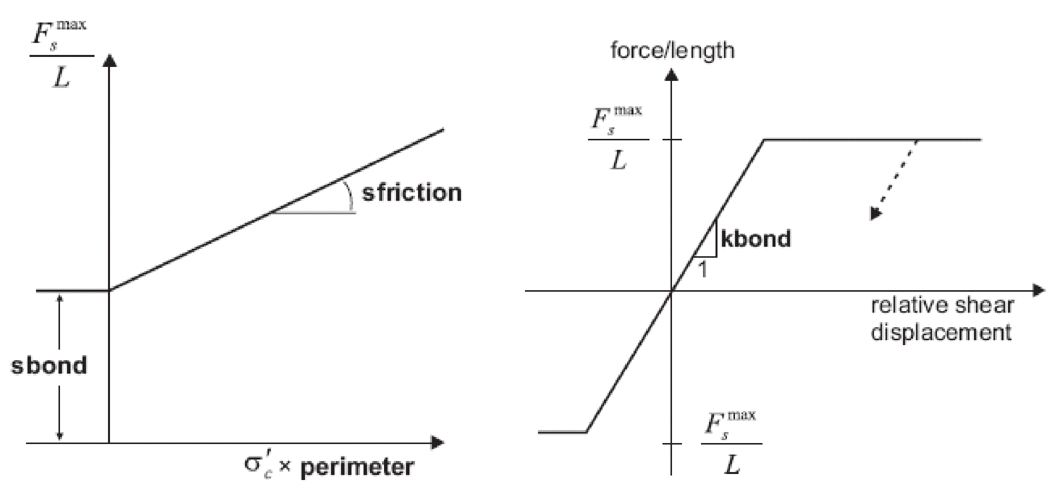

Fig. 4. 15 Interface behavior for cable material (FLAC, 2000)

The Young's modulus (E) of reinforcement was determined from published wide width tensile test results at 5% strain. This modulus was then reduced in order to consider the effect of the faster strain rate used in laboratory tests, as suggested by Lee (2000) (20% reduction for polyester woven reinforcement). Tensile yield strength (*yield*) and compressive yield strength (*comp*) were assigned values of 35 kN and 0.01 kN, respectively.

In this research, different interface properties of reinforcement elements were assigned to simulate the reinforcements located within the block elements and within the soil (backfill) elements (Fig. 4.16). Within the soil elements, the reinforcement (cable) elements were attached to the nodes of the soil element assuming that there was no slippage between the soil and the geosynthetic reinforcement. This technique was successfully used by Lee (2000) and Hatami and Bathurst (2003). In their discussions, it was suggested that this technique made it possible to avoid the violation of strain compatibility, such as when soil elements penetrate the cable elements at large strains. With this technique, it is not necessary to assign the interface element properties (*kbond*, *sbond*, and *sfriction*).

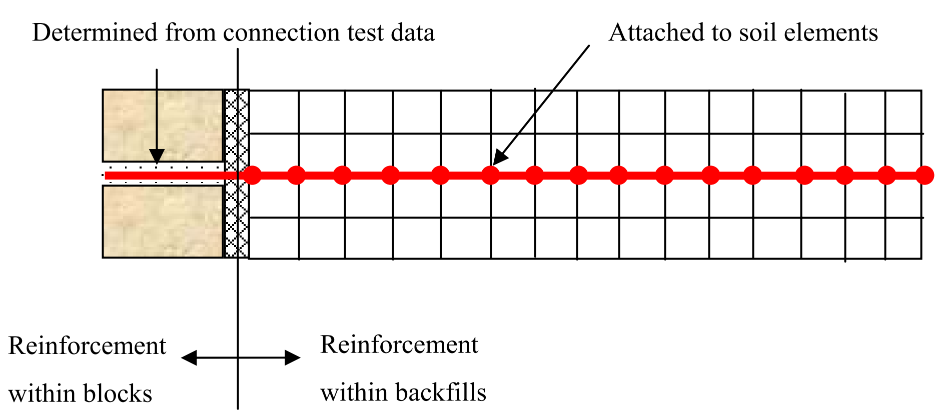

Fig. 4. 16   Determination of reinforcement interface properties

The interface properties of the cable located within the blocks were determined from connection test data (Table 4.5). Figure 4.17 shows the shear stiffness of reinforcement (*kbond*) determined from the connection strengths at the displacements of 1.27cm and 1.91cm. Shear stiffness corresponding to the displacement of 1.91cm was adopted in this research. Cohesive strength (*sbond*) and friction angle (*sfric*) were computed from the peak connection strengths. As shown in Fig. 4.18, the shear strength behavior of reinforcement was approximated by bilinear regression. Cohesive strength (*sbond*) increases from 6.8 kN/m/m to 28 kN/m/m, and friction angle (*sfric*) decreases from 48.7° to 20.5° as normal stress exceeds 34.3 kPa. The reinforcement material properties used in the FLAC model are summarized in Table 4.6.

Table 4. 5 Rockwood Classic Modular Block Unit and Fortrac 35/20-20 Polyester Geogrid Connection (after Bathurst, 1995;1997)

Test No.	Approx. Wall Height (m)	Approx. No. of Classic Blocks	Normal Stress on Connection (kPa)	Connection Strength Displacement @ 1.27cm – 1.91cm (kN/m)		Peak Connection strength (kPa/m)
1	0.6	2	8.6	4.3	5.4	8.6
2	1.2	4	17.2	8.0	9.3	12.1
3	2.4	8	34.2	8.0	10.8	16.9
4	3.7	12	51.5	11.3	14.9	18.5
5	3.7	12	64.4	10.5	14.2	19.0
6	3.7	12	51.5	12.1	15.9	18.6
7	4.6	15	51.5	11.0	14.9	18.0

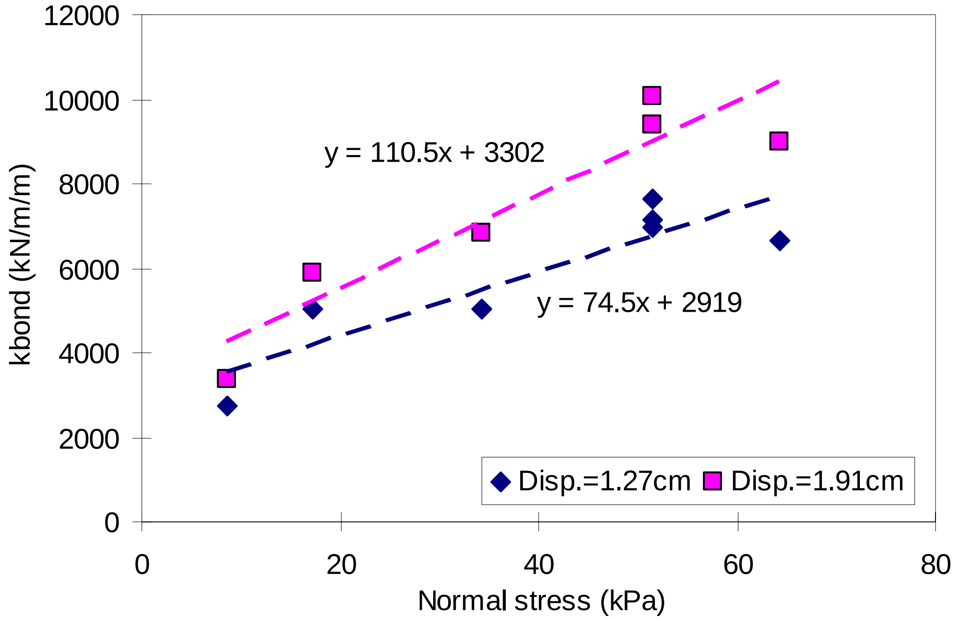

Fig. 4. 17 Shear stiffness vs. normal stress determined from connection test (after Bathurst, 1995;1997)

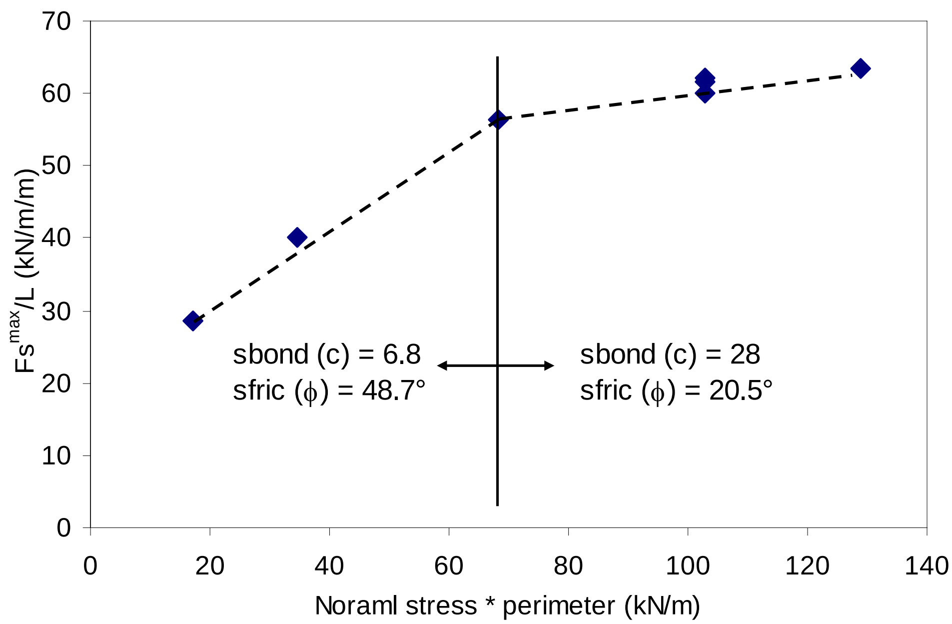

Fig. 4. 18 Shear strength behavior of reinforcement determined from connection test (after Bathurst, 1995;1997)

Table 4. 6 Summary of reinforcement input properties

Reinforcement Input properties	Within blocks	Within backfills
E (kN/m^2)	84	84
Yield (kN)	35	35
ycomp (kN)	0.01	0.01
kbond (kN/m/m)	110.5× (normal stress)+3302	-
sbond (kN/m/m)	6.8 (if normal stress < 34.3 kPa) 28 (if normal stress >= 34.3 kPa)	-
sfric (degree)	20.5(if normal stress < 34.3 kPa) 48.7(if normal stress >= 34.3 kPa)	-

Interface

Interface elements, which are characterized by sliding and/or tensile separation elements in FLAC, are used to describe the interaction between different materials. Figure 4.19 shows the mechanical representation of the interface. The input properties for the interface elements include friction, cohesion, normal stiffness (k_n), shear stiffness (k_s), and tensile strength (T). For the MSE wall model, the interface elements were used for: (1) the interface between structural blocks and (2) the interface between modular block and gravel (gravel column) that was installed behind the modular block face.

The normal stiffness (k_n) of the interfaces was assigned with a value at least ten times the stiffness of the softer material. The shear stiffness (k_s) of the interface between facing blocks was assumed to be 8500 kN/m/m, which was extracted from Hatami and Bathurst (2001). This stiffness was determined from interface shear tests of the blocks used for their study. Properties of the interface between block and gravel material were not clearly described in the documentation (Bathust et al., 1993). The same shear stiffness of 8500 kN/m/m was assumed in this research. The interface friction angle between facing blocks, and facing block and gravel column were set to the peak plain-strain friction angle of gravel as recommended by Lee (2000). The interface properties used in this research are summarized in Table 4.7.

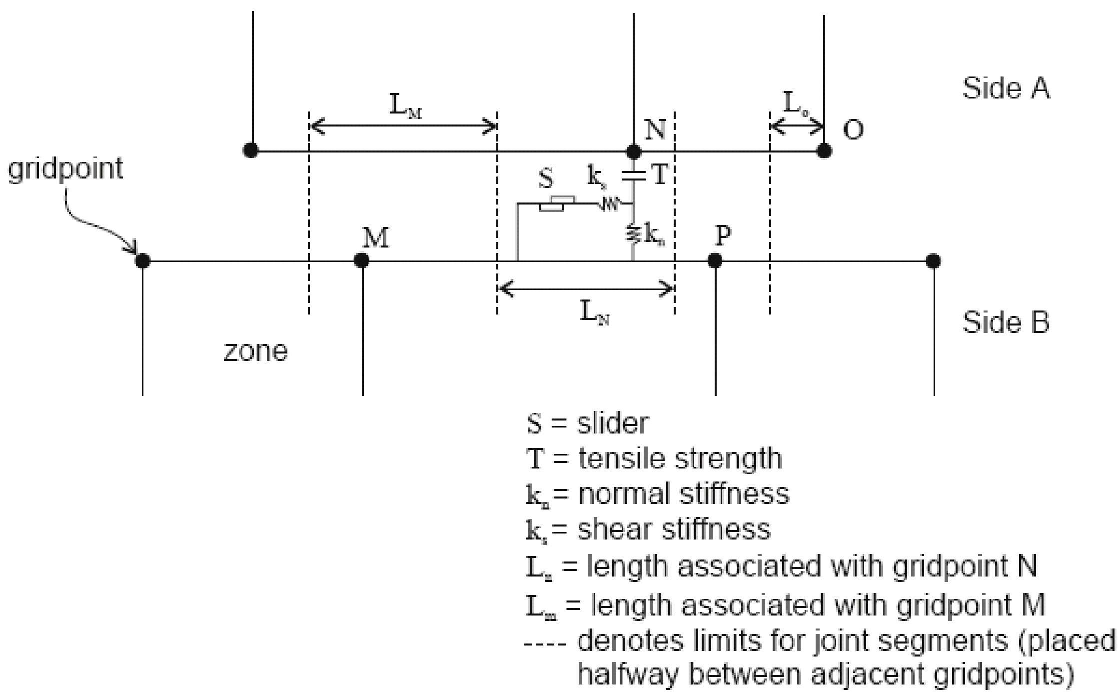

Fig. 4. 19 Mechanical representation of the interface (Itasca, 2000).

Table 4. 7 Summary of interface input properties

Interface input properties	Block-Block	Block-Soil
k_n (kN/m/m)	10.95×10^7	1×10^6
k_s (kN/m/m)	8500	8500
fric (degrees)	55°	55°
coh	0	0

4.5 RESULTS

The results of numerical simulations are presented in this section. Figures 4.20 and 4.21 show contours of stresses and displacements of the wall (both vertical and lateral) at the end of construction (for case 1 and case 2, respectively). Distinct differences between the vertical stress distributions for each case are observed in a comparison of Fig. 4.20(a) and Fig. 4.21(a). Compared to the vertical stress distribution for case 1, relatively low vertical stress is developed in the poorly compacted zone behind the wall face for case 2. This is because some of the vertical stress induced during construction within this zone is transmitted to the adjacent high stiffness materials (gravel column and well compacted backfills). Figures 4.20(b) and 4.21(b) show that the lateral stress contour for case 1 reaches deeper than that for case 2 within a 1.6m-wide zone behind the wall face. Distinct difference between the vertical displacement distributions for cases 1 and 2 is also observed from Fig. 4.20(c) and Fig. 4.21(c) showing that relatively high vertical displacements occur within the poorly compacted zone. As expected, higher lateral displacements are predicted for case 2 as shown in Figs. 4.20(d) and 4.21(d) due to the existence of the poorly compacted zone.

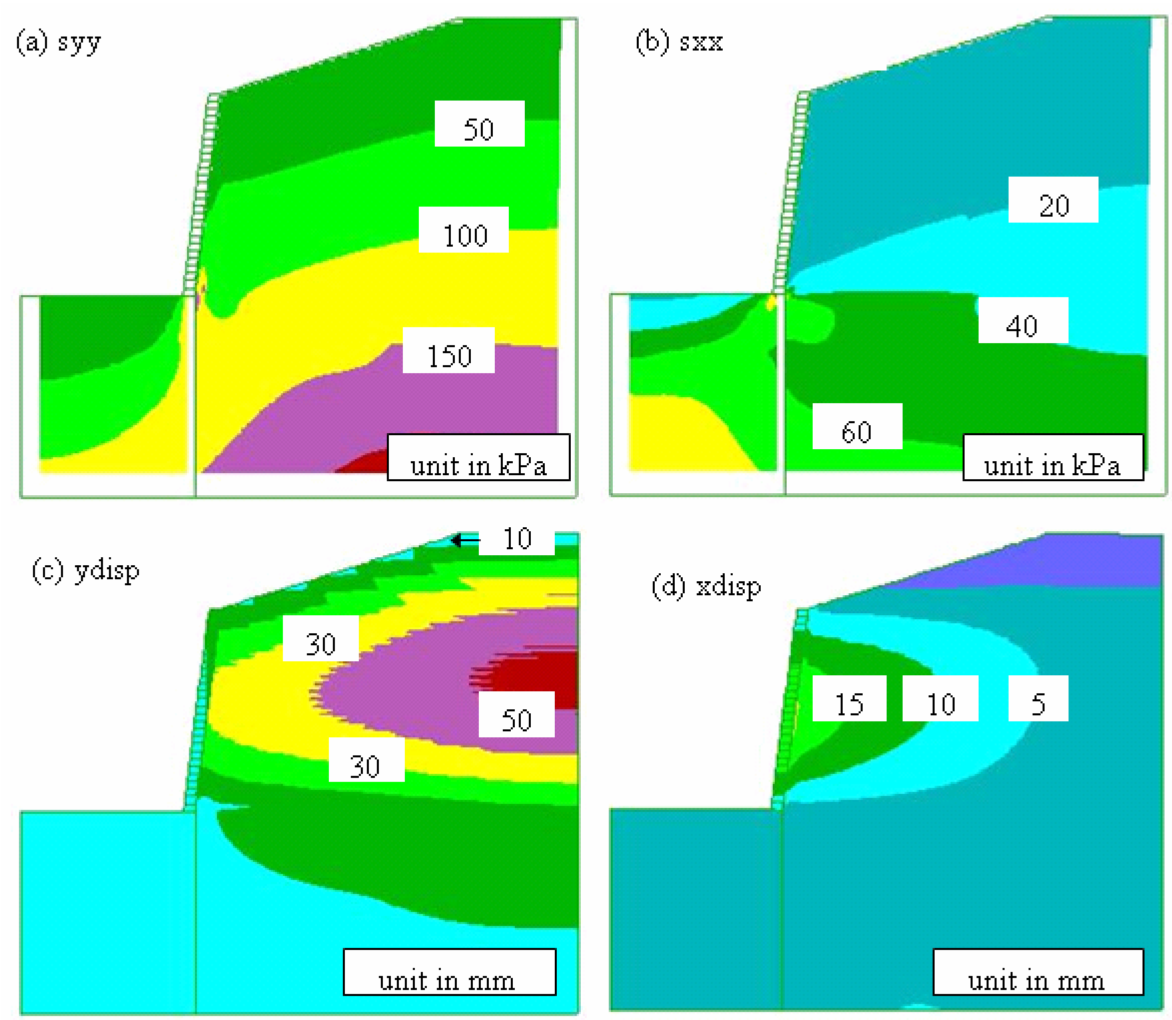

Fig. 4. 20 FLAC results at the end of construction for case 1; (a) vertical stress (b) lateral stress (c) vertical displacement and (d) lateral displacement

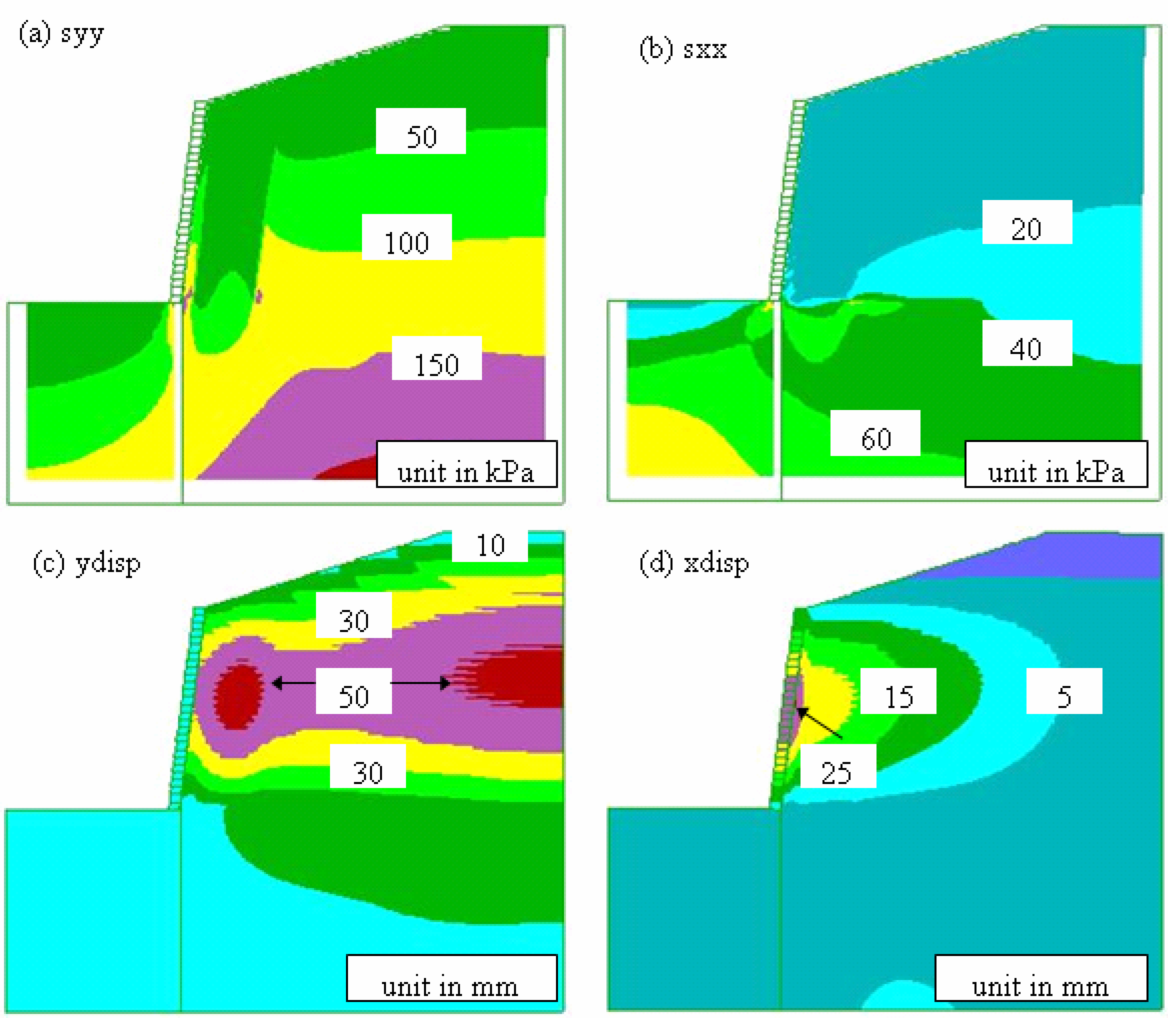

Fig. 4. 21 FLAC results at the end of construction for case 2; (a) vertical stress (b) lateral stress (c) vertical displacement and (d) lateral displacement

Figure 4.22 illustrates the development of wall movements at the end of construction. It is shown from Fig. 4.22(a) that the maximum wall face deflections for cases 1 and 2 are 19 mm and 29 mm, respectively and located near the middle of the wall (at a height of 0.43H and 0.5H, respectively). The backfill settlements profile at 1.4 m behind the wall facing (at the middle of poorly compacted zone) are plotted as a function of position along the wall height in Fig. 4.22(b). Modeling results indicate that the values of settlement increase with increasing depth below the top of the wall in the upper half of the wall, and they decreased with increasing depth in the lower half of the wall. Maximum values of 36 and 55 mm are predicted for cases 1 and 2, respectively. The existence of the 1.6m-wide poorly-compacted zone behind the wall face increased both wall face deflection and settlement by approximately 152 %. In Figs. 4.22 and 4.23, "folds" and "jogs" were observed in the predicted displacement curves (especially for vertical displacement). This numerical problem was the results of simulating incremental lifts of backfill.

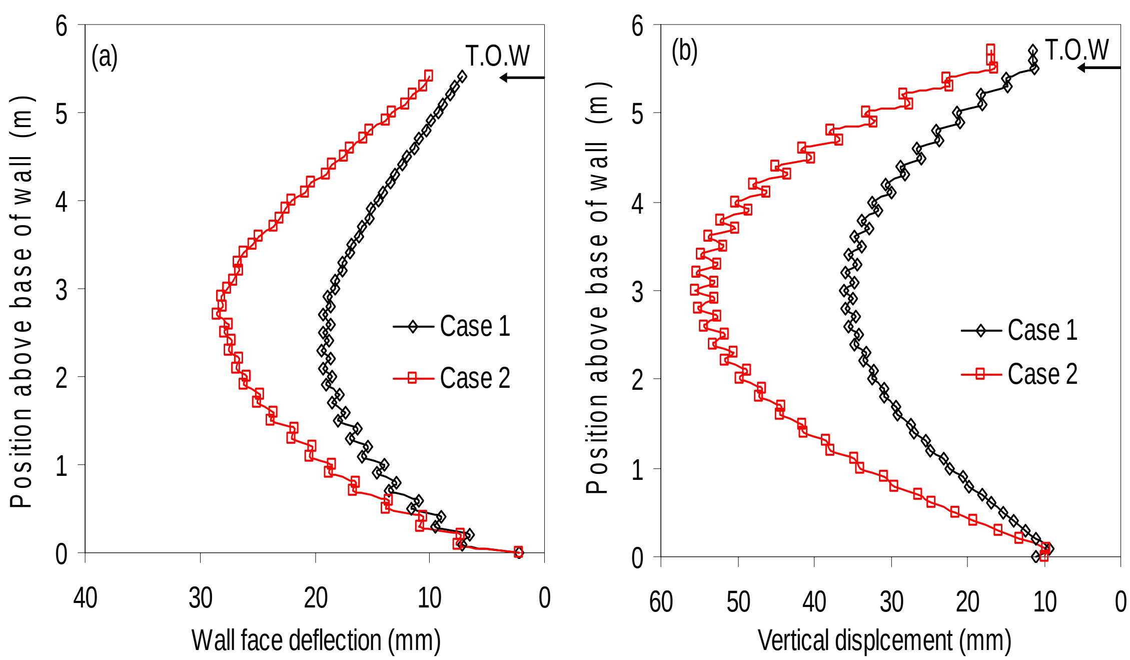

Fig. 4. 22 Predicted wall movements at the end of construction; (a) wall face lateral deflection (b) vertical displacement at 1.4m behind the wall face

The computed tension forces as a function of position along the reinforcement from the top layer (layer 11) to the bottom layer (layer 1) are shown in Fig. 4.23. These results show that the maximum reinforcement tensions, T_{peak}, for case 2 are higher than those for case 1, and that the T_{peak} values for both cases occur near the back face of the block wall facing. Obviously, relatively larger vertical displacement occurs within backfills (or gravel column) compared to the very small vertical displacement within the facing blocks. This differential displacement at 0.3m behind the wall face induces high tension in the reinforcement. Therefore, higher values of T_{peak} are developed as the backfill is not properly compacted behind the wall face (case 2). Discontinuities of tension observed at the boundary of poorly and well compacted zones (at 2.2m behind the wall face) also can be explained by the differential settlements between poorly and well compacted backfill soils.

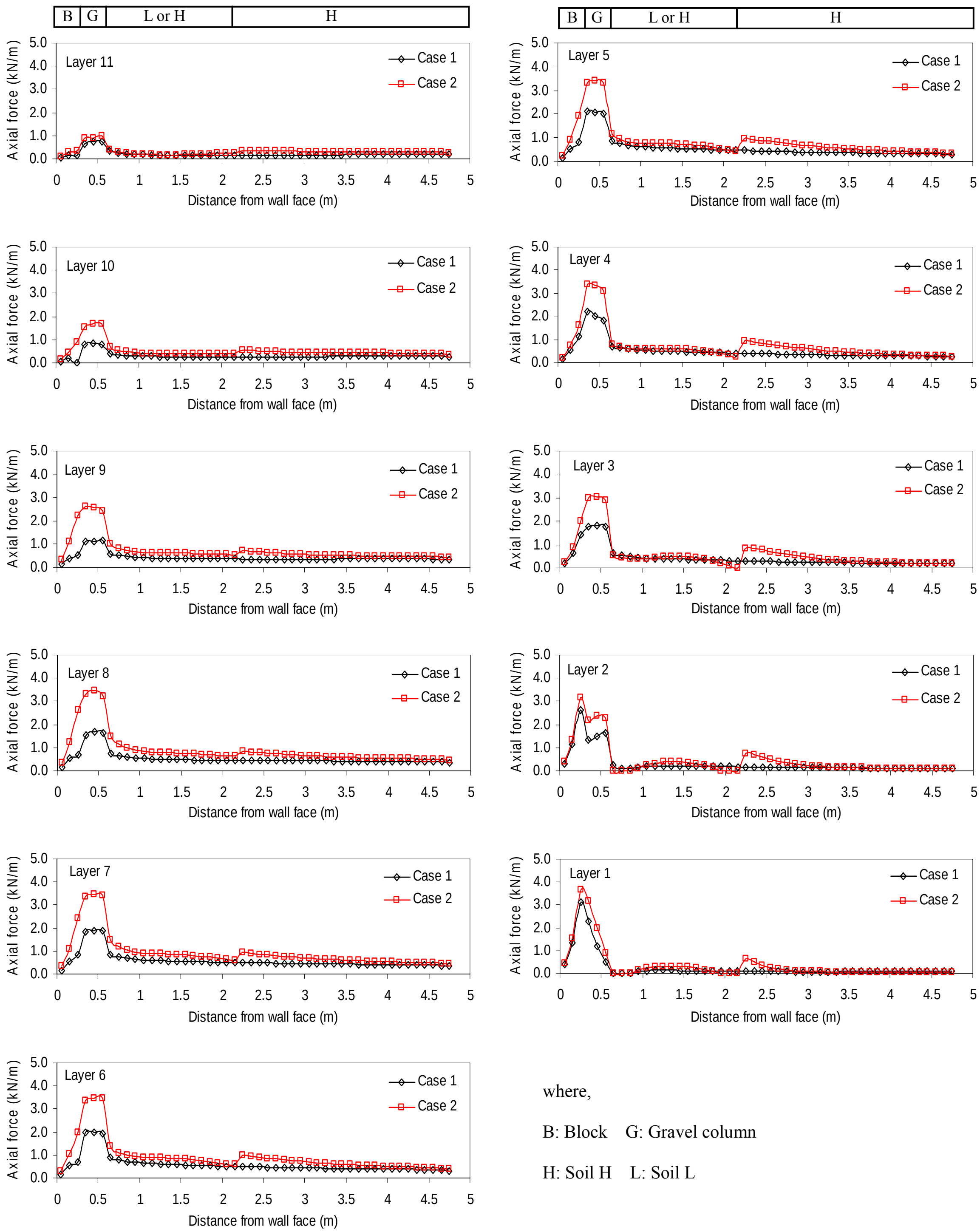

Fig. 4. 23 Computed reinforcement tension forces for both cases 1 and 2 at the end of construction

Besides the maximum tension (T_{peak}) at the back edge of the facing block; no remarkable peak tension is shown within the reinforced soil mass. The absence of peak tension within the reinforced soil mass is due to the very small shear induced deformation during the wall construction that results from the high shear strength of the unsaturated backfill, which results from high soil suction.

The maximum tension force, T_{peak}, and the average tension force for each layer, T_{avg}, are plotted along the wall elevation as shown in Figs. 4.24(a) and 4.24(b), respectively. T_{avg} increases with increasing depth below the top-of-wall in the upper half of the wall, and then decreases with increasing depth in the lower half of the wall (both cases 1 and 2). The T_{peak} distributions are more difficult to characterize than the T_{avg} distributions, showing that T_{peak} again increases with increasing depth in the upper half of the wall but no symmetrical trends are observed in the lower half.

The maximum values of T_{peak} in all layers for cases 1 and 2 were 3.1kN/m and 3.7kN/m, respectively. The maximum values of T_{avg} were predicted to be less than 1 kN/m for both cases. These values are well below the yield strength of the reinforcement material (35kN/m). The possible reasons for these small reinforcement tensions at the end of construction are that there are again that these is little shear induced deformations due to high shear strength of backfills that result from high suction, and stiff face blocks carry a large portion of the lateral earth forces. As shown in Figs. 4.24(a) and 4.24(b), the biggest increases in reinforcement tension (both T_{peak} and T_{avg}) are found near the middle of wall height.

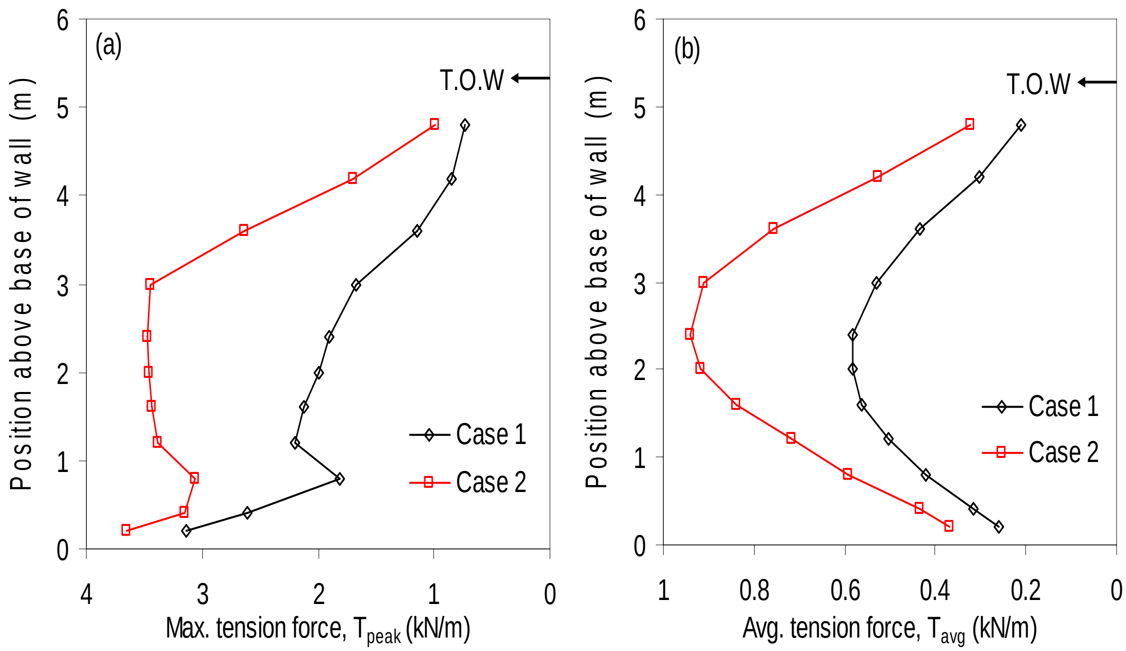

Fig. 4. 24 Tension force distributions at the end of construction; (a) maximum tension, T_{peak} and (b) average tension, T_{avg}

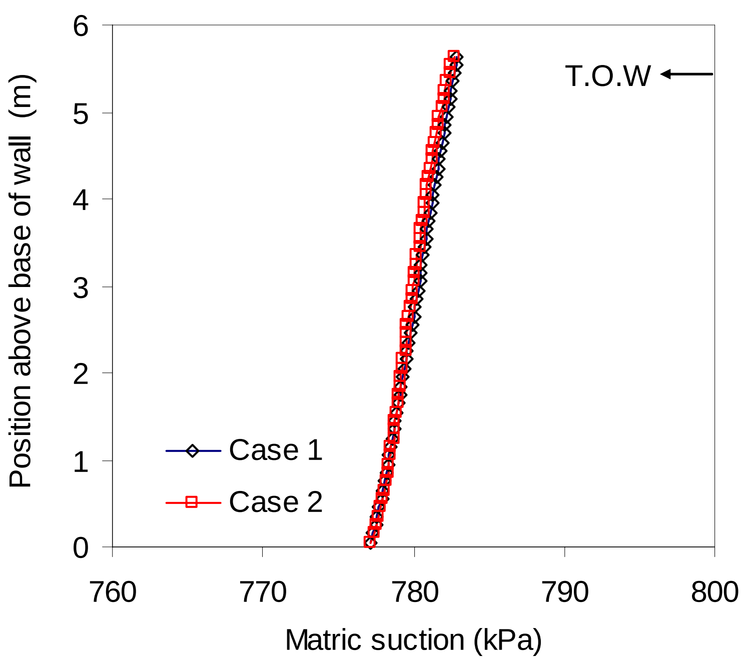

Fig. 4. 25 Matric suction distribution at the end of construction for cases 1 and 2

Finally, Fig. 4.25 shows the matric suction distribution along the wall height at 1.4m behind the wall face at the end of construction. It can be seen that very small changes in matric suction were induced by the incremental loadings (lifts of backfill) that occurred during construction because the backfill was compacted very dry of optimum. These matric suction distributions were saved in the data files and used as initial condition for the unsaturated flow analysis to be presented in the next chapter.

4.6 SUMMARY AND CONCLUSIONS

In order to better predict the end of construction behavior of a MSE wall constructed with marginal fill, a numerical model, which accounts for unsaturated soil properties (elastic modulus and shear strength), was developed using FLAC. The developed model takes into account the staged construction of a MSE wall, and uses FISH subroutines programmed in the FLAC model to update the unsaturated soil properties based on changes in both normal stress and matric suction.

This research focused on the behavior of a MSE wall constructed with backfill compacted very dry of optimum (w = 4.7%, -7 % of OMC). Also, the effect of the existence of a poorly compacted zone behind the wall face on the wall behavior was investigated. From the results of the numerical simulations presented, the following conclusions can be drawn:

1) The existence of a 1.6m-wide poorly-compacted zone behind the wall face increased the wall displacements (vertical and lateral displacements) and reinforcement tensions (peak and average tensions) significantly. The maximum increases of these

displacements and the tension forces occurred near the mid-height of the wall.

2) The peak tension forces in the reinforcements were found at the back face of the blocks due to the differential displacements between blocks and backfill, which resulted from the stiffness difference of the materials.
3) The small magnitudes of reinforcement tension forces (less than 4kN), which were well below the yield strength (35kN), were predicted for the end of construction condition are believed to be the result of the high shear strength of backfill induced by high soil suction.
4) Very little change in matric suction during the construction phase was predicted.

4.7 REFERENCES

Allen, T. M., Bathurst, R. J., and Berg, R. R. (2002). Global level of safety and performance of geosynthetic walls: A historical perspective. Geosynthetics International, (9), pp. 395-450.

Arya, L. M., and Paris, J. F. (1981). A physico-empirical model to predict the soil moisture characteristic from particle-size distribution and bulk density data, Soil Science Society of America Journal, 45, pp. 1023-1030.

Bathurst, R. J. (1995; 1997) Report results connection capacities with rockwood classic retaining wall system.

Bathurst, R. J., Simac, M. R., Christopher, B. R., and Bonczkiewicz, C. (1993). A database of results from a geosynthetic reinforced modular block soil retaining wall, Proceedings of

International Symposium of Soil Reinforcement, Paris, pp. 341-362.

Catana, M. C., Vanapalli, S. K., and Garga, V. K. (2006). The water retention characteristics of compacted clays, Proceedings of the fourth international conference on unsaturated soils, Geotechnical Special Publication, No. 147, Vol.2, pp. 1348-1359.

Cho, S. E., and Lee, S. R. (2001). Instability of unsaturated soil slope due to infiltration, Computers and Geotechnics, Vol. 28, pp. 185-208.

Collin, J. G. (1997). Design manual for segmental retaining walls-Edition 2, National Concrete Masonry Association, NCMA.

Duncan, J. M., Byrne, P., Wong, K. S., and Mabry, P. (1980). Strength, stress-strain and bulk modulus parameters for finite-element analysis of stress and movements in soil masses, Reports No. UCB/GT/80-01. University of California, Berkley.

Fredlund, D. G., and Rahardjo, H. (1993). Soil mechanics for unsaturated soils, New York: Wiley.

Fredlund, M. D., Wilson, G.. W., and Fredlund, D. G.. (2002). Use of the grain-size distribution for estimation of the soil-water characteristic curve, Canadian Geotechnical Journal, 39, pp. 1103-1117.

Fredlund, D. G., and Xing, Anqing. (1994). Equations for the soil-water characteristic curve, Canadian Geotechnical Journal, 31, pp. 521-532.

Hatami, K., and Bathurst, R.J. (2001). Modeling static response of a geosynthetic reinforced soil segmental retaining wall using FLAC, FLAC and Numerical Modeling in Geomechanics, pp. 223-231.

Hatami, K., and Bathurst, R. J. (2003). A calibrated FLAC model for geosynthetic reinforced soil modular block walls at end of construction, FLAC and Numerical Modeling in Geomechanics, pp. 223-231.

Itasca Consulting Group. (2000). FLAC-Fast Lagrangian Analysis of Continua, Version 4.0, Minneapolis.

Lee, W. F. (2000). Internal stability analyses of geosynthetic reinforced retaining walls, Ph.D. dissertation, University of Washington, Seattle.

Ng, Charles, W. W., and Pang, Y. W. (2000). Influence of stress state soil-water characteristics and slope stability, Journal of Geotechnical and Geoenvironmental Engineering, Vol. 126, No. 2, pp. 156- 166.

Rorie, D. (2006). Investigation of soil suction in low density silty sands, MS thesis, North Carolina State University, Raleigh.

Soong, T. and Koerner, R. M. (1999). Geosynthetic reinforced and geocomposite drained retaining walls utilizing low permeability backfill soils, GRI Report #24, Geosynthetic Research Institute, Folsom, PA, 140p.

Thu, T. M., Rahardjo, H., and Leong, E. C., (2006). Shear strength and pore-water pressure characteristics during constant water content triaxial tests. Journal of Geotechnical and Geoenvironmental Engineering, 132(3), pp. 411-419.

Tinjum, J. M. and Benson, C. H. and Blotz, L. R. (1997). Soil-water characteristic curves for compacted clays, Journal of Geotechnical and Geoenvironmental Engineering, Vol. 123, No. 11, pp. 1060-1069.

Tripathy, S., Leong, E. C., and Rahardjo, H. (2003). Suction of compacted residual soils, Unsaturated soils, Experimental Studies, pp. 111-122

Vanapalli, S.K., Fredlund, D.G., and Pudahl, D.E. (1999). The influence of soil structure and stress history on the soil-water characteristics of a compacted till, Geotechnique, 49(2), pp. 143-159.

Yoo, C., and Jung, H. (2006). Case history of geosynthetic reinforced segmental retaining wall failure, Journal of Geotechnical and Geoenvironmental Engineering, Vol. 132, No. 12, pp. 1538- 1548.

CHAPTER 5

Numerical simulation of MSE wall behavior induced by rainfall infiltration

5.1 INTRODUCTION

Prediction of MSE wall deformation due to rainfall infiltration is a complicated problem which includes seepage, shear strength, and volume change based on unsaturated soil mechanics principles. Several researchers (Ng and Pang, 2000; Yoo and Jung, 2006) have showed the failure mechanism of an earth structure due to rain infiltration using unsaturated shear strength based on limit equilibrium analysis. However, there are still several existing limitations for performing stress-deformation analyses based on unsaturated soil behavior. This is mainly due to the complexities of analysis utilizing the unsaturated soil constitutive law and the increased difficulties of performing experimental studies on unsaturated soils. Another major limitation is that most numerical simulation programs were developed assuming saturated soil mechanics and therefore adopted one stress state variable (either total stress or effective stress) to predict soil behavior. However, unsaturated soil behavior is explained using two stress state variables (net normal stress and matric suction) (Fredlund and Rahardjo, 1993). For the reasons mentioned above, prediction of soil behavior subjected to changes of both stress state variables is challenging.

A series of numerical analyses, using the finite difference code FLAC (Fast Lagrangian analysis of Continua) were performed in order to predict the behavior of an MSE wall subjected to surface-water infiltration (either rainfall or irrigation). Through the development of FISH subroutines within FLAC, the effects of both stress-state variables could be incorporated. First, the simulation with unsaturated soil properties was performed taking into account the staged construction. Transient flow analysis was then carried out to compute the changes of matric suction within backfill due to rainfall infiltration. Finally, the revised matric suction distribution determined from seepage analysis was used as an input for stress-deformation analysis in order to consider the effect of matric suction change on the wall deformation. The wall behavior due to wetting was predicted by superimposing the results of two simulations, one for estimating shear induced deformations, and the second for volumetric deformations.

A 5.4m high MSE wall constructed with marginal fills in the Research Triangle Park (RTP) of North Carolina experienced a localized collapse during rainfall in the spring of 2001. The objective of this study was to provide better understanding of the behavior of MSE walls subjected to rainfall infiltration based on the unsaturated soil mechanics. The behavior of the wall constructed with very low as-compacted water content backfill was the focus of this study. Also, the effect of a poor quality compaction zone behind the wall face was investigated.

5.2 PERMEABILIY OF UNSATURATED SOILS

The flow of water in a saturated-unsaturated soil is governed by Darcy's law. Darcy (1856) postulated the rate of water flow through a soil mass was proportional to the hydraulic head gradient, as shown in Eq. 5.1:

$$v_x = -k_x \frac{\partial h}{\partial x} \ , \ v_y = -k_y \frac{\partial h}{\partial y} , \ v_z = -k_z \frac{\partial h}{\partial z} \tag{5.1}$$

where v_x , v_y, and v_z are flow rates of water in the x, y, and z directions, respectively;

k_x, k_y, and k_z are the coefficients of permeability in the x, y, and z directions, respectively; and

$\partial h/\partial x$, $\partial h/\partial y$, $\partial h/\partial z$ are hydraulic head gradients in the x, y, and z directions, respectively.

Based on Darcy's equation, the governing equation of the flow of water in a saturated-unsaturated soil can be expressed as:

$$\frac{\partial}{\partial x}\left(k_x \frac{\partial h}{\partial x}\right) + \frac{\partial}{\partial y}\left(k_y \frac{\partial h}{\partial y}\right) + \frac{\partial}{\partial z}\left(k_z \frac{\partial h}{\partial z}\right) + q = \frac{\partial \theta}{\partial t} \tag{5.2}$$

where h is the total fluid head;

q is the applied external boundary flux;

θ is the volumetric water content; and

t is the time.

The coefficient of permeability is relatively constant for a specific saturated soil at a given void ratio or density. However, the coefficient of permeability in unsaturated soil cannot generally be assumed to be constant because it is significantly affected by combined changes in the void ratio and the degree of saturation (or water content) of the soil. To model the flow of water in an unsaturated soil, it is necessary to define the relationship between the coefficient of permeability and degree of saturation (or soil suction). One method of defining this relationship is to use one of a number of empirical equations (Brooks and Corey, 1964; Gardner, 1958; and Richards, 1931). However, this method requires measured data for the permeability function to determine the parameters in the permeability equation.

Since establishing the soil-water characteristic curve (SWCC) is generally neither as difficult nor demanding as measuring the coefficient of permeability at various suction levels, the task of defining the permeability function can be simplified by calculating the coefficient of permeability from the soil-water characteristic curve.

5.2.1 Permeability from the soil-water characteristic curve

Various equations have been proposed to determine the permeability function for an unsaturated soil using the SWCC. The two most common equations are those proposed by van Genuchten (1980) and Fredlund et al.(1994).

van Genuchten (1980)

Van Genuchten (1980) proposed the following closed form equation to describe the hydraulic conductivity of an unsaturated soil as a function of matric suction, combining Mualem's model (1976) with his empirical equation (Eq.3.3) for the soil-water characteristic curve:

$$k_r = \frac{\{1-(a\psi)^{(n-1)})[1+(a\psi)^n]^{-m}\}^2}{[1+(a\psi)^n]^{m/2}} \tag{5.3}$$

where k_r = relative coefficient of permeability ($=k(\psi) / k_s$);

k_s= saturated hydraulic conductivity ;

a, m, and n =curve fitting parameter (n=1-1/m) ; and,

ψ= matric suction.

From the above equation, the hydraulic conductivity function of a soil can be estimated once the saturated conductivity and the two curve fitting parameters, a and m, are known.

Fredlund et al. (1994)

Fredlund et al. proposed a method to predict the unsaturated hydraulic conductivity function from the Fredlund and Xing SWCC function (Eq.3.4). This method consists of developing the unsaturated hydraulic conductivity function by integrating along the entire curve of the volumetric water content function, as shown in Eq. 5.4.

$$k_r = \frac{\int_{\psi}^{\psi_r} \frac{\theta(y)-\theta(\psi)}{y^2}\theta'(y)dy}{\int_{\psi_{aev}}^{\psi_r} \frac{\theta(y)-\theta_s}{y^2}\theta'(y)dy} \tag{5.4}$$

where ψ_{aev} = the air-entry value of the soil under consideration;

ψ_r =the suction corresponding to the residual water content;

y = dummy variable of integration representing suction; and

θ' = the derivative of the volumetric function by Fredlund and Xing (Eq. 3.4)

5.3 PROJECT AND METHOD OF ANALSYIS

5.3.1 Project description

The 5.4m high MSE wall constructed with marginal fills in the Research Triangle Park of North Carolina that experienced a localized collapse during rainfall in 2001 is the focus of this study. Details of the MSE wall geometry and properties of the backfill materials are presented in Chapter 4.

5.3.2 Method of analysis

A series of numerical simulations were performed in order to investigate the MSE wall behavior constructed during rainfall infiltration. Figure 5.1 shows a procedural flow chart that was used in this study. Details of each step of analysis are described as follows.

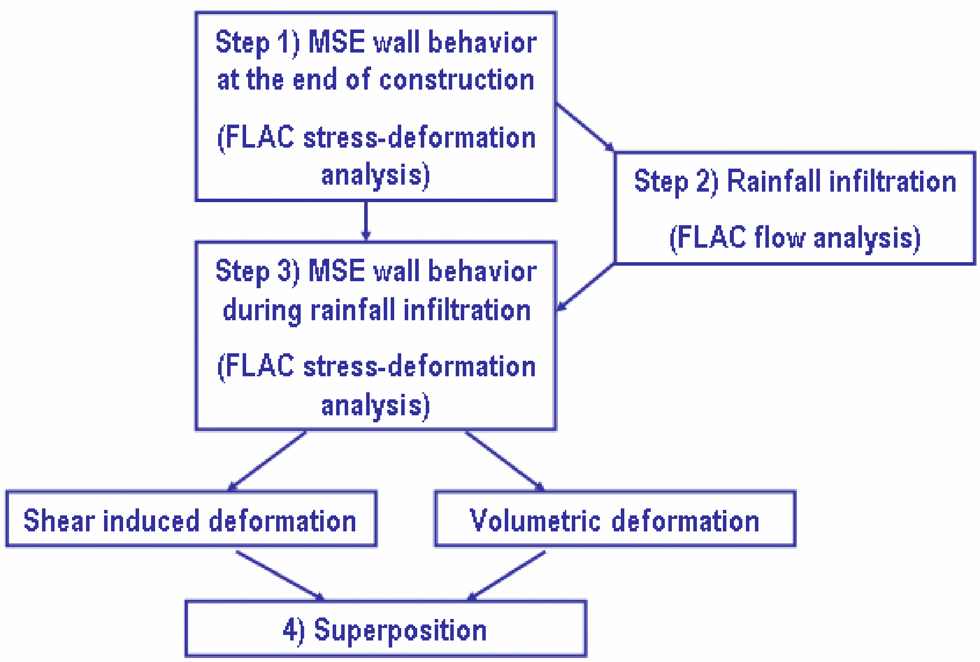

Fig. 5. 1 Analysis algorithm flow chart

Step 1) Numerical simulation of the MSE wall behavior during the construction

The behavior of the MSE wall at the end of construction was predicted using the developed FLAC model that accounted for unsaturated soil properties (elastic modulus and shear strength) and the staged construction of the wall (Chapter 4). The matric suction change due to loading (lifts of backfill) was computed in the model, and the properties of construction materials such as reinforcement, interfaces, and backfills were updated by the developed FISH subroutines based on changes in normal stress and matric suction. The matric suction distribution within the backfill at the end of construction was stored in a data file and used as initial values in the subsequent flow analysis.

Step 2) Transient seepage analysis for rainfall infiltration

Transient seepage analysis using unsaturated permeability was conducted in order to estimate changes of matric suction within the backfill due to rainfall infiltration. Deformation of soils was not considered in the seepage analysis (uncoupled analysis). The matric suction distribution at the end of wall construction, which was computed in the previous step (step 1), was used as the initial condition for the seepage analysis. When the desired rainfall period was reached during the simulation, the matric suction distribution was stored in a data file. These stored values of matric suction were recalled and used in the following stress-deformation analysis.

Step 3) Numerical simulation of the MSE wall behavior during rainfall infiltration

Post-construction wetting of compacted backfill causes wall deformations. Two factors that induce the wall deformation due to wetting were considered in this study. These two factors are described as following:

a. Shear induced deformation

Wetting generally results in significant loss of shear strength as well as increases in total unit weight. These adverse changes induce yielding of soil, and, in turn, plastic deformations.

b. Volumetric deformation

Matric suction change due to wetting causes volumetric deformation. Expansive behavior occurs in high density soils with high plasticity under relatively low stress conditions, and collapse behavior is observed in an open, partially unstable, partially unsaturated soil (i.e. soils compacted dry of optimum at low density) under relatively high stress conditions (Barden et al., 1973).

Details of the modeling techniques are described later in sections 5.4.2 and 5.4.3.

Step 4) Superposition of the results

As a final step, the results (lateral and vertical displacements within the solution domain and axial strain in the reinforcement) from the two numerical simulations described in step 3 were combined.

5.3.3 Cases used for numerical analysis

Four different conditions of the backfill were considered for numerical simulation. Table 5.1 lists the compaction conditions and permeabilities of backfill soils used for each case. Cases 1 and 2 were set up to represent the wall behavior constructed without and with the poor quality backfill zone behind the wall face (1.6m-wide), respectively. Additionally, cases 3 and 4 were introduced to consider possible variation of the backfill permeability. A saturated coefficient of permeability two times higher than that measured in the lab (k_{sat}) was adopted for cases 3 and 4.

Table 5. 1 Cases used for numerical simulations

	(1.6m wide zone)	**(Beyond 1.6m)**	**Permeability**
Case 1	Soil H*	Soil H	k_{sat}*
Case 2	Soil L*	Soil H	k_{sat}
Case 3	Soil H	Soil H	2 times k_{sat}
Case 4	Soil L	Soil H	2 times k_{sat}

* Soil H: ρ_d = 1.79g/cm3, w = 4.8% (R.C. = 94%); Soil L: ρ_d = 1.60g/cm3, w = 4.8% (R.C. = 84%); k_{sat} = saturated permeability obtained from laboratory tests

5.4. MODELING DESCRIPTION AND INPUT PROPERTIES

5.4.1 Simulation for rainfall infiltration

A two phase flow option in FLAC, which allows numerical modeling of the flow of two immiscible fluids (wetting fluid and non wetting fluid) through porous media, was used for the seepage analysis. In FLAC, the flow of each fluid (wetting fluid and non wetting fluid) is described using Darcy's law, and the relationship between matric suction and permeability is accounted for in FLAC through an empirical law of the van Genuchten form (1980).

The MSE wall elements used for a seepage analysis are presented in Fig. 5.2. The backfill elements (ABCD) were only selected for the flow analysis because it was believed that the properties of backfills were most influenced by rainfall infiltration (or matric suction change). In this study only water flow was considered, ignoring air flow by assuming the air pressure to be atmospheric (i.e. zero). The side (AC and BD) and bottom (CD) boundaries of the model were defined as a "seepage boundary" in FLAC (Itasca, 2000). At a seepage boundary, the non-wetting fluid pressure (air pressure) is atmospheric (zero) and the boundary is impermeable to the wetting fluid (water pressure), as long as the wetting pressure is negative. The pore water pressure ($u_w = 0$) and degree of saturation ($S = 1$) was applied on the ground surface boundary (AB) in order to simulate the rainfall. The matric suction at the end of construction (Chapter 4) was assigned to the model. Upon generation of the initial condition, the simulation was carried out for a total of 12 days with intermediate results at three additional times (3, 6, and 9 days). This was done to explore the influence of rainfall infiltration and not because the wall in question experienced 12 days of continuous rainfall.

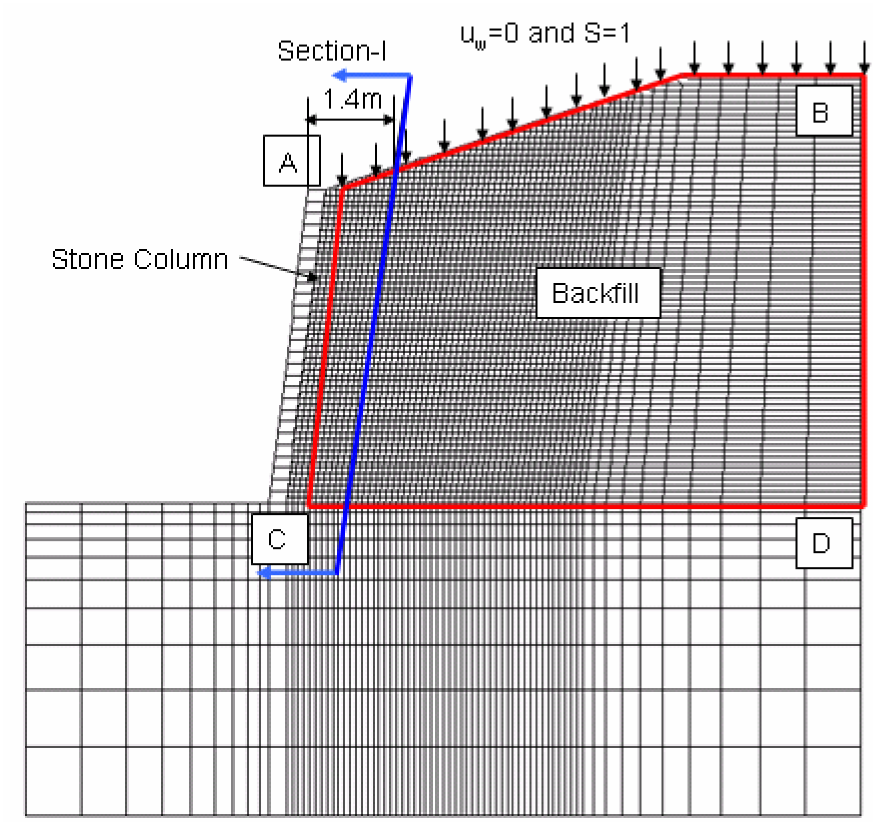

Fig. 5. 2 FLAC mesh and boundary conditions used for flow analysis

Table 5.2 shows the van Genuchten fitting parameters and saturated coefficients of permeability for soils H and L that are needed to define unsaturated flow. The fitting parameters for van Genuchten's equation (Eq. 5.3) and residual degree of saturation, S_r were determined from the best fit of the corrected pressure plate test data (Chapter 4). Rorie (2006) performed the falling head permeability tests for the backfill materials that were compacted at varying dry densities and as-compacted water contents. Figure 5.3 shows the saturated coefficients of permeability (k_{sat}) for the specimens compacted to dry densities of 1.53g/cm^3 and 1.60g/cm^3 at an as-compacted water content of 4.7%. The saturated coefficient of permeability for soil H (ρ_d=1.79g/cm^3, w = 4.7%) was estimated based on the log-linear relationship between permeability and void ratio as shown in Fig. 5.3. Figure 5.4 shows the coefficient of permeability functions with respect to matric suction for each case used in the simulation. The soil permeability decreases with increasing matric suction.

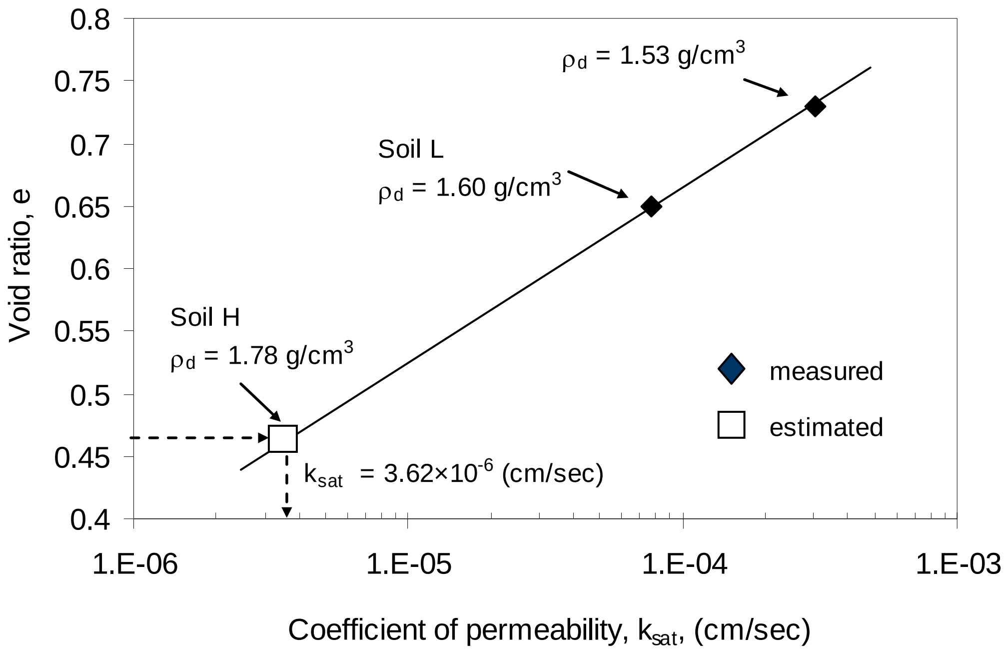

Fig. 5. 3 Determination of k_{sat} (Soil H) based on log-linear relation (under 5kPa overburden pressure)

Table 5. 2 Values of van Genuchten parameter and k_{sat} for soils H and L

	Soil H	**Soil L**
a (1/kPa)	0.0237	0.0226
n	1.380	1.300
m	0.275	0.231
S_r	0.02	0.00
k_{sat} (cm/sec)	3.62×10^{-6}	7.75×10^{-5}

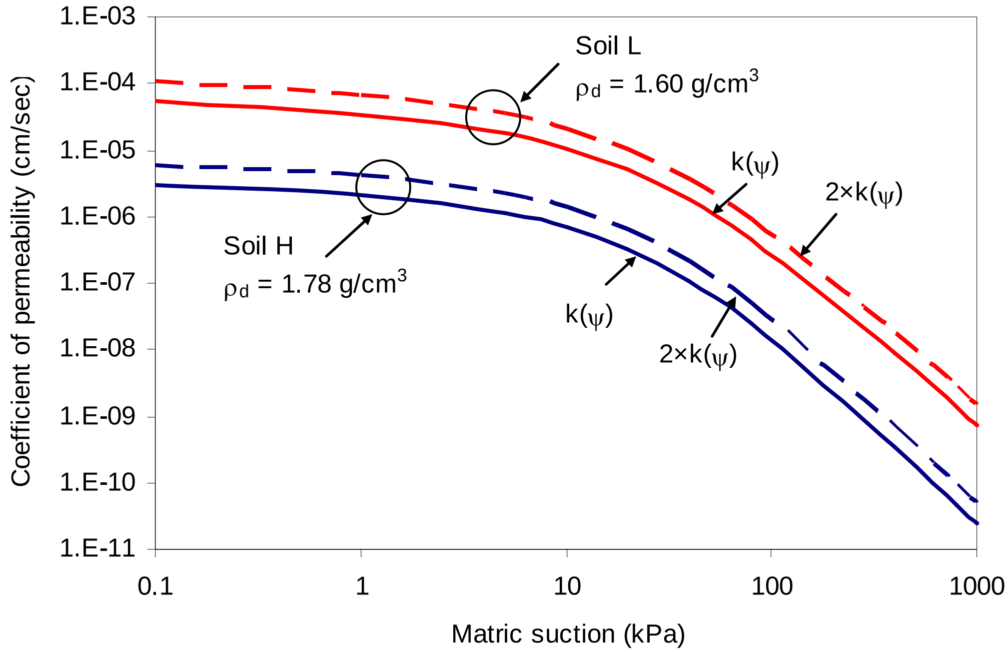

Fig. 5. 4 Coefficients of permeability with respect to matric suction for soils H and L

5.4.2 Simulation for shear induced deformation due to wetting

Figure 5.5 shows the shear strength for soils H and L under zero net normal stress (total cohesion intercept, *c*) determined from the saturated shear strength parameters and the SWCCs using Vanapalli et al.'s 2nd approach (Chapter 4). Once the value of *c* is determined as a function of matric suction, the shear strength at any net normal stress can be calculated using a constant internal friction angle, ϕ', as follows:

$$\tau_f = c + (\sigma_n - u_a)\tan\phi' \tag{5.5}$$

where, $c = c' + (u_a - u_w)[(\tan\phi')\left(\frac{S - S_r}{1 - S_r}\right)]$ from Vanapalli et al.'s 2nd approach.

By the FISH subroutine developed in the FLAC model, the total cohesion of backfill elements was updated according to the changes of the matric suction (determined from transient flow analysis). As an example, Fig. 5.6 shows the matric-suction and total cohesion profiles for case 2 during rainfall infiltration (3, 6, 9, and 12 days) along Section-I located at 1.4m from the wall face (in the middle of the poor quality backfill zone as shown in Fig. 5.2). Significant decreases (from 93kPa to 0kPa) in total cohesion are observed in the upper portion of the wall and the depth of this shear strength decreased zone increases as the rainfall period increases. In addition to consideration of cohesion decrease, the increase in the total unit weight of the backfill soil due to wetting was updated by the FISH subroutine. The FLAC model with the increased total unit weight and decreased shear strength, as a result of the decreased total cohesion, was then cycled to equilibrium. The shear induced deformation was predicted from this analysis.

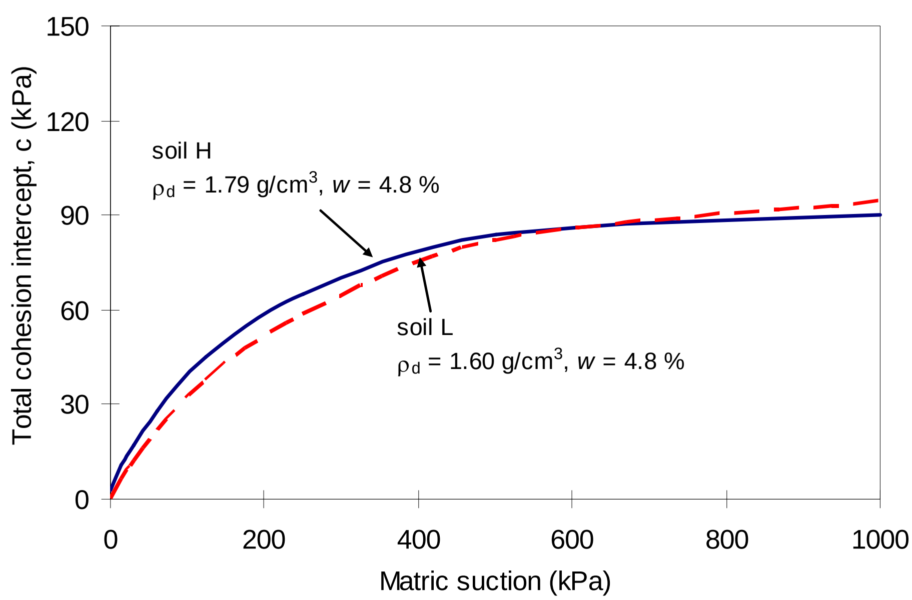

Fig. 5. 5 Total cohesion intercepts with matric suction for soils H and L

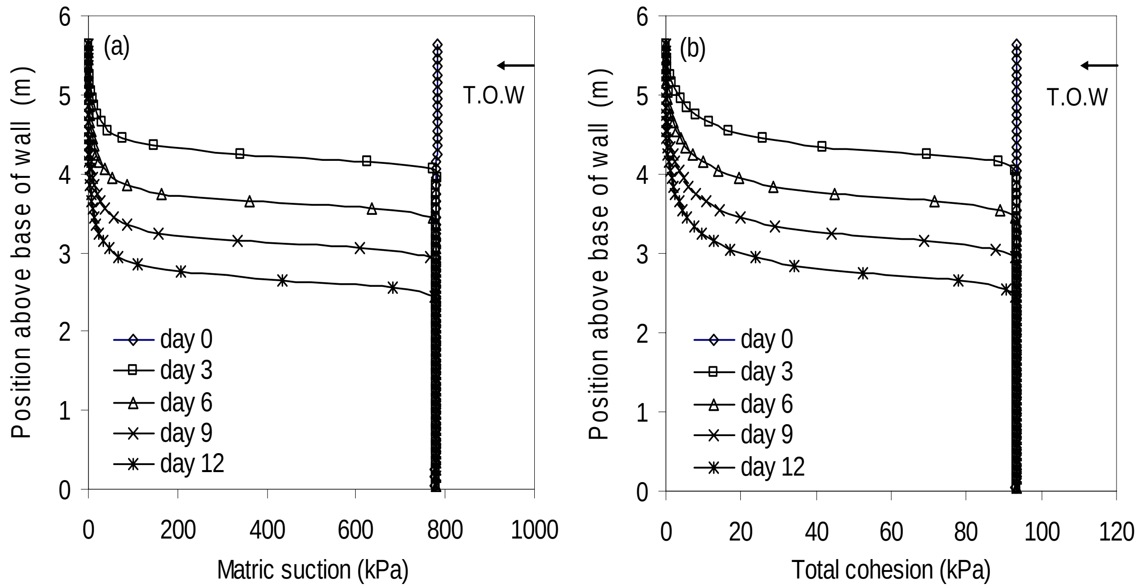

Fig. 5. 6 Variations of (a) pore-water pressure and (b) total cohesion along Section-I (Case 2)

5.4.3 Simulation for volumetric deformation due to wetting

In addition to shear-induced deformations, wetting can also produce volumetric deformations of soil. Wetting-induced volumetric strain (collapse/swell) of soils can be measured in laboratory tests, such as one dimensional oedometer tests (either single or double oedometer tests). Also, a triaxial cell can be used to determine the wetting induced strain under both isotropic and anisotropic stress conditions.

Noorany et al. (1992) developed a model for slope response analysis to compute wetting-induced slope deformation using the numerical simulation code, SWELL (Sweet, 1991). In their model, laboratory measured volumetric strains (both lateral and vertical) induced by wetting at various stress levels were used as input, thus simplifying the analysis and not requiring that the fundamental unsaturated material behavior be modeled. The same model was implemented in FLAC by Noorany et al. (1999) and can be described as follows:

Step 1) An initial state of equilibrium is computed under gravitational and applied stresses.

Step 2) Based on the results of the laboratory test, the wetting induced strains can be expressed by logarithmic functions (Eqs. 5.6 and 5.7) or linear function (Eqs. 5.8 and 5.9) of vertical stress, σ_{yy} normalized by atmospheric pressure, p_a:

$$\Delta\varepsilon_{yy} = c_1 \log\left\{a_1\left(\frac{\sigma_{yy}}{p_a}\right)\right\} \tag{5.6}$$

$$\Delta\varepsilon_{xx} = \Delta\varepsilon_{zz} = c_3 \log\left\{a_3\left(\frac{\sigma_{yy}}{p_a}\right)\right\} \tag{5.7}$$

$$\Delta\varepsilon_{yy} = c_1 - a_1(\sigma_{yy} / p_a) \tag{5.8}$$

$$\Delta\varepsilon_{xx} = \Delta\varepsilon_{zz} = c_3 - a_3(\sigma_{yy} / p_a) \tag{5.9}$$

where a_1,a_3, c_1, and c_3 are the fitting parameters.

Step 3) The wetting stresses are calculated from the wetting strain using the incremental form of Hooke's law as follows:

$$\Delta\sigma_{xx} = \left[(K+\frac{4}{3}G)\cdot\Delta\varepsilon_{xx} + (K-\frac{2}{3}G)(\Delta\varepsilon_{yy}+\Delta\varepsilon_{zz})\right] \tag{5.10}$$

$$\Delta\sigma_{yy} = \left[(K+\frac{4}{3}G)\cdot\Delta\varepsilon_{yy} + (K-\frac{2}{3}G)(\Delta\varepsilon_{xx}+\Delta\varepsilon_{zz})\right] \tag{5.11}$$

$$\Delta\sigma_{zz} = \left[(K+\frac{4}{3}G)\cdot\Delta\varepsilon_{zz} + (K-\frac{2}{3}G)(\Delta\varepsilon_{xx}+\Delta\varepsilon_{yy})\right] \tag{5.12}$$

where K and G are the bulk and shear modulus, respectively.

Step 4) For the wetting zone above the prescribed wetting front, the wetting stresses are added to the initial stresses of soil elements, and the FLAC model is cycled to equilibrium.

In this research, several advanced features were added to the model developed by Noorany et al. (1999). These features are described as:

(1) The matric suction distribution within the backfill was computed by a seepage analysis that involves saturated and unsaturated flow. Therefore, the changes in degree of saturation due to water infiltration were smoothly defined, as intermediate values between initial and saturated conditions were evaluated, rather than defined as one of two extreme conditions (either initial or saturated) by the prescribed wetting front.

(2) The amount of volumetric strain in the process of wetting (between initial and saturated conditions) was estimated by multiplying the maximum collapse (or swell) potentials (Eq. 5.6 through 5.9) by the Percent Collapse Potential, *PCP*. The value of *PCP* was determined from the SWCC, assuming the wetting strain magnitude is proportional to the amount of moisture gain (or loss) (Rodrigues and Vilar, 2006). Figure 5.7 shows an example for the determination of *PCP*. The values of *PCP* are 0 % and 100% for point 1 and point 3, respectively. The calculation of *PCP* for point 2 is shown in Fig. 5.7. The vertical and horizontal volumetric strains of soil during the wetting process are now expressed by the logarithmic functions 5.13 and 5.14, respectively.

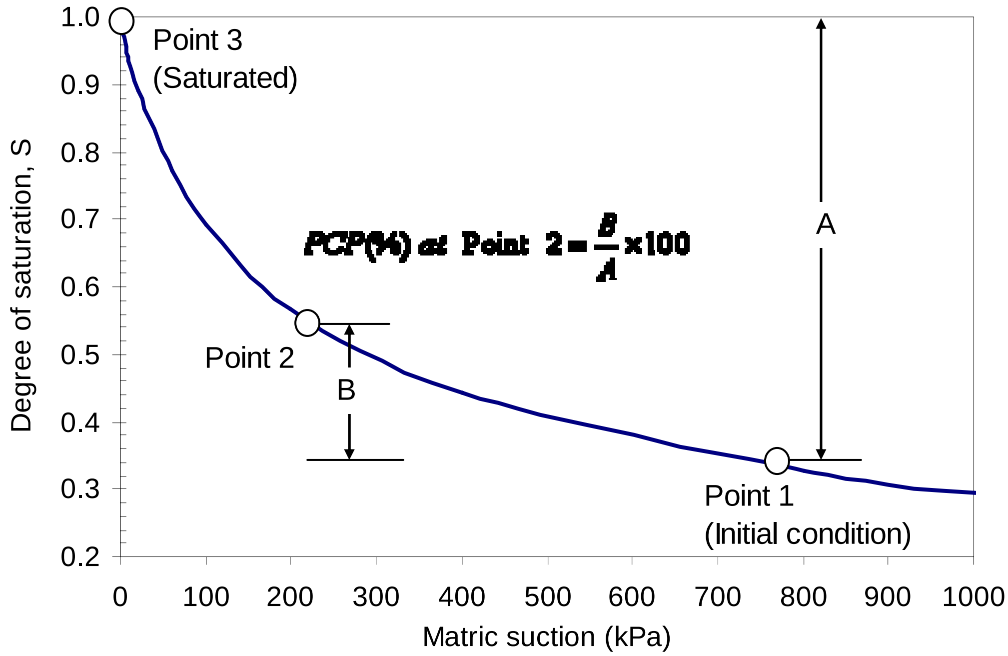

Fig. 5. 7 Example of determination of *PCP* from SWCC

$$\Delta\varepsilon_{yy} = \left[c_1 \log\left\{ a_1 \left(\frac{\sigma_{yy}}{p_a} \right) \right\} \right] \times \left(\frac{PCP(\%)}{100} \right) \tag{5.13}$$

$$\Delta\varepsilon_{xx} = \Delta\varepsilon_{zz} = \left[c_3 \log\left\{ a_3 \left(\frac{\sigma_{yy}}{p_a} \right) \right\} \right] \times \left(\frac{PCP(\%)}{100} \right) \tag{5.14}$$

(3) Both lateral and vertical displacements were restricted at the grids of the "non-wetting zone" where the values of *PCP* were computed to be zero. Figure 5.8 shows the results of simulations that were performed without (a and c) and with (b and d) application of restrictions at the grids of the "non wetting" zone. It was believed that wetting deformations must be shown in the wetting zone (not in the "non-wetting" zone) and soil settlement could only occur once the compressive stresses were assigned to the elements. However, the

computed simulation results indicated that no restriction at the grids below the wetting front allowed the soil elements in the wetting zone to compress in both directions (Fig. 5.8a) when the assigned stresses were compressive. This caused the elements nearby the wetting front to move upward (Fig. 5.8c). This unreasonable result of the simulation was improved by fixing the grids in the "non-wetting" zone in both lateral and vertical directions (Figs. 5.8b and 5.8d).

(4) For the purpose of this portion of the analysis, very large values for the cohesion and tensile strength were assigned to the backfill, forcing the material to behave elastically. Therefore, shear induced deformation could not occur in this simulation, even though high wetting stresses were added to the elements.

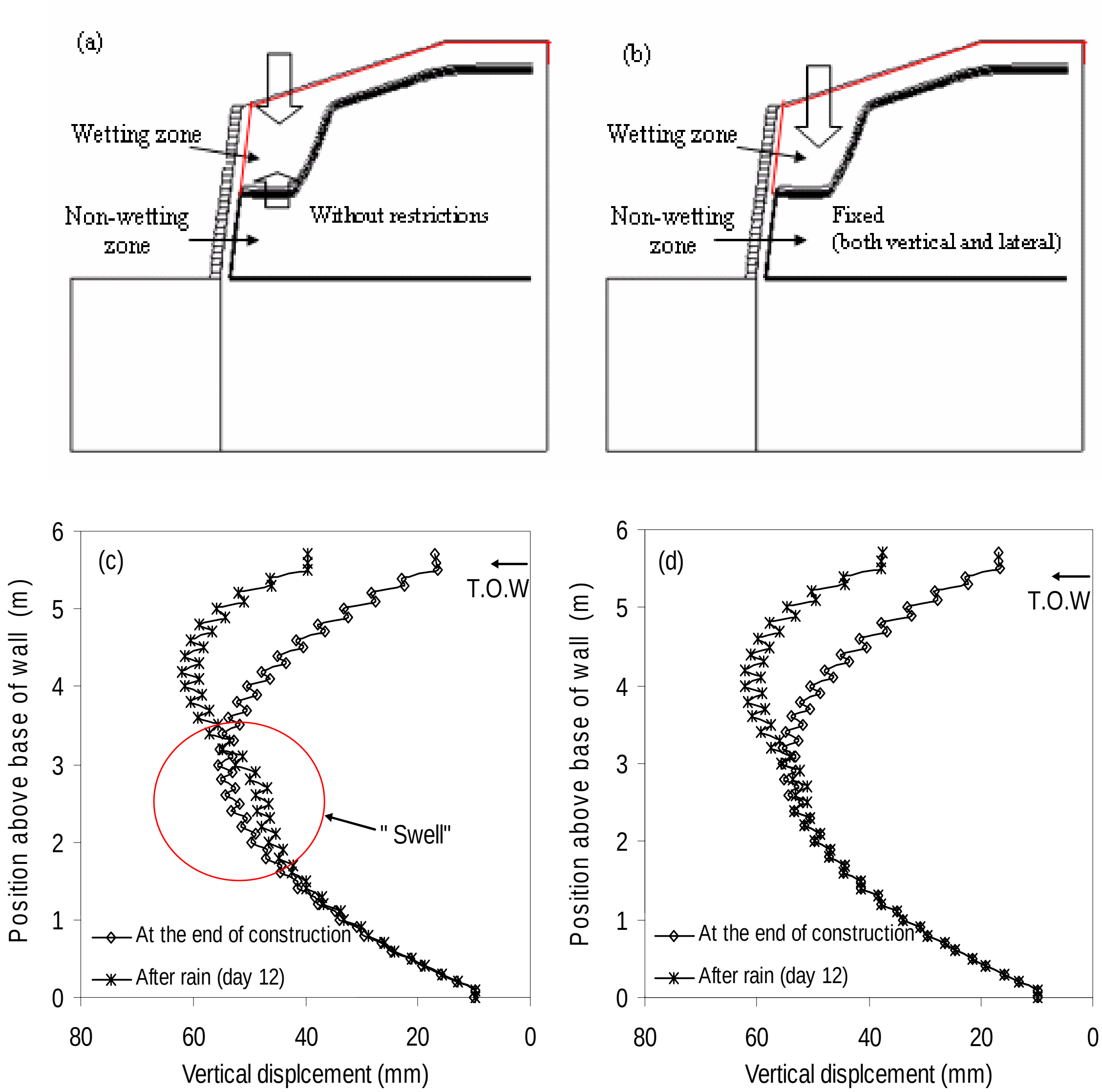

Fig. 5. 8 Comparison of the results without and with the application of restriction at the grids below wetting front

In this study, only vertical strains measured in the one dimensional oedometer tests were used as input to the FLAC model, assuming there were no lateral displacements (K_0 condition). Figure 5.9 shows the results of one dimensional oedometer tests for soils H and L (Rorie, 2006). As would be expected, it is observed that the low density soil (soil L) has a higher collapse potential than the high density soil (soil H) at a given stress. The fitting of collapse potential data to the logarithmic function prescribed in Eq.5.6 resulted in the parameters summarized in Table 5.3. The upper bounds (Max. swell) were used at the volumetric strain determined at overburden pressure at 5 kPa (Fig. 5.9).

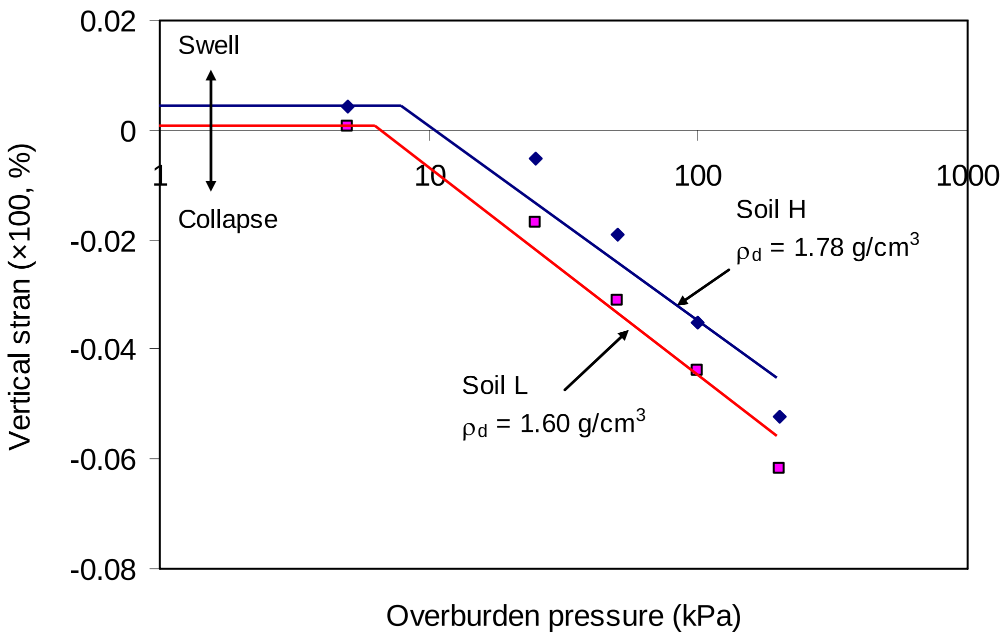

Fig. 5. 9 Measured collapse potentials (soils H and L) and the best fit functions

Table 5. 3 Collapse potential fitting parameters

	Soil H	**Soil L**
a_1	9.963	15.280
c_1	-0.0352	-0.0385
Max. swell	0.004	0.00053

5.5 RESULTS

5.5.1 Transient seepage analysis

The matric suction distributions for Cases 2 and 4 during rainfall periods are shown in Figs. 5.10 and 5.11, respectively. It is clearly shown that there is a substantial difference between the infiltration depths in the poorly and well compacted zones. Also, it is observed that the transition zone between the wetting zone and the non-wetting zone is very sharp and distinct because of the high initial matric suction. From the results of Case 2 as shown in Fig. 5.10, the infiltration depth in the poor quality compaction zone is about 3m after the 12-days rainfall, while a relative shallow advancing “wetting front” (less than 1m) is developed in the well compacted zone, as most of the rainfall cannot infiltrate into the soil because of relatively low water permeability. The matric suction distribution of Case 4 that was performed using the higher coefficients of permeability (2 times) is shown in Fig. 5.11. The matric suctions almost disappear in the low quality compaction zone after 12 days of rainfall infiltration. However, the depth of the wetting front is still only about 1m below the ground surface for the well compacted zone. Although the matric suction distributions for Cases 1 and 3 are not presented in this study, one might approximate them by extending the wetting fronts in the good quality compaction zones, which were determined from Cases 2 and 4, across the low quality compaction zone.

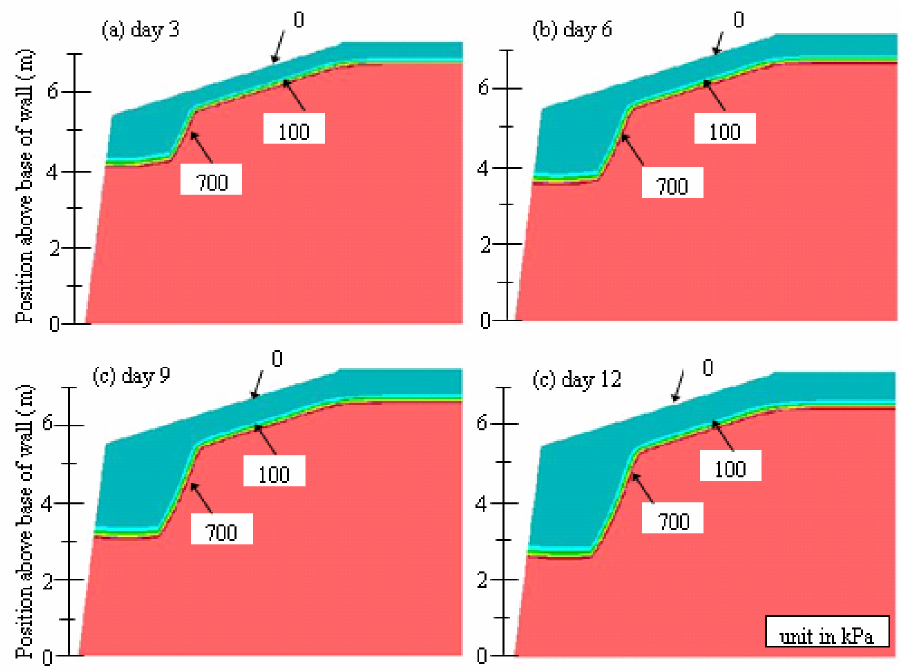

Fig. 5. 10 Matric suction contours during rainfall infiltration for Case 2

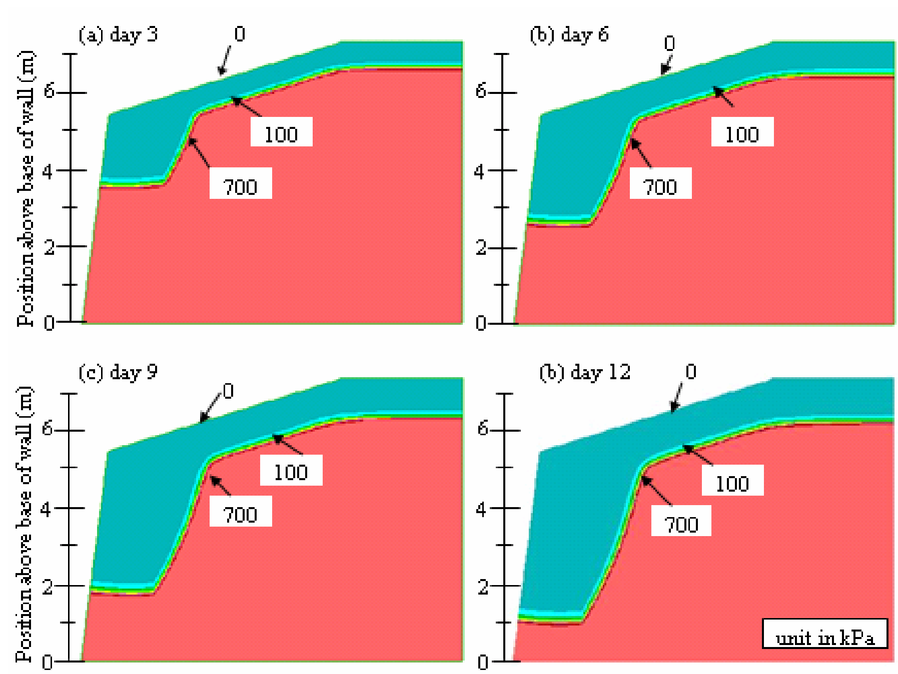

Fig. 5. 11 Matric suction contours during rainfall infiltration for Case 4

5.5.2 Stress-deformation analysis

This section provides the results of simulations for determining the wetting induced deformation and corresponding tension forces in the layers of reinforcement. The results of Case 2, which considers the low quality compaction zone behind the wall face space (1.6m-wide), are presented first and then the effect of varying permeability on the behavior of the wall is investigated through comparison between the results of Cases 2 and 4. Finally, the behaviors of the walls that were constructed with high density backfill using two different values of coefficients of permeability are presented (Cases 1 and 3).

Results for Case 2

a. Shear induced deformation

The variations of pore pressures and corresponding total cohesions with depth during the rainfall periods are shown along Section-I in Fig. 5.12. The "day 0" in the figure indicates the time when the wall construction was completed (the end of wall construction). Figures 5.13 and 5.14 illustrate the development of lateral and vertical displacements in the MSE wall that result from the decrease in backfill shear strength due to wetting. It should be noted that only the "change" in the displacements after beginning of the rain is shown in the figures (not the cumulative displacements from the construction of the wall). It is clearly seen from the figures that the wall movement tends to increase as the rain infiltrates into the wall system. As shown in Figs. 5.13(a) and 5.14(a), no significant increases in lateral and vertical displacements are observed during the first 3-day rainfall. The displacements, however, start to gradually increase with increasing rainfall (Figs. 5.13b-5.13d, and Figs. 5.14b-5.14d). Most displacements occur within the poorly compacted zone. The changes of the displacements along the wall height during the rainfall periods are more clearly shown in Fig. 5.15.

Figure 5.16 shows the variation of reinforcement tension along the length of each layer during rainfall infiltration. As can be seen in this figure, the increases in reinforcement tension appear to be in the low quality compaction zone and the upper layers (layers 8-11). Figure 5.17 shows the maximum tension forces, T_{peak}, and the average tension forces, T_{avg}, for each layer along the wall height.

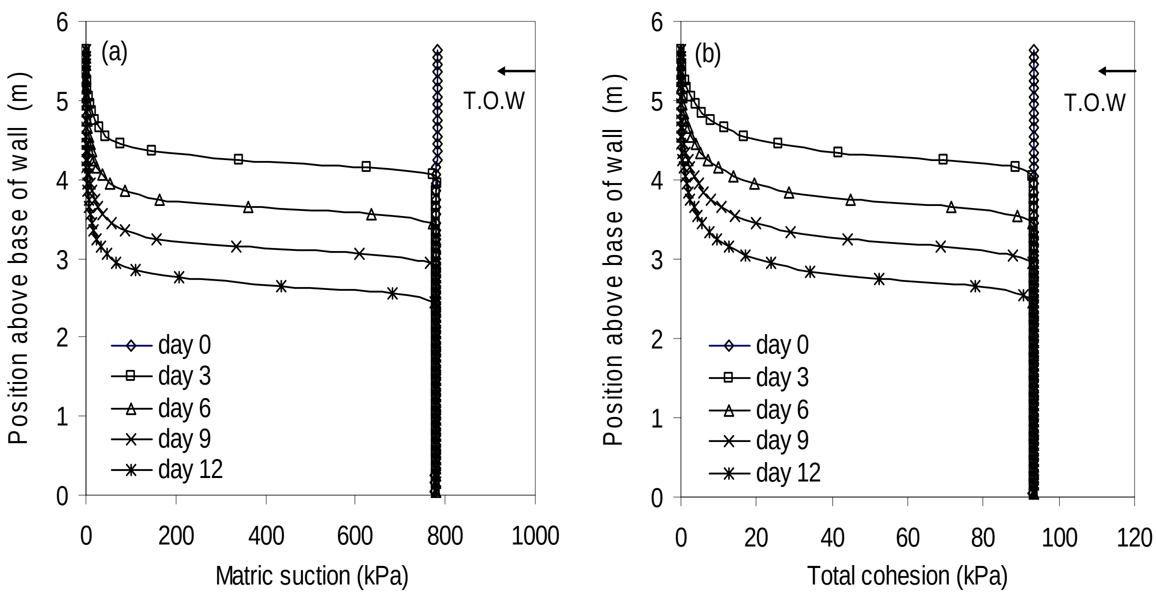

Fig. 5. 12 Profiles of (a) matric suction and (b) total cohesion for Case 2

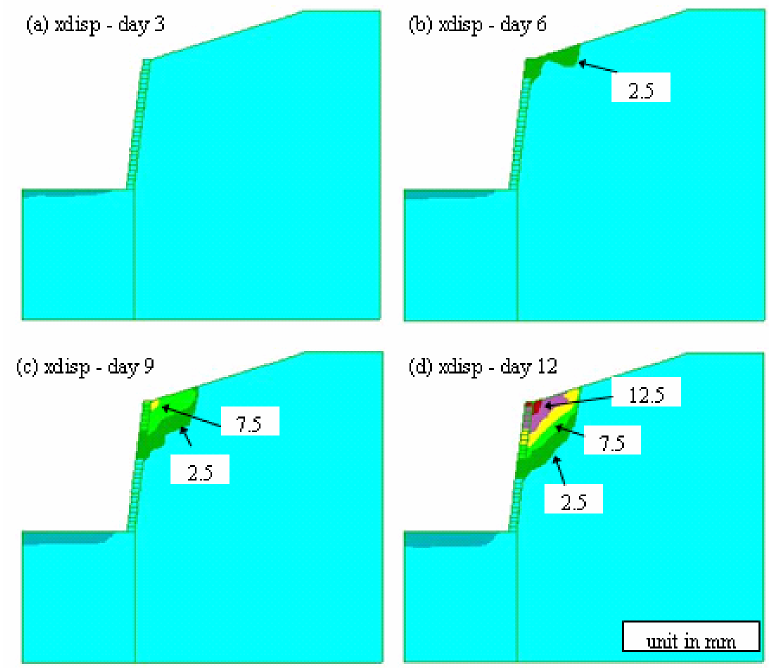

Fig. 5. 13 Shear-induced deformation (lateral displacement) due to wetting for Case 2

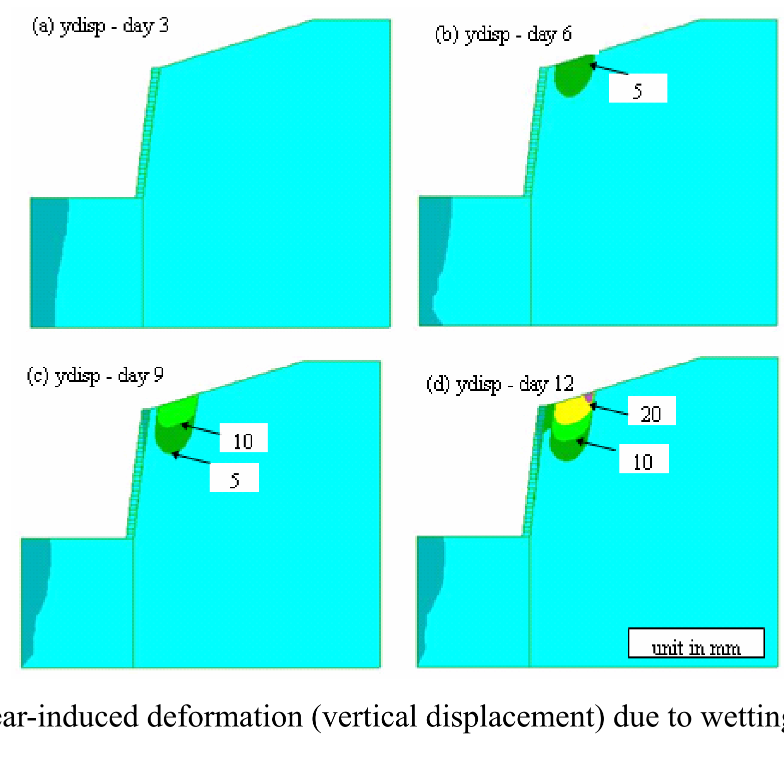

Fig. 5. 14 Shear-induced deformation (vertical displacement) due to wetting for Case 2

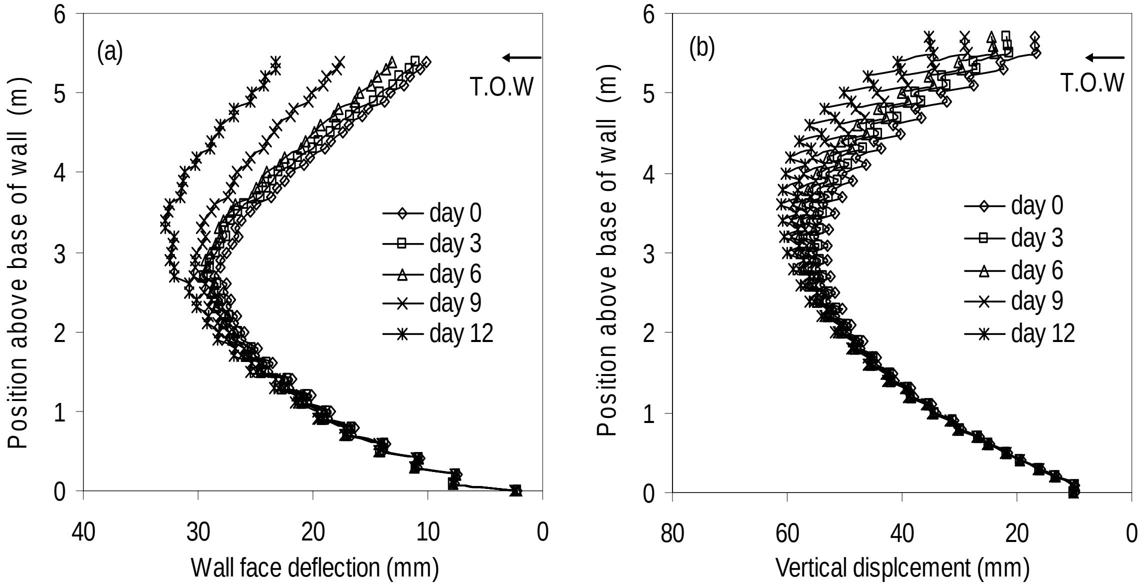

Fig. 5. 15 Variation of wall movements due to shear-induced deformation during rainfall infiltration for Case 2:(a)Wall face lateral deflection and (b)Vertical displacement at Section-I

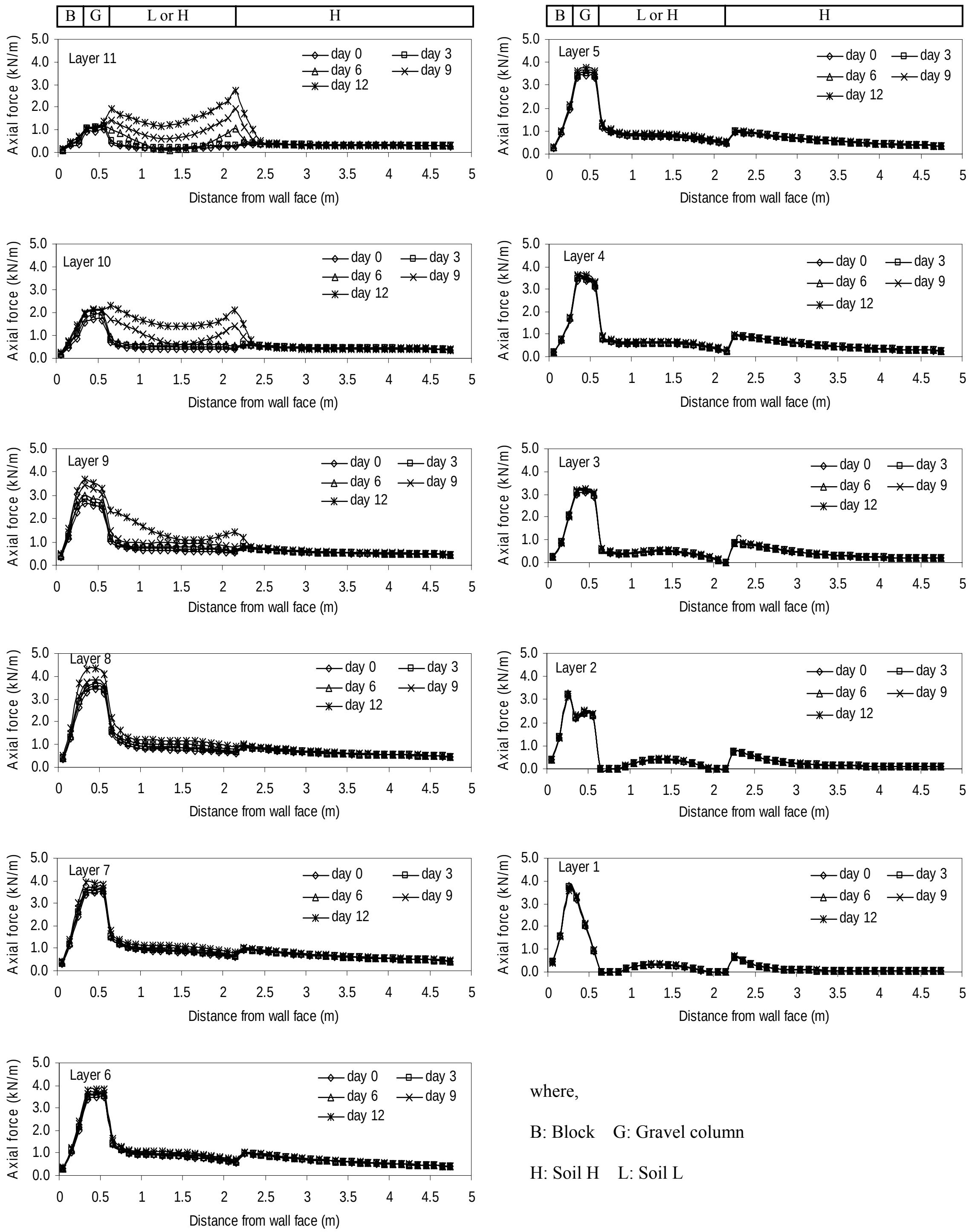

Fig. 5. 16 Variation of reinforcement tensions due to shear-induced deformation during rainfall infiltration for Case 2.

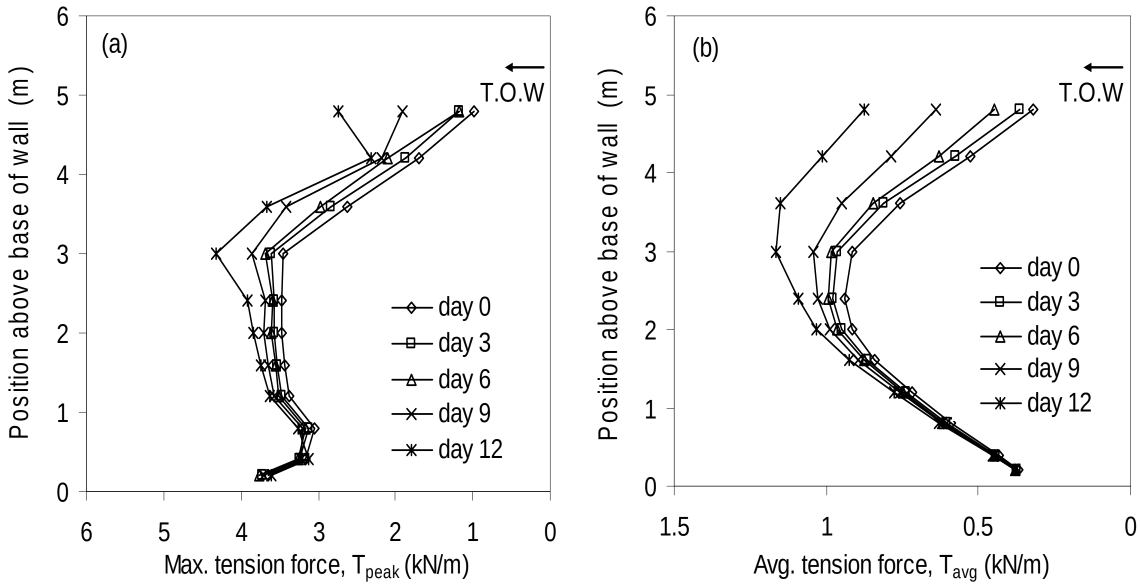

Fig. 5. 17 Variation of reinforcement tension along wall height due to shear-induced deformation during rainfall infiltration for Case 2: (a) maximum tension, T_{peak} and (b) average tension, T_{avg}

b. Volumetric deformation (Case 2)

Figures 5.18 and 5.19 show the wetting-induced changes in lateral and vertical displacements, respectively, as a result of the volumetric strains. It is seen from these figures that the vertical displacements are dominant in the wall behavior since only the vertical wetting strain, which was determined from the one-dimensional oedometer test, was used as an input in the simulation (assuming that the lateral volumetric strain due to wetting is equal to zero). However, small lateral displacements are still found in the wall behavior because settlements in the poorly compacted zone cause the wall face and nearby soil to move toward that zone (Fig. 5.20). For this reason, inward displacements are observed in the upper portion of the wall face. The variations of the wall face deflection and vertical displacement (along the section-I) induced by the volumetric strain during the rainfall periods are shown in Figs. 5.21(a) and (b).

Figure 5.22 presents the changes in reinforcement tension along the length of each layer during the rainfall periods, which result from the wetting-induced volumetric strain of backfill. The reinforcement tension of the layers within the wetting zone (layers 8-11) are seen to increase significantly near the wall facing because of the increasing differential settlements between the block and backfill during the rainfall. Also, it is observed that there is a slight decrease in the reinforcement tension (for layers 10-11) in the low quality compaction zone (Fig. 5.23). This behavior occurs because the reinforcement tension is released by the lateral wall displacements that move toward that zone, as described previously in Fig. 5.20. The maximum tension forces, T_{peak}, and the average tension forces, T_{avg}, along the wall height are shown in Figs. 5.24(a) and (b), respectively. The increases in the maximum tension force are significant in the upper layers, however, the changes in the average tension force are small along the entire height of the wall

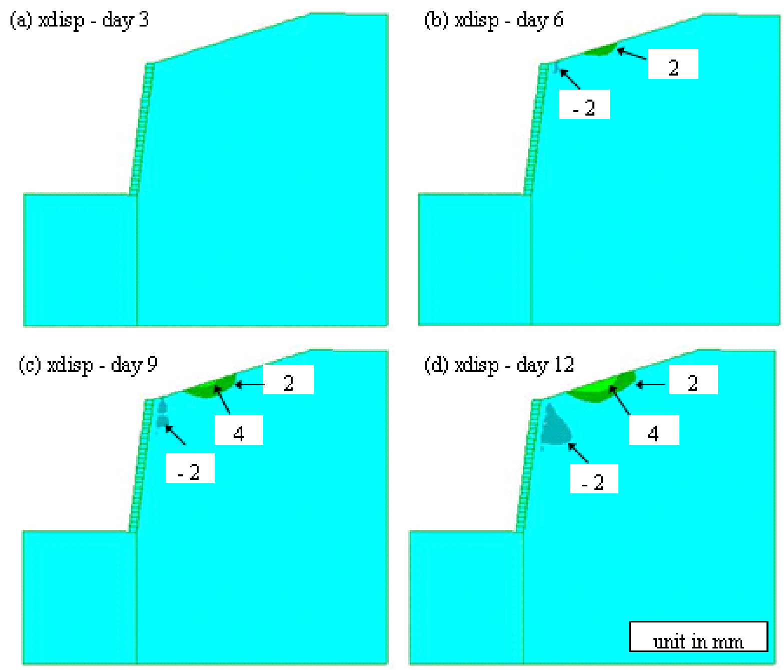

Fig. 5. 18 Wetting-induced volumetric deformation: lateral displacement for Case 2

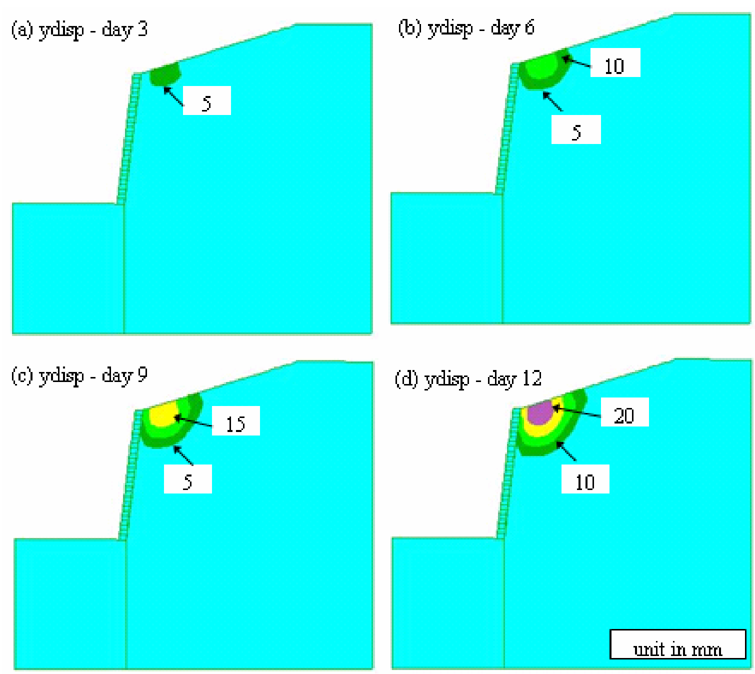

Fig. 5. 19 Wetting-induced volumetric deformation: vertical displacement for Case 2

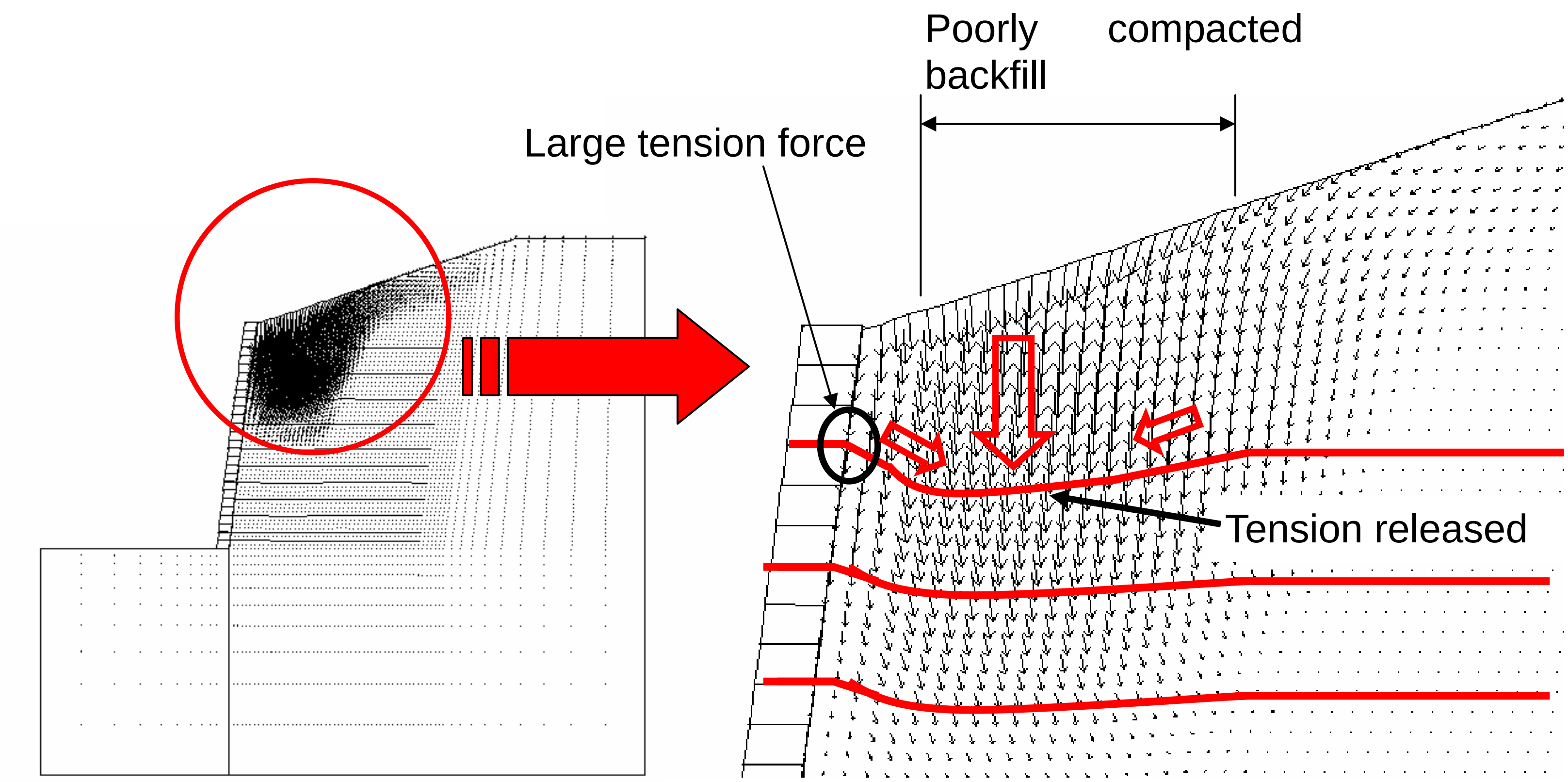

Fig. 5. 20 Displacement vectors induced by wetting (volumetric deformation)

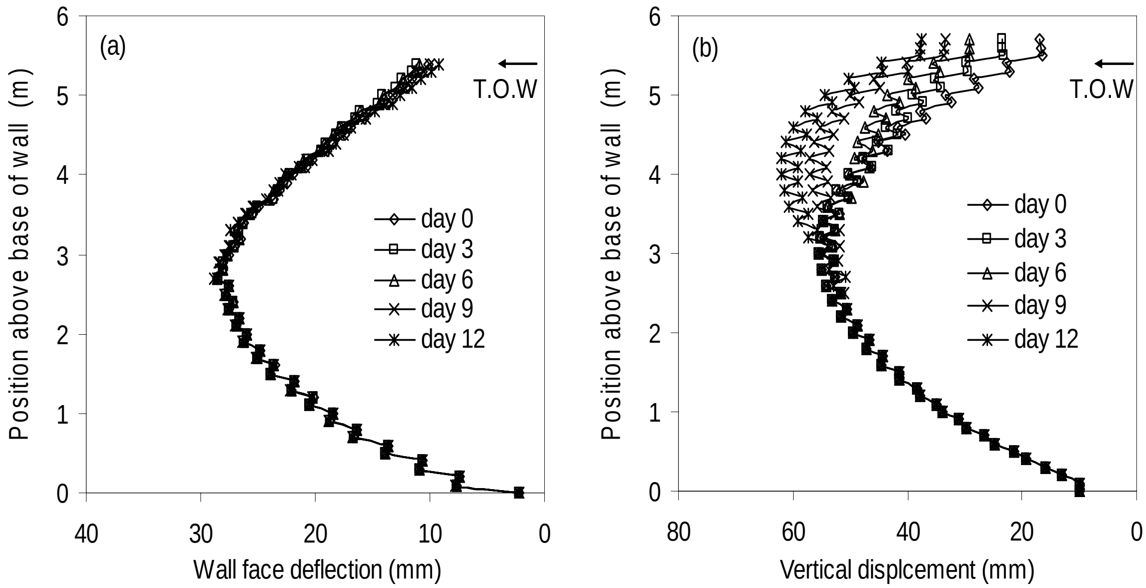

Fig. 5. 21 Variation of wall movements due to volumetric strain during rainfall infiltration for Case 2: (a) Wall face lateral deflection and (b) Vertical displacement at Section-I

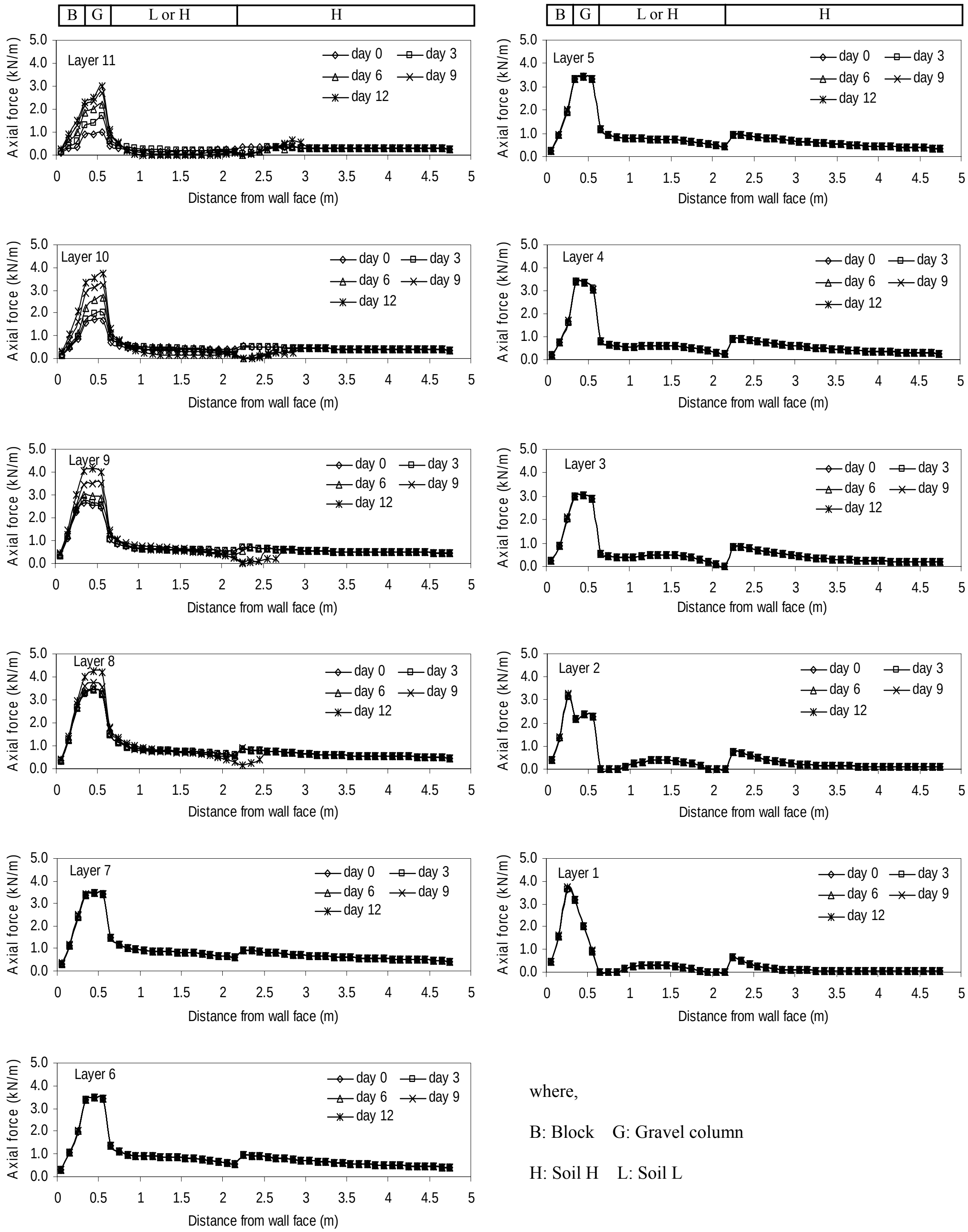

Fig. 5. 22 Variation of reinforcement tensions due to volumetric strain during rainfall infiltration for Case 2

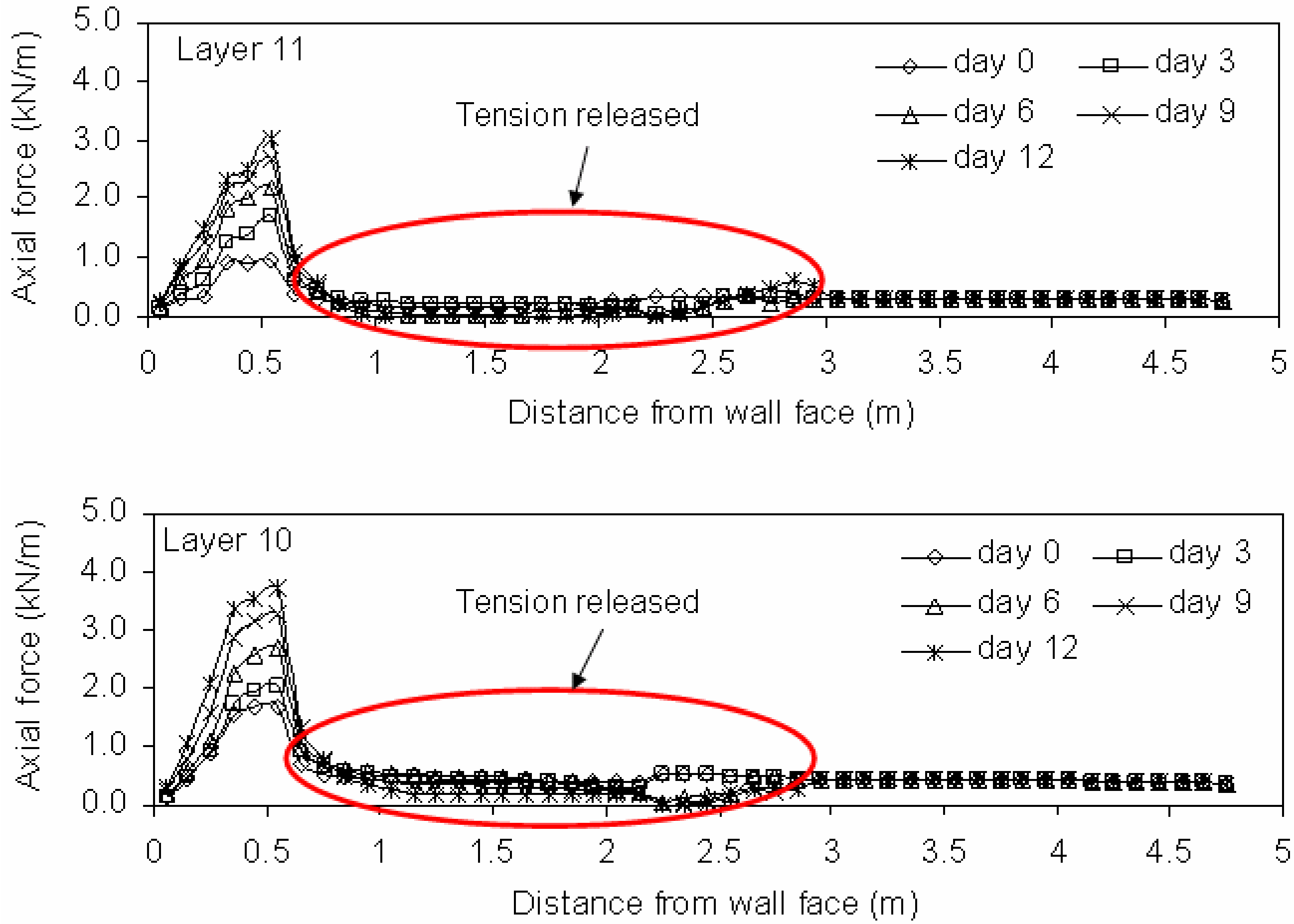

Fig. 5. 23 Decrease in reinforcement tension in low quality compaction zone

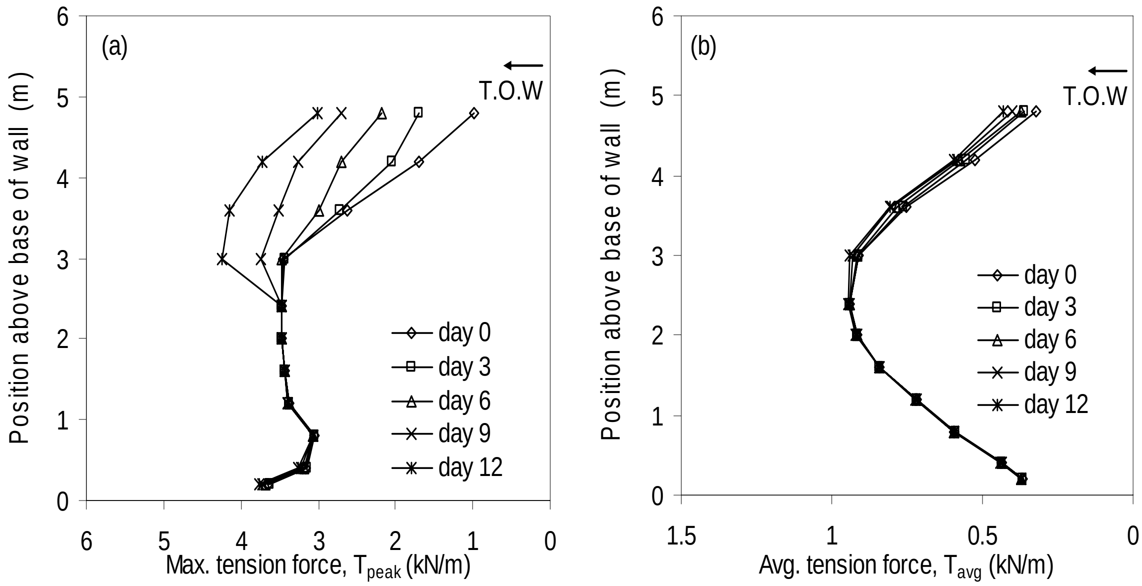

Fig. 5. 24 Variation of reinforcement tension along wall height due to volumetric strain during rainfall infiltration for Case 2:(a)maximum tension, T_{peak} and (b) average tension, T_{avg}

c. Total deformation –Combined results (Case 2)

The "total" displacements are estimated by summing up the displacements induced by (1) decreases of shear strength and (2) volumetric strain of backfill soils due to wetting. Figure 5.25 shows the face-deflection and vertical-displacement profiles during the 12-day rainfall from the end of the construction condition. It can be seen that the magnitude of the increased displacements become larger from the top of the wall (ground surface), and that the zone of significant displacement increases in depth. After 12-days of rainfall, the maximum values of the wall-face deflection and vertical displacements are predicted to be 33 mm and 74 mm, respectively. The locations of these maximum values are found at 0.6H and 0.8H, respectively (where H is the height of the MSE wall), which are higher than those at the end of construction (approximately 0.5H).

In the simulation, the compressive axial force in the reinforcement is restricted by assigning the compressive yield strength to a very small number (*ycomp* = 0.01kN). This implies that the axial forces cannot be superimposed once the reinforcement meets the compressive yield criteria. Therefore, the axial strains of reinforcements for each simulation are superimposed and then converted to the tension force using the reinforcement cross-sectional area and stiffness. Figure 5.26 illustrates the variation of reinforcement tension distribution along the length of each layer during rainfall infiltration. The maximum tension forces, T_{peak}, and the average tension forces, T_{avg}, for each layer along the wall height are shown in Figures 5.27(a) and (b), respectively. After the 12-day rainfall, the maximum values of T_{peak} and T_{avg} of all layers inside the MSE wall (defined as T_{peak_max} and T_{avg_max}, respectively) are computed to be 5.1kN and 1.2kN, respectively, and both are found at the top third layer.

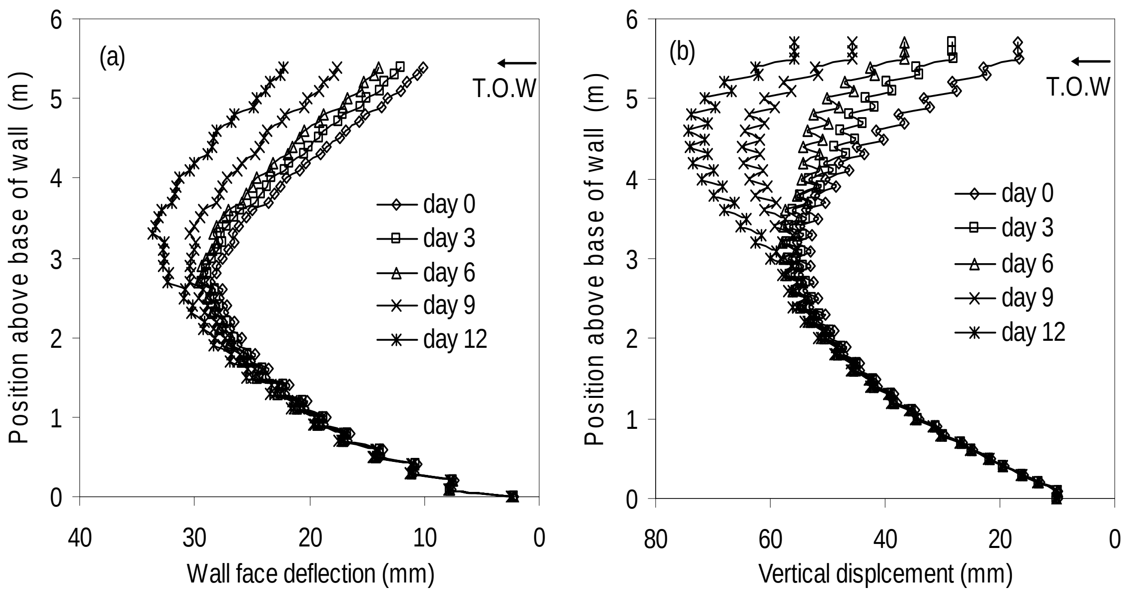

Fig. 5. 25 Variation of wall movements during rainfall infiltration for Case 2: (a) wall face lateral deflection and (b) vertical displacement at Section-I

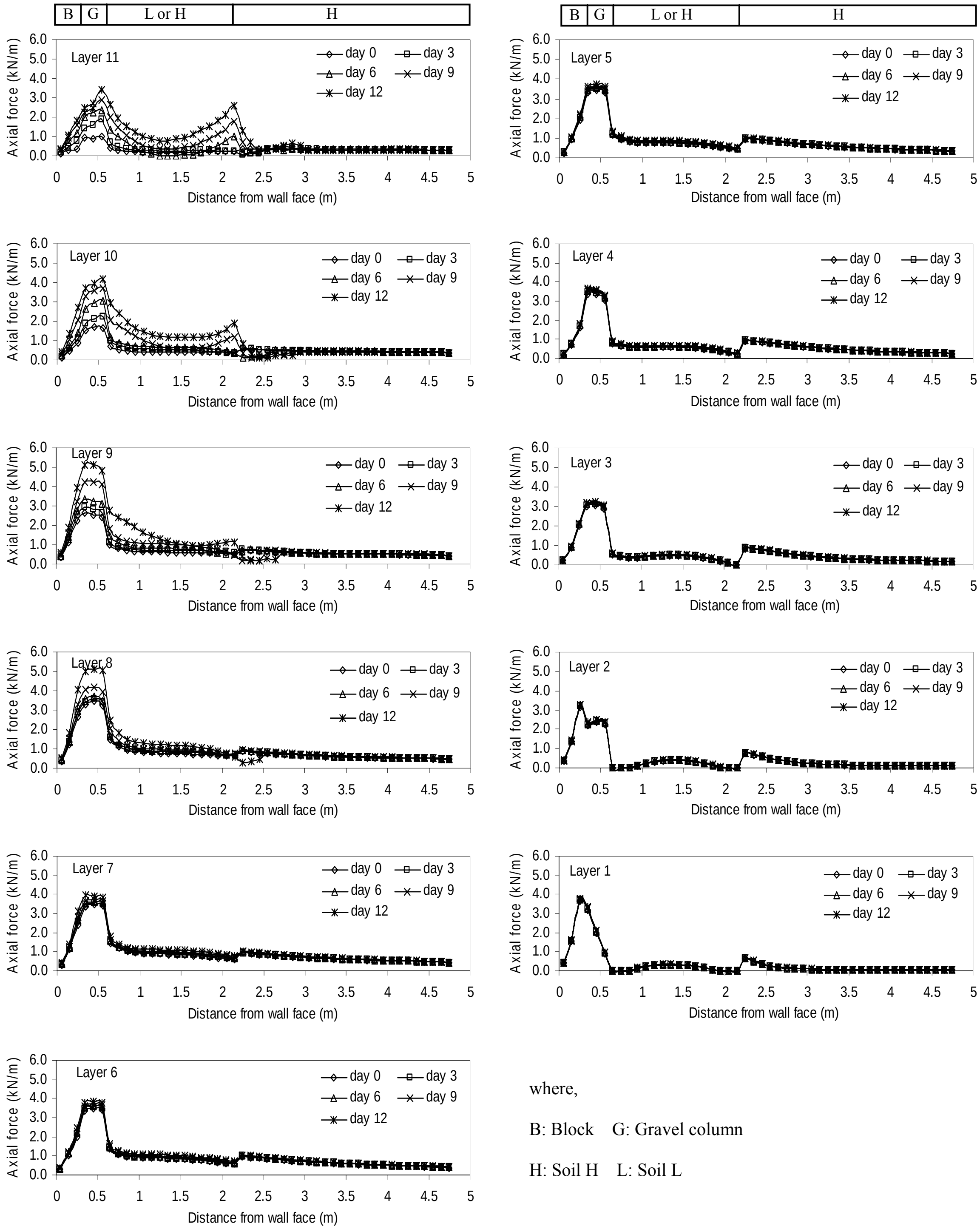

Fig. 5. 26 Variation of reinforcement tension during rainfall infiltration for Case 2

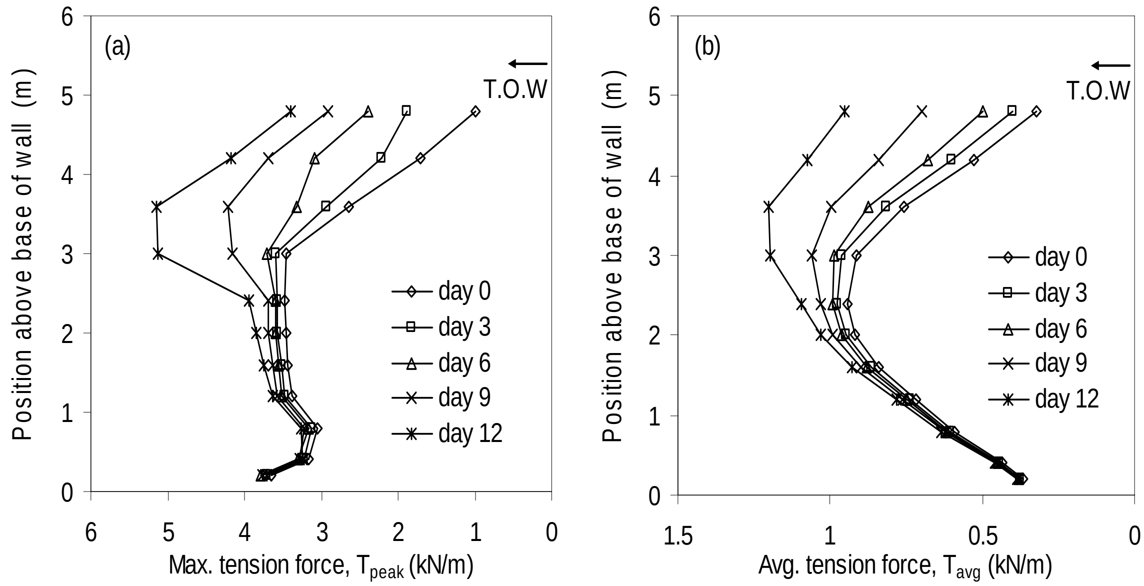

Fig. 5. 27 Variation of reinforcement tension during rainfall infiltration for Case 2: (a) maximum tension, T_{peak} and (b) average tension, T_{avg}

Results for Case 4

Figures 5.28 through 5.30 show the simulation results for Case 4 that were obtained using values of k_{sat} two times higher than those used for Case 2. It is seen in Fig. 5.28(a) that at 12days the wetting front for Case 4 is approximately 2m deeper than it is for Case 2. The simulation results are only presented for the "total" displacements and reinforcement tensions after the 12-day rainfall. The results for Case 2 are also presented in the graphs for the comparison. As expected, the results for Case 4 show the higher values of displacements and reinforcement tensions than those for Case 2 because of the extended wetting zone. The maximum values of 47mm and 107mm are observed for the wall face deflection and vertical displacements along the wall height (Fig. 5.29). The maximum values of 47mm and 107mm indicate a 42% and 44% increase, respectively, compared to those values of Case 2. However, these values are found at the same locations that were observed for Case 2 (at 0.6H and 0.8H, respectively). The values of T_{peak_max} and T_{avg_max} are predicted to be 7.7 kN and 2.0 kN, respectively (increases over 45% and 80%, respectively, compared to Case 2) and are still found at the top third layer.

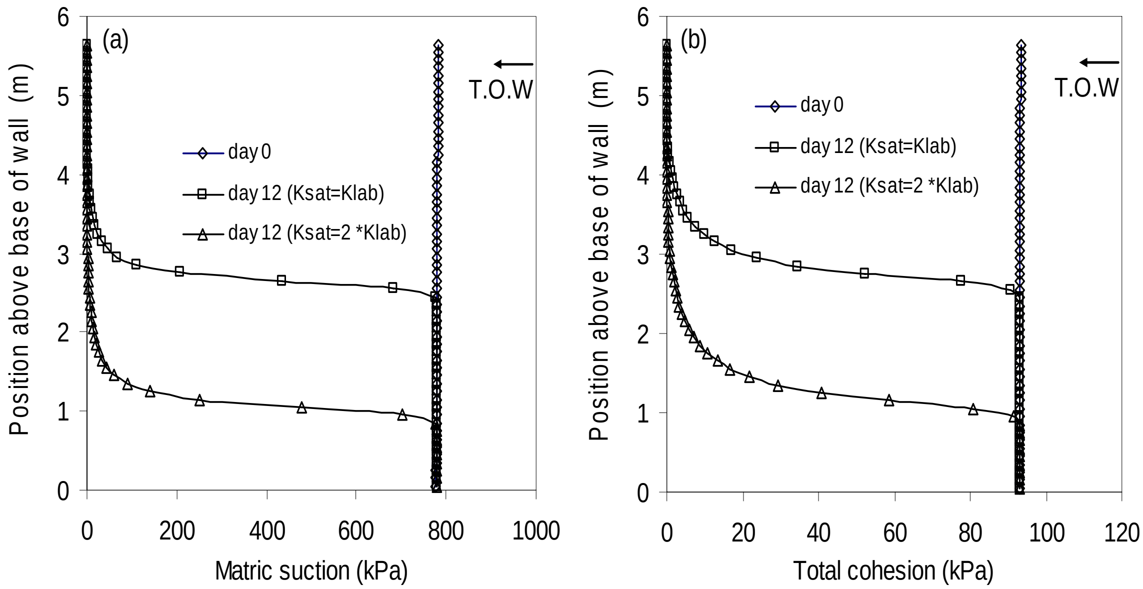

Fig. 5. 28 Profiles of (a) matric suction and (b) total cohesion after the 12-days rainfall for Cases 2 and 4

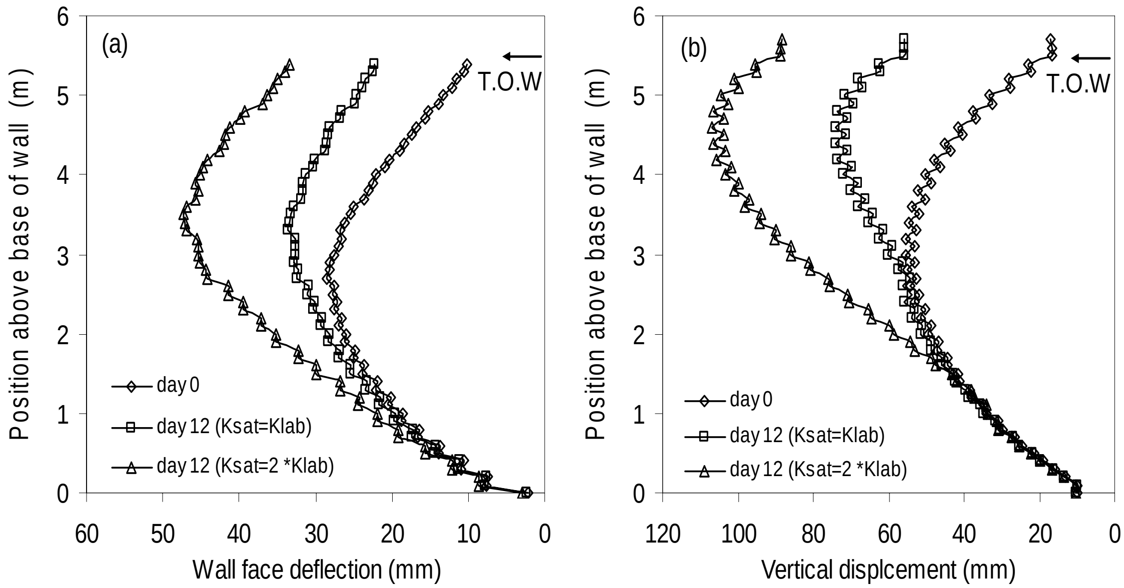

Fig. 5. 29 Wall movements after the 12-days rainfall for Cases 2 and 4: (a) wall face lateral deflection and (b) vertical displacement at Section-I

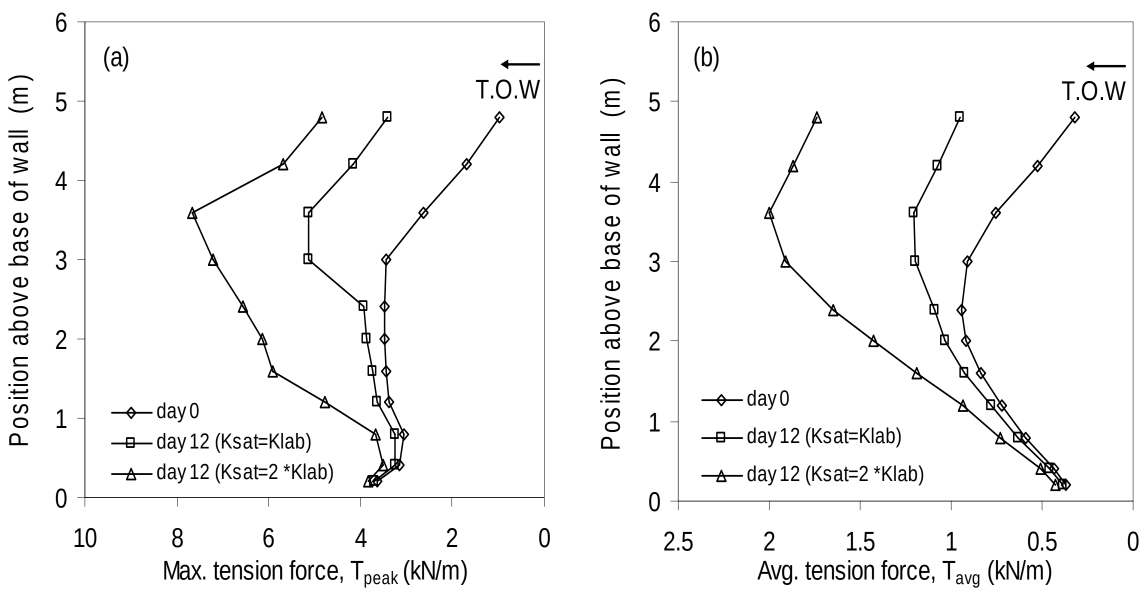

Fig. 5. 30 Reinforcement tensions after the 12-days rainfall for Cases 2 and 4: (a) maximum tension, T_{peak} and (b) average tension, T_{avg}

Results for Cases 1 and 3

The results for Cases 1 and 3 after 12-days of rainfall are shown in Figs. 5.31 through 5.33. Due to the shallow depths of rainfall infiltration, as shown in Fig. 5.31(a), there are only small changes in the displacements (Fig. 5.32) and reinforcement forces (Fig. 5.33).

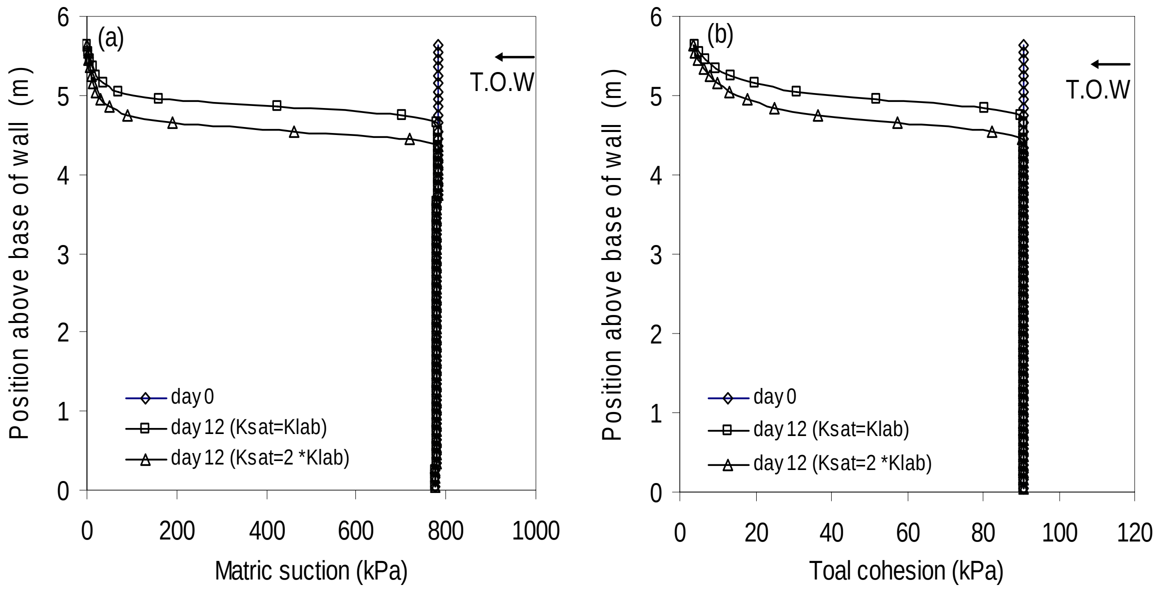

Fig. 5. 31 Profiles of (a) matric suction and (b) total cohesion after the 12-days rainfall for Cases 1 and 3

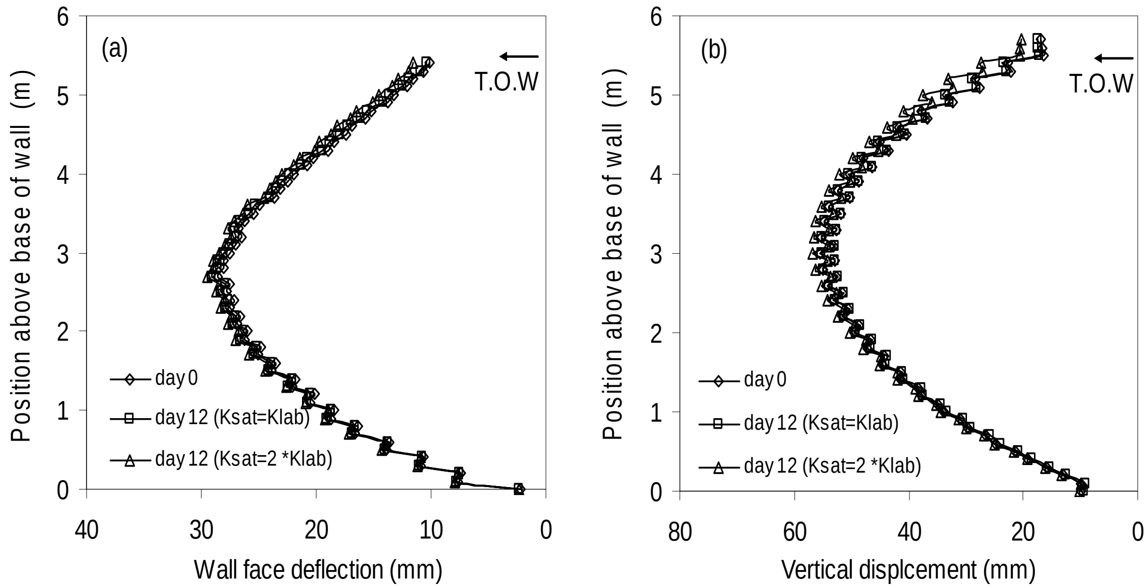

Fig. 5. 32 Wall movements after the 12-days rainfall for Cases 1 and 3: (a) wall face lateral deflection and (b) vertical displacement at Section-I

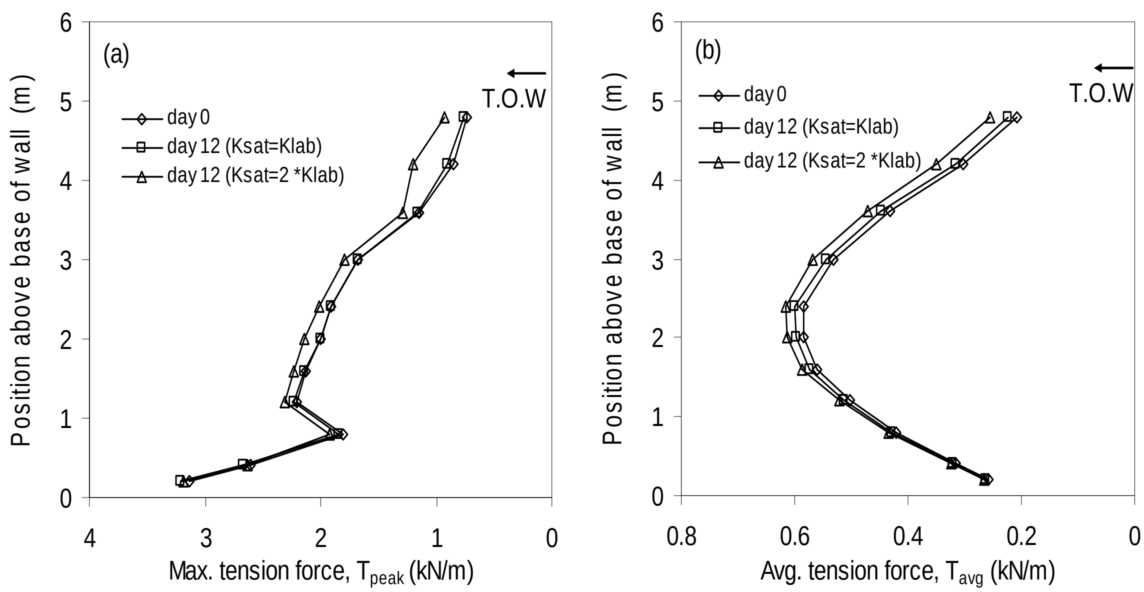

Fig. 5. 33 Reinforcement tensions after the 12-days rainfall for Cases 1 and 3: (a) maximum tension, T_{peak} and (b) average tension, T_{avg}

5.6 DISCUSSION

5.6.1 Influence of infiltration zone on wall behavior

Figures 5.34 through 5.37 show the magnitudes of increases in wall displacements and reinforcement forces after 12 days of water infiltration for all four cases. The wetting fronts in the low quality compaction zone are 1.0, 3.2, 1.3 and 4.8m below the ground surface for Cases 1, 2, 3, and 4, respectively. The depth of the wetting front for each case is shown for reference in each of the figures. It is clearly seen that the displacements (wall face deflection and settlement along section-I) become much more significant as the infiltration depth increases (Figs. 5.34 and 5.36). As an example, when the wetting front reached 1.3m below the ground surface (Case 3), a very small increase of the wall face deflection (less than 2 mm) is observed. However, as the wetting front reached 3.2 m and 4.8m from the ground surface, the wall face deflections increased greatly reaching maximum values of 12mm and 24mm, respectively. The same trends are shown for the maximum tension force and average tension force in the reinforcement, as shown in Figs. 5.36-5.38.

The increases in deflections and reinforcement tension discussed above (shown in Figs. 5.34-5.37) are predominantly caused by wetting of the backfill that is in the 1.6m-wide poorly compacted zone behind the wall face because of the shallow depth of infiltration in the well compacted zone. However, it should be noted that the displacements and reinforcement tensions of the wall would increase tremendously if the infiltration depth also increased in this zone.

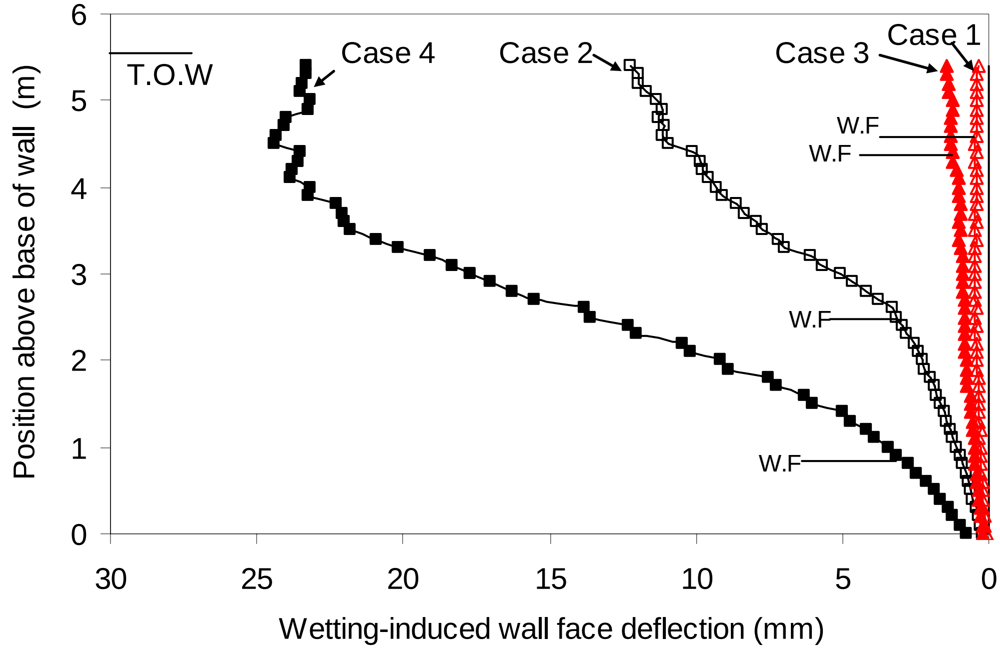

Fig. 5. 34 Increases of wall face deflections after 12-days rainfall of infiltration (all Cases)

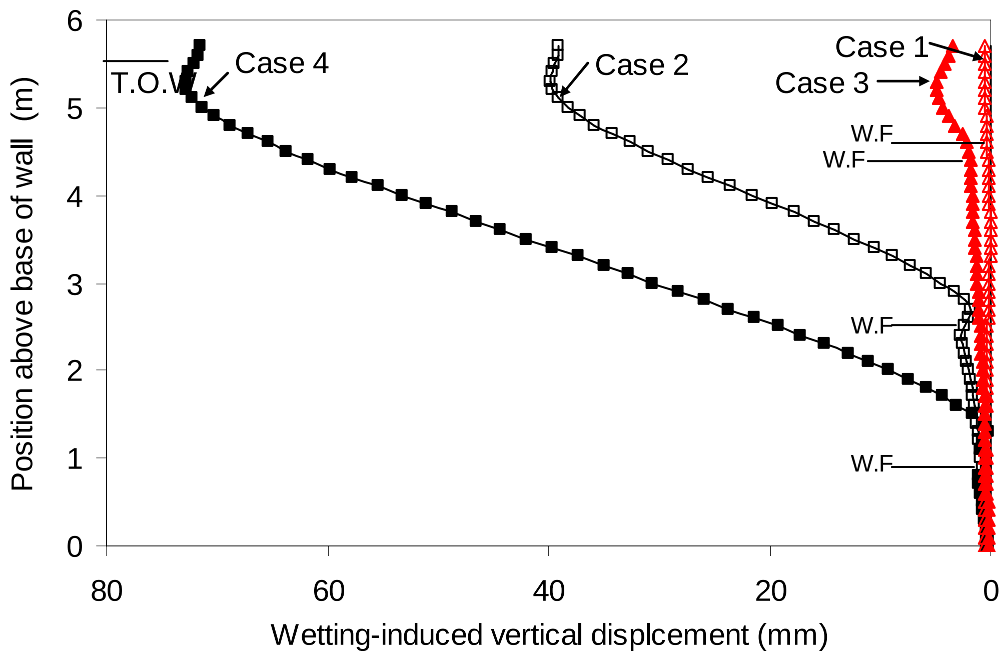

Fig. 5. 35 Increases of vertical displacements after 12-days of infiltration (all Cases)

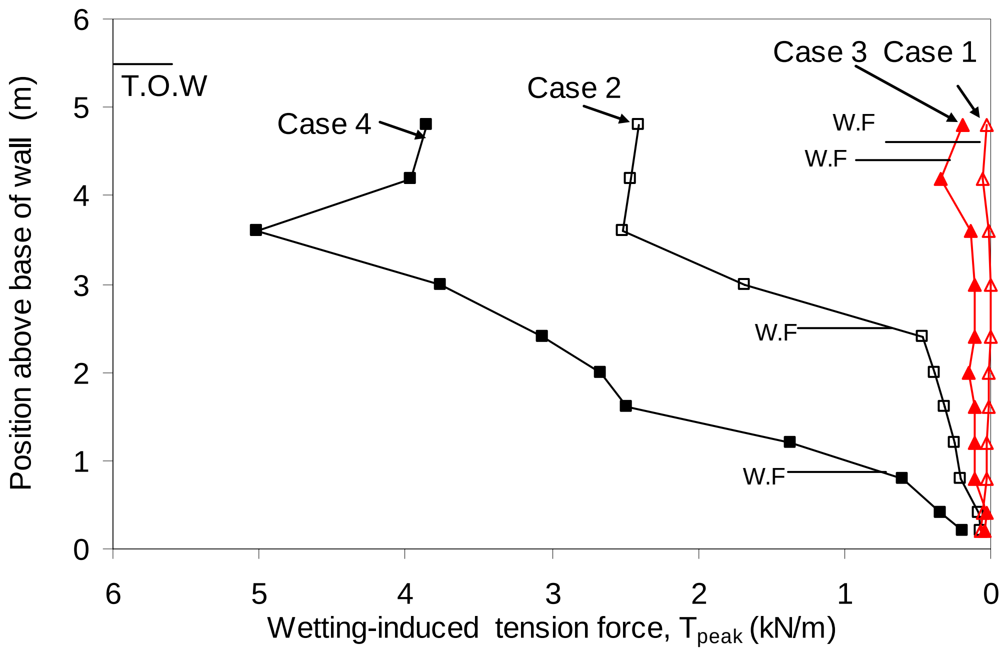

Fig. 5. 36 Increases of maximum tension force, T_{peak}, after 12-days of infiltration (all Cases)

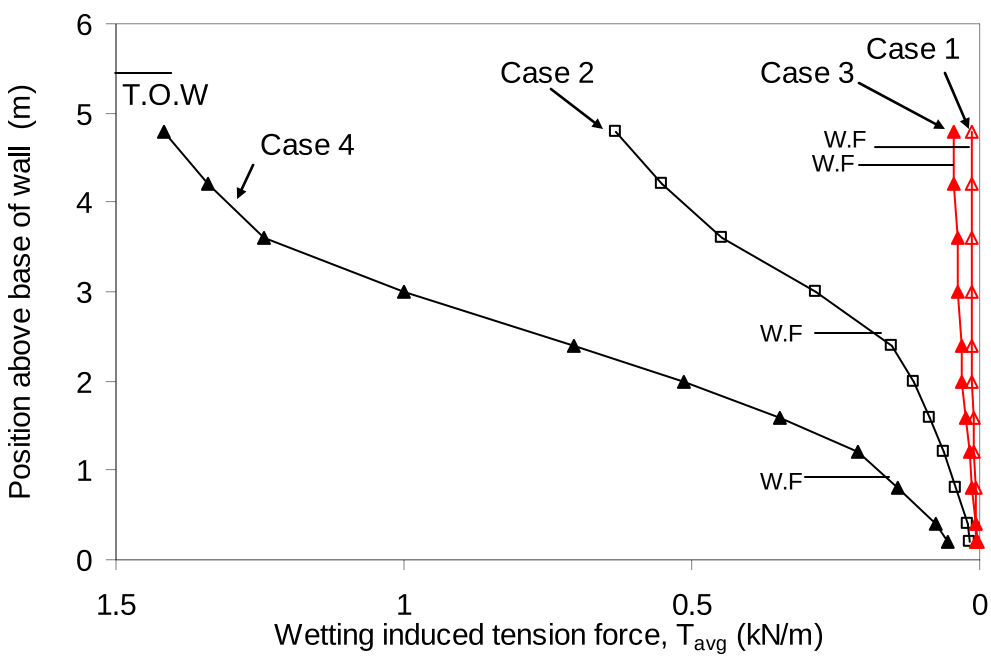

Fig. 5. 37 Increases of maximum tension force, T_{avg}, after 12-days of infiltration (all Cases)

5.6.2 Comparison with measured settlements

Although the simulation results did not show that the wall would fail under the conditions used in this study, it was clearly seen that the behavior of the wall would be significantly influenced by rainfall infiltration, showing significantly increased magnitudes of displacements and reinforcement tensions.

During the site investigation of the wall failure, a test pit was dug behind a portion of the adjacent wall that had not failed (Borden, 2004). It was seen that the fill behind the wall face had settled more than 102 mm at 1.6m above the wall base and 229 mm at 3.5m above the wall base. It was also observed that some portion of the grid had been ruptured, and that the reinforcement was in a state of distress. Figure 5.38 shows the condition of the grid behind the block wall face as exposed during hand excavation. The measured settlements were compared with the computed settlements for Case 4, which provided the largest values among the cases investigated (Fig. 5.39). It is seen that the measured settlements are far in excess of the predicted settlements. The large settlement behind the facing blocks would have caused an even more significant increase in the reinforcement tension near the wall face; therefore, it could be a one of the possible factors that caused the wall failure.

Fig. 5. 38 Condition of the grid behind the block

Based on analysis of the predicted results and observations made during the site investigation, one could suggest the possible factors that contributed to the wall failure (and the difference between the magnitudes of measured and computed settlements) as follows:

1) Wetting zone

The wetting zone in the backfill (especially for the well compacted zone) due to the rainfall might be larger than that predicted from the simulation. The permeability of the compacted soil may vary over several orders of magnitude depending on compaction condition. This implies rather large changes in permeability may accompany very small changes in as-compacted water content (Michelle et al., 1965). In addition, the field permeability tends to be higher than that measured in the lab. If there is a weak portion in the backfill where the rain infiltrates into the wall easily (i.e. crack), the wetting zone could be significantly deeper than predicted.

2) Collapse potential

The collapse potential results for the backfill materials (Rorie, 2006) showed that the magnitude of collapse increased significantly when the dry density of the material changed from 1.60 g/cm^3 (used in the simulation) to 1.53 g/cm^3. If the properties of more compressible backfill were used as an input in the simulation, the results would show worse wall performance.

3) Lateral forces

Several types of lateral forces, which have not been simulated in the model, could have been acting behind the wall face. For a low permeability soil, a perched water table could be developed during the rain infiltration (Cho and Lee, 2001). Positive pore water pressure is then generated and could be applied behind the wall face. Also, some amount of radial swelling could occur within the backfill behind the wall face during rainfall infiltration (Lawton et al., 1991).

4) Length of the geogrid embedded within the blocks

Another possible reason for the wall failure could be found in the embedded length of reinforcement between the blocks. If the reinforcement was not embedded the full length of block (as is called for in design), it could be pulled out from the blocks when the upper portion of the wall moved out and the reinforcement was pulled down vertically due to the compressing behavior of the fill behind the wall face.

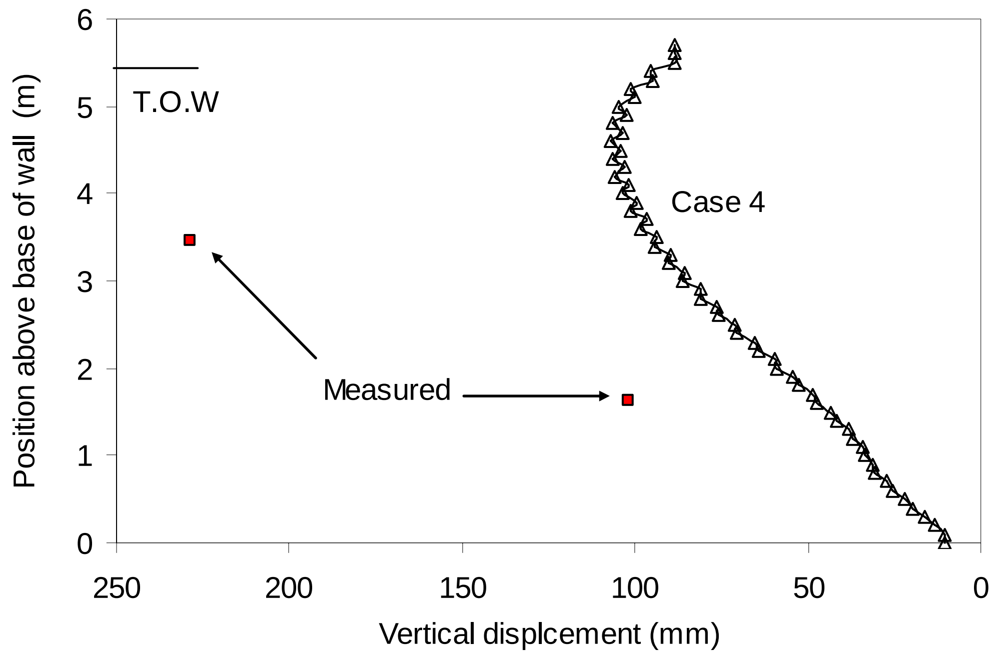

Fig. 5. 39 Measured settlements at the back of the block wall face and computed settlements at Section-I

5.6.3 The behavior of an MSE wall constructed with the backfill compacted at optimum

Even though numerical simulations for the wall constructed with backfill compacted at optimum (or wet of optimum), were not performed in this research, some idea about the behavior of this wall could be gained from this research. Since the elastic modulus and shear strength of the wetter soil are lower than those of backfill compacted dry of optimum (due to the initial low matric suction within the soil), the movements of the wall during construction would be somewhat larger than those of the wall constructed with dry-compacted backfill. However, the wall deformation during the rainfall would be significantly smaller because the fills compacted at optimum (or wet of optimum) would be expected to have permeability values two or three orders of magnitude lower than the fills compacted dry of optimum, other conditions being equal (Michelle et al., 1965; Daniel and Benson, 1990). Also, the decrease of shear strength due to wetting is very small for the fill compacted near optimum (or wet of optimum). Finally, the wetting induced volumetric strain is often small enough to be ignored when soils are compacted at optimum or wet of optimum (Lawton et al., 1991).

5.7 SUMMARY AND CONCLUSIONS

In order to predict the MSE wall behavior induced by rainfall or ground surface water infiltration, a series of numerical analyses that included transient flow analysis and stress-deformation analysis were performed using the finite difference code FLAC. Incorporating the effect of matric suction (permeability, shear strength, and volume change) into the simulation with use of the FISH programming language, it was possible to produce an analysis in the context of unsaturated soil response that provided a better understanding of MSE wall behavior. The distribution of matric suction during infiltration was estimated from transient flow analysis, and then used in the stress-deformation analysis for the prediction of wall response. Two separate simulations were used to compute both the shear-induced and volumetric deformations due to wetting. The results from each simulation were then superimposed.

The simulations were performed for a 5.4m high MSE wall in North Carolina that experienced a localized collapse during rainfall. Based on the results of the simulations, some general conclusion can be made as follows:

1) For the MSE wall constructed with fill compacted very dry of optimum (w = 4.8 %), the

results showed good wall performance during wall construction, with small displacements and reinforcement tensions. However, during the rainfall infiltration, the results showed large increases in wall and soil deformation and reinforcement tension that could lead to wall failure. This behavior was caused by:

- Shear strength decrease: The backfill shear strength at the end construction was very high (more than 90kPa) due to the high initial suction, but decreased significantly when water infiltrated into the soils.

- Settlements behind the wall face: The settlements behind the wall induced high tension at the back of the blocks making up the wall face. Since the soil compacted to a low density showed higher compressive behavior due to wetting, the wall was shown to perform more poorly when an improperly compacted zone (low quality compaction zone) existed behind the wall face.

2) The simulation results showed the wall displacements and reinforcement tension increased at a increasing rate as the infiltration depth increased. Since the permeability of fill can vary by a significant amount depending on the field compaction conditions (i.e. dry density and as-compacted water content), determination of reliable permeability values for the backfill (therefore, infiltration depth) is an important factor to enable one to predict wall behavior.

3) The behavior of a MSE wall which is constructed with fills compacted near optimum could be suggested based on the results of the simulations performed in this research. The deformation of the wall face during wall construction would be larger than that of a wall constructed with dry-compacted backfills. However, no significant increases in wall

deformation and reinforcement tension would occur during exposure to surface water infiltration, be it either by rainfall or surface irrigation.

5.8 REFERENCES

Barden, L., McGown, A., and Collins, K. (1973). The collapse mechanism in partly saturated soil, Engrg. Geol., 7(1), pp. 49-60.

Borden, R. H. (2004). Personal communication.

Brooks, R. H., and Corney, A. T. (1964). Hydraulic properties of porous medium, Colorado State University (Fort Collins), Hydrology paper 3.

Cho, S. E., and Lee, S. R. (2001). Instability of unsaturated soil slope due to infiltration, Computers and Geotechnics, Vol. 28, pp. 185-208.

Daniel, E. D., and Benson, C. H. (1990). Water content-density criteria for compacted soil liners, Journal of Geotechnical Engineering, Vol. 116, No. 2, pp. 1811- 1830..

Fredlund, D. G., and Rahardjo, H. (1993). Soil mechanics for unsaturated soils, New York: Wiley.

Fredlund, D. G., Xing, A., and Huang, S. (1994). Predicting the permeability for unsaturated soils using the soil-water characteristic curve, Canadian Geotechnical Journal, 31, pp. 533-

546.

Garner, W. R., (1958). Some steady state solutions of the unsaturated moisture flow equation with application to evaporation from a water-table, Soil Science, 85, pp. 228-232.

Itasca Consulting Group. (2000) FLAC-Fast Lagrangian Analysis of Continua, Version 4.0, Minneapolis.

Lawton, E. C., Fragaszy, R. J., and Hardcastle, J. H. (1991). Stress ratio effects on collapse of compacted clayey sand, Journal of Geotechnical and Geoenvironmental Engineering, Vol. 117, No. 5, pp. 1252-1267.

Lawton, E. C., Fragaszy, R. J., and Hetherington, M. D. (1991). View of wetting-induced collapse in compacted soil, Journal of Geotechnical Engineering, 118(9), pp. 1376-1394.

Mitchell, J. K., Hooper, D. R., and Campanella, R. G. (1965). Permeability of compacted clay, Journal of Soil Mechanics and Foundations, ASCE, 91(4), pp. 41-65.

Mualem, Y. (1976a). A new model for predicting the hydraulic conductivity of unsaturated porous media, Water Resources Research, 12, pp. 593-622.

Ng, Charles, W. W., and Pang, Y. W. (2000). Influence of stress state soil-water characteristics and slope stability, Journal of Geotechnical and Geoenvironmental

Engineering, Vol. 126, No. 2, pp. 156- 166.

Noorany, I., Frydman, S., and Detournay, C. (1999). Prediction of soil slope deformation due to wetting, FLAC and Numerical Modeling in Geomechanics, pp. 101-107.

Noorany, I., Sweet, J. A, and Smith, I. M. (1992). Deformation of fill slopes caused by wetting, Proceedings of the ASCE Conference on Stability and Performance of Slope and Embankments II, ASCE Geotechnical Special Publication No.31, New York.

Richards, L.A. (1931). Capillary conduction of liquids through porous medium, Physics, 1: 318-333.

Rodrigues, R. A. and Vilar, O. M. (2006) Relationship between collapse and soil-water retention curve of a sandy soil, Proceedings of the fourth international conference on unsaturated soils, Geotechnical Special Publication No. 147, Vol.1, pp. 1025-1036.

Rorie, D., (2006). Investigation of soil suction in low density silty sands, MS thesis, North Carolina State University, Raleigh.

Sweet, J. A. (1991). SWELL – A finite-element program that predicts the deformation and stress state resulting from the swelling or compression of soils, Coast Analytics, Inc., California.

van Genuchten, M. TH. (1980). A closed-form equation for predicting the hydraulic conductivity of unsaturated soils, Soil Science Society of America Journal, 44, pp. 892-898.

Yoo, C., and Jung, H. (2006). Case History of Geosynthetic Reinforced Segmental Retaining Wall Failure, Journal of Geotechnical and Geoenvironmental Engineering, Vol. 132, No. 12, pp. 1538- 1548.

CHAPTER 6

SUMMARY, CONCLUSIONS, AND RECOMMENDATIONS FOR FUTURE STUDY

6.1 SUMMARY AND CONCLUSIONS

A study on the MSE wall behavior due to water infiltration has been conducted using the theory of unsaturated soil mechanics. The summary and major conclusions from this study are briefly as follows:

In Chapter 2, the drained moduli of as-compacted and soaked specimens prepared under various initial conditions were estimated based on assumed Poisson's ratios and the relationships between volumetric stress and strain, which were measured from as-compacted and soaked specimens in double oedometer tests. The undrained modulus was also able to be computed from the constitutive relation for undrained loading, which was determined using the procedures suggested in this paper. Determination of the constitutive relation for undrained loading was accomplished by using Hilf's equation (1948) along with the compressibility of as-compacted soil to compute changes in pore pressure. The secant and tangent pore pressure parameters were then determined from the computed pore pressures. From the analyses of computed modulus and pore pressure presented in this paper, the following conclusions can be drawn:

1) At the dry densities studied (1.6 g/cm^3 or 1.79 g/cm^3), the drained elastic modulus of a series of as-compacted specimens increased significantly as the as-compacted water

content decreased to 4.7% while the drained elastic modulus of soaked specimens remained almost constant.

2) For specimens with water contents of 4.7% and tested in their as-compacted state, the drained elastic modulus increased significantly as dry density increased from 1.53 g/cm^3 to 1.79 g/cm^3, while the elastic drained modulus of soaked specimens increased very little.
3) Specimens compacted at high degrees of saturation and tested in either soaked or unsoaked conditions showed little difference in the drained elastic moduli.
4) The induced pore pressures due to loading increased with increasing as-compacted water content and decreasing dry density.
5) The specimens compacted at the lowest water content of w = 4.7% showed no significant difference in drained and undrained moduli. However, there was an increasing difference in these moduli for specimens with increasing as-compacted water content.
6) The linearly increasing elastic modulus was defined using a modulus number, K . The ratios, K_{DU}/K_{DS} and K_{UN}/K_{DS}, were seen to vary from about 1 to 3.

In Chapter 3, comparisons among the shear strengths predicted from three empirical procedures (1st and 2nd approaches of Vanapalli et al., and Khalili and Khabbaz model) that use SWCCs were presented. In order to study the influence of the SWCC on the predicted shear strength for these procedures a parametric study was performed by varying the a and n values of the Fredlund and Xing SWCC model. A comprehensive analysis was undertaken to examine shear strength data of fifteen soils published in the literature using these procedures.

Comparisons are presented between measured and predicted shear strengths taking into account soil type, net normal stress range, and stress state under which the SWCCs were measured.

From the results of the parametric study, the following conclusions can be drawn:

1) For 1st and 2nd approaches of Vanapalli et al., the predicted shear strength increases as the *a* value increases or the *n* value decreases.
2) For the Khalili and Khabbaz model, the predicted shear strength for a given net normal stress increases as the *a* value increases. However, the predicted shear strength is independent of the *n* value.
3) There is a difference in the shear strengths predicted using the three procedures although the same SWCC is used for the prediction. This difference was shown to be either insignificant or significant depending on the shape of SWCC.

From the comparisons between the measured and predicted shear strengths, the following conclusion can be summarized:

1) For low plasticity clays, all prediction methods provide relatively good comparisons between measured and predicted shear strengths with the predicted values slightly smaller than those measured. In contrast, for sandy soils the predicted shear strengths are greater than the measured shear strengths. The Khalili and Khabbaz model generally provides the smallest value of shear strength for the low plasticity clays and sandy soils.
2) For soils that desaturate relatively fast ($n > 2$), the 1st and 2nd approaches of Vanapalli

et al. provide very poor comparison between the measured and predicted shear strengths, predicting significantly smaller values of shear strength with high variation of data. More meaningful results are found using the Khalili and Khabbaz model.

3) Among soil types with n values higher than 2, the predicted shear strengths are highly underestimated for fine grained soils (clay or silt), while the predicted shear strengths are slightly overestimated for sandy soils

4) From the results of analysis for the limited amount of data, it could be suggested that the relationship between the κ value and plasticity index (Eq. 3.7) can be used for natural soils as well as compacted soils and that a residual suction of 3000 kPa can be reasonably used to predict shear strength using Vanapalli et al.'s 2nd approach for the sandy soils and low plasticity clays. The Khalili and Khabbaz model predicts values of shear strength much smaller than those measured for soils in which the air entry value is small (< 35 kPa).

5) The effect of net normal stress state on the predicted shear strength would be significant if the friction angle of the soil increases significantly with increasing matric suction.

6) The shear strengths predicted using the SWCCs performed at different net normal stresses would be significantly higher than those predicted using the one SWCC performed at zero or nominal net normal stress, if the SWCCs, are highly dependent on stress state.

In Chapter 4, a numerical model, which accounts for unsaturated soil properties (elastic modulus and shear strength), was developed using FLAC, in order to better predict the end of construction behavior of a MSE wall constructed with marginal fill (i.e. high fined contents). The developed model takes into account the staged construction of a MSE wall, and uses FISH subroutines programmed in the FLAC model to update the unsaturated soil properties based on changes in both normal stress and matric suction. This research focused on the behavior of a MSE wall constructed with backfill compacted very dry of optimum (w = 4.7%, -7 % of OMC). Also, the effect of the existence of a poorly compacted zone behind the wall face on the wall behavior was investigated. From the results of the numerical simulations presented, the following conclusions can be drawn:

1) The existence of a 1.6m-wide poorly-compacted zone behind the wall face increased the wall displacements (vertical and lateral displacements) and reinforcement tensions (peak and average tensions) significantly. The maximum increases of these displacements and the tension forces occurred near the mid-height of the wall.
2) The peak tension forces in the reinforcements were found at the back face of the block facing because of the differential displacements between blocks and backfill, which resulted from the stiffness difference of the materials.
3) The small magnitudes of reinforcement tension forces (less than 4kN), which were well below the yield strength (35kN), were predicted for the end of construction condition are believed to be the result of the high shear strength of backfill induced by high soil suction.

In Chapter 5, a series of numerical analyses that included transient flow analysis and stress-deformation analysis were performed using the finite difference code FLAC in order to predict the MSE wall behavior induced by rainfall or ground-surface water infiltration. Incorporating the effect of matric suction (permeability, shear strength, and volume change) into the simulation with use of the FISH programming language, it was possible to produce an analysis in the context of unsaturated soil response that provided a better understanding of MSE wall behavior. The distribution of matric suction during infiltration was estimated from transient flow analysis, and then used in the stress-deformation analysis for the prediction of wall response. Two separate simulations were used to compute both the shear-induced and volumetric deformations due to wetting. The results from each simulation were then superimposed. Based on the results of the simulations, some general conclusion can be made as follows:

1) For the MSE wall constructed with fill compacted very dry of optimum (w = 4.8 %), the results showed good wall performance during wall construction, with small displacements and reinforcement tensions. However, during the rainfall infiltration, the results showed large increases in wall and soil deformation and reinforcement tension that could lead to wall failure. This behavior was caused by:

   - Shear strength decrease: The backfill shear strength at the end construction was very high (more than 90kPa) due to the high initial suction, but decreased significantly when water infiltrated into the soils.

   - Settlements behind the wall face: The settlements behind the wall induced high tension at the back of the blocks making up the wall face. Since the soil compacted to a low density showed higher compressive behavior due to wetting, the wall was shown to perform more poorly when an improperly compacted zone (low quality compaction zone) existed behind the wall face.

2) The simulation results showed the wall displacements and reinforcement tension increased at an increasing rate as the infiltration depth increased. Since the permeability of fill can vary by a significant amount depending on the field compaction conditions (i.e. dry density and as-compacted water content), determination of reliable permeability values for the backfill (therefore, infiltration depth) is an important factor to enable one to predict wall behavior.

3) The behavior of a MSE wall which is constructed with fills compacted near optimum, could be suggested based on the results of the simulations performed in this research. The deformation of the wall face during construction would be larger than that of a wall constructed with dry-compacted backfills. However, no significant increases in wall deformation and reinforcement tension would occur during exposure to surface water infiltration, be it either by rainfall or surface irrigation.

6.2 RECOMMENDATIONS FOR FUTURE RESEARCH

Based on the results of this research, the author provides the following recommendations for further research:

1) to investigate wetting curves for various compaction conditions (initial water content, compactive effort, and stress state): Drying curves have been usually measured and wetting curves have been ignored due to experimental difficulties involved in their measurement. However, recent researchers have emphasized that it is more appropriate to use the wetting curve for analyzing infiltration problems and the drying curve for analyzing evaporation problems, because the SWCC shows hysteresis for wetting and drying (Fig. 6.1a).

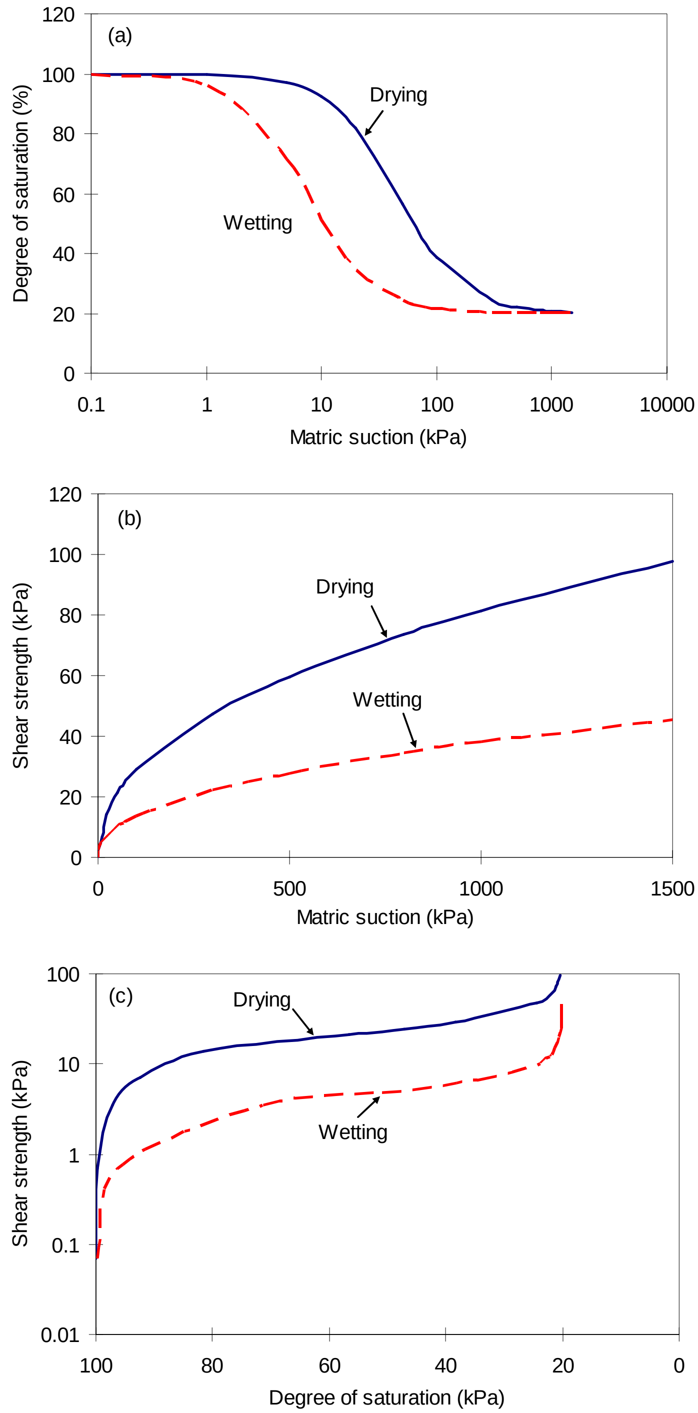

Fig. 6. 1 (a) soil-water characteristic curves (b) shear strength versus matric suction (c)shear strength versus degree of saturation (shear strength predicted using the Khalili and Khabbaz model)

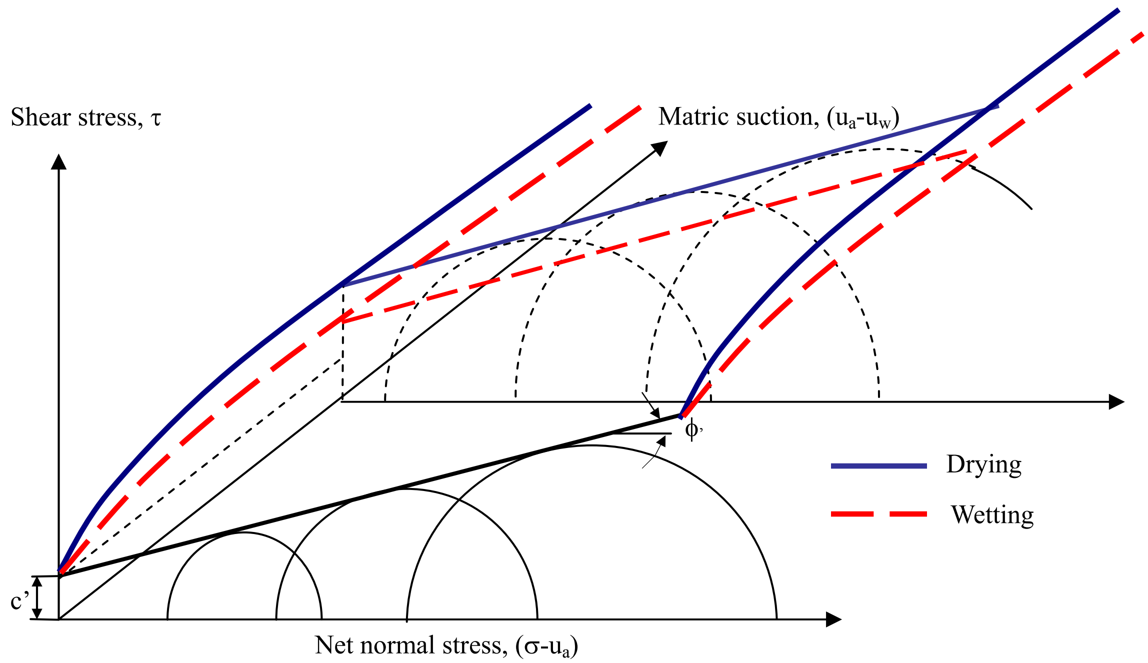

Fig. 6. 2 Failure envelopes for unsaturated soils in dying process and wetting process

2) to determine shear failure envelop for soil in wetting process: The shear strength of an unsaturated soil in both drying and wetting processes can be estimated from the drying and wetting curves, respectively, using the empirical shear strength equations (Eqs.3.8-3.10) and the results from the Khalili and Khabbaz model are plotted against both matric suction and degree of saturation as shown in Figs. 6.1(b) and (c). The results show a hysteresis on the shear strength from both the matric suction and degree of saturation. Figure 6.2 shows the failure envelopes estimated from both the drying curve and the wetting curve. It is clearly observed that at given matric suction or degree of saturation the shear strength predicted from the drying curve is higher than that predicted from the wetting curve. However, most of the measured shear strengths in the literature were determined during drying, and therefore the empirical

equations were also developed based on the shear strength data of soils subjected to drying. For further study, measurement of shear strength of soil in wetting condition is required in order to investigate the magnitude of the shear strength hysteresis. It is also recommended that the measured shear strength be compared to the shear strength predicted from the SWCC based equations (Eqs.3.8-3.10) using the measured wetting curve.

3) to investigate the influence of possible lateral forces acting behind the wall face on the wall behavior through a numerical simulation: Several types of lateral forces (pore water pressure and radial swelling of backfill), which have not been simulated in this research, could be acting behind the wall face.

4) to develop a numerical simulation program based on unsaturated soil mechanics principle: Most numerical simulation programs were developed assuming saturated soil mechanics and therefore adopted one stress state variable (either total stress or effective stress) to predict soil behavior. However, unsaturated soil behavior is explained using two stress state variables (net normal stress and matric suction).

APPENDIX A: STRESS-STRAIN RELATIONSHIPS

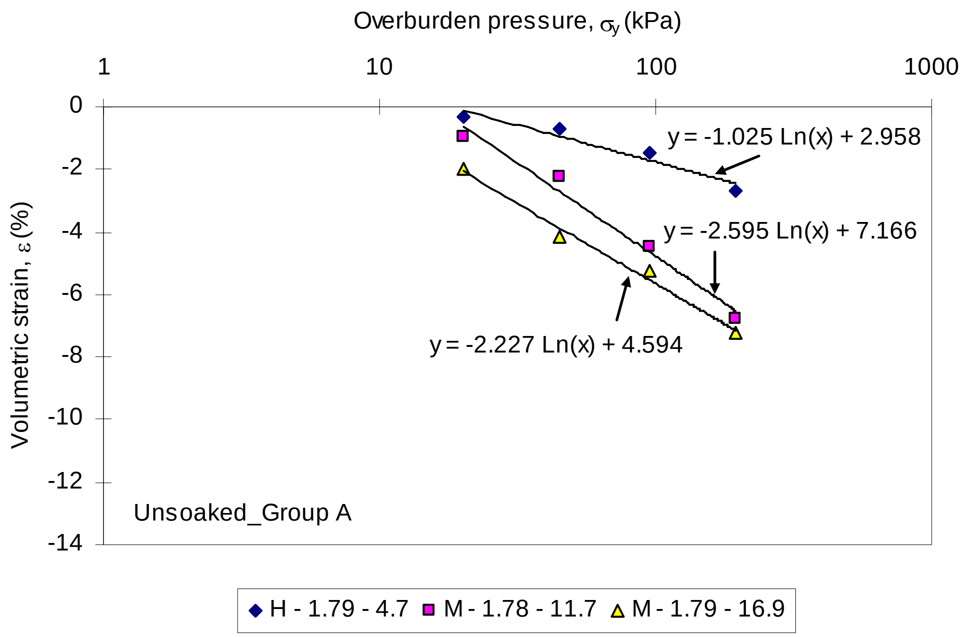

Measured volumetric strain vs. overburden pressure for unsoaked specimens (Group A-Drained)

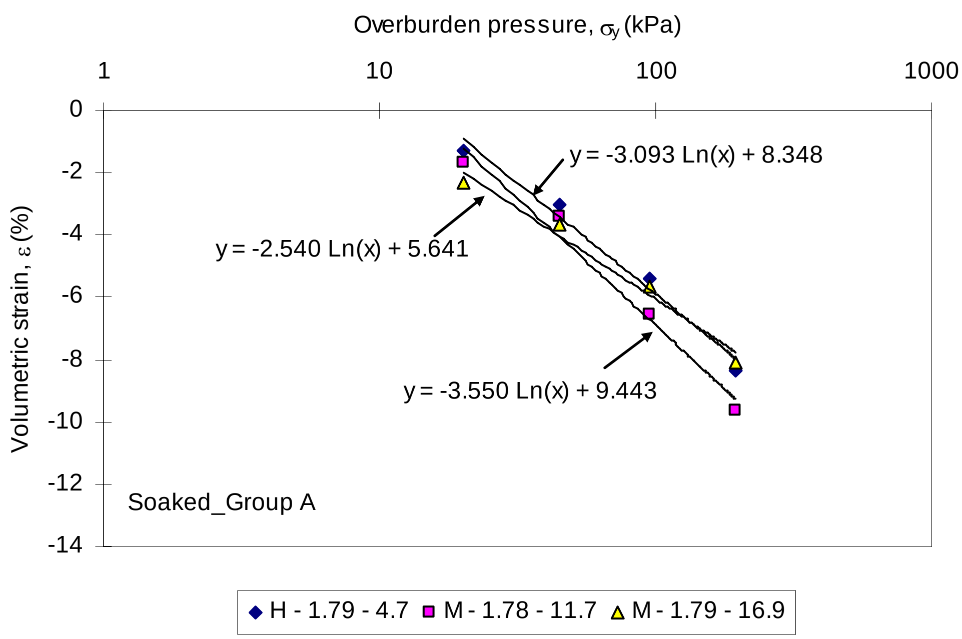

Measured volumetric strain vs. overburden pressure for soaked specimens (Group A-Drained)

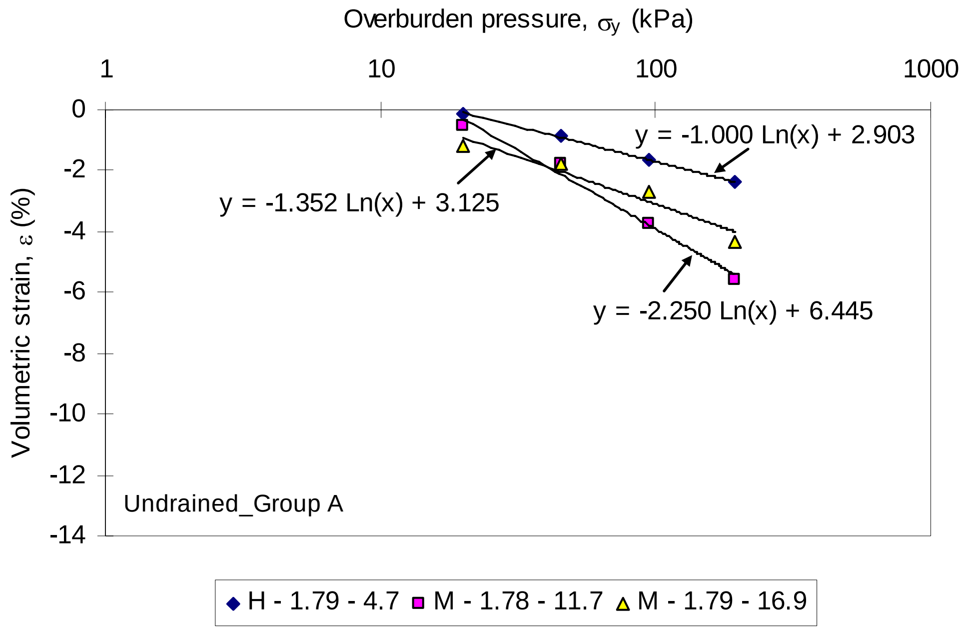

Predicted volumetric strain vs. overburden pressure for unsoaked specimens (Group A-Undrained)

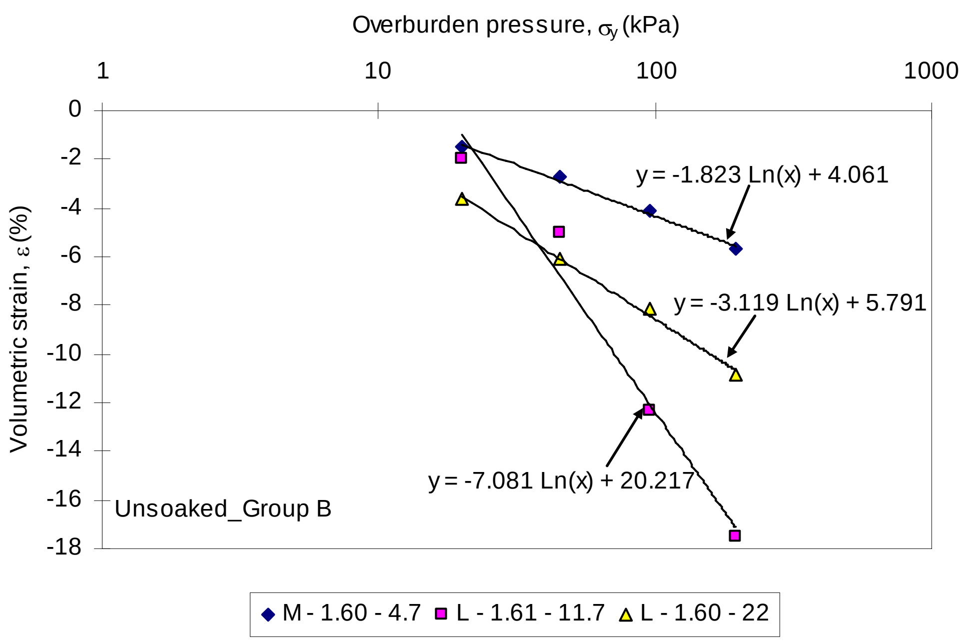

Measured volumetric strain vs. overburden pressure for unsoaked specimens (Group B-Drained)

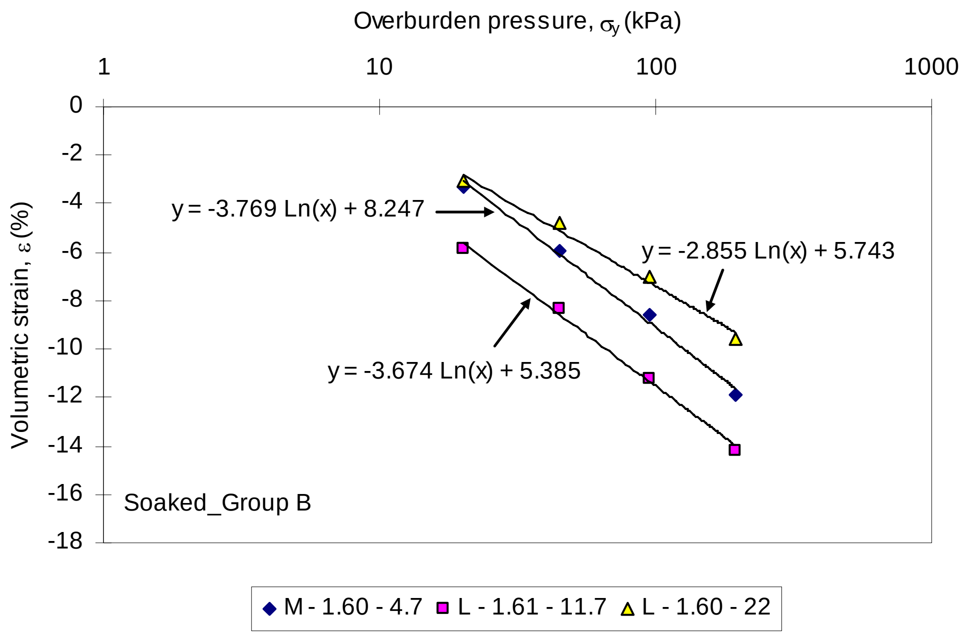

Measured volumetric strain vs. overburden pressure for soaked specimens (Group B-Drained)

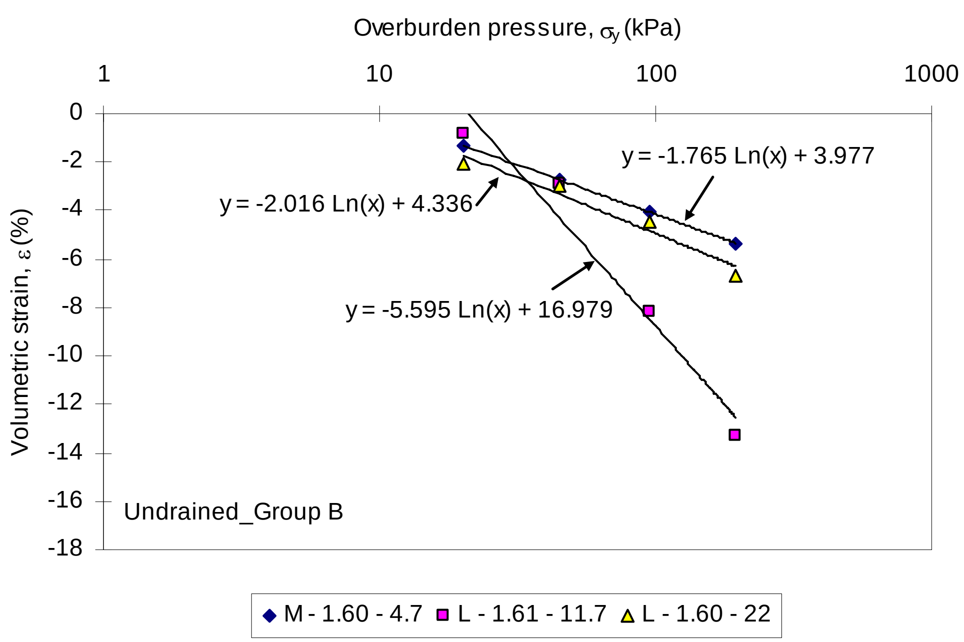

Predicted volumetric strain vs. overburden pressure for unsoaked specimens (Group B-Undrained)

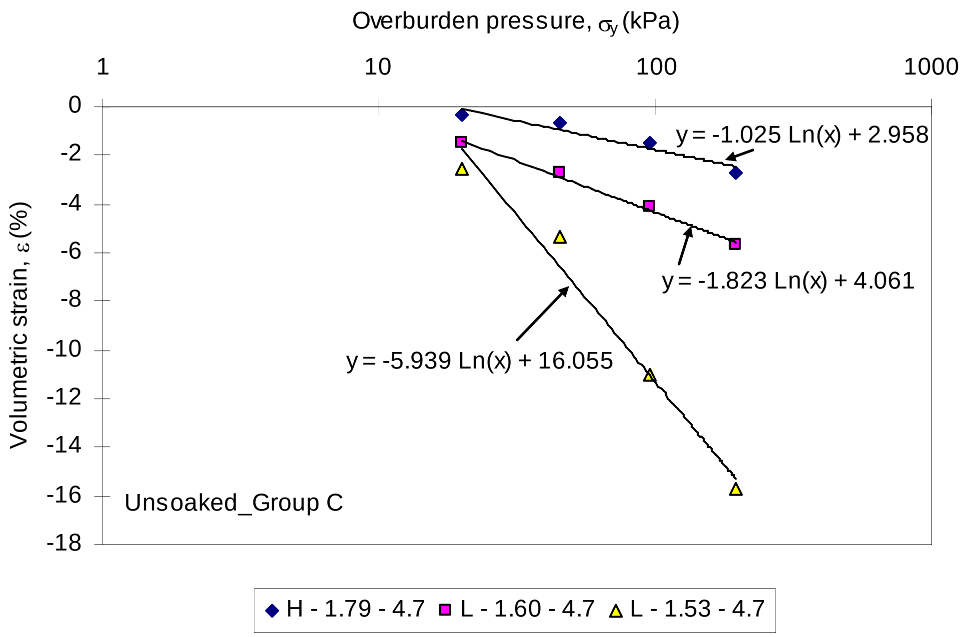

Measured volumetric strain vs. overburden pressure for unsoaked specimens (Group C-Drained)

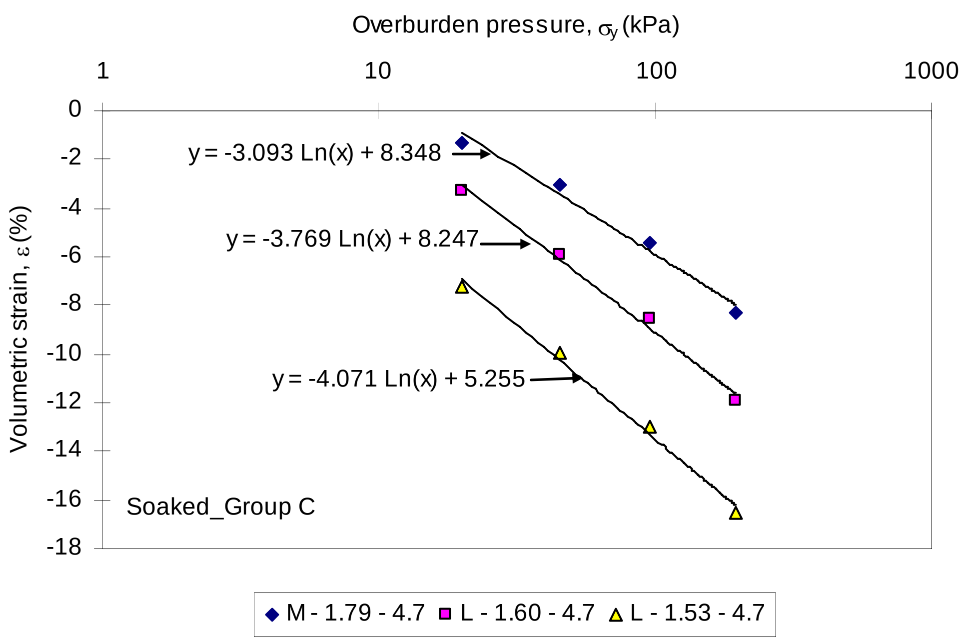

Measured volumetric strain vs. overburden pressure for soaked specimens (Group C-Drained)

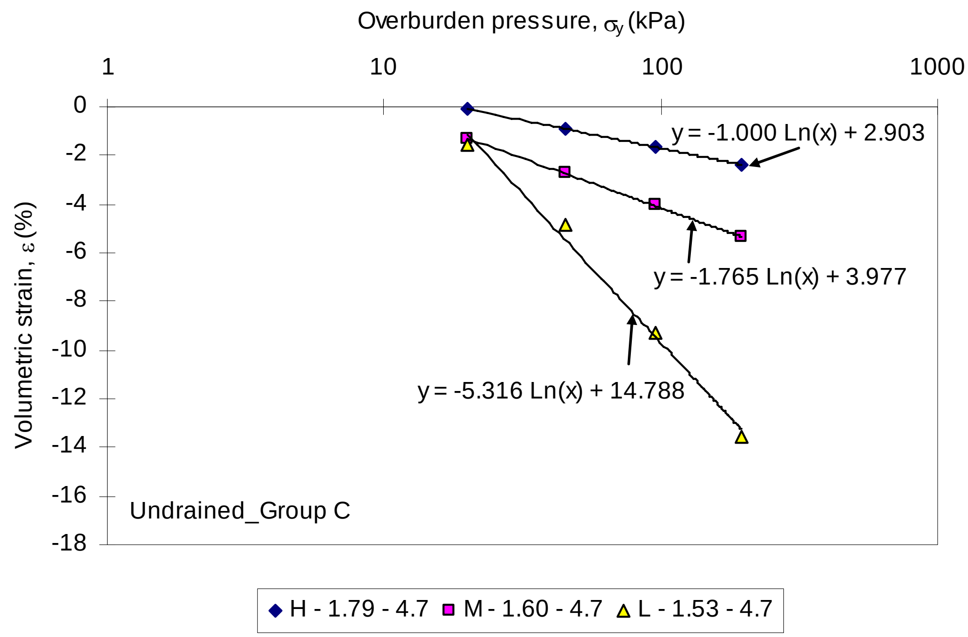

Predicted volumetric strain vs. overburden pressure for unsoaked specimens (Group C-Undrained)

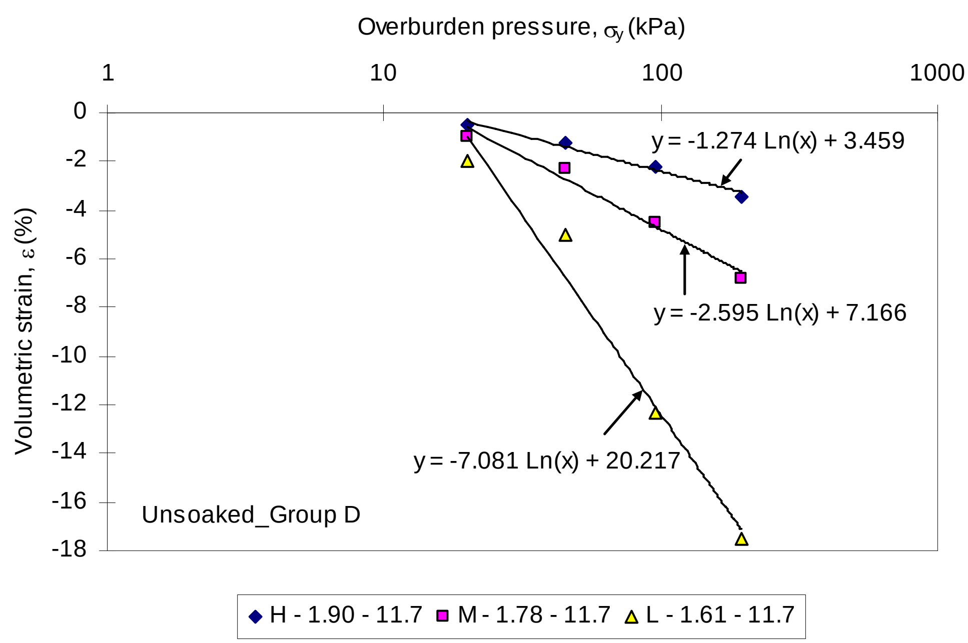

Measured volumetric strain vs. overburden pressure for unsoaked specimens (Group D-Drained)

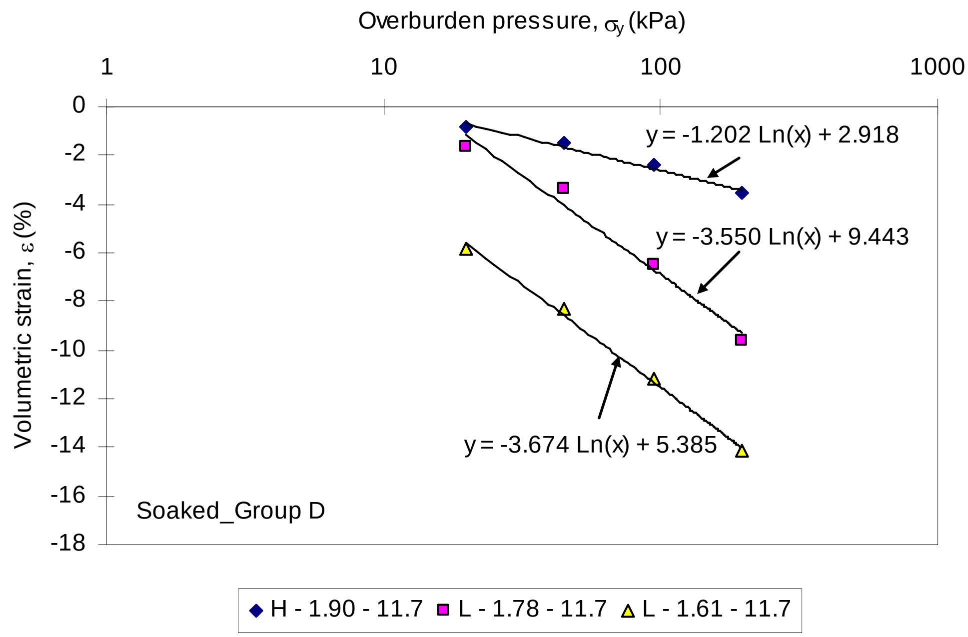

Measured volumetric strain vs. overburden pressure for soaked specimens (Group D-Drained)

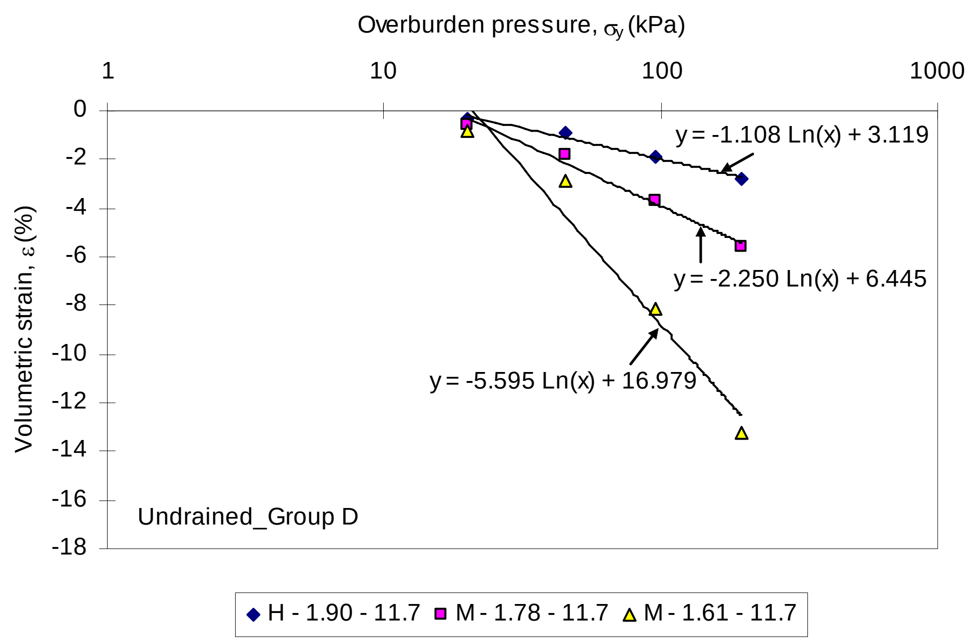

Predicted volumetric strain vs. overburden pressure for unsoaked specimens (Group D-Undrained)

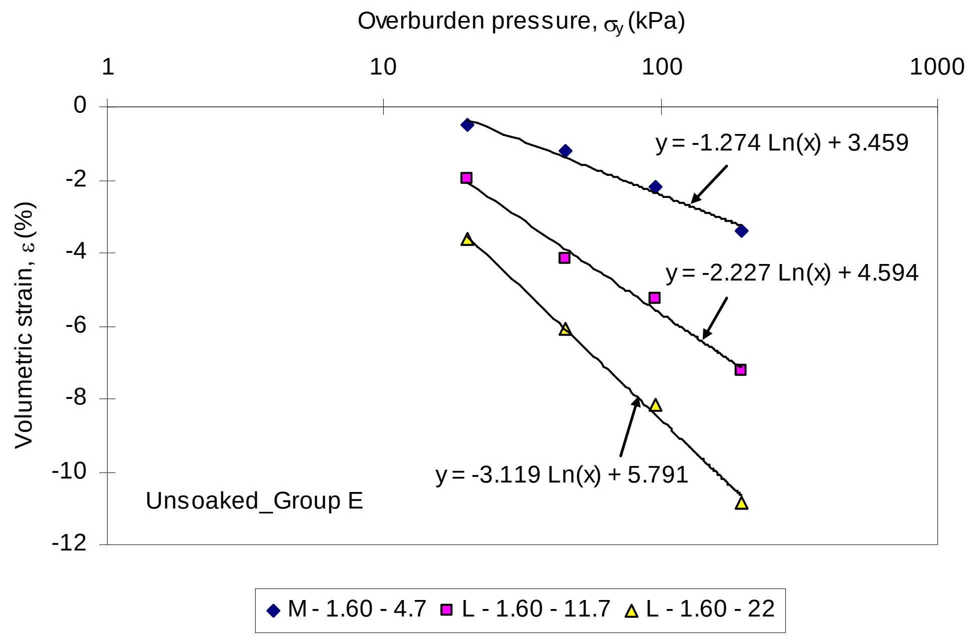

Measured volumetric strain vs. overburden pressure for unsoaked specimens (Group E-Drained)

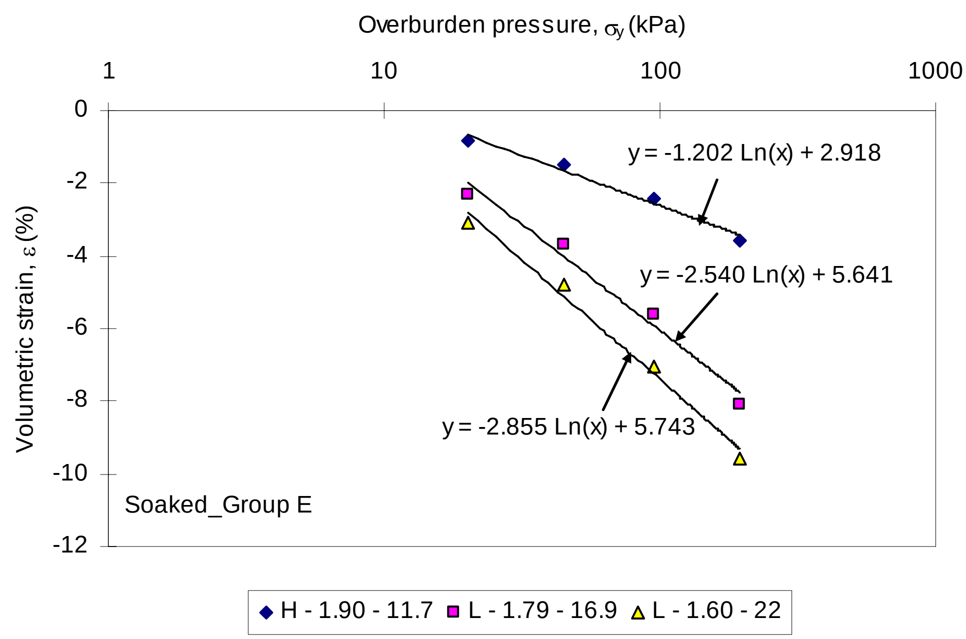

Measured volumetric strain vs. overburden pressure for soaked specimens (Group E-Drained)

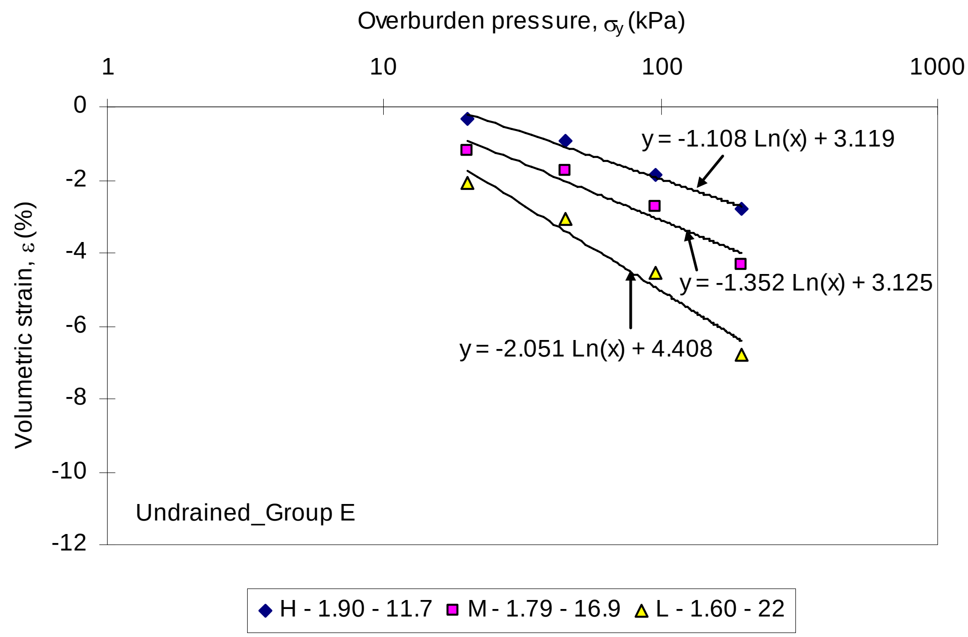

Predicted volumetric strain vs. overburden pressure for unsoaked specimens (Group E-Undrained)

APPENDIX B: SHEAR STRENGTH DATA

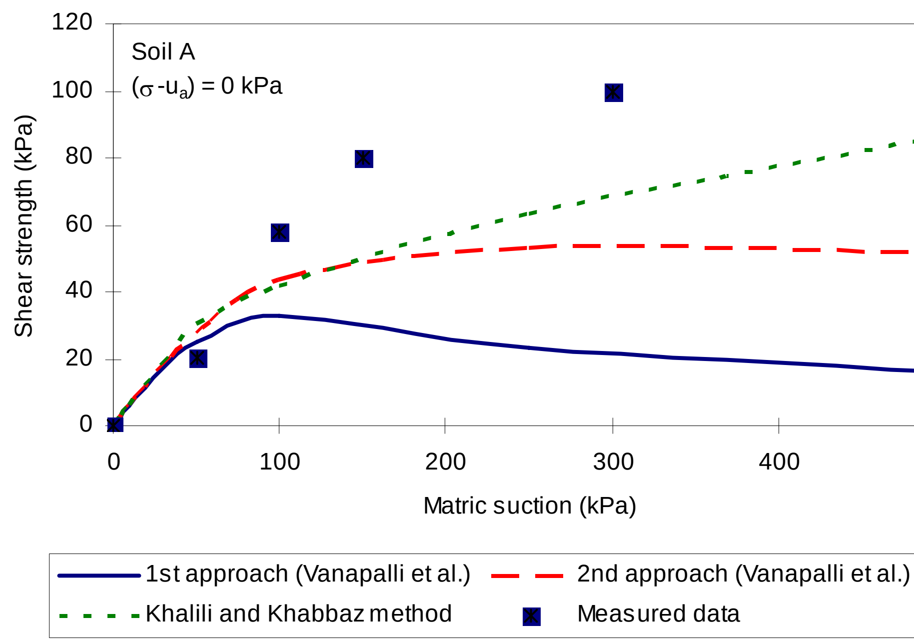

Measured and predicted shear strength values for Soil A (σ-u_a = 0kPa)

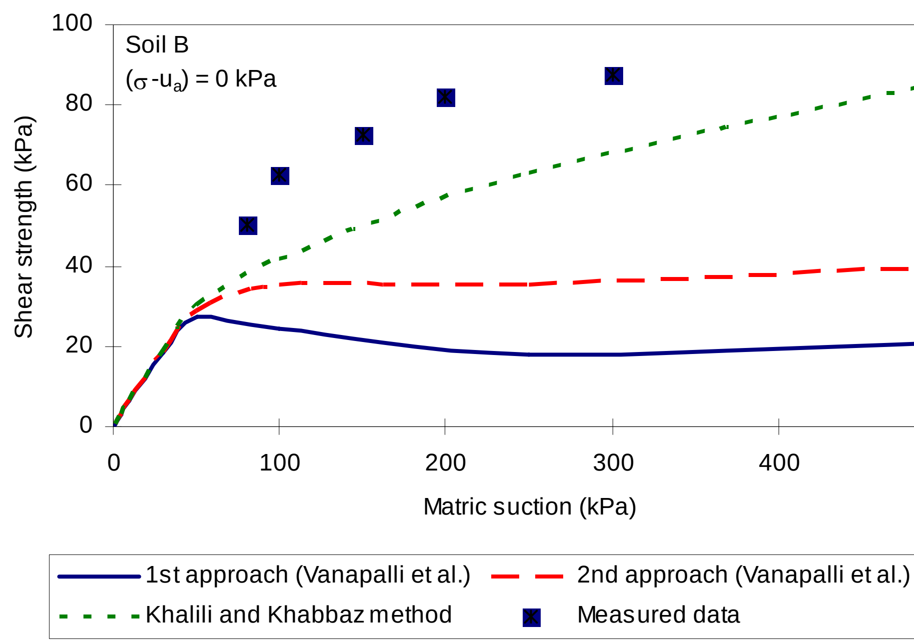

Measured and predicted shear strength values for Soil B (σ-u_a = 0kPa)

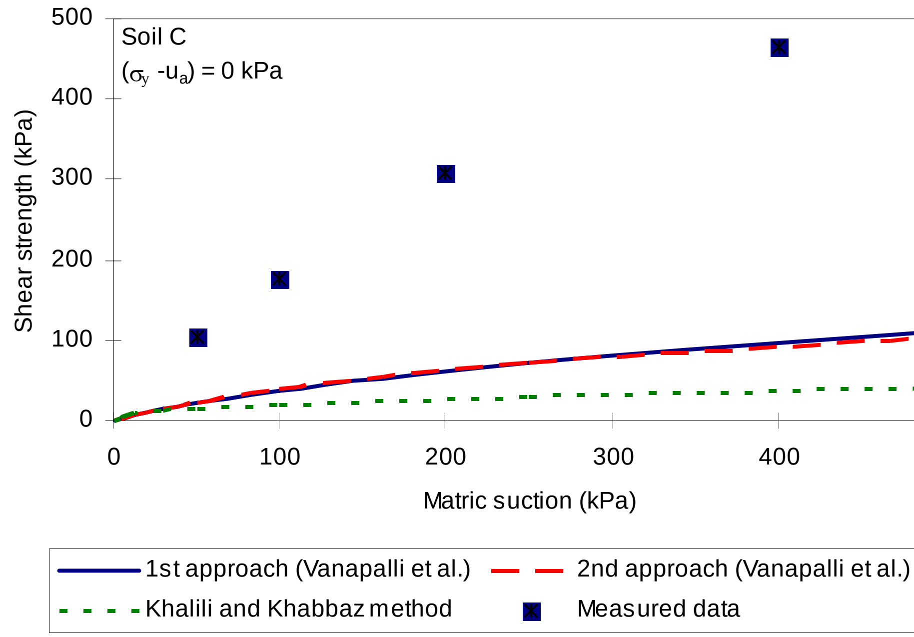

Measured and predicted shear strength values for Soil C (σ_y-u_a = 0kPa)

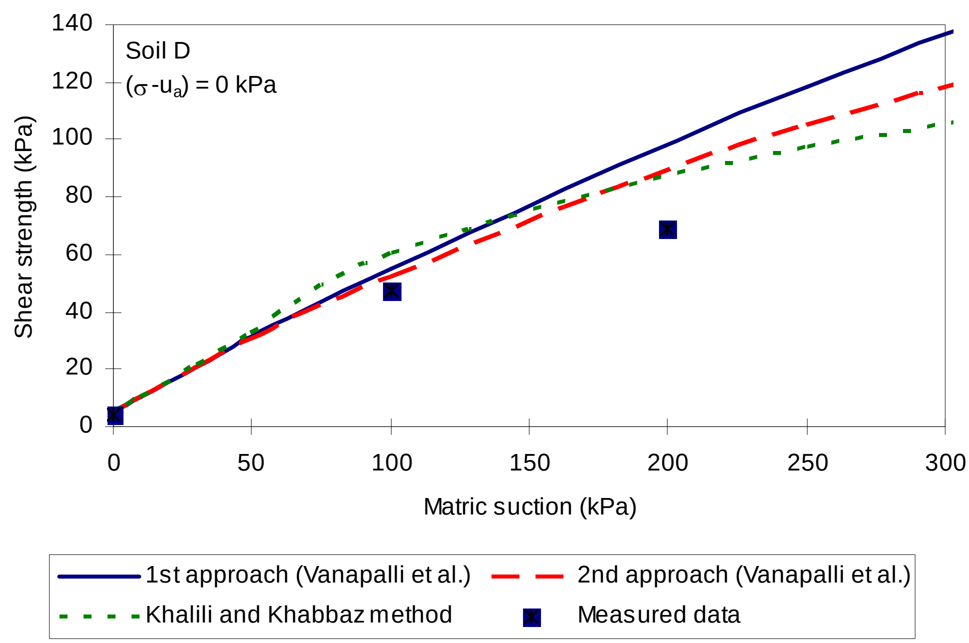

Measured and predicted shear strength values for Soil D (σ-u_a = 0kPa)

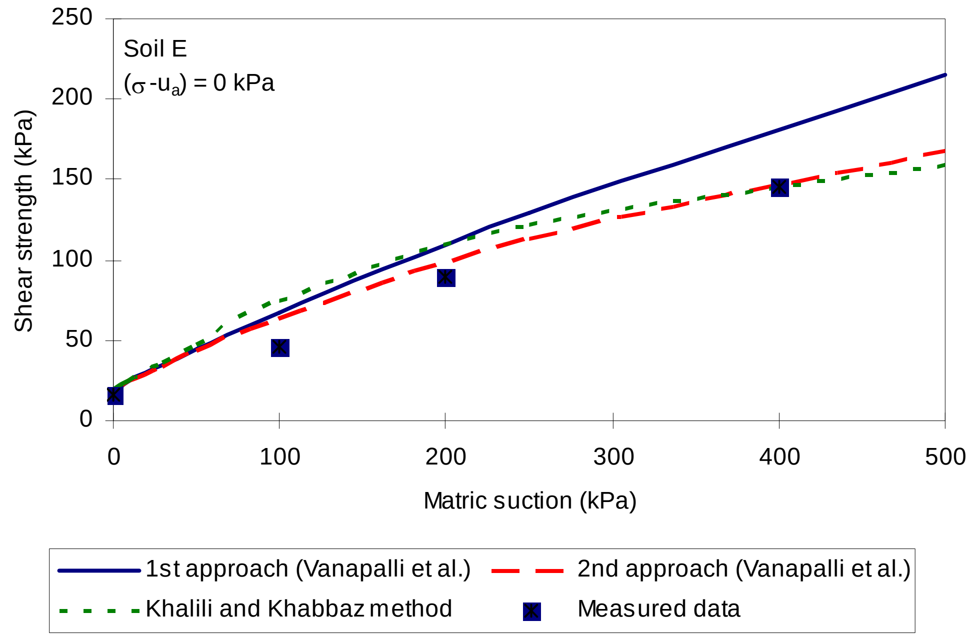

Measured and predicted shear strength values for Soil E (σ-u_a = 0kPa)

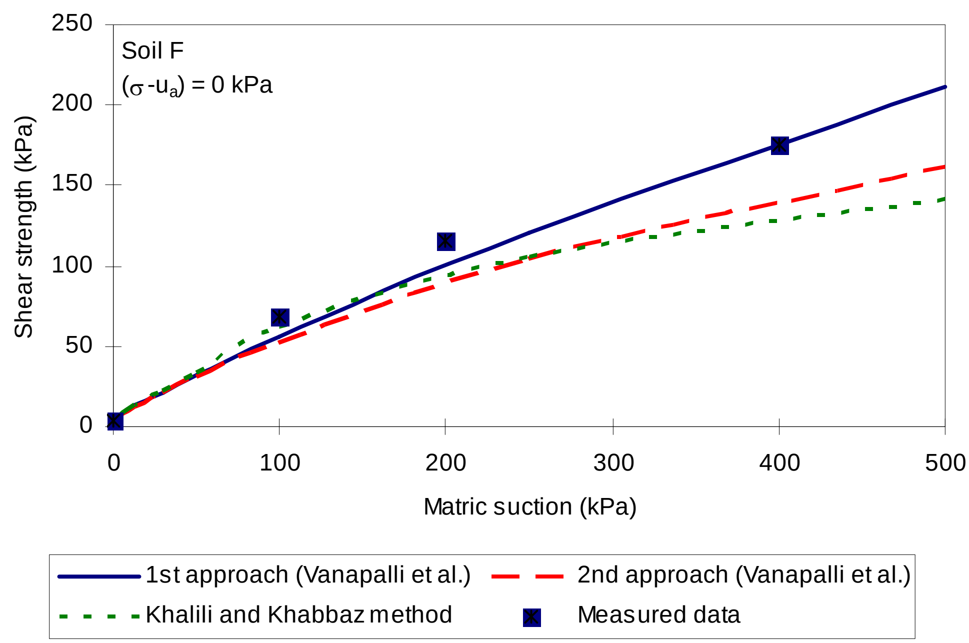

Measured and predicted shear strength values for Soil F (σ-u_a = 0kPa)

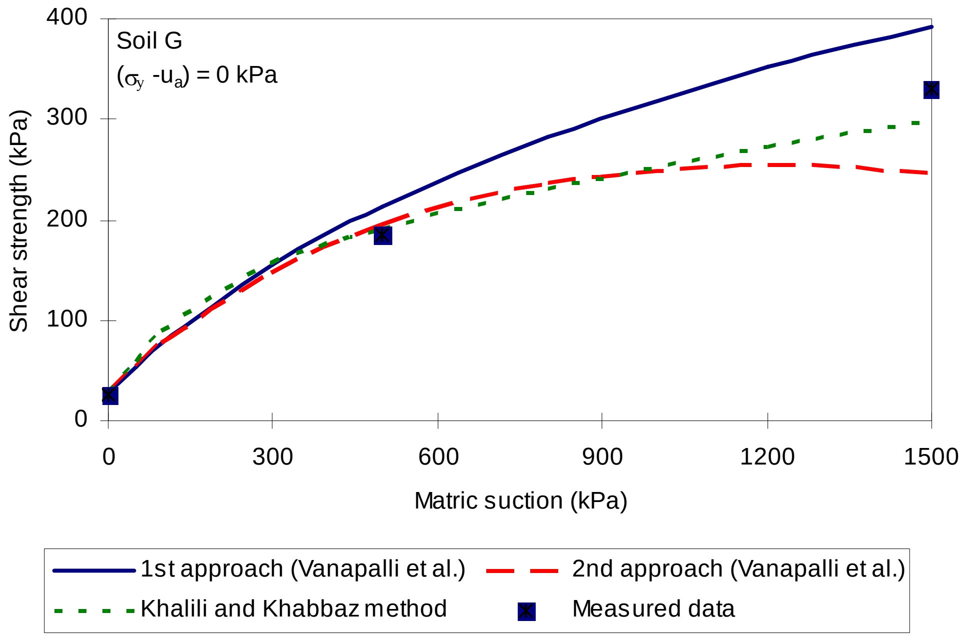

Measured and predicted shear strength values for Soil G (σ_y-u_a = 0kPa)

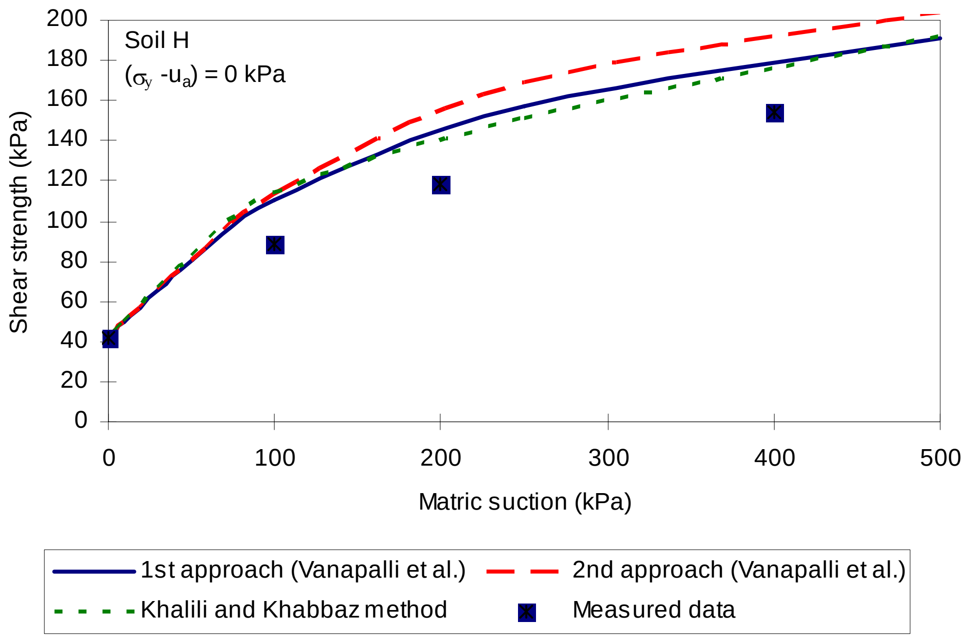

Measured and predicted shear strength values for Soil H (σ_y-u_a = 0kPa)

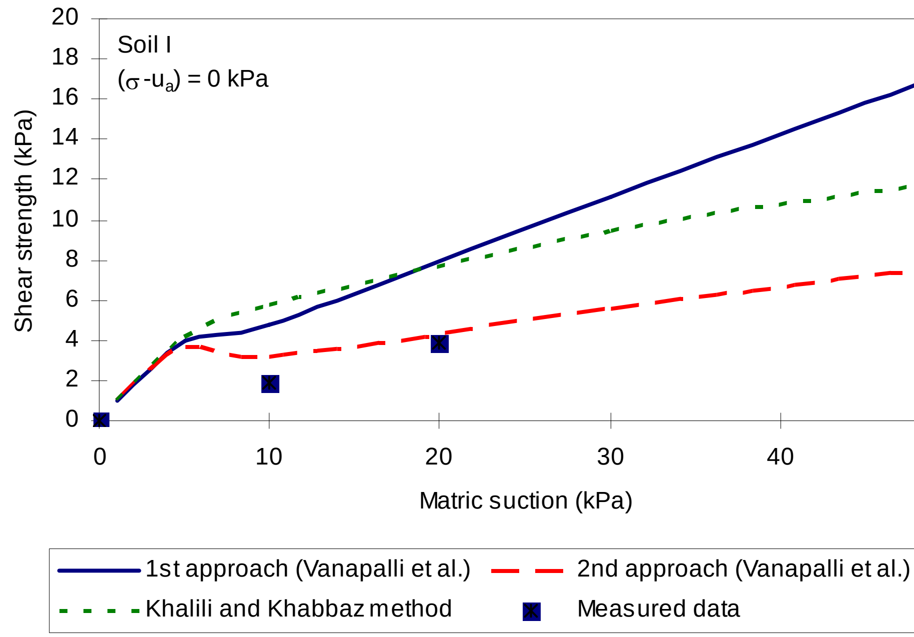

Measured and predicted shear strength values for Soil I (σ-u_a = 0kPa)

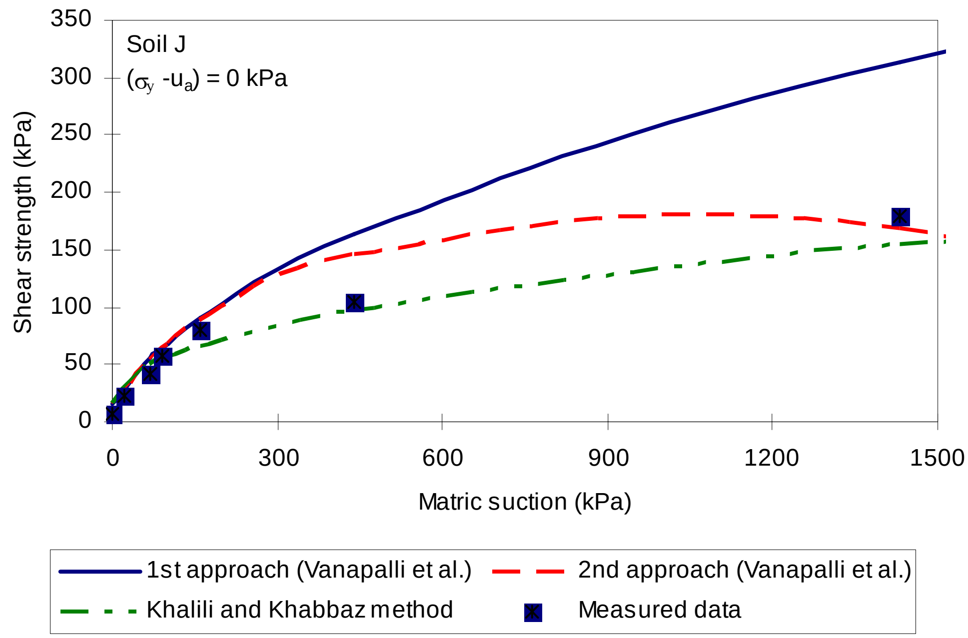

Measured and predicted shear strength values for Soil J (σ_y-u_a = 0kPa)

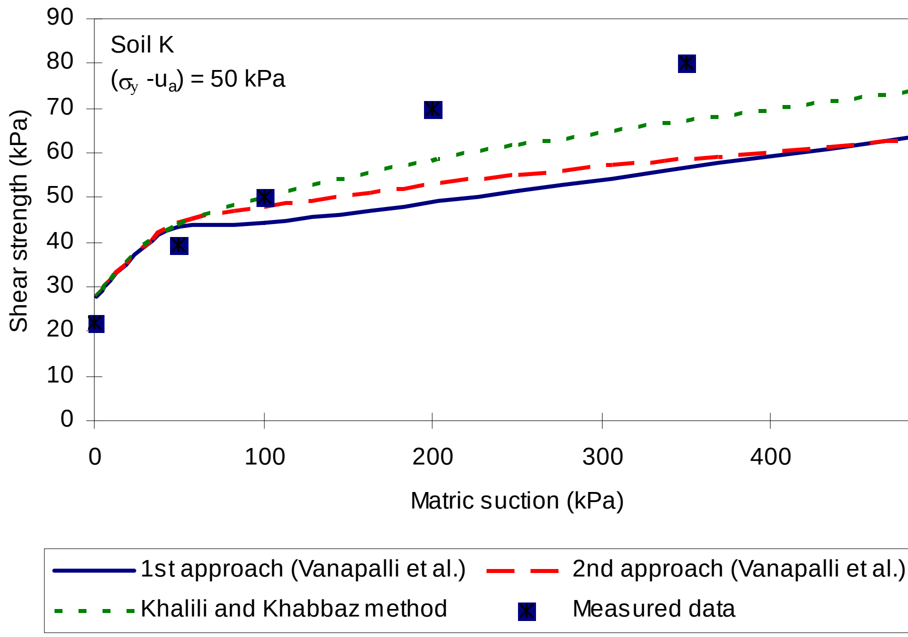

Measured and predicted shear strength values for Soil K (σ_y-u_a = 50kPa)

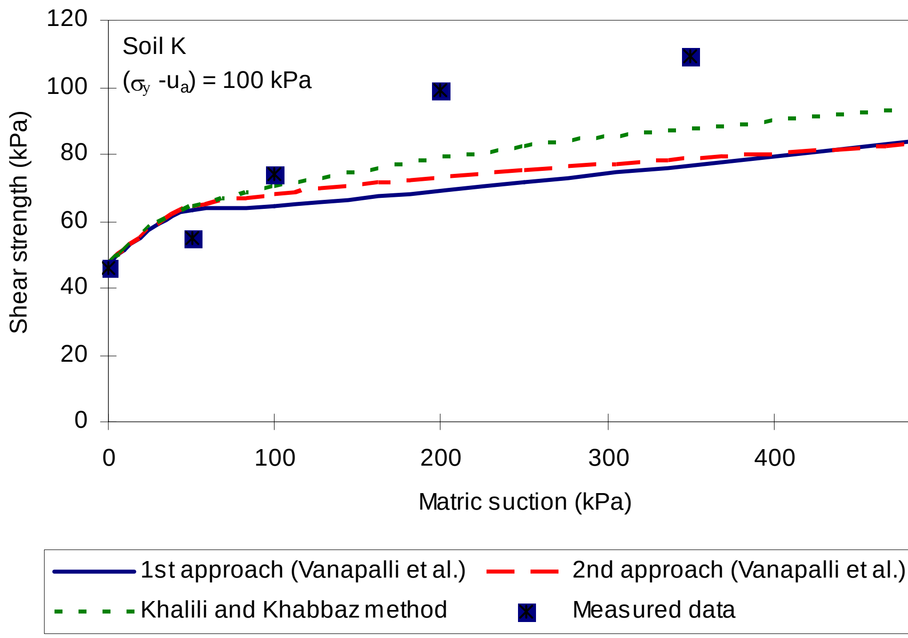

Measured and predicted shear strength values for Soil K (σ_y-u_a = 100kPa)

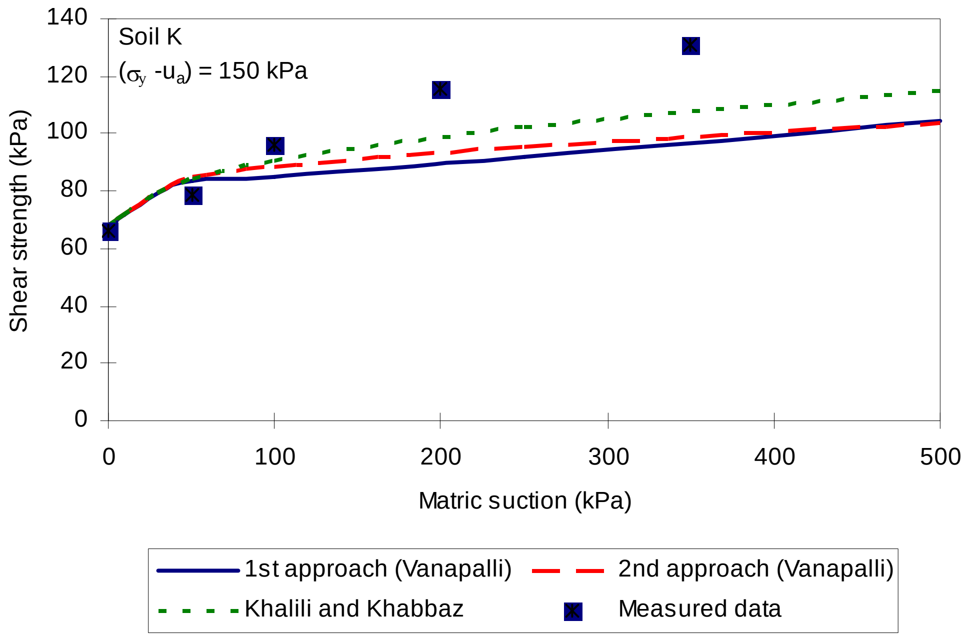

Measured and predicted shear strength values for Soil K (σ_y-u_a = 150kPa)

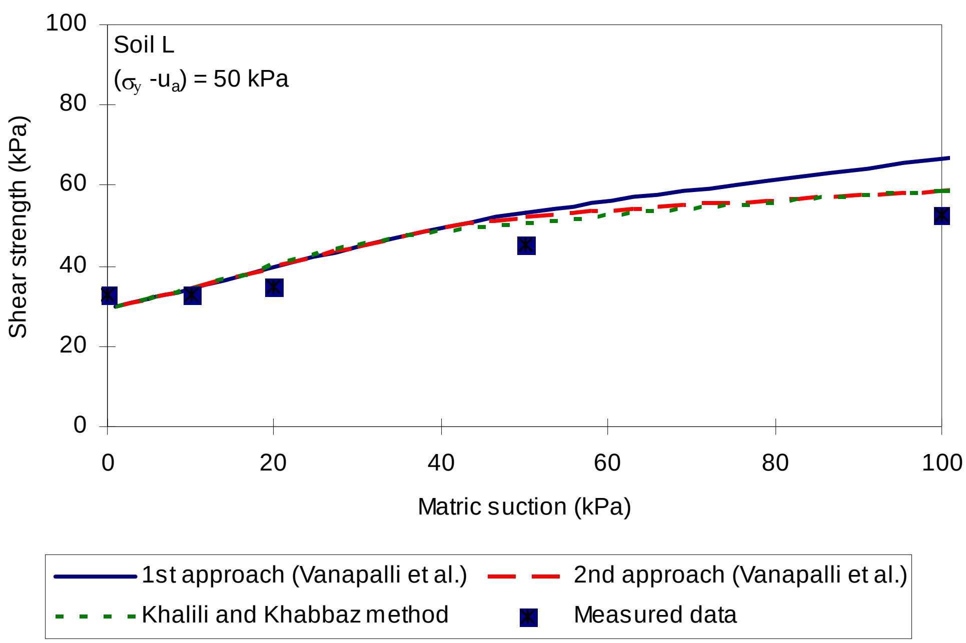

Measured and predicted shear strength values for Soil L (σ_y-u_a = 50kPa)

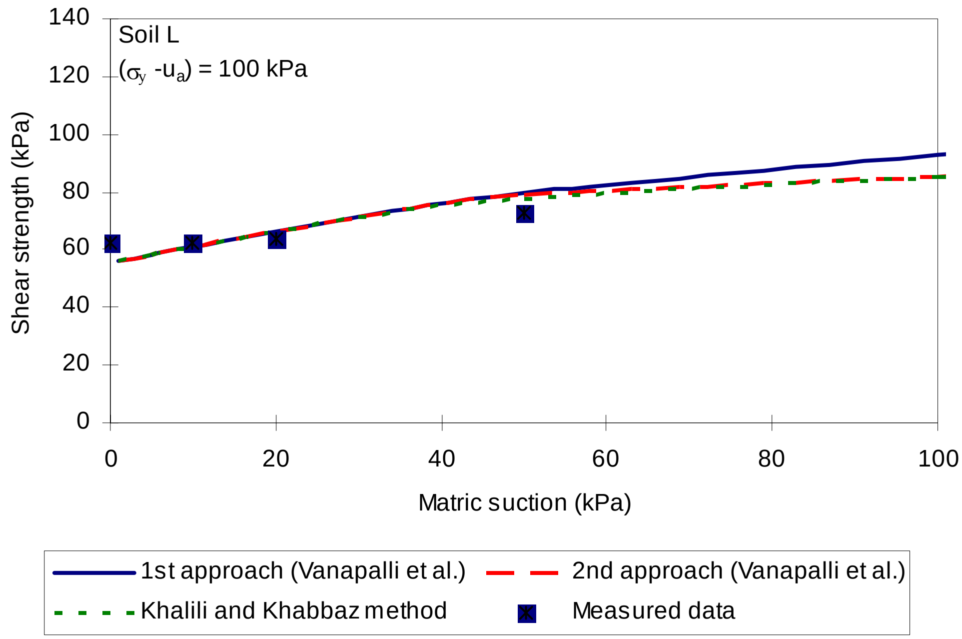

Measured and predicted shear strength values for Soil L (σ_y-u_a = 100kPa)

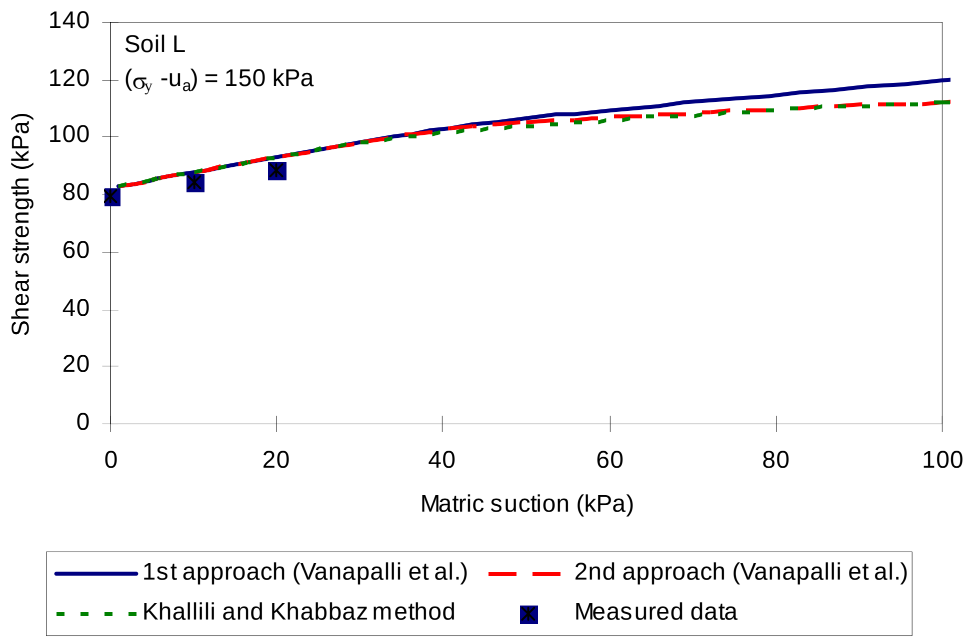

Measured and predicted shear strength values for Soil L (σ_y-u_a = 150kPa)

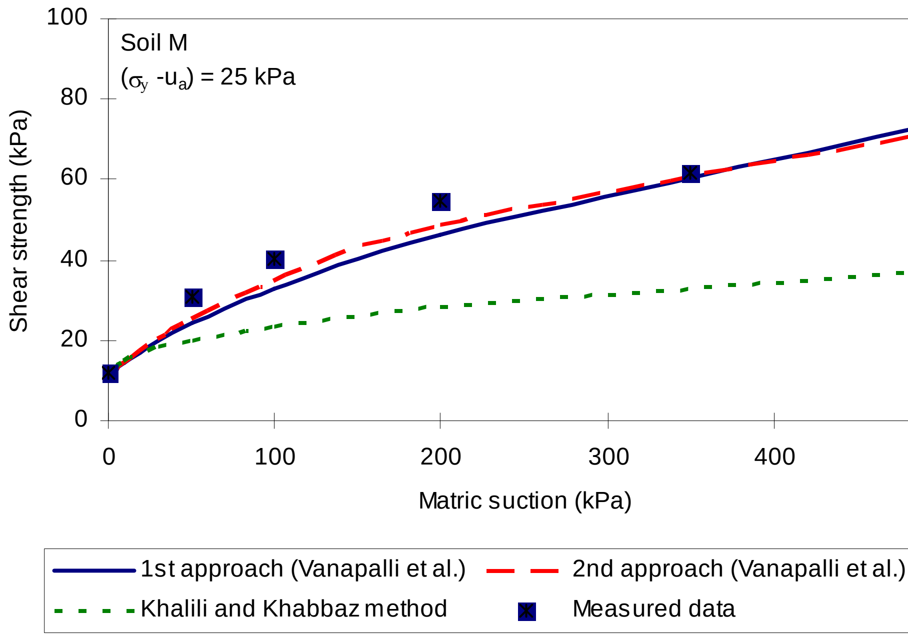

Measured and predicted shear strength values for Soil M (σ_y-u_a = 25kPa)

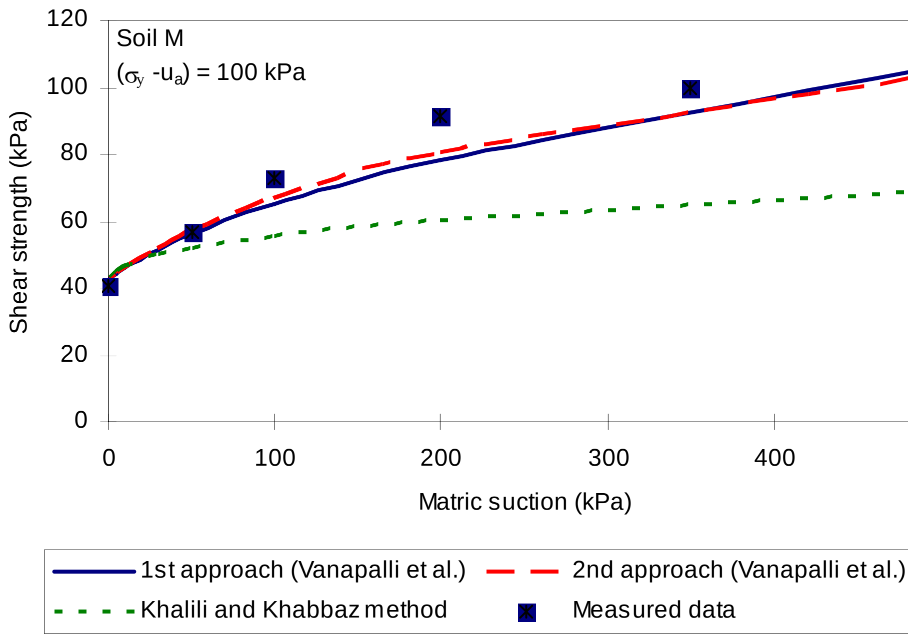

Measured and predicted shear strength values for Soil M (σ_y-u_a = 100kPa)

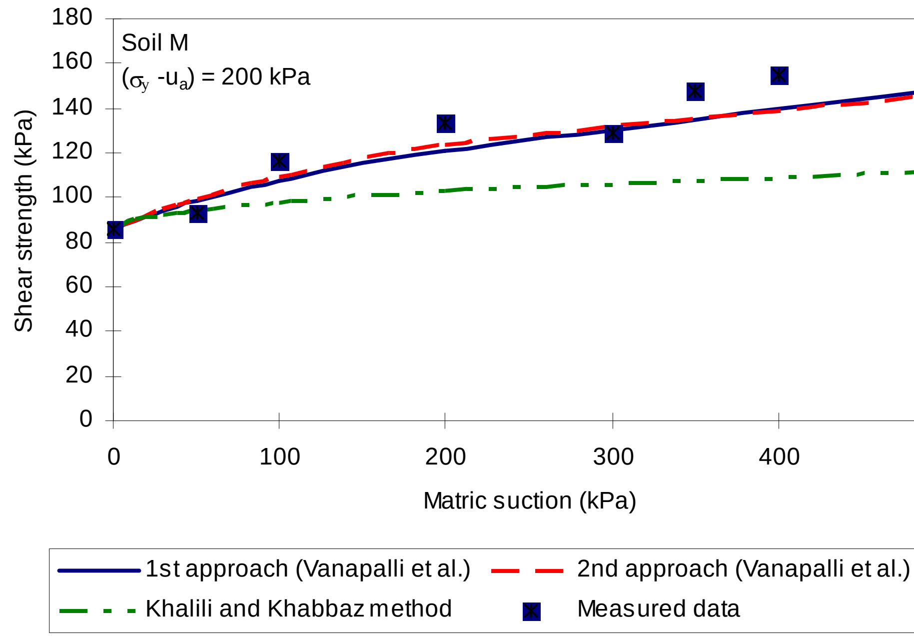

Measured and predicted shear strength values for Soil H (σ_y-u_a = 200kPa)

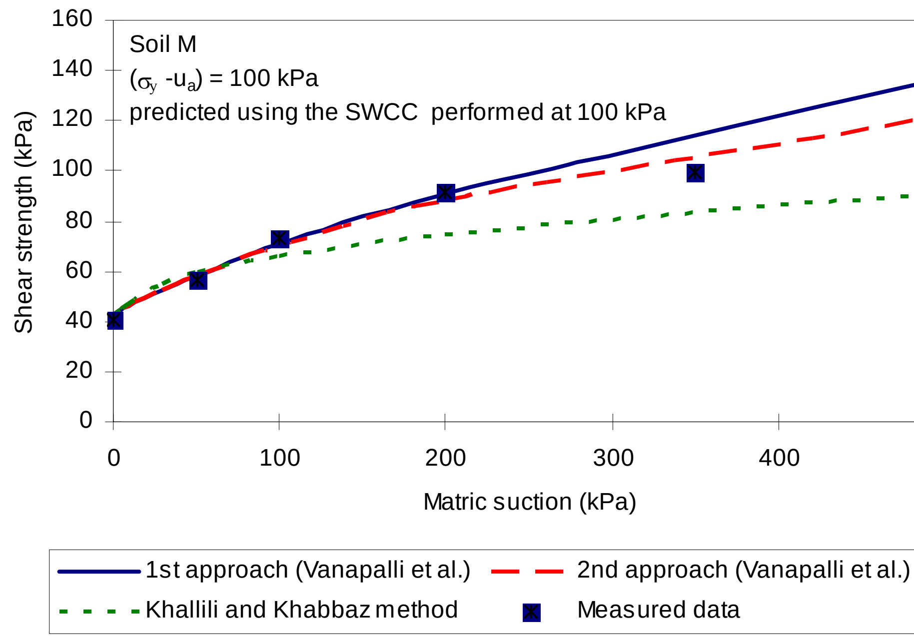

Measured and predicted shear strength values for Soil M (σ_y-u_a = 100kPa)
[predicted using the SWCC performed at (σ_y-u_a) = 100kPa]

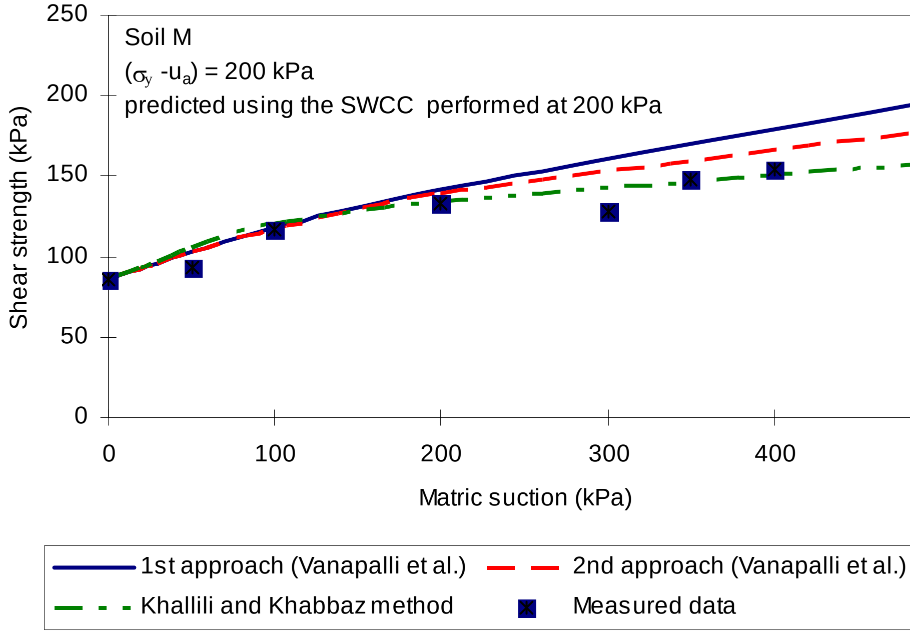

Measured and predicted shear strength values for Soil M (σ_y-u_a = 200kPa)
[predicted using the SWCC performed at (σ_y-u_a) = 200kPa]

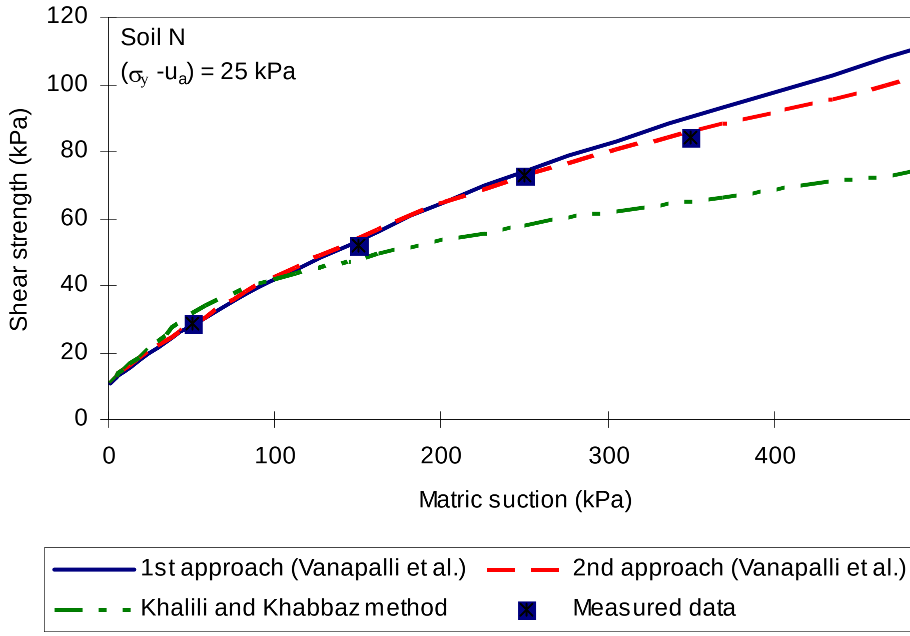

Measured and predicted shear strength values for Soil N (σ_y-u_a = 25kPa)

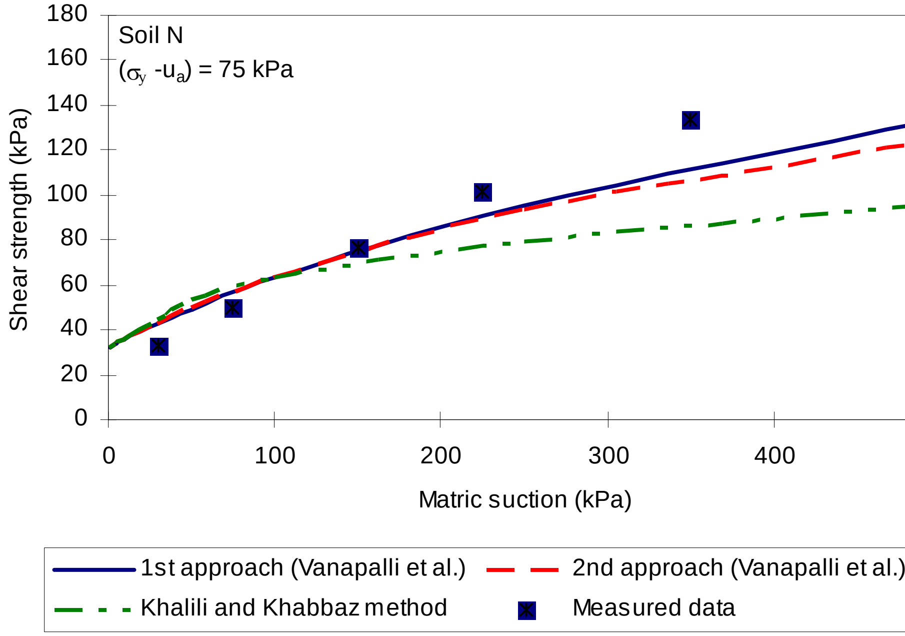

Measured and predicted shear strength values for Soil N (σ_y-u_a = 75kPa)

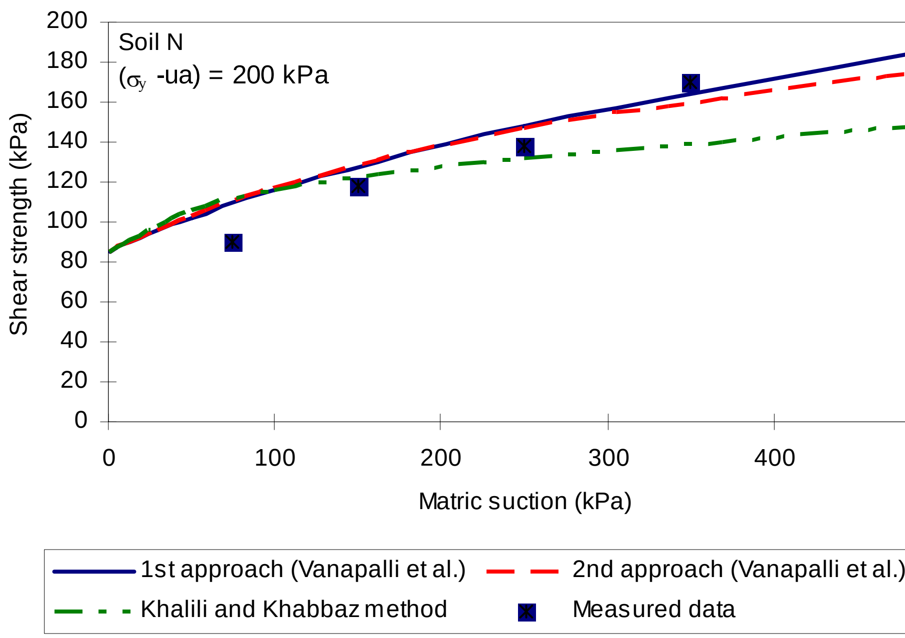

Measured and predicted shear strength values for Soil N (σ_y-u_a = 200kPa)

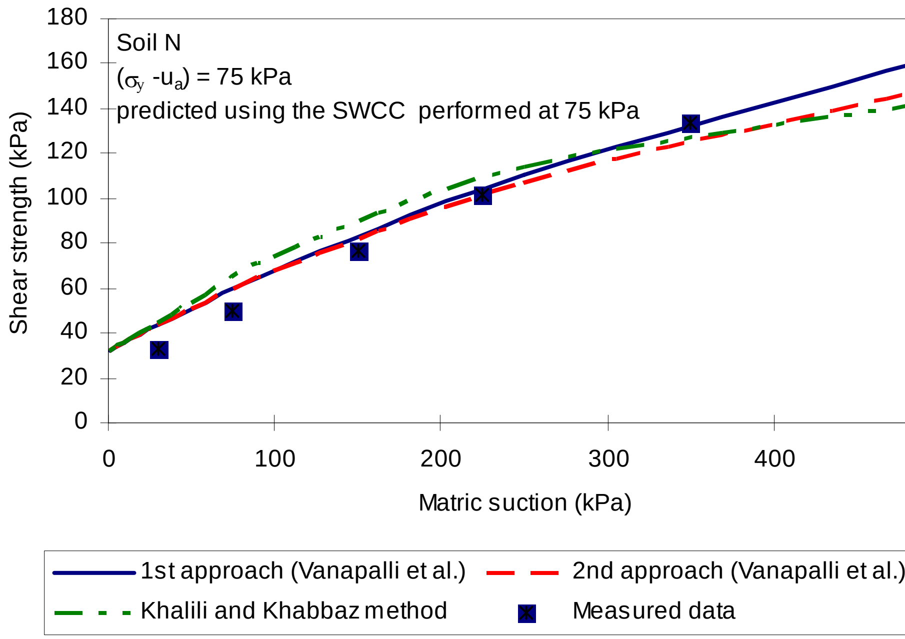

Measured and predicted shear strength values for Soil N (σ_y-u_a = 75kPa)
[predicted using the SWCC performed at (σ_y-u_a) = 75kPa]

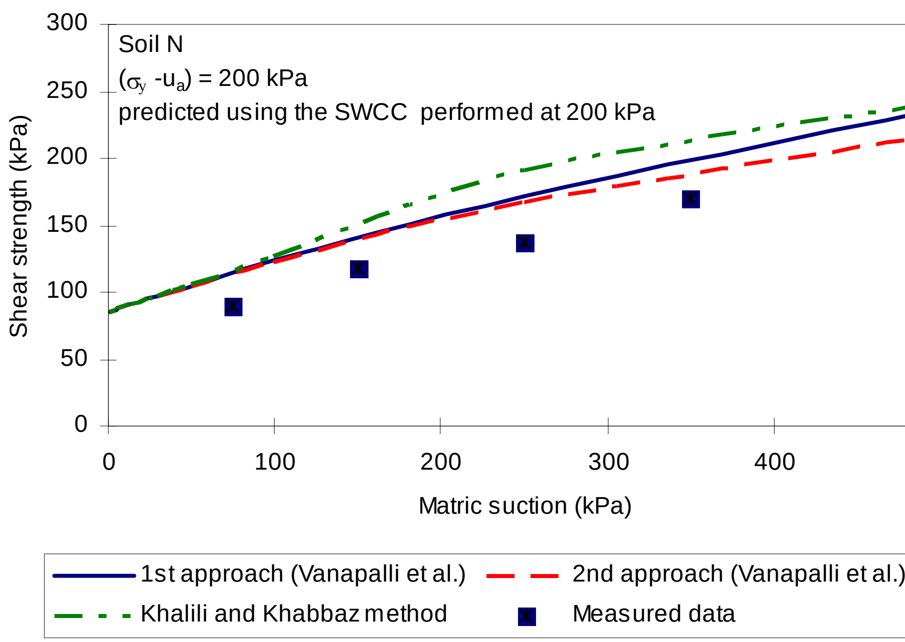

Measured and predicted shear strength values for Soil N (σ_y-u_a = 200kPa)
[predicted using the SWCC performed at (σ_y-u_a) = 200kPa]

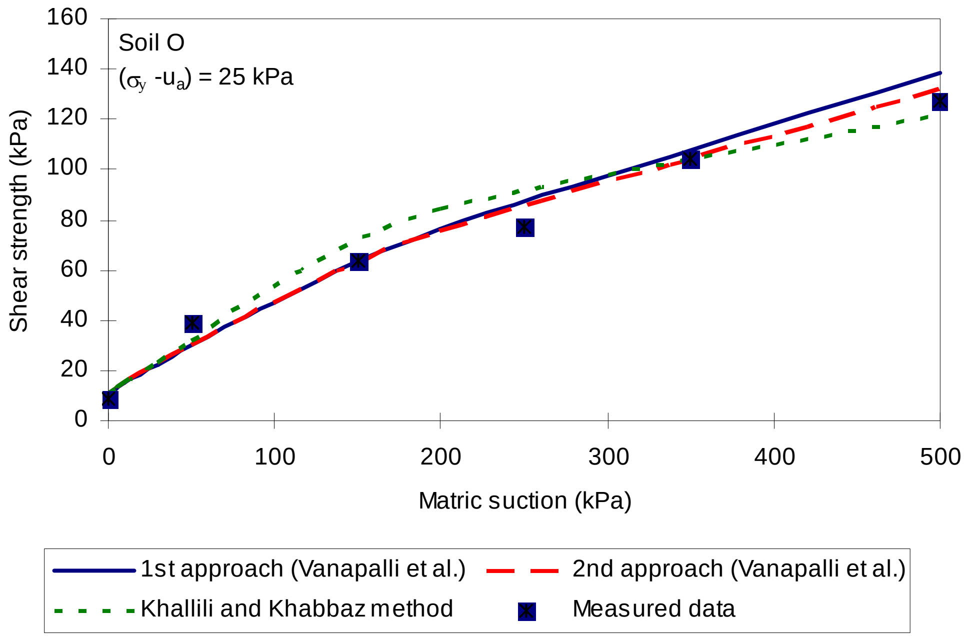

Measured and predicted shear strength values for Soil O (σ_y-u_a = 25kPa)

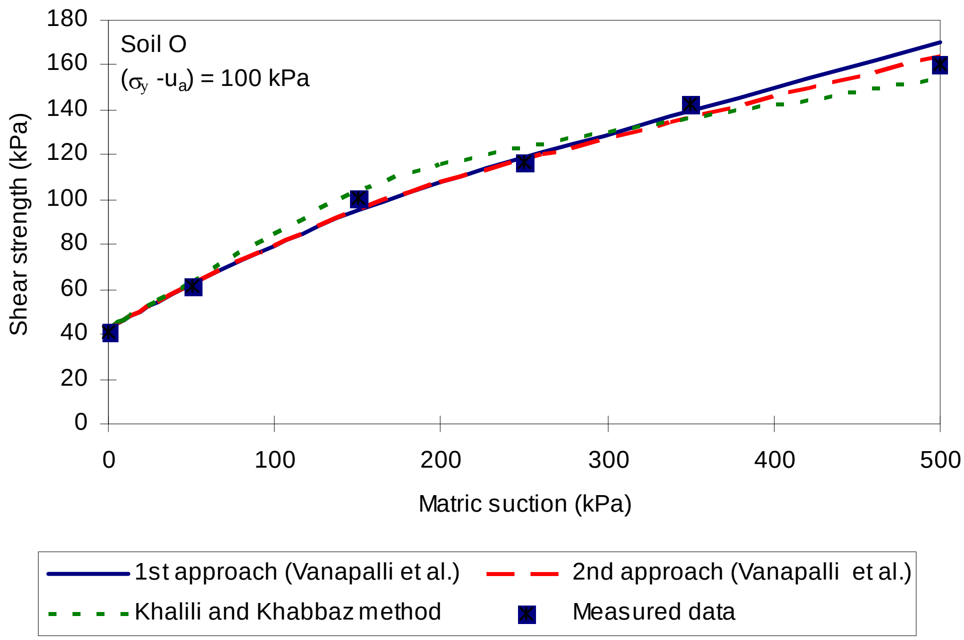

Measured and predicted shear strength values for Soil O (σ_y-u_a = 100kPa)

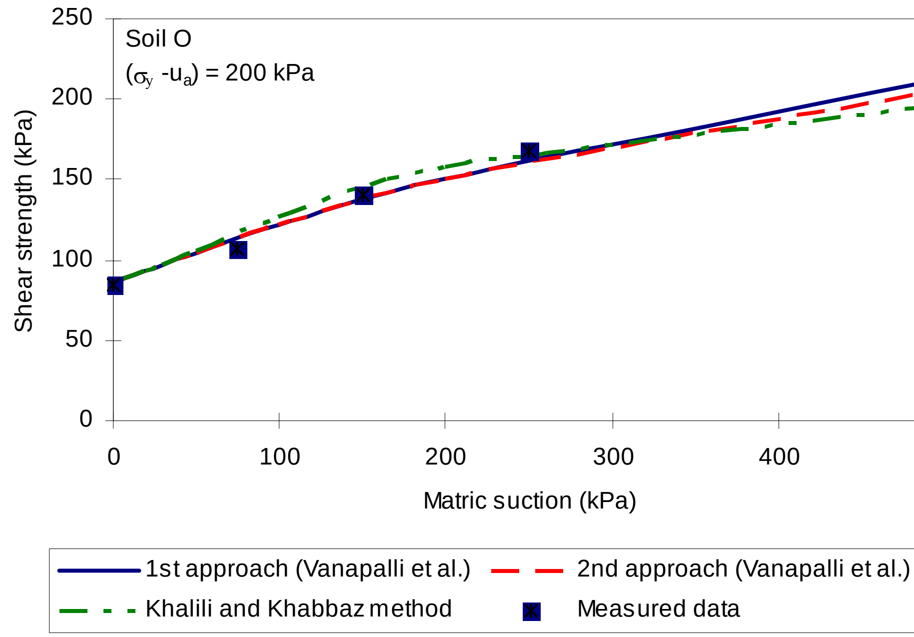

Measured and predicted shear strength values for Soil O (σ_y-u_a = 200kPa)

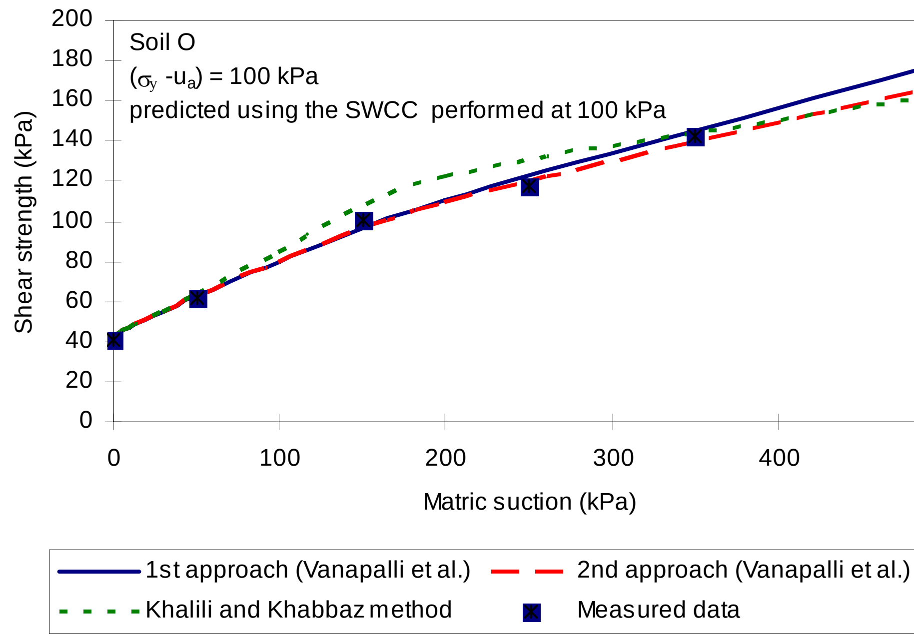

Measured and predicted shear strength values for Soil O (σ_y-u_a = 100kPa)
[predicted using the SWCC performed at (σ_y-u_a) = 100kPa]

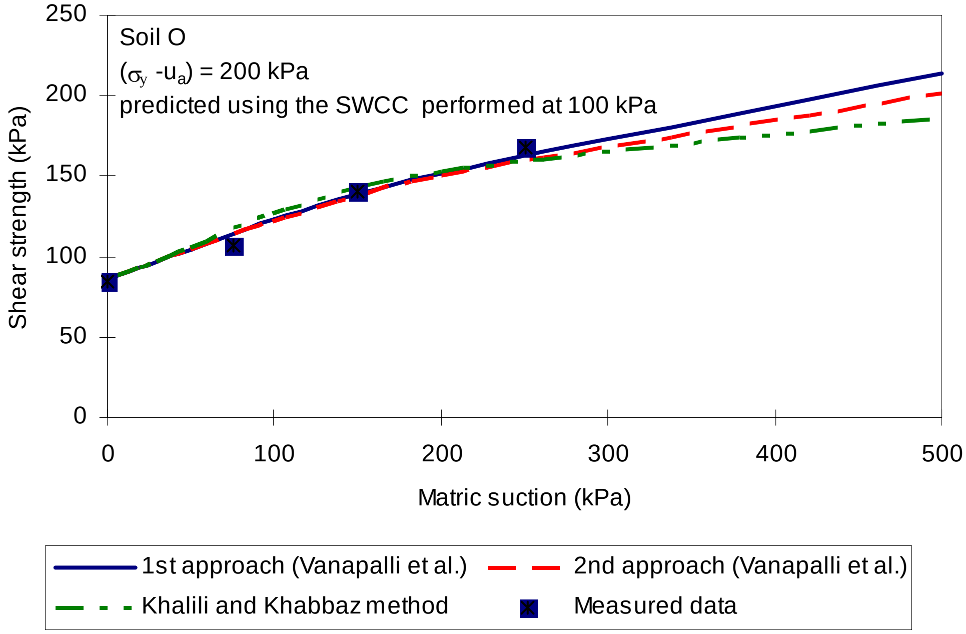

Measured and predicted shear strength values for Soil O (σ_y-u_a = 200kPa)
[predicted using the SWCC performed at (σ_y-u_a) = 200kPa]

APPENDIX C: FLAC CODE
(Simulation for wall behavior at the end of construction)

```
********************************************************************************
* MSE wall behavior during construction based on unsaturated soil properties
* Fish files (Extrap.fis and Luda.fis) are needed for running this code)
********************************************************************************
config ex 12
grid 72,84
gen -4.5,-5.4 -4.5,0.0 -0.3,0.0 -0.3,-5.4 ratio 0.8,0.8 i 1 10 j 1 11
gen -4.5,0.0 -4.5,7.4 0.625,7.4 -0.3,0.0 ratio 0.8,1.0 i 1 10 j 11 85
gen -0.3,-5.4 -0.3,0.0 0.0,0.0 0.0,-5.4 ratio 1.0,0.8 i 10 11 j 1 11
gen -0.3,0.0 0.625,7.4 0.925,7.4 0.0,0.0 i 10 11 j 11 85
gen 0.0,-5.4 0.0,0.0 5.2,0.0 5.2,-5.4 ratio 1.0,0.8 i 11 63 j 1 11
gen 0.0,0.0 0.925,7.4 6.125,7.4 5.2,0.0 i 11 63 j 11 85
gen 5.2,-5.4 5.2,0.0 10.0,0.0 10.0,-5.4 ratio 1.2,0.8 i 63 73 j 1 11
gen 5.2,0.0 6.125,7.4 10.0,7.4 10.0,0.0 ratio 1.2,1.0 i 63 73 j 11 85
m m i=1,72 j=1,10 ;foundation
m null i=11 ;interface
m null i=1,9 j=11,84 ;front of the wall
m e i=10 j=11,84 ;blocks
m m i=12,72 j=11,64 ;backfill soil
m m i=12,72 j=65,84 ;surcharge
ini x add -0.1 i 12 85
********************************************************************************
def blockgrid ;-grid generation for blocks
 x1=-0.3
 y1=0.0
 l1=10
 m1=11
 loop n (1,27)
      x2=x1
      x22=x2+0.025
      x3=x2+0.3
      x33=x22+0.3
      y2=y1
      y3=y2+0.2
      y1=y3
      x1=x22
      l1=l1+2
      m1=m1+2
           command
           gen x2,y2 x22,y3 x33,y3 x3,y2 I=10,11 j=l1,m1
           end_command
  end_loop
end
********************************************************************************
blockgrid
mark i=1
mark i=84
mark j=1
mark j=11
mark i=12
mark i=12,73 j=85
m null i=10 j=11,84
table 1 0.675,5.4 6.875,7.4
```

```
gen table 1
m null reg 13,83
m null reg 40 70
fix y j=1
fix x i=1
fix x i=73
set g=9.81
set large
hist 1 unbal
m null
*******************************************************************************
def prop_comp_setup ;-grid generation for blocks
;1.6m wide zone
;dry density = 1.60      water content = 4.7
Gs01=2.64                                   ; specific gravity
pd01=1.60                                   ; dry density
w01=0.047                                   ; as-compacted water content
den1=pd01*(1.0+w01)                         ; wet density (1.67)
e01=0.65                                    ; void ratio
n01=e01/(1+e01)                             ; porosity
nu1=0.25                                    ; poissson's ratio
Eini1=1.20e3                                ; initial E
bm1=Eini1/(3*(1-2*nu1))                     ; initial bulk modulus
sm1=Eini1/(2*(1+nu1))                       ; initial shear modulus
cohsat1=0.0                                 ; effective cohesion
phi1=26.0                                   ; effective friction angle
dil1=10.0                                   ; dilation angle
ms_ascomp1=783.0                            ; matric suction of ascompacted soil
Bavg1=0.10                                  ; Average B'- hilf pore pressure parpmeter
fa1=248.4                                   ; Fredlund and Xing model parameter
fn1=0.66                                    ; Fredlund and Xing model parameter
fm1=1.78                                    ; Fredlund and Xing model parameter
fhr1=3000.0                                 ; Fredlund and Xing model parameter
;fk1=1.82                                   ; Fredlund and Xing model parameter
Sr1=0.24                                    ; Residual degree of saturation
;airentry1=21.0                             ; airentry value

;beyond 1.6m
;dry density = 1.79    water content = 4.7
Gs02=2.64                                   ; specific gravity
pd02=1.79                                   ; dry density
w02=0.047                                   ; as-compacted water content
den2=pd02*(1.0+w02)                         ; wet density (1.874)
e02=0.47                                    ; void ratio
n02=e02/(1+e02)                             ; porosity
nu2=0.25                                    ; poissson's ratio
Eini2=4.10e3                                ; initial E
bm2=Eini2/(3*(1-2*nu2))                     ; initial bulk modulus
sm2=Eini2/(2*(1+nu2))                       ; initial shear modulus
cohsat2=3.0                                 ; effective cohesion
phi2=30.0                                   ; effective friction angle
dil2=10.0                                   ; dilation angle
ms_ascomp2=783.0                            ; matric suction of ascompacted soil
```

```
Bavg2=0.06                          ; Average B'- hilf pore pressure parpmeter
fa2=138.9                           ; Fredlund and Xing model parameter
fn2=0.81                            ; Fredlund and Xing model parameter
fm2=1.64                            ; Fredlund and Xing model parameter
fhr2=3000.0                         ; Fredlund and Xing model parameter
;fk2=1.82                           ; Fredlund and Xing model parameter
Sr2=0.17                            ; Residual degree of saturation
;airentry2=19.5                     ; airentry value

CASEOF shear_est_method             ; choose the prediction method!
CASE 1                              ; Total Coshesion-Vanapalli et al.'s 1st app.
Cf1=1-(ln(1+ms_ascomp1/fhr1))/(ln(1+(1000000/fhr1)))
theta1=Cf1*(n01)/(ln(2.718+(ms_ascomp1/fa1)^fn1))^fm1
cohin1=cohsat1+ms_ascomp1*(theta1/n01)^fk1*tan(phi1*degrad)
Cf2=1-(ln(1+ms_ascomp2/fhr2))/(ln(1+(1000000/fhr2)))
theta2=Cf2*(n02)/(ln(2.718+(ms_ascomp2/fa2)^fn2))^fm2
cohin2=cohsat2+ms_ascomp2*(theta2/n02)^fk2*tan(phi2*degrad)

CASE 2                              ; Total Coshesion-Vanapalli et al.'s 2st app.
Cf1=(1-(ln(1+ms_ascomp1/fhr1))/(ln(1+(1000000/fhr1))))
S1=Cf1*(1/(ln(2.718+(ms_ascomp1/fa1)^fn1)))^(fm1)
cohin1=cohsat1+ms_ascomp1*((S1-Sr1)/(1-Sr1))*tan(phi1*degrad)
Cf2=(1-(ln(1+ms_ascomp2/fhr2))/(ln(1+(1000000/fhr2))))
S2=Cf2*(1/(ln(2.718+(ms_ascomp2/fa2)^fn2)))^(fm2)
cohin2=cohsat2+ms_ascomp2*((S2-Sr2)/(1-Sr2))*tan(phi2*degrad)

CASE 3                              ; Total Coshesion-Khalli and Khabaz
cohin1=cohsat1+ms_ascomp1*(ms_ascomp1/airentry1)^(-0.55)*tan(phi1*degrad)
cohin2=cohsat2+ms_ascomp2*(ms_ascomp2/airentry2)^(-0.55)*tan(phi2*degrad)
ENDCASE
end
******************************************************************************
set shear_est_method=2 ;(1: Vanapalli et al.'s 1st app., 2: Vanapalli et al.'s 2nd app., 3: Khalili and Khabbaz method)
prop_comp_setup


*Foundation
m m i=1,10 j=1,10
prop den=1.92 b=3.3e4 shear=2.0e4 fric=30 coh=10.0 i=1,10 j=1,10
m m i=12,72 j=1,10
prop den=1.92 b=3.3e4 shear=2.0e4 fric=30 coh=10.0 i=12,72 j=1,10
int 1 Aside from 11,1 to 11,11 Bside from 12,1 to 12,11
int 1 kn=1.98e6 ks=1.98e6 glued
solve
sav D160179-i.sav

******************************************************************************
*     (The following FISH function step-wise alters the geometry and properties
*           of the layer being constructed)
******************************************************************************
def batter
   p0=p1
```

```
      p2=p0+1
      p22=p2+1
      p2_1=p2-2
      P22_1=P22-2
      p3=p2+2
      p33=p3+1
      p3_1=p3-2
      P33_1=P33-2
      p4=p3+2
      p1=p33
      s2=s1+1
      s3=s2+1
      s4=s3+1
      s5=s4+1
      s6=s5+1
      s1=s5
      I0=I1
      I2=I0+1
      I3=I2+1
      I4=I3+1
      I5=I4+1
      I6=I5+1
      I7=I6+1
      I1=I7
      hh=hh+4
end
*******************************************************************************
set p1=11 I1=2 s1=10 hh=10

*******************************************************************************
* Hyperbolic model for gravel column
*
*******************************************************************************
def Hyperbolic
           loop j (11,hh)
              loop i (12,14)
                    temp1=-0.5*(sxx(i,j)+syy(i,j))
              temp2=sqrt(sxy(i,j)^2+0.25*(sxx(i,j)-syy(i,j))^2)
              sigma3=min(temp1-temp2, -szz(i,j))
              if sigma3<0 then
                   sigma3=0.0
              end_if
              sl=max(temp1+temp2, -szz(i,j))
              sl=0.5*(sl-sigma3)*(1-sin(fri1*degrad))
              sl=sl/(coh*cos(fri1*degrad)+sigma3*sin(fri1*degrad))
              ela=(1-rf*sl)^2*k2*pat*(sigma3/pat)^nd
              bulk_mod(i,j)=ela/(3*(1-2*nu3))
              shear_mod(i,j)=ela/(2*(1.0+nu3))
      end_loop
     end_loop
      end
*******************************************************************************
set pat=101.3 k2=4000 nd=0.5 rf=0.73 nu3=0.25
```

```
set coh=0 fri1=55

******************************************************************************
* Update stress dependent elastic modulus for backfills
* (Using unsaturated soil properties)
******************************************************************************
def update_mod ;
    loop j (11,hh)
        loop i (15,72)
            Smean=-0.333*(sxx(i,j)+syy(i,j)+szz(i,j))
CASEOF ela_est_method
CASE 1                          ;Quadratic fuction
            if i<=30 then
              nu=nu1
;- 3-dimensional loading (Smean) --->    Ko loading    (Sy)
              Sy=3*((1-nu)/(1+nu))*Smean
              ms1=abs((2*a1*Sy+b1)/100) ; slope-differentiate
              ela=((1+nu)*(1-2*nu))/((1-nu)*(ms1))
              if ela<E_min1
              ela=E_min1
              end_if
            else
              nu=nu2
              Sy=3*((1-nu)/(1+nu))*Smean
              ms1=abs((2*a2*Sy+b2)/100) ; slope-differentiate
              ela=((1+nu)*(1-2*nu))/((1-nu)*(ms1))
              if ela<E_min2
              ela=E_min2
              end_if
            end_if
CASE 2                            ;Log fuction
            if i<=30 then
              nu=nu1
;- 3-dimensional loading (Smean) --->    Ko loading    (Sy)
              Sy=3*((1-nu)/(1+nu))*Smean
              if Sy<=0.0
              Sy=0.01
              end_if
              ms1=abs(a1*(1/Sy)/100) ; a1 = slope of log function
              ela=((1+nu)*(1-2*nu))/((1-nu)*(ms1))
              if ela<E_min1
              ela=E_min1
              end_if
            else
              nu=nu2
              Sy=3*((1-nu)/(1+nu))*Smean
              if Sy<=0.0
              Sy=0.01
              end_if
              ms1=abs(a2*(1/Sy)/100) ; a2 = slope of log function
              ela=((1+nu)*(1-2*nu))/((1-nu)*(ms1))
              if ela<E_min2
              ela=E_min2
```

```
                    end_if
                end_if
ENDCASE
                  bulk_mod(i,j)=ela/(3*(1-2*nu))
                  shear_mod(i,j)=ela/(2*(1.0+nu))
              end_loop
        end_loop
end
********************************************************************************
set ela_est_method=2 ;(1: Qaudratic, 2: Log)
set a1=-1.765 E_min1=1.20e3
set a2=-1.000 E_min2=4.10e3

********************************************************************************
* Update cohesion intercept for backfills
* (based on the change in matric suction due to loading)
********************************************************************************
def update_coh;
        loop j (11,hh)
              loop i (15,72)
                if i<=30 then
                  n=n01
                  nu=nu1
                  ms_ascomp=ms_ascomp1
                  Bavg=Bavg1                  ; Hilf's secant pore pressure parameter
                  cohsat=cohsat1
                  phi=phi1
                  airentry=airentry1
                  fa=fa1
                  fn=fn1
                  fm=fm1
                  fhr=fhr1
                  fk=fk1
                  Sr=Sr1
                else
                  n=n02
                  nu=nu2
                  ms_ascomp=ms_ascomp2
                  Bavg=Bavg2                  ; Hilf's secant pore pressure parameter
                  cohsat=cohsat2
                  phi=phi2
                  airentry=airentry2
                  fa=fa2
                  fn=fn2
                  fm=fm2
                  fhr=fhr2
                  fk=fk2
                  Sr=Sr2
                endif
; excess pore pressure calcullated based on the Modified Hilf's eqatuion.
; Smean used instead of syy becuase 2-D loading condtion
                  Smean=-0.333*(sxx(i,j)+syy(i,j)+szz(i,j))
                  Sy=3*((1-nu)/(1+nu))*Smean
```

```
            ex_1(i,j)=ms_ascomp-Bavg*Sy
            if ex_1(i,j)<=0 then
              command
                prop coh cohsat i=i j=j
              end_command
            else
Cf=1-(ln(1+ex_1(i,j)/fhr))/(ln(1+(1000000/fhr)))
theta=Cf*(n)/(ln(2.718+(ex_1(i,j)/fa)^fn))^fm
S=Cf/(ln(2.718+(ex_1(i,j)/fa)^fn))^fm

CASEOF shear_est_method
CASE 1                          ; Vanapalli et al.'s 1st App
totalcoh=cohsat+ex_1(i,j)*(theta/n)^fk*tan(phi*degrad)
CASE 2                          ; Vanapalli et al.'s 2nd App
totalcoh=cohsat+ex_1(i,j)*((S-Sr)/(1-Sr))*tan(phi*degrad)
CASE 3                          ; Khalli and Khabaz
totalcoh=cohsat+ex_1(i,j)*(ex_1(i,j)/airentry)^(-0.55)*tan(phi*degrad)
ENDCASE
              command
                prop coh totalcoh i=i j=j
              end_command
            end_if
          end_loop
    end_loop
end
******************************************************************************

******************************************************************************
def build1
    command
      m e i=10 j=p2
      prop den=2.00 b=10.95e6 s=10e6 i=10 j=p2
      m e i=10 j=p3
      prop den=2.00 b=10.95e6 s=10e6 i=10 j=p3
      m m i=12,14 j=s2,s3
      prop den=2.1 b=10000 s=7000 fric=55 di=20 coh=0 i=12,14 j=s2,s3
      m m i=15,30 j=s2,s3
      prop den=den1 b=bm1 s=sm1 fric=phi1 di=dil1 coh=cohin1 i=15,30 j=s2,s3
      m m i=31,72 j=s2,s3
      prop den=den2 b=bm2 s=sm2 fric=phi2 di=dil2 coh=cohin2 i=31,72 j=s2,s3
      int I2 Aside from 11,p2 to 11,p22 Bside from 12,s2 to 12,s4
      int I2 kn=1e6 ks=8.5e3 fric=55
      int I3 Aside from 11,p22_1 to 11,p2_1 Bside from 12,s2 to 12,s4
      int I3 kn=1e6 ks=8.5e3 fric=55
      int I4 Aside from 10,p22 to 11,p22 Bside from 10,p3 to 11,p3
      int I4 kn=10.95e7 ks=8.5e3 fric=55 t=0
      solve srat=0.01
    end_command
end
******************************************************************************
******************************************************************************
def build2
    command
```

```
        m e I=10 j=p4
        prop den=2.00 b=10.95e6 s=10e6 i=10 j=p4
        m m i=12,14 j=s4,s5
        prop den=2.1 b=10000 s=7000 fric=55 di=20 coh=0 i=12,14 j=s4,s5
        m m i=15,30 j=s4,s5
        prop den=den1 b=bm1 s=sm1 fric=phi1 di=dil1 coh=cohin1 i=15,30 j=s4,s5
        m m i=31,72 j=s4,s5
        prop den=den2 b=bm2 s=sm2 fric=phi2 di=dil2 coh=cohin2 i=31,72 j=s4,s5
        int I5 Aside from 11,p3 to 11,p33 Bside from 12,s4 to 12,s6
        int I5 kn=1e6 ks=8.5e3 fric=55
        int I6 Aside from 11,p33_1 to 11,p3_1 Bside from 12,s4 to 12,s6
        int I6 kn=1e6 ks=8.5e3 fric=55
        int I7 Aside from 10,p33 to 11,p33 Bside from 10,p4 to 11,p4
        int I7 kn=10.95e7 ks=8.5e3 fric=55 t=0
        solve srat=0.01
    end_command
end
********************************************************************************

********************************************************************************
def Hrein
    h1=Rbeg
    f1=f1
    v0=v0
    kk=Rend-1
    loop i (Rbeg,kk)
        h2=h1+1
        command
        struct cable begin grid h1,v0 end grid h2,v0 seg=1 pr=f1
        end_command
        h1=h2
    end_loop
end
********************************************************************************
*   (Type 3)
*use (in-situ modulus) for Fortrac Geogrid
struct prop=1 a=2.5e-3 peri=2 e=84e3
struct prop=1 yield=35.0 ycomp=0.01
set Rbeg=12 Rend=57 f1=1

********************************************************************************
* Update properties of reinforcement
*
********************************************************************************
def update_rein
bn=14    ; Block Number from bottom
rn=2     ; property number
loop k (1,2)
overburden=-syy(10,bn)
reinstiff=110.5*overburden+3302
if overburden < 34.3 then
   reinfric=28.0
   reincoh=20.5
```

```
else
     reinfric=6.8
     reincoh=48.7
endif
command
struc prop=rn kbond=reinstiff sbond=reincoh sfric=reinfric
end_command
bn=bn+2    ; Number of block between reinforcements
rn=rn+1
end_loop

bn=20       ; Block Number from bottom
rn=4        ; property number
loop k (1,6)
overburden=-syy(10,bn)
reinstiff=110.5*overburden+3302
if overburden < 34.3 then
     reinfric=28.0
     reincoh=20.5
else
     reinfric=6.8
     reincoh=48.7
endif
command
struc prop=rn kbond=reinstiff    sbond=reincoh sfric=reinfric
end_command
bn=bn+4    ; Number of block between reinforcements
rn=rn+1
end_loop

bn=48       ; Block Number from bottom
rn=10       ; property number
loop k (1,3)
overburden=-syy(10,bn)
reinstiff=110.5*overburden+3302
if overburden < 34.3 then
     reinfric=28.0
     reincoh=20.5
else
     reinfric=6.8
     reincoh=48.7
endif
command
struc prop=rn kbond=reinstiff    sbond=reincoh sfric=reinfric
end_command
bn=bn+6      ; Number of block between reinforcements
rn=rn+1
end_loop
end
********************************************************************************

********************************************************************************
def supstep
```

```
        Hyperbolic
        update_mod
        update_coh
        update_rein
        command
           step 100
        end_command
end

def supsolve
        loop kk(1,10)
        supstep
        end_loop
end
*******************************************************************************

; Start building the MSE wall
*1
batter
m e i=10 j=p2
prop den=2.00 b=10.95e6 s=10e6 i=10 j=p2
m e i=10 j=p3
prop den=2.00 b=10.95e6 s=10e6 i=10 j=p3
m m i=12,14 j=s2,s3
prop den=2.1 b=10000 s=7000 fric=55 di=20 coh=0 i=12,14 j=s2,s3
m m i=15,30 j=s2,s3
prop den=den1 b=bm1 s=sm1 fric=phi1 di=dil1 coh=cohin1 i=15,30 j=s2,s3
m m i=31,72 j=s2,s3
prop den=den2 b=bm2 s=sm2 fric=phi2 di=dil2 coh=cohin2 i=31,72 j=s2,s3
int 2 Aside from 10,11 to 11,11 Bside from 10,12 to 11,12
int 2 kn=10e6 ks=8.5e3 fric=55 ;glued
int I2 Aside from 11,p2 to 11,p22 Bside from 12,s2 to 12,s4
int I2 kn=1e6 ks=8.5e3 fric=55
int I4 Aside from 10,p22 to 11,p22 Bside from 10,p3 to 11,p3
int I4 kn=10.95e7 ks=8.5e3 fric=55 t=0
solve srat=0.01
*geosynthetic layer #1
set v0=13
struct cable begin -0.27,0.2 end grid Rbeg,v0 seg=3 pr=2
struct prop=2 a=2.5e-3 peri=2 e=84e3 yield=35.0 ycomp=0.01
struct prop=2 sbond=20.5 sfric=28.0
Hrein

*2
build2
supsolve
*geosynthetic layer #2
set v0=15
struct cable begin -0.245,0.4 end grid Rbeg,v0 seg=3 pr=3
struct prop=3 a=2.5e-3 peri=2 e=84e3 yield=35.0 ycomp=0.01
struct prop=3 sbond=20.5 sfric=28.0
Hrein
```

```
*3
batter
build1
*4
build2
supsolve
*geosynthetic layer #3
set v0=19
struct cable begin -0.195,0.8 end grid Rbeg,v0 seg=3 pr=4
struct prop=4 a=2.5e-3 peri=2 e=84e3 yield=35.0 ycomp=0.01
struct prop=4 sbond=20.5 sfric=28.0
Hrein

*5
batter
build1
*6
build2
supsolve
*geosynthetic layer #4
set v0=23
struct cable begin -0.145,1.2 end grid Rbeg,v0 seg=3 pr=5
struct prop=5 a=2.5e-3 peri=2 e=84e3 yield=35.0 ycomp=0.01
struct prop=5 sbond=20.5 sfric=28.0
Hrein

*7
batter
build1
*8
build2
supsolve
*geosynthetic layer #5
set v0=27
struct cable begin -0.095,1.6 end grid Rbeg,v0 seg=3 pr=6
struct prop=6 a=2.5e-3 peri=2 e=84e3 yield=35.0 ycomp=0.01
struct prop=6 sbond=20.5 sfric=28.0
Hrein
sav D160179-8.sav

*9
batter
build1
*10
build2
supsolve
*geosynthetic layer #6
set v0=31
struct cable begin -0.045,2.0 end grid Rbeg,v0 seg=3 pr=7
struct prop=7 a=2.5e-3 peri=2 e=84e3 yield=35.0 ycomp=0.01
struct prop=7 sbond=20.5 sfric=28.0
Hrein
```

```
*11
batter
build1
*12
build2
supsolve
*geosynthetic layer #7
set v0=35
struct cable begin 0.005,2.4 end grid Rbeg,v0 seg=3 pr=8
struct prop=8 a=2.5e-3 peri=2 e=84e3 yield=35.0 ycomp=0.01
struct prop=8 sbond=20.5 sfric=28.0
Hrein

*13
batter
build1
*14
build2
supsolve

*15
batter
build1
*geosynthetic layer #8
set v0=41
struct cable begin 0.08,3.0 end grid Rbeg,v0 seg=3 pr=9
struct prop=9 a=2.5e-3 peri=2 e=84e3 yield=35.0 ycomp=0.01
struct prop=9 sbond=20.5 sfric=28.0
Hrein

*16
build2
supsolve

*17
batter
build1
*18
build2
supsolve
*geosynthetic layer #9
set v0=47
struct cable begin 0.155,3.6 end grid Rbeg,v0 seg=3 pr=10
struct prop=10 a=2.5e-3 peri=2 e=84e3 yield=35.0 ycomp=0.01
struct prop=10 sbond=20.5 sfric=28.0
Hrein
sav D160179-18.sav

*19
batter
build1
*20
build2
```

```
supsolve

*21
batter
build1
*geosynthetic layer #10
set v0=53
struct cable begin 0.23,4.2 end grid Rbeg,v0 seg=3 pr=11
struct prop=11 a=2.5e-3 peri=2 e=84e3 yield=35.0 ycomp=0.01
struct prop=11 sbond=20.5 sfric=28.0
Hrein
*22
build2
supsolve

*23
batter
build1
*24
build2
supsolve
*geosynthetic layer #11
set v0=59
struct cable begin 0.305,4.8 end grid Rbeg,v0 seg=3 pr=12
struct prop=12 a=2.5e-3 peri=2 e=84e3 yield=35.0 ycomp=0.01
struct prop=12 sbond=20.5 sfric=28.0
Hrein

*25
batter
build1
*26
build2
supsolve

;*27
batter
m m i=12,14 j=s2,s3
prop den=2.1 b=10000 s=7000 fric=55 di=20 coh=0 i=12,14 j=s2,s3
m m i=15,30 j=s2,s3    ; poor compaction
prop den=den1 b=bm1 s=sm1 fric=phi1 di=dil1 coh=cohin1 i=15,30 j=s2,s3
m m i=31,72 j=s2,s3      ; high compaction
prop den=den2 b=bm2 s=sm2 fric=phi2 di=dil2 coh=cohin2 i=31,72 j=s2,s3
int I2 Aside from 11,p2 to 11,p22 Bside from 12,s2 to 12,s4
int I2 kn=1e6 ks=8.5e3 fric=55
int I3 Aside from 11,p22_1 to 11,p2_1 Bside from 12,s2 to 12,s4
int I3 kn=1e6 ks=8.5e3 fric=55
solve srat=0.01
set hh=64
supsolve
sav D160179-27.sav

******************************************************************************
```

```
def supstep1
       update_mod
       update_coh
       update_rein
       command
          step 100
       end_command
end
def supsolve1
       loop kk(1,10)
       supstep1
       end_loop
end
******************************************************************************

*Surcharge
m m i=12,72 j=65,68
prop den=den1 b=bm1 s=sm1 fric=phi1 di=dil1 coh=cohin1 i=12,30 j=65,68
prop den=den2 b=bm2 s=sm2 fric=phi2 di=dil2 coh=cohin2 i=31,72 j=65,68
m null reg 12,66

set hh=84
solve srat=0.01
supsolve1 ; define modulus for surcharge

m m i=12,72 j=69,72
prop den=den1 b=bm1 s=sm1 fric=phi1 di=dil1 coh=cohin1 i=12,30 j=69,72
prop den=den2 b=bm2 s=sm2 fric=phi2 di=dil2 coh=cohin2 i=31,72 j=69,72
m null reg 12,70
solve srat=0.01
supsolve1 ; define modulus for surcharge

m m i=12,72 j=63,76
prop den=den1 b=bm1 s=sm1 fric=phi1 di=dil1 coh=cohin1 i=12,30 j=73,76
prop den=den2 b=bm2 s=sm2 fric=phi2 di=dil2 coh=cohin2 i=31,72 j=73,76
m null reg 12,74
solve srat=0.01
supsolve1 ; define modulus for surcharge

m m i=12,72 j=77,80
prop den=den1 b=bm1 s=sm1 fric=phi1 di=dil1 coh=cohin1 i=12,30 j=77,80
prop den=den2 b=bm2 s=sm2 fric=phi2 di=dil2 coh=cohin2 i=31,72 j=77,80
m null reg 12,78
solve srat=0.01
supsolve1 ; define modulus for surcharge

m m i=12,72 j=81,84
prop den=den1 b=bm1 s=sm1 fric=phi1 di=dil1 coh=cohin1 i=12,30 j=81,84
prop den=den2 b=bm2 s=sm2 fric=phi2 di=dil2 coh=cohin2 i=31,72 j=81,84
m null reg 12,82
solve
supsolve1
sav D160179-f.sav
```

```
*******************************************************************************
*; Store matric suctions (grid & zone)
*******************************************************************************

model null i 1 72 j 1 10
model null i 10 14 j 11 84

;call fish to extrappolates zone-based field to gridpoints
call extrap.fis
set gp_avg=1 ; simple average=1 least square=0
extrap_to_gp

def setup
   a_size = 5000
   IO_READ    = 0
   IO_WRITE = 1
   IO_FISH    = 0
   IO_ASCII = 1
end
setup

def io
array pp_zone(a_size)
status = open('160179ppzone.dat', IO_WRITE, IO_FISH)
ibuf=0
loop i (15,72)
loop j (11,84)
pp_zone(ibuf+1)    = ex_1(i,j)
ibuf=ibuf+1
end_loop
end_loop
status = write(pp_zone,5000)
status = close
end
;
io

def io
array pp_grid(a_size)
status = open('160179gpp.dat', IO_WRITE, IO_FISH)
ibuf=0
loop i (15,73)
loop j (11,85)
pp_grid(ibuf+1)    = ex_2(i,j)
ibuf=ibuf+1
end_loop
end_loop
status = write(pp_grid,5000)
status = close
end
;
io
sav D160179-s.sav
```

APPENDIX D: FLAC CODE
(Transient seepage analysis)

```
********************************************************************************
* FLOW ANALYSIS - UNSATURATED SOIL
********************************************************************************

config tpflow ex 2
grid 72,84
gen -4.5,-5.4 -4.5,0.0 -0.3,0.0 -0.3,-5.4 ratio 0.8,0.8 i 1 10 j 1 11
gen -4.5,0.0 -4.5,7.4 0.625,7.4 -0.3,0.0 ratio 0.8,1.0 i 1 10 j 11 85
gen -0.3,-5.4 -0.3,0.0 0.0,0.0 0.0,-5.4 ratio 1.0,0.8 i 10 11 j 1 11
gen -0.3,0.0 0.625,7.4 0.925,7.4 0.0,0.0 i 10 11 j 11 85
gen 0.0,-5.4 0.0,0.0 5.2,0.0 5.2,-5.4 ratio 1.0,0.8 i 11 63 j 1 11
gen 0.0,0.0 0.925,7.4 6.125,7.4 5.2,0.0 i 11 63 j 11 85
gen 5.2,-5.4 5.2,0.0 10.0,0.0 10.0,-5.4 ratio 1.2,0.8 i 63 73 j 1 11
gen 5.2,0.0 6.125,7.4 10.0,7.4 10.0,0.0 ratio 1.2,1.0 i 63 73 j 11 85
m m i=1,72 j=1,10 ;foundation
m null i=11 ;interface
m null i=1,9 j=11,84 ;front of the wall
m e i=10 j=11,84 ;blocks
m m i=12,72 j=11,64 ;backfill soil
m m i=12,72 j=65,84 ;surcharge
ini x add -0.1 i 12 85
mark i=1
mark i=84
mark j=1
mark j=11
mark i=12
mark i=12,73 j=85
m null i=10 j=11,84
table 1 0.675,5.4 6.875,7.4
gen table 1
m null reg 13,83
m null reg 5,5
m null reg 15,5
m null i=12,14 j=11,85;stone colume
********************************************************************************

********************************************************************************
* Input parameters (Sat.Perm and van Genuchten parameters)
********************************************************************************
def perm_setup ;parameters for permeability
;1.6m backfill zone behind the wall
;dry density = Soil 1 ;H- 1.79-4.7
     va_1          = 0.231
     p0_1          = 42.2
     rs_1          = 0.0
     poros_1       = 0.39
     wperm_1   = 7.91e-8

;backfill zone after 1.6m
;dry density = Soil 2 ;M- 1.60-4.7
     va_2          = 0.275
     p0_2          = 44.2
     rs_2          = 0.02
```

```
    poros_2       = 0.32
    wperm_2   = 3.69e-9
end
******************************************************************************
perm_setup

ini wperm=wperm_1 por=poros_1 udcoe 0 visrat 1 i=15,30 j=11,84
ini vga=va_1 vgpcw=0.5 vgpcnw=0.5 vgp0=p0_1 rsat=rs_1 i=15,30 j=11,84
ini wperm=wperm_2 por=poros_2 udcoe 0 visrat 1 i=31,72 j=11,84
ini vga=va_2 vgpcw=0.5 vgpcnw=0.5 vgp0=p0_2 rsat=rs_2 i=31,72 j=11,84
water den 1.0 nwden 0
ini fmod 1e4 f2mod 0.1

******************************************************************************
def setup
   a_size = 5000
   IO_READ    = 0
   IO_WRITE = 1
   IO_FISH    = 0
   IO_ASCII = 1
end
setup

def ini_gpp
array bb(a_size)
status = open('160179gpp.dat', IO_READ, IO_FISH)
status = read(bb, 5000)
status = close
ibuf=0
loop i (15,73)
loop j (11,85)
ex_2(i,j)=bb(ibuf+1);****************
ibuf=ibuf+1
end_loop
end_loop
end
ini_gpp
******************************************************************************

******************************************************************************
* Asign initial matric suction
******************************************************************************

def ini_pps ; Soil 1 <---1.5m
   n = 1.0/(1.0-va_1)
   loop jj (11,85)
   loop ii (15,30)
      pc=ex_2(ii,jj)
         ;if pc<0 then
               ;sat(ii,jj)=1.0
         ;else
               se = ((pc/p0_1)^n + 1.0)^(-va_1)
               sw = se * (1.0 - rs_1) + rs_1
```

```
                gpp(ii,jj)=-pc
                sat(ii,jj)=sw
            ;endif
    end_loop
    end_loop
end
ini_pps

def ini_pps1 ; Soil 2 1.5m ---->
    n = 1.0/(1.0-va_2)
    loop jj (11,85)
    loop ii (31,73)
        pc=ex_2(ii,jj)
            ;if pc<0 then
                ;sat(ii,jj)=1.0
            ;else
                se = ((pc/p0_2)^n + 1.0)^(-va_2)
                sw = se * (1.0 - rs_2) + rs_2
                gpp(ii,jj)=-pc
                sat(ii,jj) = sw
            ;endif
    end_loop
    end_loop
end
ini_pps1
*******************************************************************************

set grav=9.81
set step 1000000
set mech off flow on
ini nwpp 0 ;atmosphereic presuure
fix nwpp

;Boundary condition
fix seepage i=15 j=11,85
fix seepage i=72,73 j=11,85
fix seepage i=15,73 j=11
save R160179_i.sav

ini udcoe 0
*******************************************************************************
* Water Infiltration
*******************************************************************************
def infiltration
command
initial pp 0.0 i 15 16 j 66
initial sat 1.0 i 15 16 j 66
fix pp i 15 16 j 66
fix sat i 15 16 j 66
initial pp 0.0 i 16 j 66 67
initial sat 1.0 i 16 j 66 67
fix pp i 16 j 66 67
fix sat i 16 j 66 67
```

```
end_command

loop n (1,16)
x0=x1
x2=x0+3
x1=x2
y0=y1
y2=y0+1
y1=y2
command
initial pp 0.0 i x0 x2 j y0
initial sat 1.0 i x0 x2 j y0
fix pp i x0 x2 j y0
fix sat i x0 x2 j y0
initial pp 0.0 i x2 j y0 y2
initial sat 1.0 i x2 j y0 y2
fix pp i x2 j y0 y2
fix sat i x2 j y0 y2
end_command
end_loop

command
initial pp 0.0 i 64 65 j 83
initial sat 1.0 i 64 65 j 83
fix pp i 64 65 j 83
fix sat i 64 65 j 83
initial pp 0.0 i 65 j 83 84
initial sat 1.0 i 65 j 83 84
fix pp i 65 j 83 84
fix sat i 65 j 83 84
initial pp 0.0 i 65 67 j 84
initial sat 1.0 i 65 67 j 84
fix pp i 65 67 j 84
fix sat i 65 67 j 84
initial pp 0.0 i 67 j 84 85
initial sat 1.0 i 67 j 84 85
fix pp i 67 j 84 85
fix sat i 67 j 84 85
end_command

command
initial pp 0.0 i 67 73 j 85
initial sat 1.0 i 67 73 j 85
fix pp i 67 73 j 85
fix sat i 67 73 j 85
end_command
end
*****************************************************************************

*****************************************************************************
* DAY 3
*****************************************************************************
```

```
set x1=16 y1=67
infiltration
m n i 72 ; to solve zone variable problem

set gwtime 0
solve age 259200

def pp_adjust
command
m e i 72 j 11 84
end_command
loop j (11,85)
gpp(73,j)=gpp(72,j)
sat(73,j)=sat(72,j)
end_loop
end
pp_adjust

def io
array ppzone1(a_size)
status = open('160179ppzone_d3.dat', IO_WRITE, IO_FISH)
ibuf=0
loop i (15,72)
loop j (11,84)
avgpp=-((gpp(i,j)+gpp(i+1,j)+gpp(i,j+1)+gpp(i+1,j+1))/4)
ppzone1(ibuf+1)    =avgpp
ibuf=ibuf+1
end_loop
end_loop
status = write(ppzone1,5000)
status = close
end
;
io
save R160179_d3.sav
m n i 72
********************************************************************************
* DAY 6
********************************************************************************
solve age 518400
pp_adjust
def io
array ppzone3(a_size)
status = open('160179ppzone_d6.dat', IO_WRITE, IO_FISH)
ibuf=0
loop i (15,72)
loop j (11,84)
avgpp=-((gpp(i,j)+gpp(i+1,j)+gpp(i,j+1)+gpp(i+1,j+1))/4)
ppzone3(ibuf+1)    =avgpp
ibuf=ibuf+1
end_loop
end_loop
status = write(ppzone3,5000)
```

```
status = close
end
;
io
save R160179_d6.sav
m n i 72
********************************************************************************
* DAY 9
********************************************************************************
solve age 777600
pp_adjust
def io
array ppzone5(a_size)
status = open('160179ppzone_d9.dat', IO_WRITE, IO_FISH)
ibuf=0
loop i (15,72)
loop j (11,84)
avgpp=-((gpp(i,j)+gpp(i+1,j)+gpp(i,j+1)+gpp(i+1,j+1))/4)
ppzone5(ibuf+1)    =avgpp
ibuf=ibuf+1
end_loop
end_loop
status = write(ppzone5,5000)
status = close
end
;
io
save R160179_d9.sav
m n i 72
********************************************************************************
* DAY 12
********************************************************************************
solve age 1036800
pp_adjust
def io
array ppzone7(a_size)
status = open('160179ppzone_d12.dat', IO_WRITE, IO_FISH)
ibuf=0
loop i (15,72)
loop j (11,84)
avgpp=-((gpp(i,j)+gpp(i+1,j)+gpp(i,j+1)+gpp(i+1,j+1))/4)
ppzone7(ibuf+1)    =avgpp
ibuf=ibuf+1
end_loop
end_loop
status = write(ppzone7,5000)
status = close
end
;
io
save R160179_d12.sav
*************************************************************************
```

APPENDIX E: FLAC CODE
(Simulation for shear-induced deformation due to wetting)

```
;Shear-induced deformation due to water infiltraion.

res D160179-f.sav

;---- reset displacement to zero----
ini xv 0 yv 0 xd 0 yd 0

set step 1000000
********************************************************************************
* DAY 3
********************************************************************************
def setup
   a_size = 5000
   IO_READ    = 0
   IO_WRITE = 1
   IO_FISH    = 0
   IO_ASCII = 1
   filename = '160179ppzone_d3.dat'
end
setup

; assign the matric suction distrubution from transient seepage analysis
def mid_ppzone
array arain(a_size)
;***** Choose the file corresponding to the desired rainy days!!!
status = open(filename, IO_READ, IO_FISH)
status = read(arain, 5000)
status = close
ibuf=0
loop i (15,72)
loop j (11,84)
ex_3(i,j)=arain(ibuf+1);****************
ibuf=ibuf+1
end_loop
end_loop
end
mid_ppzone

; Update the shear strength based on new matric suction
def update_den_coh
       loop j (11,hh)
            loop i (15,72)

               if i<=30 then
                 Gs=Gs01
                 pd=pd01
                 n=n01
                 e=e01
                 nu=nu1
                 ms_ascomp=ms_ascomp1
                 Bavg=Bavg1                  ; Hilf's secant pore pressure parameter
                 cohsat=cohsat1
                 phi=phi1
```

```
        airentry=airentry1
        fa=fa1
        fn=fn1
        fm=fm1
        fhr=fhr1
        fk=fk1
        Sr=Sr1
       else
        Gs=Gs02
        pd=pd02
        n=n02
        e=e02
        nu=nu2
        ms_ascomp=ms_ascomp2
        Bavg=Bavg2            ; Hilf's secant pore pressure parameter
        cohsat=cohsat2
        phi=phi2
        airentry=airentry2
        fa=fa2
        fn=fn2
        fm=fm2
        fhr=fhr2
        fk=fk2
        Sr=Sr2
       endif

        if ex_3(i,j)<=0 then
          command
            prop coh cohsat i=i j=j
          end_command
        else

wsat=e/Gs ; ( Wsat = e / Gs) ; water content at saturation
Cf=1-(ln(1+ex_3(i,j)/fhr))/(ln(1+(1000000/fhr)))
theta=Cf*(n)/(ln(2.718+(ex_3(i,j)/fa)^fn))^fm     ; volumetric water content
S=Cf/(ln(2.718+(ex_3(i,j)/fa)^fn))^fm             ; degree of saturation
w=Cf*(wsat)/(ln(2.718+(ex_3(i,j)/fa)^fn))^fm      ; gravimetric water content

CASEOF shear_est_method
CASE 1     ;update cohesion based on change in matric suction- Vanapalli et al.'s 1st App
totalcoh=cohsat+ex_3(i,j)*(theta/n)^fk*tan(phi*degrad)
CASE 2     ;update cohesion based on change in matric suction- Vanapalli et al.'s 2nd App
totalcoh=cohsat+ex_3(i,j)*((S-Sr)/(1-Sr))*tan(phi*degrad)
CASE 3     ;update cohesion based on change in matric suction-Khalili and Khabaz
totalcoh=cohsat+ex_3(i,j)*(ex_3(i,j)/airentry)^(-0.55)*tan(phi*degrad)
ENDCASE

pt=pd*(1+w) ; increase density due to water infiltration

                         if ex_3(i,j)<=ex_1(i,j)
                            command
                           prop den pt i=i j=j
                            end_command
```

```
                                        end_if

                    command
                       prop coh totalcoh i=i j=j
                    end_command
                end_if
            end_loop
        end_loop
end
update_den_coh

set hh=64 ; (define the region for gravel column-- divided by 0)
def supstep2
        Hyperbolic
        update_rein
        command
           step 200
        end_command
end
def supsolve2
        loop kk(1,100)
        supstep2
        end_loop
end
supsolve2

solve
sav 160179pla_d3.sav


********************************************************************************
* DAY 6
********************************************************************************
def setup
   filename = '160179ppzone_d6.dat'
end
setup

mid_ppzone
update_den_coh
supsolve2
solve
sav 160179pla_d6.sav

********************************************************************************
* DAY 9
********************************************************************************
def setup
   filename = '160179ppzone_d9.dat'
end
setup

mid_ppzone
```

```
update_den_coh
supsolve2
solve
sav 160179pla_d9.sav

******************************************************************************
* DAY 12
******************************************************************************
def setup
   filename = '160179ppzone_d12.dat'
end
setup

mid_ppzone
update_den_coh
supsolve2
solve
sav 160179pla_d12.sav
```

APPENDIX F: FLAC CODE
(Simulation for volumetric strain due to wetting)

```
; Voluemtric deformation due to water infiltraion.

res D160179-f.sav
set step 1000000

; Increase coshesion and tenstion not to cause plastic strain.
Prop coh=100000 t=100000 i=15,72 j=11,84

;---- reset displacement to zero----
ini xv 0 yv 0 xd 0 yd 0

def setup
   a_size = 5000
   IO_READ    = 0
   IO_WRITE = 1
   IO_FISH    = 0
   IO_ASCII = 1
end
setup

; assign the intitial matric suction distrubution computed from construction stage
def ini_ppzone
array aa(a_size)
status = open('160179ppzone.dat', IO_READ, IO_FISH)
status = read(aa, 5000)
status = close
ibuf=0
loop i (15,72)
loop j (11,84)
ex_1(i,j)=aa(ibuf+1);****************
ibuf=ibuf+1
end_loop
end_loop
end
ini_ppzone

; assign the matric suction distrubution from transient seepage analysis
def mid_ppzone
array arain(a_size)
status = open('160179ppzone_d12.dat', IO_READ, IO_FISH)
status = read(arain, 5000)
status = close
ibuf=0
loop i (15,72)
loop j (11,84)
ex_3(i,j)=arain(ibuf+1);****************
ibuf=ibuf+1
end_loop
end_loop
end
mid_ppzone
;-------------------------------------------------------------
```

```
def makesize
p_size=2 ; 2 properites sets
end
makesize
def setup
p_a=1.01325E2
array v_a1(p_size)
array v_a3(p_size)
array v_c1(p_size)
array v_c3(p_size)
array e_m1(p_size)
array e_m3(p_size)
; swelling laws parameter sets;
;vertical direction: v_a1, v_c1
;hor. Plane; v_a3,v_c3
;properties: set 1 (soil 1-log law; 179179)
v_a1(1)=15.28
v_c1(1)=-3.85e-2
e_m1(1)=0.00053
v_a3(1)=1.0
v_c3(1)=0.0
e_m3(1)=0.0
;properties: set 2 (soil 2-dummy, not used)
v_a1(2)=9.96
v_c1(2)=-3.35e-2
e_m1(2)=0.004
v_a3(2)=1.0
v_c3(2)=0.0
e_m3(2)=0.0
end
setup
;------------------------------------------------------------
; call file containing fish function to model swelling
ca swellpa.fis
; specify the swelling law in grid variable ex_1:
;1 is for log
;2 is for linear
ini ex_4 1 i=15,72 j=11,84
;specify the property set number in grid extra variable ex_2;
ini ex_5 1 i=15,30 j=11,84
ini ex_5 2 i=31,72 j=11,84
set v_step=100
set hh=64 ;(define the region for gravel column-- divided by 0)
v_str_inc

def swell
loop ii(1,v_step)
app_str_inc
Hyperbolic
update_rein
command
cyc 1000
end_command
```

```
endloop
end

swell
solve
sav 160179ela_d12.sav
ret
sweallpa.fis

Set echo off
def v_str_inc
; -------basic checking---------
if v_step<=0 then
v_step=1
endif
;-----store stress increments due to swelling-------
loop i (15,72)
loop j (11,84)
;------ skip zones with null model
if model (i,j)#1 then
; ---- tension cut-off----
sigv=-syy(i,j)
if sigv<=0.0 then
sigv=0.0
endif
; ------- retrieve model number (default is 1)----
modnum=int(ex_4(i,j))
if modnum=0 then
modnum=1
endif
;;-------retrieve property set number--
prodnum=int(ex_5(i,j))

;-----determine PCP(percent collapse potential)-------
if i<30
        Cf1=1-(ln(1+ex_1(i,j)/fhr1))/(ln(1+(1000000/fhr1)))
        theta1=Cf1*(n01)/(ln(2.718+(ex_1(i,j)/fa1)^fn1))^fm1
        Cf2=1-(ln(1+ex_3(i,j)/fhr1))/(ln(1+(1000000/fhr1)))
        theta2=Cf2*(n01)/(ln(2.718+(ex_3(i,j)/fa1)^fn1))^fm1
        PCP=(n01-theta2)/(n01-theta1)
    if PCP<=0.0 then
    PCP=0.0
    endif
    if PCP>=1.0 then
    PCP=1
    endif
    PCP=1-PCP
    ex_11(i,j)=PCP
else
        Cf1=1-(ln(1+ex_1(i,j)/fhr2))/(ln(1+(1000000/fhr2)))
        theta1=Cf1*(n02)/(ln(2.718+(ex_1(i,j)/fa2)^fn2))^fm2
        Cf2=1-(ln(1+ex_3(i,j)/fhr2))/(ln(1+(1000000/fhr2)))
        theta2=Cf2*(n02)/(ln(2.718+(ex_3(i,j)/fa2)^fn2))^fm2
```

```
        PCF=(n02-theta2)/(n02-theta1)
        if PCP<=0.0 then
        PCP=0.0
        endif
        if PCP>=1.0 then
        PCP=1.0
        endif
        PCP=1-PCP
        ex_11(i,j)=PCP
endif

if PCP<0.01
command
fix y i=i j=j
fix x i=i j=j
end_command

if i =72
command
fix y i=73 j=j
end_command
endif
endif

;
;------swelling law
caseof modnum
default: no swelling stresses
vdex=0.0
vdez=0.0
vdey=0.0
case 1              ;log law
if sigv=0.0 then    ; get max swell, as defined
vdex=e_m3(prodnum)
vdez=e_m3(prodnum)
vdey=e_m1(prodnum)
else
val3=v_a3(prodnum)
val1=v_a1(prodnum)
;--- if a3 or a1 is negative, it is taken as 1 ---
if val1<=0.0 then
val1=1.0
endif
if val3<=0.0 then
val3=1.0
endif
vdex=v_c3(prodnum)*log((sigv/p_a)*val3)
vdex=vdex*PCP
vdez=vdex
vdey=v_c1(prodnum)*log((sigv/p_a)*val1)
vdey=vdey*PCP
endif
;ensure that swell is not greater rhan max possible value
```

```
if vdex>e_m3(prodnum) then
vdex=e_m3(prodnum)
endif
if vdez>e_m3(prodnum) then
vdez=e_m3(prodnum)
endif
if vdey>e_m1(prodnum) then
vdey=e_m1(prodnum)
endif
case 2 ;             linear law
vdex=(sigv/p_a)
vdex=v_c3(prodnum)-vdex*v_a3(prodnum)
vdez=vdex
vdey=(sigv/p_a)
vdey=v_c1(prodnum)-vdey*v_a1(prodnum)
endcase

;----save swelling stress increments-----
al1=bulk_mod(i,j)+shear_mod(i,j)*4.0/3.0
al2=bulk_mod(i,j)-shear_mod(i,j)*2.0/3.0
ds=float(v_step)
ex_6(i,j)=-(al1*vdex+al2*(vdey+vdez))/ds;dsxx
ex_7(i,j)=-(al1*vdey+al2*(vdex+vdez))/ds;dsyy
ex_8(i,j)=-(al1*vdez+al2*(vdex+vdey))/ds;dszz
;------save swelling strains----
ex_9(i,j)=vdey
ex_10(i,j)=vdex
endif
endloop
endloop
end
;----------------
;app_str_inc
;apply one swelling stress increment above wetting front input:
; -----------------
def app_str_inc
loop i (15,72)
loop j (11,84)
;apply swelling stress increments to zones above wetting front
sxx(i,j)=sxx(i,j)+ex_6(i,j)
syy(i,j)=syy(i,j)+ex_7(i,j)
szz(i,j)=szz(i,j)+ex_8(i,j)
endloop
endloop
end
set echo on
```

APPENDIX G: FLAC CODE
(Reinforcement strain)

```
; --- Save cable axial forces in table ---
res 160179ela_d12.sav
ca str.fin
def tabforce
     i1 = 0               ; Table 1:    Reinforcement 1
     i2 = 0               ; Table 2:    Reinforcement 2
     i3 = 0               ; Table 3:    Reinforcement 3
     i4 = 0               ; Table 4:    Reinforcement 4
     i5 = 0               ; Table 5:    Reinforcement 5
     i6 = 0               ; Table 6:    Reinforcement 6
     i7 = 0               ; Table 7:    Reinforcement 7
     i8 = 0               ; Table 8:    Reinforcement 8
     i9 = 0               ; Table 9:    Reinforcement 9
     i10 = 0              ; Table 10: Reinforcement 10
     i11 = 0              ; Table 11: Reinforcement 11
     nin = imem(str_pnt + $ksels)        ;
     loop while nin # 0
if imem(nin+$kelcod) = 2 then
       if imem(nin+$keltyp) = 2 then    ;
          i1 = i1+1
          p1 = imem(nin + $keln1)
          p2 = imem(nin + $keln2)
          xe = (fmem(p2+$kndx)+fmem(p1+$kndx))*0.5
          ye = (fmem(p2+$kndy)+fmem(p1+$kndy))*0.5
          xtable(1,i1) = xe
          ytable(1,i1) = -fmem(nin+$keleax)
       endif
       if imem(nin+$keltyp) = 1 then
          p1 = imem(nin + $keln1)
          p2 = imem(nin + $keln2)
          xe = (fmem(p2+$kndx)+fmem(p1+$kndx))*0.5
          ye = (fmem(p2+$kndy)+fmem(p1+$kndy))*0.5
          if ye <= 0.21
          i1 = i1+1
          xtable(1,i1) = xe
          ytable(1,i1) = -fmem(nin+$keleax)
          endif
       endif
;**************************************************
       if imem(nin+$keltyp) = 3 then    ;
          i2 = i2+1
          p1 = imem(nin + $keln1)
          p2 = imem(nin + $keln2)
          xe = (fmem(p2+$kndx)+fmem(p1+$kndx))*0.5
          ye = (fmem(p2+$kndy)+fmem(p1+$kndy))*0.5
          xtable(2,i2) = xe
          ytable(2,i2) = -fmem(nin+$keleax)
       endif
       if imem(nin+$keltyp) = 1 then
          p1 = imem(nin + $keln1)
          p2 = imem(nin + $keln2)
          xe = (fmem(p2+$kndx)+fmem(p1+$kndx))*0.5
          ye = (fmem(p2+$kndy)+fmem(p1+$kndy))*0.5
```

```
      if ye > 0.21 then
      if ye <= 0.41 then
      i2 = i2+1
      xtable(2,i2) = xe
      ytable(2,i2) = -fmem(nin+$keleax)
      endif
      endif
    endif
;****************************************************
    if imem(nin+$keltyp) = 4 then    ;
      i3 = i3+1
      p1 = imem(nin + $keln1)
      p2 = imem(nin + $keln2)
      xe = (fmem(p2+$kndx)+fmem(p1+$kndx))*0.5
      ye = (fmem(p2+$kndy)+fmem(p1+$kndy))*0.5
      xtable(3,i3) = xe
      ytable(3,i3) = -fmem(nin+$keleax)
    endif
    if imem(nin+$keltyp) = 1 then
      p1 = imem(nin + $keln1)
      p2 = imem(nin + $keln2)
      xe = (fmem(p2+$kndx)+fmem(p1+$kndx))*0.5
      ye = (fmem(p2+$kndy)+fmem(p1+$kndy))*0.5
      if ye > 0.41 then
      if ye <= 0.81 then
      i3 = i3+1
      xtable(3,i3) = xe
      ytable(3,i3) = -fmem(nin+$keleax)
      endif
      endif
    endif
;****************************************************
    if imem(nin+$keltyp) = 5 then    ;
      i4 = i4+1
      p1 = imem(nin + $keln1)
      p2 = imem(nin + $keln2)
      xe = (fmem(p2+$kndx)+fmem(p1+$kndx))*0.5
      ye = (fmem(p2+$kndy)+fmem(p1+$kndy))*0.5
      xtable(4,i4) = xe
      ytable(4,i4) = -fmem(nin+$keleax)
    endif
    if imem(nin+$keltyp) = 1 then
      p1 = imem(nin + $keln1)
      p2 = imem(nin + $keln2)
      xe = (fmem(p2+$kndx)+fmem(p1+$kndx))*0.5
      ye = (fmem(p2+$kndy)+fmem(p1+$kndy))*0.5
      if ye > 0.81 then
      if ye <= 1.21 then
      i4 = i4+1
      xtable(4,i4) = xe
      ytable(4,i4) = -fmem(nin+$keleax)
      endif
      endif
```

```
    endif
;**************************************************
    if imem(nin+$keltyp) = 6 then    ;
      i5 = i5+1
      p1 = imem(nin + $keln1)
      p2 = imem(nin + $keln2)
      xe = (fmem(p2+$kndx)+fmem(p1+$kndx))*0.5
      ye = (fmem(p2+$kndy)+fmem(p1+$kndy))*0.5
      xtable(5,i5) = xe
      ytable(5,i5) = -fmem(nin+$keleax)
    endif
    if imem(nin+$keltyp) = 1 then
      p1 = imem(nin + $keln1)
      p2 = imem(nin + $keln2)
      xe = (fmem(p2+$kndx)+fmem(p1+$kndx))*0.5
      ye = (fmem(p2+$kndy)+fmem(p1+$kndy))*0.5
      if ye > 1.21 then
      if ye <= 1.61 then
      i5 = i5+1
      xtable(5,i5) = xe
      ytable(5,i5) = -fmem(nin+$keleax)
      endif
      endif
    endif
;**************************************************
    if imem(nin+$keltyp) = 7 then    ;
      i6 = i6+1
      p1 = imem(nin + $keln1)
      p2 = imem(nin + $keln2)
      xe = (fmem(p2+$kndx)+fmem(p1+$kndx))*0.5
      ye = (fmem(p2+$kndy)+fmem(p1+$kndy))*0.5
      xtable(6,i6) = xe
      ytable(6,i6) = -fmem(nin+$keleax)
    endif
    if imem(nin+$keltyp) = 1 then
      p1 = imem(nin + $keln1)
      p2 = imem(nin + $keln2)
      xe = (fmem(p2+$kndx)+fmem(p1+$kndx))*0.5
      ye = (fmem(p2+$kndy)+fmem(p1+$kndy))*0.5
      if ye > 1.61 then
      if ye <= 2.01 then
      i6 = i6+1
      xtable(6,i6) = xe
      ytable(6,i6) = -fmem(nin+$keleax)
      endif
      endif
    endif
;**************************************************
    if imem(nin+$keltyp) = 8 then    ;
      i7 = i7+1
      p1 = imem(nin + $keln1)
      p2 = imem(nin + $keln2)
      xe = (fmem(p2+$kndx)+fmem(p1+$kndx))*0.5
```

```
        ye = (fmem(p2+$kndy)+fmem(p1+$kndy))*0.5
        xtable(7,i7) = xe
        ytable(7,i7) = -fmem(nin+$keleax)
      endif
      if imem(nin+$keltyp) = 1 then
        p1 = imem(nin + $keln1)
        p2 = imem(nin + $keln2)
        xe = (fmem(p2+$kndx)+fmem(p1+$kndx))*0.5
        ye = (fmem(p2+$kndy)+fmem(p1+$kndy))*0.5
        if ye > 2.01 then
        if ye <= 2.41 then
        i7 = i7+1
        xtable(7,i7) = xe
        ytable(7,i7) = -fmem(nin+$keleax)
        endif
        endif
      endif
;***************************************************
      if imem(nin+$keltyp) = 9 then    ;
        i8 = i8+1
        p1 = imem(nin + $keln1)
        p2 = imem(nin + $keln2)
        xe = (fmem(p2+$kndx)+fmem(p1+$kndx))*0.5
        ye = (fmem(p2+$kndy)+fmem(p1+$kndy))*0.5
        xtable(8,i8) = xe
        ytable(8,i8) = -fmem(nin+$keleax)
      endif
      if imem(nin+$keltyp) = 1 then
        p1 = imem(nin + $keln1)
        p2 = imem(nin + $keln2)
        xe = (fmem(p2+$kndx)+fmem(p1+$kndx))*0.5
        ye = (fmem(p2+$kndy)+fmem(p1+$kndy))*0.5
        if ye > 2.41 then
        if ye <= 3.01 then
        i8 = i8+1
        xtable(8,i8) = xe
        ytable(8,i8) = -fmem(nin+$keleax)
        endif
        endif
      endif
;***************************************************
      if imem(nin+$keltyp) = 10 then    ;
        i9 = i9+1
        p1 = imem(nin + $keln1)
        p2 = imem(nin + $keln2)
        xe = (fmem(p2+$kndx)+fmem(p1+$kndx))*0.5
        ye = (fmem(p2+$kndy)+fmem(p1+$kndy))*0.5
        xtable(9,i9) = xe
        ytable(9,i9) = -fmem(nin+$keleax)
      endif
      if imem(nin+$keltyp) = 1 then
        p1 = imem(nin + $keln1)
        p2 = imem(nin + $keln2)
```

```
            xe = (fmem(p2+$kndx)+fmem(p1+$kndx))*0.5
            ye = (fmem(p2+$kndy)+fmem(p1+$kndy))*0.5
            if ye > 3.01 then
            if ye <= 3.61 then
            i9 = i9+1
            xtable(9,i9) = xe
            ytable(9,i9) = -fmem(nin+$keleax)
            endif
            endif
        endif
;**************************************************
        if imem(nin+$keltyp) = 11 then    ;
            i10 = i10+1
            p1 = imem(nin + $keln1)
            p2 = imem(nin + $keln2)
            xe = (fmem(p2+$kndx)+fmem(p1+$kndx))*0.5
            ye = (fmem(p2+$kndy)+fmem(p1+$kndy))*0.5
            xtable(10,i10) = xe
            ytable(10,i10) = -fmem(nin+$keleax)
        endif
        if imem(nin+$keltyp) = 1 then
            p1 = imem(nin + $keln1)
            p2 = imem(nin + $keln2)
            xe = (fmem(p2+$kndx)+fmem(p1+$kndx))*0.5
            ye = (fmem(p2+$kndy)+fmem(p1+$kndy))*0.5
            if ye > 3.61 then
            if ye <= 4.21 then
            i10 = i10+1
            xtable(10,i10) = xe
            ytable(10,i10) = -fmem(nin+$keleax)
            endif
            endif
        endif
;**************************************************
        if imem(nin+$keltyp) = 12 then    ;
            i11 = i11+1
            p1 = imem(nin + $keln1)
            p2 = imem(nin + $keln2)
            xe = (fmem(p2+$kndx)+fmem(p1+$kndx))*0.5
            ye = (fmem(p2+$kndy)+fmem(p1+$kndy))*0.5
            xtable(11,i11) = xe
            ytable(11,i11) = -fmem(nin+$keleax)
        endif
        if imem(nin+$keltyp) = 1 then
            p1 = imem(nin + $keln1)
            p2 = imem(nin + $keln2)
            xe = (fmem(p2+$kndx)+fmem(p1+$kndx))*0.5
            ye = (fmem(p2+$kndy)+fmem(p1+$kndy))*0.5
            if ye > 4.21 then
            if ye <= 4.81 then
            i11 = i11+1
            xtable(11,i11) = xe
            ytable(11,i11) = -fmem(nin+$keleax)
```

```
          endif
          endif
       endif
;****************************************************
endif
       nin = imem(nin)
     end_loop
end
tabforce
ret
→
```

APPENDIX H: FLAC RESULTS –Case 2
(Vertical and lateral displacements at grids after the 12-day rainfall)

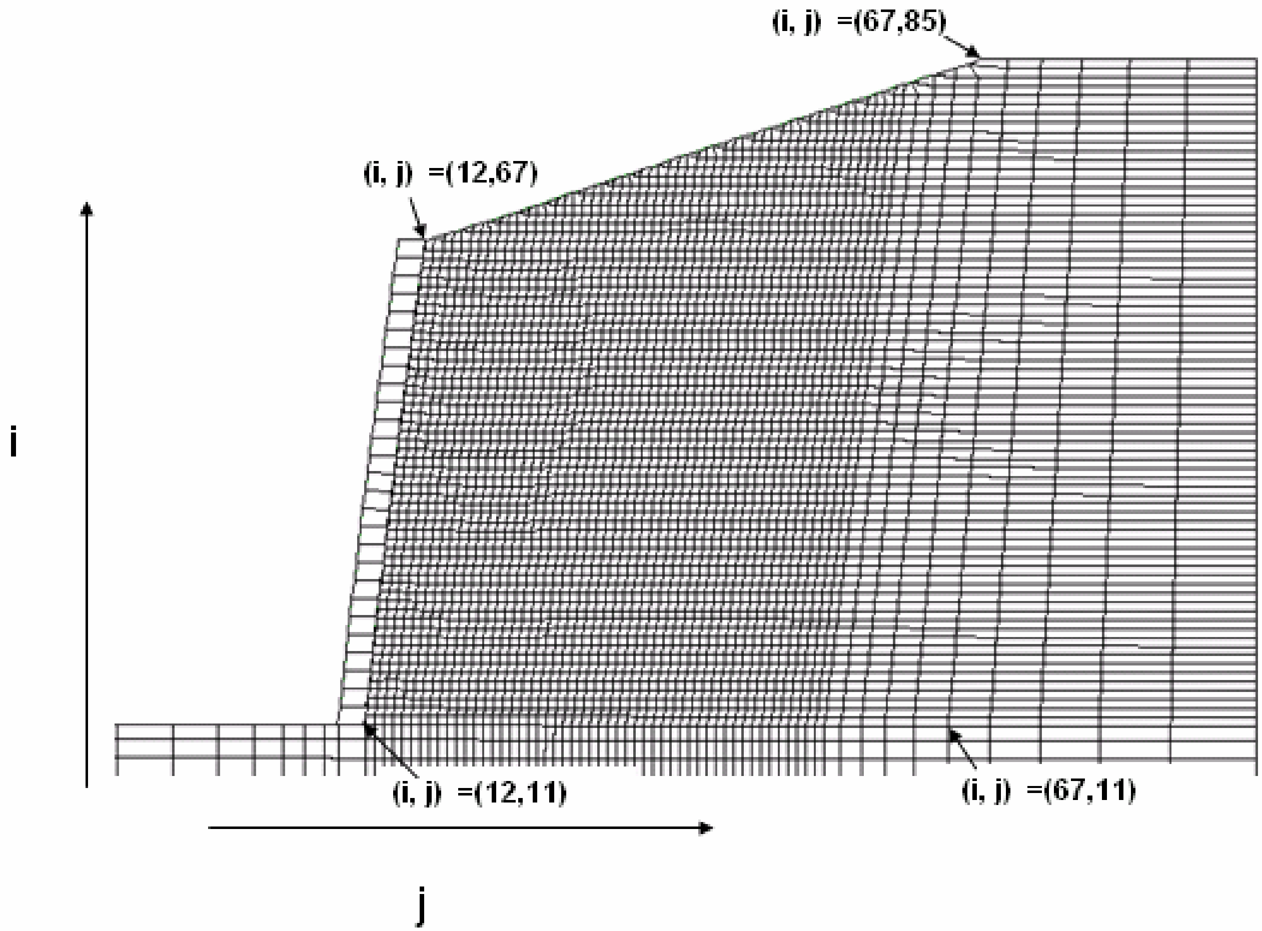

Grid number information

FLAC results: Shear-induced deformation (vertical disp.) for Case 2- day 12

(mm)

I	12	13	14	15	16	17	18	19	20	21	22	23	24	25	26	27	28	29	30	31	32	33	34	...
J																								...
73																							-3.5	...
72																				-3.9	-3.8	-3.7	-3.6	...
71																	-21.9	-21.6	-25.0	-3.9	-3.8	-3.7	-3.6	...
70														-19.5	-20.1	-20.9	-21.3	-22.1	-22.5	-3.9	-3.8	-3.7	-3.6	...
69											-18.0	-18.3	-18.8	-19.0	-19.6	-20.1	-20.9	-21.6	-22.2	-3.9	-3.8	-3.7	-3.6	...
68								-18.3	-18.4	-18.7	-18.4	-18.3	-18.4	-18.6	-19.1	-19.9	-20.6	-21.2	-21.4	-3.9	-3.8	-3.7	-3.6	...
67					-18.3	-18.6	-18.8	-18.7	-18.5	-18.3	-18.2	-18.2	-18.2	-18.4	-18.8	-19.4	-20.1	-20.5	-20.3	-3.8	-3.8	-3.7	-3.6	...
66		-5.6	-5.5	-5.4	-18.4	-18.8	-18.5	-18.3	-18.2	-18.2	-18.1	-18.1	-18.2	-18.2	-18.5	-18.9	-19.4	-19.6	-19.1	-3.8	-3.8	-3.7	-3.6	...
65	-5.7	-5.7	-5.5	-5.4	-18.6	-18.4	-18.3	-18.1	-18.0	-18.0	-18.0	-18.0	-18.0	-18.1	-18.1	-18.3	-18.5	-18.5	-17.9	-3.9	-3.8	-3.7	-3.6	...
64	-5.6	-5.7	-5.5	-5.4	-17.8	-18.0	-17.9	-17.9	-17.8	-17.9	-17.9	-17.9	-17.9	-17.9	-17.8	-17.6	-17.6	-17.5	-16.5	-3.9	-3.8	-3.7	-3.6	...
63	-5.5	-5.6	-5.5	-5.5	-16.9	-17.4	-17.5	-17.6	-17.6	-17.7	-17.7	-17.7	-17.7	-17.6	-17.3	-17.0	-16.6	-16.2	-15.2	-3.9	-3.8	-3.7	-3.6	...
62	-5.6	-5.6	-5.5	-5.4	-16.0	-16.8	-17.2	-17.3	-17.4	-17.5	-17.5	-17.4	-17.3	-17.2	-16.9	-16.4	-15.7	-15.0	-13.8	-4.0	-3.9	-3.7	-3.5	...
61	-5.6	-5.5	-5.4	-5.4	-15.1	-16.2	-16.7	-17.0	-17.1	-17.1	-17.1	-17.0	-16.8	-16.6	-16.3	-15.8	-15.0	-13.9	-12.5	-4.0	-3.9	-3.7	-3.5	...
60	-5.5	-5.4	-5.3	-5.3	-14.2	-15.6	-16.3	-16.5	-16.6	-16.6	-16.6	-16.4	-16.2	-16.0	-15.6	-15.2	-14.5	-13.3	-11.2	-4.0	-3.9	-3.6	-3.5	...
59	-5.4	-5.3	-5.3	-5.3	-13.5	-15.0	-15.6	-15.9	-16.0	-16.0	-16.0	-15.8	-15.6	-15.3	-14.9	-14.4	-13.7	-12.7	-10.3	-4.1	-3.6	-3.5	-3.4	...
58	-5.4	-5.3	-5.2	-5.2	-13.1	-14.1	-14.9	-15.2	-15.4	-15.4	-15.3	-15.1	-14.9	-14.5	-14.1	-13.6	-12.9	-11.8	-10.6	-4.0	-3.5	-3.4	-3.3	...
57	-5.3	-5.2	-5.2	-5.1	-12.2	-13.4	-14.1	-14.5	-14.7	-14.7	-14.6	-14.4	-14.1	-13.8	-13.3	-12.8	-12.0	-11.1	-10.2	-3.9	-3.5	-3.4	-3.3	...
56	-5.2	-5.1	-5.1	-5.0	-11.3	-12.7	-13.4	-13.8	-14.0	-14.0	-13.9	-13.7	-13.4	-13.1	-12.7	-12.0	-11.3	-10.5	-9.4	-3.8	-3.5	-3.3	-3.2	...
55	-5.1	-5.1	-4.9	-4.9	-10.3	-11.9	-12.6	-13.1	-13.3	-13.3	-13.2	-12.9	-12.6	-12.3	-11.9	-11.3	-10.6	-9.8	-8.6	-3.7	-3.5	-3.3	-3.2	...
54	-5.0	-4.9	-4.8	-4.8	-9.4	-11.0	-11.9	-12.3	-12.5	-12.6	-12.5	-12.2	-11.9	-11.5	-11.1	-10.7	-10.1	-9.2	-7.7	-3.6	-3.4	-3.2	-3.1	...
53	-4.9	-4.8	-4.8	-4.7	-8.5	-10.3	-11.1	-11.6	-11.8	-11.9	-11.8	-11.5	-11.2	-10.8	-10.4	-9.9	-9.4	-8.6	-6.9	-3.4	-3.2	-3.1	-3.0	...
52	-4.9	-4.7	-4.7	-4.6	-7.7	-9.3	-10.2	-10.7	-10.9	-11.0	-10.9	-10.7	-10.3	-10.0	-9.6	-9.2	-8.7	-7.9	-6.8	-3.4	-3.0	-3.0	-2.9	...
51	-4.6	-4.6	-4.6	-4.5	-6.9	-8.4	-9.4	-9.9	-10.2	-10.2	-10.1	-9.9	-9.6	-9.3	-8.9	-8.5	-8.0	-7.3	-6.2	-3.2	-3.0	-2.9	-2.9	...
50	-4.5	-4.5	-4.4	-4.4	-6.2	-7.7	-8.6	-9.2	-9.4	-9.4	-9.4	-9.2	-9.0	-8.7	-8.3	-7.9	-7.4	-6.7	-5.6	-3.0	-2.9	-2.9	-2.8	...
49	-4.2	-4.4	-4.2	-4.3	-5.7	-7.0	-7.8	-8.3	-8.5	-8.6	-8.6	-8.5	-8.3	-8.1	-7.8	-7.3	-6.8	-6.0	-5.0	-2.9	-2.8	-2.8	-2.7	...
48	-4.1	-4.2	-4.2	-4.1	-5.3	-6.3	-7.0	-7.4	-7.7	-7.8	-7.9	-7.9	-7.7	-7.5	-7.2	-6.8	-6.2	-5.5	-4.4	-2.7	-2.6	-2.7	-2.7	...
47	-3.9	-4.0	-4.1	-4.1	-4.8	-5.6	-6.2	-6.6	-7.0	-7.2	-7.2	-7.2	-7.2	-7.0	-6.7	-6.3	-5.7	-5.0	-3.9	-2.6	-2.5	-2.6	-2.6	...
46	-3.8	-3.7	-4.0	-4.0	-4.4	-5.0	-5.5	-5.9	-6.3	-6.5	-6.6	-6.6	-6.6	-6.4	-6.1	-5.8	-5.3	-4.6	-3.7	-2.5	-2.5	-2.5	-2.5	...
45	-3.7	-3.5	-3.7	-3.9	-4.0	-4.5	-5.0	-5.4	-5.7	-5.9	-6.0	-6.1	-6.0	-5.9	-5.7	-5.3	-4.9	-4.2	-3.5	-2.5	-2.4	-2.4	-2.4	...
44	-3.7	-3.3	-3.4	-3.7	-3.9	-4.2	-4.6	-5.0	-5.3	-5.5	-5.6	-5.7	-5.6	-5.5	-5.3	-5.0	-4.5	-4.0	-3.3	-2.5	-2.4	-2.3	-2.3	...
43	-3.6	-3.2	-3.1	-3.5	-3.7	-4.0	-4.3	-4.6	-4.9	-5.1	-5.2	-5.2	-5.2	-5.1	-4.9	-4.6	-4.2	-3.7	-3.1	-2.5	-2.3	-2.3	-2.2	...
42	-3.3	-3.1	-2.9	-3.2	-3.5	-3.8	-4.1	-4.3	-4.5	-4.7	-4.8	-4.8	-4.8	-4.7	-4.5	-4.3	-3.9	-3.5	-3.0	-2.4	-2.3	-2.2	-2.1	...
41	-3.0	-2.9	-2.8	-3.0	-3.3	-3.6	-3.8	-4.0	-4.2	-4.4	-4.5	-4.5	-4.5	-4.4	-4.2	-4.0	-3.7	-3.3	-2.8	-2.3	-2.2	-2.1	-2.0	...
40	-2.9	-2.7	-2.7	-2.9	-3.1	-3.4	-3.6	-3.8	-3.9	-4.0	-4.1	-4.1	-4.1	-4.0	-3.9	-3.7	-3.4	-3.1	-2.7	-2.2	-2.1	-2.0	-2.0	...
39	-2.8	-2.6	-2.5	-2.7	-2.9	-3.2	-3.3	-3.5	-3.6	-3.7	-3.8	-3.8	-3.8	-3.7	-3.6	-3.4	-3.2	-2.9	-2.5	-2.1	-2.0	-2.0	-1.9	...
38	-2.7	-2.5	-2.4	-2.6	-2.8	-3.0	-3.1	-3.3	-3.4	-3.5	-3.5	-3.5	-3.5	-3.4	-3.3	-3.2	-2.9	-2.7	-2.4	-2.0	-2.0	-1.9	-1.8	...
37	-2.5	-2.4	-2.3	-2.4	-2.6	-2.8	-2.9	-3.0	-3.1	-3.2	-3.2	-3.2	-3.2	-3.2	-3.1	-2.9	-2.7	-2.5	-2.2	-1.9	-1.9	-1.8	-1.7	...
36	-2.3	-2.3	-2.2	-2.3	-2.5	-2.6	-2.8	-2.8	-2.9	-3.0	-3.0	-3.0	-3.0	-2.9	-2.8	-2.7	-2.5	-2.3	-2.1	-1.8	-1.8	-1.7	-1.7	...
35	-2.1	-2.1	-2.1	-2.2	-2.4	-2.5	-2.6	-2.7	-2.7	-2.8	-2.8	-2.8	-2.8	-2.7	-2.6	-2.5	-2.4	-2.2	-2.0	-1.7	-1.7	-1.6	-1.6	...
34	-2.0	-2.0	-2.0	-2.1	-2.2	-2.3	-2.4	-2.5	-2.5	-2.5	-2.6	-2.6	-2.5	-2.5	-2.4	-2.3	-2.2	-2.0	-1.9	-1.7	-1.6	-1.6	-1.5	...
33	-1.9	-1.9	-1.9	-2.0	-2.1	-2.2	-2.2	-2.3	-2.3	-2.4	-2.4	-2.4	-2.3	-2.3	-2.2	-2.1	-2.0	-1.9	-1.7	-1.6	-1.5	-1.5	-1.4	...
32	-1.8	-1.8	-1.8	-1.9	-2.0	-2.0	-2.1	-2.1	-2.2	-2.2	-2.2	-2.2	-2.2	-2.1	-2.1	-2.0	-1.9	-1.8	-1.6	-1.5	-1.4	-1.4	-1.4	...
31	-1.7	-1.7	-1.7	-1.8	-1.8	-1.9	-1.9	-2.0	-2.0	-2.0	-2.0	-2.0	-2.0	-2.0	-1.9	-1.8	-1.8	-1.7	-1.5	-1.4	-1.4	-1.3	-1.3	...
30	-1.6	-1.6	-1.6	-1.7	-1.7	-1.8	-1.8	-1.8	-1.9	-1.9	-1.9	-1.9	-1.8	-1.8	-1.8	-1.7	-1.6	-1.5	-1.4	-1.3	-1.3	-1.3	-1.2	...
29	-1.6	-1.5	-1.5	-1.6	-1.6	-1.6	-1.7	-1.7	-1.7	-1.7	-1.7	-1.7	-1.7	-1.7	-1.6	-1.6	-1.5	-1.4	-1.3	-1.2	-1.2	-1.2	-1.2	...
28	-1.5	-1.4	-1.4	-1.4	-1.5	-1.5	-1.6	-1.6	-1.6	-1.6	-1.6	-1.6	-1.6	-1.5	-1.5	-1.5	-1.4	-1.3	-1.3	-1.2	-1.2	-1.1	-1.1	...
27	-1.4	-1.3	-1.3	-1.3	-1.4	-1.4	-1.4	-1.5	-1.5	-1.5	-1.5	-1.5	-1.4	-1.4	-1.4	-1.3	-1.3	-1.2	-1.2	-1.1	-1.1	-1.1	-1.0	...
26	-1.3	-1.2	-1.2	-1.3	-1.3	-1.3	-1.3	-1.4	-1.4	-1.4	-1.4	-1.3	-1.3	-1.3	-1.3	-1.2	-1.2	-1.2	-1.1	-1.0	-1.0	-1.0	-1.0	...
25	-1.2	-1.2	-1.1	-1.2	-1.2	-1.2	-1.2	-1.2	-1.3	-1.3	-1.2	-1.2	-1.2	-1.2	-1.2	-1.1	-1.1	-1.1	-1.0	-1.0	-1.0	-0.9	-0.9	...
24	-1.1	-1.1	-1.0	-1.1	-1.1	-1.1	-1.1	-1.1	-1.2	-1.2	-1.1	-1.1	-1.1	-1.1	-1.1	-1.1	-1.0	-1.0	-1.0	-0.9	-0.9	-0.9	-0.9	...
23	-1.1	-1.0	-1.0	-1.0	-1.0	-1.0	-1.0	-1.1	-1.1	-1.1	-1.1	-1.0	-1.0	-1.0	-1.0	-1.0	-0.9	-0.9	-0.9	-0.8	-0.8	-0.8	-0.8	...
22	-1.0	-0.9	-0.9	-0.9	-0.9	-0.9	-1.0	-1.0	-1.0	-1.0	-1.0	-1.0	-0.9	-0.9	-0.9	-0.9	-0.9	-0.8	-0.8	-0.8	-0.8	-0.8	-0.7	...
21	-0.9	-0.9	-0.8	-0.8	-0.8	-0.9	-0.9	-0.9	-0.9	-0.9	-0.9	-0.9	-0.9	-0.8	-0.8	-0.8	-0.8	-0.8	-0.8	-0.7	-0.7	-0.7	-0.7	...
20	-0.8	-0.8	-0.7	-0.7	-0.8	-0.8	-0.8	-0.8	-0.8	-0.8	-0.8	-0.8	-0.8	-0.8	-0.8	-0.7	-0.7	-0.7	-0.7	-0.7	-0.7	-0.7	-0.6	...
19	-0.8	-0.7	-0.7	-0.7	-0.7	-0.7	-0.7	-0.7	-0.7	-0.7	-0.7	-0.7	-0.7	-0.7	-0.7	-0.7	-0.7	-0.7	-0.6	-0.6	-0.6	-0.6	-0.6	...
18	-0.7	-0.6	-0.6	-0.6	-0.6	-0.6	-0.6	-0.6	-0.6	-0.6	-0.6	-0.6	-0.6	-0.6	-0.6	-0.6	-0.6	-0.6	-0.6	-0.6	-0.6	-0.6	-0.6	...
17	-0.6	-0.6	-0.5	-0.5	-0.5	-0.6	-0.6	-0.6	-0.6	-0.6	-0.6	-0.6	-0.6	-0.6	-0.6	-0.5	-0.5	-0.5	-0.5	-0.5	-0.5	-0.5	-0.5	...
16	-0.5	-0.5	-0.5	-0.4	-0.5	-0.5	-0.5	-0.5	-0.5	-0.5	-0.5	-0.5	-0.5	-0.5	-0.5	-0.5	-0.5	-0.5	-0.5	-0.5	-0.5	-0.5	-0.5	...
15	-0.5	-0.4	-0.4	-0.4	-0.4	-0.4	-0.5	-0.5	-0.5	-0.4	-0.4	-0.4	-0.4	-0.4	-0.4	-0.4	-0.4	-0.4	-0.4	-0.4	-0.4	-0.4	-0.4	...
14	-0.4	-0.4	-0.4	-0.3	-0.4	-0.4	-0.4	-0.4	-0.4	-0.4	-0.4	-0.4	-0.4	-0.4	-0.4	-0.4	-0.4	-0.4	-0.4	-0.4	-0.4	-0.4	-0.4	...
13	-0.3	-0.3	-0.3	-0.3	-0.3	-0.3	-0.3	-0.3	-0.3	-0.3	-0.3	-0.3	-0.3	-0.3	-0.3	-0.3	-0.3	-0.3	-0.3	-0.4	-0.3	-0.3	-0.3	...
12	-0.3	-0.3	-0.3	-0.3	-0.3	-0.3	-0.3	-0.3	-0.3	-0.3	-0.3	-0.3	-0.3	-0.3	-0.3	-0.3	-0.3	-0.3	-0.3	-0.3	-0.3	-0.3	-0.3	...
11	-0.2	-0.3	-0.2	-0.2	-0.2	-0.2	-0.2	-0.2	-0.2	-0.2	-0.2	-0.2	-0.2	-0.2	-0.2	-0.2	-0.2	-0.2	-0.2	-0.3	-0.3	-0.3	-0.3	...
...	...	...	...	...	...	...	...	...	...	...	...	...	...	...	...	...	...	...	...	...	...	...	...	...

FLAC results: Shear-induced deformation (lateral disp.) for Case 2- day 12

(mm)

I	12	13	14	15	16	17	18	19	20	21	22	23	24	25	26	27	28	29	30	31	32	33	34	...
J																								...
73																							-1.5	...
72																				-1.6	-1.6	-1.6	-1.5	...
71																	-8.5	-8.5	-5.8	-1.6	-1.5	-1.5	-1.4	...
70														-10.1	-9.9	-9.1	-8.2	-7.7	-7.6	-1.4	-1.4	-1.4	-1.4	...
69											-11.6	-12.1	-11.6	-10.6	-9.3	-8.7	-8.4	-8.0	-7.5	-1.3	-1.3	-1.3	-1.3	...
68								-12.1	-12.7	-12.2	-11.4	-10.4	-10.0	-9.8	-9.5	-9.2	-8.8	-8.3	-7.3	-1.2	-1.2	-1.2	-1.2	...
67					-12.0	-12.3	-12.3	-11.8	-10.9	-10.4	-10.2	-10.1	-10.1	-10.0	-9.9	-9.5	-9.0	-8.3	-7.0	-1.2	-1.2	-1.2	-1.1	...
66		-13.6	-13.6	-13.7	-11.4	-11.6	-11.3	-10.9	-10.5	-10.3	-10.2	-10.2	-10.2	-10.2	-10.1	-9.7	-9.1	-8.1	-6.7	-1.1	-1.1	-1.1	-1.1	...
65	-13.9	-13.6	-13.5	-13.5	-12.1	-11.5	-11.0	-10.6	-10.3	-10.2	-10.1	-10.1	-10.2	-10.2	-10.1	-9.7	-8.9	-7.7	-6.1	-1.0	-1.0	-1.0	-1.0	...
64	-13.7	-13.3	-13.3	-13.3	-12.2	-11.3	-10.7	-10.4	-10.2	-10.1	-10.1	-10.1	-10.1	-10.0	-9.9	-9.4	-8.6	-7.3	-5.7	-0.9	-1.0	-1.0	-1.0	...
63	-13.4	-13.2	-13.2	-13.0	-11.8	-11.0	-10.4	-10.2	-10.1	-10.1	-10.0	-9.9	-9.8	-9.6	-9.3	-8.9	-8.1	-6.9	-5.1	-0.9	-0.9	-0.9	-0.9	...
62	-13.2	-13.1	-13.0	-12.8	-11.7	-10.8	-10.3	-10.2	-10.1	-10.0	-9.8	-9.6	-9.4	-9.0	-8.6	-8.2	-7.6	-6.5	-4.7	-0.8	-0.9	-0.9	-0.9	...
61	-12.9	-12.9	-12.7	-12.5	-11.4	-10.7	-10.3	-10.1	-9.9	-9.7	-9.4	-9.1	-8.7	-8.3	-7.8	-7.2	-6.7	-6.0	-4.4	-0.9	-0.8	-0.8	-0.8	...
60	-12.8	-12.6	-12.5	-12.4	-11.3	-10.8	-10.5	-10.1	-9.7	-9.3	-9.0	-8.5	-8.1	-7.5	-6.9	-6.3	-5.6	-5.1	-4.1	-1.2	-0.9	-0.8	-0.7	...
59	-12.4	-12.4	-12.3	-12.1	-11.7	-11.1	-10.5	-9.9	-9.4	-8.9	-8.4	-7.9	-7.4	-6.8	-6.1	-5.4	-4.6	-3.7	-2.8	-1.8	-1.1	-0.8	-0.7	...
58	-12.3	-12.2	-12.1	-11.9	-10.9	-10.3	-9.7	-9.1	-8.7	-8.3	-7.9	-7.4	-6.9	-6.4	-5.9	-5.2	-4.5	-3.6	-3.0	-0.8	-0.6	-0.6	-0.6	...
57	-11.9	-11.9	-11.8	-11.4	-10.4	-9.7	-9.1	-8.6	-8.2	-7.8	-7.4	-6.9	-6.5	-6.0	-5.5	-4.9	-4.3	-3.5	-2.8	-0.5	-0.4	-0.4	-0.5	...
56	-11.7	-11.7	-11.4	-10.9	-9.9	-9.2	-8.7	-8.2	-7.8	-7.4	-7.0	-6.5	-6.0	-5.5	-5.0	-4.5	-4.0	-3.4	-2.7	-0.4	-0.3	-0.3	-0.4	...
55	-11.5	-11.3	-11.0	-10.6	-9.6	-8.9	-8.4	-7.9	-7.4	-7.0	-6.5	-6.1	-5.6	-5.1	-4.5	-4.0	-3.6	-3.3	-2.5	-0.5	-0.2	-0.2	-0.3	...
54	-11.3	-10.9	-10.6	-10.3	-9.5	-8.7	-8.2	-7.7	-7.1	-6.6	-6.1	-5.7	-5.2	-4.7	-4.1	-3.6	-3.2	-2.9	-2.3	-0.6	-0.2	-0.2	-0.2	...
53	-10.7	-10.5	-10.3	-10.1	-9.4	-8.7	-8.0	-7.4	-6.8	-6.2	-5.7	-5.2	-4.8	-4.3	-3.8	-3.3	-2.8	-2.2	-1.6	-0.8	-0.4	-0.3	-0.2	...
52	-10.4	-10.0	-9.8	-9.4	-8.6	-7.7	-7.1	-6.5	-6.1	-5.6	-5.1	-4.7	-4.3	-3.9	-3.6	-3.2	-2.8	-2.3	-1.7	-0.4	-0.2	-0.2	-0.2	...
51	-9.8	-9.6	-9.3	-8.7	-7.9	-7.1	-6.5	-6.1	-5.6	-5.1	-4.6	-4.2	-3.8	-3.6	-3.4	-3.1	-2.7	-2.3	-1.6	-0.3	-0.1	-0.1	-0.2	...
50	-9.5	-9.2	-8.7	-8.0	-7.4	-6.9	-6.3	-5.8	-5.2	-4.6	-4.1	-3.8	-3.5	-3.3	-3.1	-2.9	-2.6	-2.2	-1.5	-0.4	-0.1	-0.2	-0.2	...
49	-8.9	-8.7	-8.2	-7.6	-7.2	-6.7	-6.1	-5.4	-4.7	-4.2	-3.8	-3.4	-3.2	-3.0	-2.8	-2.6	-2.4	-2.0	-1.5	-0.5	-0.2	-0.2	-0.3	...
48	-8.9	-8.3	-7.8	-7.3	-7.0	-6.4	-5.6	-4.9	-4.3	-3.9	-3.5	-3.2	-3.0	-2.7	-2.6	-2.4	-2.1	-1.8	-1.4	-0.7	-0.4	-0.4	-0.3	...
47	-8.4	-7.9	-7.4	-7.0	-6.4	-5.8	-5.1	-4.6	-4.1	-3.7	-3.3	-3.0	-2.8	-2.6	-2.3	-2.1	-1.8	-1.5	-1.2	-0.8	-0.6	-0.5	-0.5	...
46	-7.8	-7.4	-6.8	-5.9	-5.3	-4.7	-4.2	-3.8	-3.5	-3.3	-3.0	-2.8	-2.6	-2.3	-2.1	-1.9	-1.7	-1.5	-1.2	-0.7	-0.6	-0.6	-0.6	...
45	-7.1	-6.8	-6.0	-4.8	-4.4	-4.0	-3.8	-3.5	-3.3	-3.1	-2.8	-2.6	-2.4	-2.2	-2.0	-1.8	-1.6	-1.4	-1.1	-0.8	-0.7	-0.7	-0.6	...
44	-6.5	-6.2	-5.4	-4.2	-4.0	-3.9	-3.7	-3.4	-3.2	-3.0	-2.8	-2.5	-2.3	-2.1	-1.9	-1.6	-1.4	-1.2	-1.0	-0.8	-0.7	-0.7	-0.6	...
43	-5.9	-5.6	-4.9	-3.9	-3.8	-3.7	-3.5	-3.3	-3.1	-2.9	-2.7	-2.4	-2.2	-2.0	-1.8	-1.6	-1.3	-1.1	-0.9	-0.8	-0.7	-0.7	-0.7	...
42	-5.6	-5.1	-4.5	-3.8	-3.6	-3.5	-3.3	-3.2	-3.0	-2.8	-2.5	-2.3	-2.1	-1.9	-1.7	-1.5	-1.3	-1.1	-0.9	-0.8	-0.7	-0.7	-0.7	...
41	-5.2	-4.7	-4.3	-3.9	-3.5	-3.3	-3.1	-3.0	-2.8	-2.6	-2.4	-2.2	-2.0	-1.8	-1.6	-1.4	-1.3	-1.1	-0.9	-0.8	-0.7	-0.7	-0.6	...
40	-4.7	-4.3	-3.9	-3.2	-3.1	-3.0	-2.9	-2.8	-2.6	-2.5	-2.3	-2.1	-1.9	-1.7	-1.5	-1.4	-1.2	-1.0	-0.9	-0.8	-0.7	-0.7	-0.6	...
39	-4.2	-3.9	-3.5	-2.9	-2.8	-2.8	-2.7	-2.6	-2.5	-2.3	-2.2	-2.0	-1.8	-1.6	-1.5	-1.3	-1.1	-1.0	-0.8	-0.7	-0.7	-0.6	-0.6	...
38	-3.8	-3.5	-3.2	-2.7	-2.6	-2.6	-2.5	-2.4	-2.3	-2.2	-2.0	-1.9	-1.7	-1.6	-1.4	-1.2	-1.1	-0.9	-0.8	-0.7	-0.7	-0.6	-0.6	...
37	-3.4	-3.2	-2.9	-2.5	-2.5	-2.4	-2.4	-2.3	-2.2	-2.0	-1.9	-1.8	-1.6	-1.5	-1.3	-1.2	-1.0	-0.9	-0.8	-0.7	-0.6	-0.6	-0.6	...
36	-3.3	-3.0	-2.7	-2.5	-2.4	-2.3	-2.2	-2.1	-2.0	-1.9	-1.8	-1.7	-1.5	-1.4	-1.3	-1.1	-1.0	-0.9	-0.8	-0.7	-0.6	-0.6	-0.6	...
35	-3.1	-2.8	-2.6	-2.4	-2.3	-2.2	-2.1	-2.0	-1.9	-1.8	-1.7	-1.6	-1.4	-1.3	-1.2	-1.1	-1.0	-0.9	-0.7	-0.7	-0.6	-0.6	-0.5	...
34	-2.9	-2.7	-2.5	-2.1	-2.1	-2.0	-1.9	-1.9	-1.8	-1.7	-1.6	-1.5	-1.3	-1.2	-1.1	-1.0	-0.9	-0.8	-0.7	-0.6	-0.6	-0.6	-0.5	...
33	-2.7	-2.5	-2.3	-2.0	-1.9	-1.9	-1.8	-1.7	-1.7	-1.6	-1.5	-1.4	-1.3	-1.2	-1.1	-1.0	-0.9	-0.8	-0.7	-0.6	-0.6	-0.5	-0.5	...
32	-2.6	-2.4	-2.1	-1.9	-1.8	-1.8	-1.7	-1.6	-1.5	-1.5	-1.4	-1.3	-1.2	-1.1	-1.0	-0.9	-0.8	-0.7	-0.7	-0.6	-0.5	-0.5	-0.5	...
31	-2.4	-2.2	-2.0	-1.9	-1.7	-1.7	-1.6	-1.5	-1.4	-1.4	-1.3	-1.2	-1.1	-1.0	-0.9	-0.9	-0.8	-0.7	-0.6	-0.6	-0.5	-0.5	-0.5	...
30	-2.3	-2.1	-1.9	-1.6	-1.6	-1.5	-1.5	-1.4	-1.3	-1.3	-1.2	-1.1	-1.0	-1.0	-0.9	-0.8	-0.7	-0.7	-0.6	-0.5	-0.5	-0.5	-0.4	...
29	-2.1	-2.0	-1.8	-1.5	-1.5	-1.4	-1.4	-1.3	-1.3	-1.2	-1.1	-1.0	-1.0	-0.9	-0.8	-0.8	-0.7	-0.6	-0.6	-0.5	-0.5	-0.5	-0.4	...
28	-2.1	-1.9	-1.7	-1.4	-1.4	-1.3	-1.3	-1.2	-1.2	-1.1	-1.0	-1.0	-0.9	-0.8	-0.8	-0.7	-0.6	-0.6	-0.5	-0.5	-0.5	-0.4	-0.4	...
27	-1.9	-1.7	-1.6	-1.4	-1.3	-1.3	-1.2	-1.1	-1.1	-1.0	-1.0	-0.9	-0.8	-0.8	-0.7	-0.7	-0.6	-0.6	-0.5	-0.5	-0.4	-0.4	-0.4	...
26	-1.8	-1.6	-1.5	-1.2	-1.2	-1.1	-1.1	-1.0	-1.0	-0.9	-0.9	-0.8	-0.8	-0.7	-0.7	-0.6	-0.6	-0.5	-0.5	-0.4	-0.4	-0.4	-0.4	...
25	-1.6	-1.5	-1.3	-1.1	-1.1	-1.0	-1.0	-1.0	-0.9	-0.9	-0.8	-0.8	-0.7	-0.7	-0.6	-0.6	-0.5	-0.5	-0.4	-0.4	-0.4	-0.4	-0.3	...
24	-1.6	-1.4	-1.2	-1.0	-1.0	-1.0	-0.9	-0.9	-0.8	-0.8	-0.8	-0.7	-0.7	-0.6	-0.6	-0.5	-0.5	-0.5	-0.4	-0.4	-0.4	-0.3	-0.3	...
23	-1.4	-1.2	-1.1	-1.0	-0.9	-0.9	-0.9	-0.8	-0.8	-0.7	-0.7	-0.7	-0.6	-0.6	-0.5	-0.5	-0.5	-0.4	-0.4	-0.4	-0.3	-0.3	-0.3	...
22	-1.3	-1.1	-1.0	-0.8	-0.8	-0.8	-0.8	-0.7	-0.7	-0.7	-0.6	-0.6	-0.6	-0.5	-0.5	-0.5	-0.4	-0.4	-0.4	-0.3	-0.3	-0.3	-0.3	...
21	-1.2	-1.0	-0.9	-0.7	-0.7	-0.7	-0.7	-0.7	-0.6	-0.6	-0.6	-0.5	-0.5	-0.5	-0.4	-0.4	-0.4	-0.4	-0.3	-0.3	-0.3	-0.3	-0.3	...
20	-1.1	-0.9	-0.8	-0.7	-0.7	-0.6	-0.6	-0.6	-0.6	-0.5	-0.5	-0.5	-0.5	-0.4	-0.4	-0.4	-0.3	-0.3	-0.3	-0.3	-0.3	-0.3	-0.2	...
19	-0.9	-0.8	-0.7	-0.6	-0.6	-0.6	-0.6	-0.5	-0.5	-0.5	-0.5	-0.4	-0.4	-0.4	-0.4	-0.3	-0.3	-0.3	-0.3	-0.3	-0.2	-0.2	-0.2	...
18	-0.9	-0.7	-0.7	-0.5	-0.5	-0.5	-0.5	-0.5	-0.4	-0.4	-0.4	-0.4	-0.4	-0.3	-0.3	-0.3	-0.3	-0.3	-0.3	-0.2	-0.2	-0.2	-0.2	...
17	-0.7	-0.7	-0.6	-0.4	-0.4	-0.4	-0.4	-0.4	-0.4	-0.4	-0.4	-0.3	-0.3	-0.3	-0.3	-0.3	-0.3	-0.2	-0.2	-0.2	-0.2	-0.2	-0.2	...
16	-0.7	-0.5	-0.5	-0.4	-0.4	-0.4	-0.4	-0.3	-0.3	-0.3	-0.3	-0.3	-0.3	-0.3	-0.2	-0.2	-0.2	-0.2	-0.2	-0.2	-0.2	-0.2	-0.2	...
15	-0.5	-0.4	-0.4	-0.3	-0.3	-0.3	-0.3	-0.3	-0.3	-0.3	-0.3	-0.2	-0.2	-0.2	-0.2	-0.2	-0.2	-0.2	-0.2	-0.2	-0.2	-0.2	-0.1	...
14	-0.5	-0.4	-0.3	-0.2	-0.3	-0.3	-0.3	-0.2	-0.2	-0.2	-0.2	-0.2	-0.2	-0.2	-0.2	-0.2	-0.2	-0.2	-0.2	-0.2	-0.1	-0.1	-0.1	...
13	-0.3	-0.3	-0.2	-0.2	-0.2	-0.2	-0.2	-0.2	-0.2	-0.2	-0.2	-0.2	-0.2	-0.1	-0.1	-0.1	-0.1	-0.1	-0.1	-0.1	-0.1	-0.1	-0.1	...
12	-0.3	-0.2	-0.2	-0.2	-0.2	-0.2	-0.1	-0.1	-0.1	-0.1	-0.1	-0.1	-0.1	-0.1	-0.1	-0.1	-0.1	-0.1	-0.1	-0.1	-0.1	-0.1	-0.1	...
11	-0.2	-0.1	-0.1	-0.1	-0.1	-0.1	-0.1	-0.1	-0.1	-0.1	-0.1	-0.1	-0.1	-0.1	-0.1	-0.1	-0.1	-0.1	-0.1	-0.1	-0.1	-0.1	-0.1	...
...	...	...	...	...	...	...	...	...	...	...	...	...	...	...	...	...	...	...	...	...	...	...	...	...

FLAC results: Volumetric deformation (vertical disp.) for Case 2- day 12

(mm)

I	12	13	14	15	16	17	18	19	20	21	22	23	24	25	26	27	28	29	30	31	32	33	34	...
J																								...
73																							-6.6	...
72																				-9.9	-9.1	-8.1	-7.3	...
71																	-14.5	-13.5	-12.2	-10.7	-9.5	-8.6	-7.7	...
70														-18.1	-17.4	-16.3	-15.4	-13.8	-12.4	-11.0	-10.1	-9.1	-8.2	...
69											-20.9	-20.4	-19.7	-19.0	-17.7	-16.6	-15.4	-14.1	-12.9	-11.6	-10.7	-9.8	-8.8	...
68								-22.1	-22.0	-21.7	-21.4	-20.7	-19.9	-19.0	-18.0	-16.9	-15.7	-14.4	-13.2	-12.2	-11.4	-10.4	-9.4	...
67					-21.6	-21.9	-22.1	-22.2	-22.2	-22.0	-21.6	-21.0	-20.2	-19.4	-18.4	-17.2	-16.0	-14.8	-13.6	-12.6	-11.8	-10.8	-9.7	...
66		-17.1	-18.0	-20.5	-21.4	-21.9	-22.2	-22.4	-22.4	-22.2	-21.8	-21.3	-20.6	-19.8	-18.8	-17.7	-16.5	-15.2	-13.9	-12.9	-12.0	-11.0	-9.8	...
65	-17.4	-16.8	-17.5	-21.0	-21.6	-22.0	-22.3	-22.5	-22.6	-22.5	-22.2	-21.7	-21.0	-20.2	-19.3	-18.1	-16.9	-15.6	-14.2	-12.9	-12.0	-10.9	-9.7	...
64	-16.4	-16.4	-17.1	-21.3	-21.5	-22.0	-22.4	-22.7	-22.8	-22.8	-22.5	-22.0	-21.3	-20.5	-19.4	-18.3	-17.0	-15.7	-14.3	-12.8	-11.8	-10.7	-9.4	...
63	-15.4	-15.9	-16.7	-21.2	-21.5	-22.0	-22.5	-22.9	-22.9	-22.8	-22.5	-22.0	-21.3	-20.4	-19.4	-18.3	-17.0	-15.6	-14.1	-12.6	-11.5	-10.3	-9.1	...
62	-14.5	-15.3	-16.2	-20.9	-21.4	-22.0	-22.4	-22.7	-22.7	-22.6	-22.3	-21.8	-21.1	-20.2	-19.2	-18.0	-16.7	-15.3	-13.8	-12.2	-11.1	-9.9	-8.6	...
61	-13.4	-14.7	-15.7	-20.2	-21.0	-21.7	-22.1	-22.3	-22.3	-22.2	-21.8	-21.3	-20.6	-19.8	-18.8	-17.6	-16.3	-14.9	-13.4	-11.8	-10.7	-9.5	-8.1	...
60	-12.6	-13.8	-15.3	-19.2	-20.5	-21.1	-21.5	-21.7	-21.7	-21.6	-21.2	-20.7	-20.1	-19.2	-18.2	-17.1	-15.8	-14.4	-12.9	-11.2	-10.1	-8.9	-7.6	...
59	-12.0	-13.2	-14.6	-18.6	-19.6	-20.2	-20.7	-20.9	-21.0	-20.8	-20.5	-20.1	-19.4	-18.6	-17.6	-16.5	-15.2	-13.8	-12.2	-10.5	-9.5	-8.3	-6.9	...
58	-11.4	-12.4	-13.9	-18.4	-18.6	-19.2	-19.7	-19.9	-20.0	-19.9	-19.6	-19.2	-18.6	-17.8	-16.8	-15.7	-14.5	-13.1	-11.6	-9.9	-8.8	-7.6	-6.4	...
57	-10.5	-11.7	-12.9	-17.2	-17.7	-18.2	-18.7	-18.9	-19.0	-18.9	-18.7	-18.2	-17.6	-16.9	-16.0	-14.9	-13.7	-12.3	-10.8	-9.2	-8.1	-7.0	-5.7	...
56	-9.8	-11.0	-12.1	-15.6	-16.7	-17.3	-17.7	-18.0	-18.0	-18.0	-17.7	-17.3	-16.7	-16.0	-15.1	-14.1	-12.9	-11.6	-10.1	-8.4	-7.4	-6.3	-5.1	...
55	-9.0	-10.2	-11.1	-14.1	-15.4	-16.2	-16.6	-16.9	-16.9	-16.9	-16.6	-16.2	-15.7	-15.0	-14.1	-13.1	-12.0	-10.7	-9.3	-7.7	-6.7	-5.6	-4.4	...
54	-8.3	-9.2	-10.4	-12.6	-14.3	-15.0	-15.5	-15.8	-15.8	-15.8	-15.5	-15.2	-14.6	-14.0	-13.2	-12.2	-11.1	-9.9	-8.5	-6.9	-6.0	-4.9	-3.7	...
53	-7.6	-8.5	-9.6	-11.7	-13.0	-13.8	-14.4	-14.7	-14.8	-14.7	-14.5	-14.1	-13.6	-13.0	-12.2	-11.3	-10.2	-9.0	-7.6	-6.2	-5.2	-4.1	-3.0	...
52	-6.7	-7.7	-8.9	-11.0	-11.6	-12.4	-13.0	-13.3	-13.4	-13.4	-13.2	-12.9	-12.4	-11.8	-11.1	-10.3	-9.3	-8.1	-6.9	-5.4	-4.5	-3.5	-2.4	...
51	-5.7	-6.9	-7.9	-9.9	-10.6	-11.2	-11.7	-12.0	-12.1	-12.1	-11.9	-11.7	-11.2	-10.7	-10.0	-9.2	-8.3	-7.2	-6.1	-4.7	-3.8	-2.8	-1.8	...
50	-4.9	-6.1	-7.1	-8.7	-9.6	-10.2	-10.6	-10.8	-10.9	-10.9	-10.8	-10.5	-10.1	-9.6	-9.0	-8.2	-7.4	-6.4	-5.3	-4.0	-3.1	-2.2	-1.3	...
49	-4.1	-5.2	-6.2	-7.7	-8.6	-9.1	-9.4	-9.6	-9.7	-9.6	-9.5	-9.2	-8.9	-8.4	-7.9	-7.2	-6.4	-5.5	-4.5	-3.3	-2.4	-1.6	-0.7	...
48	-3.4	-4.4	-5.5	-6.8	-7.6	-8.0	-8.2	-8.4	-8.5	-8.4	-8.3	-8.1	-7.7	-7.3	-6.8	-6.2	-5.4	-4.6	-3.7	-2.6	-1.9	-1.0	-0.3	...
47	-2.8	-3.7	-4.8	-6.1	-6.5	-6.8	-7.1	-7.2	-7.3	-7.2	-7.1	-6.9	-6.6	-6.3	-5.8	-5.2	-4.5	-3.7	-2.9	-1.9	-1.2	-0.4	0.1	...
46	-2.3	-3.0	-4.2	-5.5	-5.5	-5.6	-5.8	-5.9	-6.0	-5.9	-5.8	-5.7	-5.4	-5.1	-4.7	-4.2	-3.6	-2.9	-2.2	-1.3	-0.6	0.0	0.3	...
45	-1.9	-2.5	-3.4	-4.6	-4.5	-4.6	-4.6	-4.7	-4.7	-4.7	-4.6	-4.4	-4.2	-3.9	-3.6	-3.2	-2.7	-2.1	-1.4	-0.7	-0.1	0.4	0.5	...
44	-1.8	-2.0	-2.6	-3.7	-3.6	-3.6	-3.6	-3.6	-3.6	-3.5	-3.4	-3.3	-3.1	-2.8	-2.5	-2.2	-1.8	-1.3	-0.7	-0.1	0.4	0.7	0.5	...
43	-1.6	-1.6	-1.9	-2.8	-2.7	-2.6	-2.5	-2.5	-2.4	-2.3	-2.2	-2.1	-1.9	-1.7	-1.5	-1.2	-0.9	-0.5	-0.1	0.4	0.8	0.8	0.4	...
42	-1.3	-1.3	-1.4	-2.0	-1.9	-1.7	-1.5	-1.4	-1.3	-1.2	-1.1	-1.0	-0.9	-0.7	-0.5	-0.3	-0.1	0.2	0.5	0.9	1.0	0.8	0.0	...
41	-0.9	-1.0	-1.1	-1.5	-1.1	-0.8	-0.6	-0.5	-0.4	-0.3	-0.2	-0.1	0.0	0.2	0.3	0.5	0.6	0.8	1.0	1.1	1.1	0.6	0.0	...
40	-0.6	-0.7	-0.8	-1.1	-0.3	0.1	0.3	0.5	0.6	0.7	0.7	0.8	0.9	1.0	1.1	1.2	1.3	1.4	1.3	1.3	1.1	0.5	0.0	...
39	-0.5	-0.4	-0.5	-0.7	0.2	0.7	0.9	1.1	1.2	1.3	1.4	1.4	1.5	1.6	1.7	1.7	1.8	1.7	1.6	1.1	0.9	0.0	0.0	...
38	-0.3	-0.3	-0.2	-0.4	0.4	0.9	1.2	1.3	1.4	1.5	1.6	1.7	1.7	1.8	1.8	1.8	1.8	1.8	1.5	0.8	0.5	0.0	0.0	...
37	-0.2	-0.2	-0.1	-0.2	0.3	0.7	0.9	1.0	1.1	1.2	1.3	1.3	1.4	1.4	1.4	1.4	1.4	1.3	1.1	0.5	0.0	0.0	0.0	...
36	-0.1	-0.1	0.0	0.0	0.1	0.3	0.4	0.5	0.6	0.6	0.7	0.7	0.7	0.7	0.7	0.7	0.7	0.7	0.6	0.0	0.0	0.0	0.0	...
35	-0.1	-0.1	0.0	0.0	0.0	0.0	0.0	0.0	0.0	0.0	0.0	0.0	0.0	0.0	0.0	0.0	0.0	0.0	0.0	0.0	0.0	0.0	0.0	...
34	-0.1	-0.1	0.0	0.0	0.0	0.0	0.0	0.0	0.0	0.0	0.0	0.0	0.0	0.0	0.0	0.0	0.0	0.0	0.0	0.0	0.0	0.0	0.0	...
33	-0.1	-0.1	0.0	0.0	0.0	0.0	0.0	0.0	0.0	0.0	0.0	0.0	0.0	0.0	0.0	0.0	0.0	0.0	0.0	0.0	0.0	0.0	0.0	...
32	-0.1	-0.1	0.0	0.0	0.0	0.0	0.0	0.0	0.0	0.0	0.0	0.0	0.0	0.0	0.0	0.0	0.0	0.0	0.0	0.0	0.0	0.0	0.0	...
31	-0.1	0.0	0.0	0.0	0.0	0.0	0.0	0.0	0.0	0.0	0.0	0.0	0.0	0.0	0.0	0.0	0.0	0.0	0.0	0.0	0.0	0.0	0.0	...
30	0.0	0.0	0.0	0.0	0.0	0.0	0.0	0.0	0.0	0.0	0.0	0.0	0.0	0.0	0.0	0.0	0.0	0.0	0.0	0.0	0.0	0.0	0.0	...
29	0.0	0.0	0.0	0.0	0.0	0.0	0.0	0.0	0.0	0.0	0.0	0.0	0.0	0.0	0.0	0.0	0.0	0.0	0.0	0.0	0.0	0.0	0.0	...
28	0.0	0.0	0.0	0.0	0.0	0.0	0.0	0.0	0.0	0.0	0.0	0.0	0.0	0.0	0.0	0.0	0.0	0.0	0.0	0.0	0.0	0.0	0.0	...
27	0.0	0.0	0.0	0.0	0.0	0.0	0.0	0.0	0.0	0.0	0.0	0.0	0.0	0.0	0.0	0.0	0.0	0.0	0.0	0.0	0.0	0.0	0.0	...
26	0.0	0.0	0.0	0.0	0.0	0.0	0.0	0.0	0.0	0.0	0.0	0.0	0.0	0.0	0.0	0.0	0.0	0.0	0.0	0.0	0.0	0.0	0.0	...
25	0.0	0.0	0.0	0.0	0.0	0.0	0.0	0.0	0.0	0.0	0.0	0.0	0.0	0.0	0.0	0.0	0.0	0.0	0.0	0.0	0.0	0.0	0.0	...
24	0.0	0.0	0.0	0.0	0.0	0.0	0.0	0.0	0.0	0.0	0.0	0.0	0.0	0.0	0.0	0.0	0.0	0.0	0.0	0.0	0.0	0.0	0.0	...
23	0.0	0.0	0.0	0.0	0.0	0.0	0.0	0.0	0.0	0.0	0.0	0.0	0.0	0.0	0.0	0.0	0.0	0.0	0.0	0.0	0.0	0.0	0.0	...
22	0.0	0.0	0.0	0.0	0.0	0.0	0.0	0.0	0.0	0.0	0.0	0.0	0.0	0.0	0.0	0.0	0.0	0.0	0.0	0.0	0.0	0.0	0.0	...
21	0.0	0.0	0.0	0.0	0.0	0.0	0.0	0.0	0.0	0.0	0.0	0.0	0.0	0.0	0.0	0.0	0.0	0.0	0.0	0.0	0.0	0.0	0.0	...
20	0.0	0.0	0.0	0.0	0.0	0.0	0.0	0.0	0.0	0.0	0.0	0.0	0.0	0.0	0.0	0.0	0.0	0.0	0.0	0.0	0.0	0.0	0.0	...
19	0.0	0.0	0.0	0.0	0.0	0.0	0.0	0.0	0.0	0.0	0.0	0.0	0.0	0.0	0.0	0.0	0.0	0.0	0.0	0.0	0.0	0.0	0.0	...
18	0.0	0.0	0.0	0.0	0.0	0.0	0.0	0.0	0.0	0.0	0.0	0.0	0.0	0.0	0.0	0.0	0.0	0.0	0.0	0.0	0.0	0.0	0.0	...
17	0.0	0.0	0.0	0.0	0.0	0.0	0.0	0.0	0.0	0.0	0.0	0.0	0.0	0.0	0.0	0.0	0.0	0.0	0.0	0.0	0.0	0.0	0.0	...
16	0.0	0.0	0.0	0.0	0.0	0.0	0.0	0.0	0.0	0.0	0.0	0.0	0.0	0.0	0.0	0.0	0.0	0.0	0.0	0.0	0.0	0.0	0.0	...
15	0.0	0.0	0.0	0.0	0.0	0.0	0.0	0.0	0.0	0.0	0.0	0.0	0.0	0.0	0.0	0.0	0.0	0.0	0.0	0.0	0.0	0.0	0.0	...
14	-0.1	0.0	0.0	0.0	0.0	0.0	0.0	0.0	0.0	0.0	0.0	0.0	0.0	0.0	0.0	0.0	0.0	0.0	0.0	0.0	0.0	0.0	0.0	...
13	-0.1	-0.1	0.0	0.0	0.0	0.0	0.0	0.0	0.0	0.0	0.0	0.0	0.0	0.0	0.0	0.0	0.0	0.0	0.0	0.0	0.0	0.0	0.0	...
12	-0.1	-0.1	0.0	0.0	0.0	0.0	0.0	0.0	0.0	0.0	0.0	0.0	0.0	0.0	0.0	0.0	0.0	0.0	0.0	0.0	0.0	0.0	0.0	...
11	-0.1	-0.1	0.0	0.0	0.0	0.0	0.0	0.0	0.0	0.0	0.0	0.0	0.0	0.0	0.0	0.0	0.0	0.0	0.0	0.0	0.0	0.0	0.0	...
...	...	...	...	...	...	...	...	...	...	...	...	...	...	...	...	...	...	...	...	...	...	...	...	

FLAC results: Volumetric deformation (lateral disp.) for Case 2- day 12

(mm)

I	12	13	14	15	16	17	18	19	20	21	22	23	24	25	26	27	28	29	30	31	32	33	34	...
J																								...
73																							-6.2	...
72																				-6.4	-6.4	-6.3	-6.2	...
71																	-6.2	-6.3	-6.4	-6.3	-5.8	-5.7	-5.5	...
70														-5.1	-5.4	-5.8	-6.0	-5.5	-5.3	-5.2	-5.2	-5.1	-4.9	...
69											-3.0	-3.5	-4.1	-4.6	-4.5	-4.6	-4.6	-4.6	-4.5	-4.5	-4.5	-4.5	-4.4	...
68								-0.6	-1.1	-1.8	-2.4	-2.7	-3.1	-3.3	-3.6	-3.7	-3.8	-3.9	-3.9	-4.0	-4.0	-4.0	-4.0	...
67					1.5	1.1	0.5	0.0	-0.6	-1.1	-1.5	-1.9	-2.2	-2.5	-2.8	-3.0	-3.2	-3.3	-3.4	-3.4	-3.6	-3.6	-3.6	...
66		1.2	2.2	2.6	2.0	1.3	0.8	0.4	0.0	-0.5	-0.9	-1.2	-1.6	-1.9	-2.2	-2.4	-2.6	-2.8	-2.9	-2.9	-3.1	-3.1	-3.1	...
65	-1.3	0.6	1.2	1.8	1.7	1.5	1.1	0.8	0.4	0.0	-0.3	-0.7	-1.0	-1.3	-1.6	-1.8	-2.1	-2.2	-2.4	-2.4	-2.6	-2.6	-2.6	...
64	-1.2	0.2	0.9	2.0	1.8	1.7	1.4	1.1	0.7	0.4	0.1	-0.3	-0.6	-0.8	-1.1	-1.4	-1.6	-1.8	-1.9	-1.9	-2.1	-2.1	-2.2	...
63	-1.2	0.2	0.8	2.4	2.2	1.9	1.6	1.3	1.0	0.7	0.4	0.1	-0.1	-0.4	-0.6	-0.9	-1.1	-1.3	-1.4	-1.4	-1.6	-1.7	-1.7	...
62	-1.2	0.1	0.9	2.7	2.5	2.2	1.9	1.6	1.3	1.0	0.7	0.5	0.2	0.0	-0.2	-0.5	-0.6	-0.8	-0.9	-0.9	-1.1	-1.2	-1.3	...
61	-1.2	0.0	1.0	3.0	2.7	2.4	2.1	1.8	1.5	1.3	1.1	0.8	0.6	0.4	0.2	0.0	-0.2	-0.4	-0.5	-0.5	-0.7	-0.8	-0.9	...
60	-1.3	0.2	1.1	3.0	2.5	2.3	2.1	1.9	1.7	1.5	1.3	1.1	0.9	0.7	0.5	0.3	0.2	0.0	-0.1	-0.1	-0.3	-0.5	-0.6	...
59	-0.6	0.1	0.8	1.7	2.0	2.1	2.1	2.0	1.9	1.8	1.6	1.4	1.2	1.0	0.8	0.6	0.5	0.4	0.3	0.2	0.0	-0.2	-0.3	...
58	-1.4	-0.4	0.4	3.1	2.8	2.6	2.5	2.3	2.2	2.0	1.8	1.6	1.4	1.3	1.1	0.9	0.8	0.7	0.6	0.5	0.3	0.1	-0.1	...
57	-1.3	-0.5	0.6	3.7	3.5	3.1	2.9	2.6	2.4	2.2	2.0	1.8	1.7	1.5	1.3	1.2	1.0	0.9	0.8	0.8	0.5	0.3	0.1	...
56	-1.3	-0.5	1.0	4.1	3.8	3.4	3.1	2.8	2.6	2.4	2.2	2.0	1.8	1.7	1.5	1.4	1.2	1.1	1.0	1.0	0.7	0.4	0.2	...
55	-1.3	-0.3	1.5	4.0	3.7	3.4	3.1	2.8	2.6	2.5	2.3	2.1	2.0	1.8	1.7	1.6	1.4	1.3	1.2	1.1	0.8	0.5	0.3	...
54	-1.5	0.3	1.7	3.6	3.2	3.1	2.9	2.8	2.6	2.5	2.4	2.2	2.1	2.0	1.8	1.7	1.6	1.4	1.3	1.3	0.9	0.6	0.4	...
53	-0.3	0.5	1.4	2.3	2.6	2.7	2.7	2.7	2.6	2.5	2.4	2.3	2.2	2.0	1.9	1.8	1.7	1.5	1.4	1.3	0.9	0.7	0.5	...
52	-1.0	0.3	1.2	3.4	3.0	2.8	2.7	2.7	2.6	2.5	2.4	2.3	2.2	2.1	2.0	1.9	1.8	1.6	1.5	1.4	1.0	0.7	0.5	...
51	-0.8	0.2	1.5	3.7	3.3	3.0	2.7	2.6	2.5	2.4	2.4	2.3	2.2	2.1	2.0	1.9	1.8	1.7	1.6	1.5	1.1	0.8	0.5	...
50	-0.8	0.3	1.6	3.6	3.2	2.9	2.7	2.5	2.4	2.4	2.3	2.3	2.2	2.1	2.0	2.0	1.9	1.8	1.7	1.5	1.1	0.8	0.5	...
49	-0.7	0.3	1.7	3.3	2.9	2.7	2.5	2.4	2.3	2.3	2.2	2.2	2.1	2.1	2.0	1.9	1.9	1.8	1.7	1.6	1.1	0.7	0.5	...
48	-0.9	0.4	1.5	2.7	2.4	2.3	2.3	2.2	2.2	2.2	2.1	2.1	2.1	2.0	2.0	1.9	1.8	1.7	1.6	1.5	1.1	0.7	0.4	...
47	-0.5	0.2	0.9	1.7	1.9	2.0	2.0	2.0	2.0	2.0	2.0	2.0	2.0	1.9	1.9	1.8	1.7	1.6	1.5	1.4	1.0	0.7	0.4	...
46	-0.7	-0.2	0.6	2.2	1.9	1.9	1.9	1.9	1.9	1.9	1.9	1.9	1.9	1.9	1.8	1.8	1.7	1.7	1.6	1.4	1.0	0.6	0.4	...
45	-0.8	-0.5	0.4	2.2	2.0	1.8	1.8	1.7	1.7	1.8	1.8	1.8	1.8	1.8	1.8	1.7	1.7	1.6	1.5	1.4	0.9	0.6	0.3	...
44	-0.9	-0.5	0.4	2.1	1.9	1.7	1.7	1.6	1.6	1.6	1.7	1.7	1.7	1.7	1.7	1.6	1.6	1.5	1.5	1.3	0.9	0.5	0.3	...
43	-0.7	-0.4	0.4	1.8	1.6	1.5	1.5	1.5	1.5	1.5	1.5	1.5	1.5	1.5	1.5	1.5	1.5	1.4	1.3	1.2	0.8	0.4	0.2	...
42	-0.6	-0.2	0.4	1.4	1.2	1.2	1.3	1.3	1.3	1.4	1.4	1.4	1.4	1.4	1.4	1.4	1.3	1.3	1.2	1.0	0.6	0.3	0.0	...
41	-0.4	-0.1	0.3	0.7	0.9	1.0	1.1	1.1	1.2	1.2	1.2	1.2	1.2	1.2	1.2	1.2	1.1	1.1	0.9	0.8	0.4	0.2	0.0	...
40	-0.4	-0.1	0.2	0.8	0.8	0.9	1.0	1.0	1.0	1.1	1.1	1.1	1.1	1.0	1.0	1.0	1.0	0.9	0.9	0.7	0.4	0.1	0.0	...
39	-0.2	-0.1	0.2	0.7	0.8	0.8	0.9	0.9	0.9	0.9	0.9	0.9	0.9	0.8	0.8	0.8	0.8	0.7	0.7	0.5	0.2	0.0	0.0	...
38	-0.1	0.0	0.1	0.6	0.7	0.8	0.8	0.8	0.8	0.7	0.7	0.7	0.7	0.6	0.6	0.6	0.5	0.5	0.4	0.3	0.1	0.0	0.0	...
37	0.0	0.0	0.1	0.3	0.5	0.6	0.6	0.6	0.6	0.5	0.5	0.5	0.5	0.4	0.4	0.3	0.3	0.2	0.2	0.1	0.0	0.0	0.0	...
36	0.0	0.0	0.0	0.0	0.3	0.4	0.4	0.4	0.3	0.3	0.3	0.3	0.2	0.2	0.2	0.1	0.1	0.0	0.0	0.0	0.0	0.0	0.0	...
35	0.0	0.0	0.0	0.0	0.0	0.0	0.0	0.0	0.0	0.0	0.0	0.0	0.0	0.0	0.0	0.0	0.0	0.0	0.0	0.0	0.0	0.0	0.0	...
34	0.0	0.0	0.0	0.0	0.0	0.0	0.0	0.0	0.0	0.0	0.0	0.0	0.0	0.0	0.0	0.0	0.0	0.0	0.0	0.0	0.0	0.0	0.0	...
33	0.0	0.0	0.0	0.0	0.0	0.0	0.0	0.0	0.0	0.0	0.0	0.0	0.0	0.0	0.0	0.0	0.0	0.0	0.0	0.0	0.0	0.0	0.0	...
32	0.0	0.0	0.0	0.0	0.0	0.0	0.0	0.0	0.0	0.0	0.0	0.0	0.0	0.0	0.0	0.0	0.0	0.0	0.0	0.0	0.0	0.0	0.0	...
31	0.0	0.0	0.0	0.0	0.0	0.0	0.0	0.0	0.0	0.0	0.0	0.0	0.0	0.0	0.0	0.0	0.0	0.0	0.0	0.0	0.0	0.0	0.0	...
30	0.0	0.0	0.0	0.0	0.0	0.0	0.0	0.0	0.0	0.0	0.0	0.0	0.0	0.0	0.0	0.0	0.0	0.0	0.0	0.0	0.0	0.0	0.0	...
29	0.0	0.0	0.0	0.0	0.0	0.0	0.0	0.0	0.0	0.0	0.0	0.0	0.0	0.0	0.0	0.0	0.0	0.0	0.0	0.0	0.0	0.0	0.0	...
28	0.0	0.0	0.0	0.0	0.0	0.0	0.0	0.0	0.0	0.0	0.0	0.0	0.0	0.0	0.0	0.0	0.0	0.0	0.0	0.0	0.0	0.0	0.0	...
27	0.0	0.0	0.0	0.0	0.0	0.0	0.0	0.0	0.0	0.0	0.0	0.0	0.0	0.0	0.0	0.0	0.0	0.0	0.0	0.0	0.0	0.0	0.0	...
26	0.0	0.0	0.0	0.0	0.0	0.0	0.0	0.0	0.0	0.0	0.0	0.0	0.0	0.0	0.0	0.0	0.0	0.0	0.0	0.0	0.0	0.0	0.0	...
25	0.0	0.0	0.0	0.0	0.0	0.0	0.0	0.0	0.0	0.0	0.0	0.0	0.0	0.0	0.0	0.0	0.0	0.0	0.0	0.0	0.0	0.0	0.0	...
24	0.0	0.0	0.0	0.0	0.0	0.0	0.0	0.0	0.0	0.0	0.0	0.0	0.0	0.0	0.0	0.0	0.0	0.0	0.0	0.0	0.0	0.0	0.0	...
23	0.0	0.0	0.0	0.0	0.0	0.0	0.0	0.0	0.0	0.0	0.0	0.0	0.0	0.0	0.0	0.0	0.0	0.0	0.0	0.0	0.0	0.0	0.0	...
22	0.0	0.0	0.0	0.0	0.0	0.0	0.0	0.0	0.0	0.0	0.0	0.0	0.0	0.0	0.0	0.0	0.0	0.0	0.0	0.0	0.0	0.0	0.0	...
21	0.0	0.0	0.0	0.0	0.0	0.0	0.0	0.0	0.0	0.0	0.0	0.0	0.0	0.0	0.0	0.0	0.0	0.0	0.0	0.0	0.0	0.0	0.0	...
20	0.0	0.0	0.0	0.0	0.0	0.0	0.0	0.0	0.0	0.0	0.0	0.0	0.0	0.0	0.0	0.0	0.0	0.0	0.0	0.0	0.0	0.0	0.0	...
19	0.0	0.0	0.0	0.0	0.0	0.0	0.0	0.0	0.0	0.0	0.0	0.0	0.0	0.0	0.0	0.0	0.0	0.0	0.0	0.0	0.0	0.0	0.0	...
18	0.0	0.0	0.0	0.0	0.0	0.0	0.0	0.0	0.0	0.0	0.0	0.0	0.0	0.0	0.0	0.0	0.0	0.0	0.0	0.0	0.0	0.0	0.0	...
17	0.0	0.0	0.0	0.0	0.0	0.0	0.0	0.0	0.0	0.0	0.0	0.0	0.0	0.0	0.0	0.0	0.0	0.0	0.0	0.0	0.0	0.0	0.0	...
16	0.0	0.0	0.0	0.0	0.0	0.0	0.0	0.0	0.0	0.0	0.0	0.0	0.0	0.0	0.0	0.0	0.0	0.0	0.0	0.0	0.0	0.0	0.0	...
15	0.0	0.0	0.0	0.0	0.0	0.0	0.0	0.0	0.0	0.0	0.0	0.0	0.0	0.0	0.0	0.0	0.0	0.0	0.0	0.0	0.0	0.0	0.0	...
14	0.0	0.0	0.0	0.0	0.0	0.0	0.0	0.0	0.0	0.0	0.0	0.0	0.0	0.0	0.0	0.0	0.0	0.0	0.0	0.0	0.0	0.0	0.0	...
13	0.0	0.0	0.0	0.0	0.0	0.0	0.0	0.0	0.0	0.0	0.0	0.0	0.0	0.0	0.0	0.0	0.0	0.0	0.0	0.0	0.0	0.0	0.0	...
12	0.0	0.0	0.0	0.0	0.0	0.0	0.0	0.0	0.0	0.0	0.0	0.0	0.0	0.0	0.0	0.0	0.0	0.0	0.0	0.0	0.0	0.0	0.0	...
11	0.0	0.0	0.0	0.0	0.0	0.0	0.0	0.0	0.0	0.0	0.0	0.0	0.0	0.0	0.0	0.0	0.0	0.0	0.0	0.0	0.0	0.0	0.0	...
...	...	...	...	...	...	...	...	...	...	...	...	...	...	...	...	...	...	...	...	...	...	...	...	...

FLAC results: Total deformation (vertical disp.) for Case 2- day 12

(mm)

I	12	13	14	15	16	17	18	19	20	21	22	23	24	25	26	27	28	29	30	31	32	33	34	...
J																								...
73																							-10.1	...
72																				-13.7	-12.8	-11.8	-10.9	...
71																0.0	-36.3	-35.1	-37.2	-14.7	-13.3	-12.3	-11.2	...
70														-37.7	-37.4	-37.2	-36.6	-35.9	-35.0	-14.9	-13.9	-12.8	-11.8	...
69											-38.9	-38.7	-38.4	-37.9	-37.3	-36.7	-36.3	-35.8	-35.1	-15.5	-14.5	-13.4	-12.4	...
68								-40.4	-40.4	-40.4	-39.8	-39.0	-38.3	-37.6	-37.1	-36.7	-36.2	-35.6	-34.6	-16.1	-15.1	-14.1	-13.0	...
67						-40.5	-40.9	-40.8	-40.7	-40.2	-39.8	-39.2	-38.5	-37.8	-37.2	-36.7	-36.1	-35.3	-33.9	-16.5	-15.6	-14.5	-13.3	...
66		-22.7	-23.5	-25.9	-39.8	-40.8	-40.7	-40.7	-40.6	-40.3	-39.9	-39.4	-38.8	-38.0	-37.2	-36.6	-35.9	-34.8	-33.0	-16.7	-15.8	-14.6	-13.4	...
65	-23.2	-22.6	-23.0	-26.5	-40.1	-40.4	-40.6	-40.6	-40.6	-40.5	-40.2	-39.7	-39.1	-38.3	-37.4	-36.4	-35.4	-34.1	-32.1	-16.8	-15.7	-14.6	-13.3	...
64	-22.0	-22.1	-22.6	-26.7	-39.3	-40.0	-40.3	-40.6	-40.7	-40.6	-40.4	-39.9	-39.2	-38.3	-37.2	-35.9	-34.6	-33.1	-30.8	-16.7	-15.6	-14.4	-13.0	...
63	-21.0	-21.5	-22.2	-26.7	-38.4	-39.4	-40.1	-40.4	-40.6	-40.5	-40.2	-39.7	-39.0	-38.0	-36.7	-35.2	-33.6	-31.8	-29.4	-16.5	-15.3	-14.0	-12.6	...
62	-20.1	-20.9	-21.7	-26.3	-37.5	-38.8	-39.6	-40.0	-40.2	-40.1	-39.7	-39.2	-38.4	-37.4	-36.1	-34.4	-32.4	-30.4	-27.6	-16.2	-15.0	-13.6	-12.2	...
61	-19.0	-20.1	-21.0	-25.6	-36.1	-37.8	-38.8	-39.3	-39.4	-39.3	-38.9	-38.3	-37.4	-36.4	-35.1	-33.4	-31.4	-28.9	-25.8	-15.8	-14.6	-13.1	-11.6	...
60	-18.1	-19.3	-20.6	-24.5	-34.7	-36.7	-37.7	-38.2	-38.3	-38.2	-37.8	-37.2	-36.3	-35.2	-33.8	-32.2	-30.3	-27.7	-24.0	-15.2	-14.0	-12.5	-11.0	...
59	-17.4	-18.5	-19.9	-23.8	-33.1	-35.2	-36.3	-36.9	-37.0	-36.9	-36.5	-35.9	-35.0	-33.8	-32.5	-30.8	-28.9	-26.4	-22.5	-14.6	-13.1	-11.8	-10.3	...
58	-16.8	-17.7	-19.1	-23.6	-31.7	-33.4	-34.6	-35.2	-35.4	-35.3	-34.9	-34.3	-33.4	-32.3	-30.9	-29.3	-27.4	-24.9	-22.1	-13.9	-12.3	-11.0	-9.7	...
57	-15.8	-16.9	-18.1	-22.3	-29.9	-31.6	-32.8	-33.4	-33.7	-33.6	-33.3	-32.6	-31.8	-30.7	-29.3	-27.7	-25.7	-23.5	-21.0	-13.1	-11.7	-10.3	-9.0	...
56	-15.0	-16.2	-17.2	-20.6	-28.0	-30.0	-31.1	-31.8	-32.1	-32.0	-31.6	-31.0	-30.1	-29.1	-27.8	-26.1	-24.2	-22.0	-19.5	-12.2	-10.9	-9.6	-8.3	...
55	-14.2	-15.3	-16.0	-19.0	-25.7	-28.1	-29.3	-29.9	-30.2	-30.2	-29.8	-29.1	-28.3	-27.3	-26.0	-24.5	-22.6	-20.5	-17.9	-11.3	-10.1	-8.9	-7.6	...
54	-13.4	-14.1	-15.2	-17.4	-23.6	-26.1	-27.4	-28.1	-28.4	-28.3	-28.0	-27.4	-26.5	-25.5	-24.3	-22.9	-21.2	-19.1	-16.2	-10.5	-9.3	-8.1	-6.8	...
53	-12.5	-13.3	-14.4	-16.4	-21.4	-24.1	-25.5	-26.2	-26.5	-26.5	-26.2	-25.6	-24.8	-23.8	-22.6	-21.2	-19.6	-17.6	-14.6	-9.6	-8.3	-7.3	-6.1	...
52	-11.6	-12.4	-13.6	-15.6	-19.4	-21.7	-23.2	-24.0	-24.3	-24.4	-24.1	-23.5	-22.7	-21.8	-20.7	-19.4	-18.0	-16.1	-13.7	-8.8	-7.5	-6.5	-5.4	...
51	-10.4	-11.6	-12.5	-14.4	-17.5	-19.7	-21.1	-21.9	-22.3	-22.3	-22.0	-21.5	-20.8	-20.0	-18.9	-17.7	-16.3	-14.5	-12.3	-7.9	-6.7	-5.7	-4.7	...
50	-9.5	-10.6	-11.5	-13.1	-15.9	-17.9	-19.2	-20.0	-20.3	-20.3	-20.1	-19.7	-19.1	-18.3	-17.3	-16.1	-14.7	-13.0	-10.8	-7.0	-6.0	-5.0	-4.1	...
49	-8.3	-9.6	-10.4	-12.0	-14.3	-16.0	-17.2	-17.9	-18.2	-18.2	-18.1	-17.7	-17.2	-16.5	-15.6	-14.5	-13.1	-11.5	-9.4	-6.1	-5.2	-4.3	-3.5	...
48	-7.5	-8.5	-9.6	-10.9	-12.9	-14.2	-15.2	-15.8	-16.2	-16.3	-16.2	-15.9	-15.5	-14.8	-14.0	-13.0	-11.7	-10.1	-8.1	-5.3	-4.5	-3.7	-3.0	...
47	-6.7	-7.7	-8.9	-10.2	-11.3	-12.4	-13.3	-13.8	-14.2	-14.4	-14.4	-14.2	-13.8	-13.2	-12.5	-11.5	-10.2	-8.7	-6.8	-4.5	-3.7	-3.0	-2.5	...
46	-6.1	-6.7	-8.2	-9.6	-9.8	-10.6	-11.3	-11.8	-12.2	-12.4	-12.4	-12.3	-12.0	-11.5	-10.8	-9.9	-8.8	-7.5	-5.9	-3.8	-3.1	-2.5	-2.1	...
45	-5.6	-6.0	-7.1	-8.5	-8.6	-9.1	-9.6	-10.1	-10.4	-10.6	-10.6	-10.5	-10.3	-9.8	-9.3	-8.5	-7.5	-6.3	-4.9	-3.2	-2.5	-2.0	-1.9	...
44	-5.5	-5.3	-6.0	-7.4	-7.5	-7.8	-8.2	-8.6	-8.8	-9.0	-9.0	-8.9	-8.7	-8.3	-7.8	-7.1	-6.3	-5.2	-4.0	-2.6	-2.0	-1.7	-1.8	...
43	-5.1	-4.8	-5.0	-6.2	-6.4	-6.6	-6.9	-7.1	-7.3	-7.4	-7.4	-7.3	-7.1	-6.8	-6.4	-5.8	-5.1	-4.2	-3.2	-2.0	-1.6	-1.5	-1.9	...
42	-4.6	-4.4	-4.3	-5.2	-5.4	-5.5	-5.6	-5.7	-5.8	-5.9	-5.9	-5.8	-5.7	-5.4	-5.0	-4.6	-4.0	-3.3	-2.5	-1.6	-1.3	-1.4	-2.1	...
41	-4.0	-3.9	-3.9	-4.5	-4.4	-4.4	-4.4	-4.5	-4.6	-4.6	-4.6	-4.6	-4.4	-4.2	-3.9	-3.5	-3.0	-2.4	-1.8	-1.2	-1.1	-1.5	-2.0	...
40	-3.6	-3.4	-3.5	-4.0	-3.5	-3.3	-3.2	-3.3	-3.3	-3.4	-3.4	-3.3	-3.2	-3.0	-2.7	-2.4	-2.1	-1.7	-1.3	-1.0	-1.0	-1.6	-2.0	...
39	-3.3	-3.0	-3.0	-3.4	-2.8	-2.5	-2.4	-2.4	-2.4	-2.4	-2.4	-2.4	-2.3	-2.1	-1.9	-1.7	-1.4	-1.2	-1.0	-1.0	-1.2	-2.0	-1.9	...
38	-3.0	-2.7	-2.6	-2.9	-2.4	-2.1	-2.0	-1.9	-1.9	-1.9	-1.9	-1.9	-1.8	-1.7	-1.5	-1.3	-1.1	-0.9	-0.9	-1.2	-1.4	-1.9	-1.8	...
37	-2.6	-2.5	-2.3	-2.6	-2.3	-2.1	-2.1	-2.0	-2.0	-2.0	-2.0	-1.9	-1.9	-1.8	-1.6	-1.5	-1.3	-1.2	-1.2	-1.4	-1.9	-1.8	-1.7	...
36	-2.4	-2.4	-2.2	-2.3	-2.4	-2.3	-2.3	-2.3	-2.3	-2.4	-2.3	-2.3	-2.3	-2.2	-2.1	-2.0	-1.8	-1.7	-1.6	-1.8	-1.8	-1.7	-1.7	...
35	-2.2	-2.2	-2.2	-2.2	-2.4	-2.5	-2.6	-2.7	-2.7	-2.8	-2.8	-2.8	-2.8	-2.7	-2.6	-2.5	-2.4	-2.2	-2.0	-1.7	-1.7	-1.6	-1.6	...
34	-2.1	-2.1	-2.1	-2.1	-2.2	-2.3	-2.4	-2.5	-2.5	-2.5	-2.6	-2.6	-2.5	-2.5	-2.4	-2.3	-2.2	-2.0	-1.9	-1.7	-1.6	-1.6	-1.5	...
33	-2.0	-2.0	-1.9	-2.0	-2.1	-2.2	-2.2	-2.3	-2.3	-2.4	-2.4	-2.4	-2.3	-2.3	-2.2	-2.1	-2.0	-1.9	-1.7	-1.6	-1.5	-1.5	-1.4	...
32	-1.9	-1.8	-1.8	-1.9	-2.0	-2.0	-2.1	-2.1	-2.2	-2.2	-2.2	-2.2	-2.2	-2.1	-2.1	-2.0	-1.9	-1.8	-1.6	-1.5	-1.4	-1.4	-1.4	...
31	-1.7	-1.7	-1.7	-1.8	-1.8	-1.9	-1.9	-2.0	-2.0	-2.0	-2.0	-2.0	-2.0	-2.0	-1.9	-1.8	-1.8	-1.7	-1.5	-1.4	-1.4	-1.3	-1.3	...
30	-1.7	-1.6	-1.6	-1.7	-1.7	-1.8	-1.8	-1.8	-1.9	-1.9	-1.9	-1.9	-1.8	-1.8	-1.8	-1.7	-1.6	-1.5	-1.4	-1.3	-1.3	-1.3	-1.2	...
29	-1.6	-1.5	-1.5	-1.6	-1.6	-1.6	-1.7	-1.7	-1.7	-1.7	-1.7	-1.7	-1.7	-1.7	-1.6	-1.6	-1.5	-1.4	-1.3	-1.2	-1.2	-1.2	-1.2	...
28	-1.5	-1.4	-1.4	-1.4	-1.5	-1.5	-1.6	-1.6	-1.6	-1.6	-1.6	-1.6	-1.6	-1.5	-1.5	-1.5	-1.4	-1.3	-1.3	-1.2	-1.2	-1.1	-1.1	...
27	-1.4	-1.4	-1.3	-1.3	-1.4	-1.4	-1.4	-1.5	-1.5	-1.5	-1.5	-1.5	-1.4	-1.4	-1.4	-1.3	-1.3	-1.2	-1.2	-1.1	-1.1	-1.1	-1.0	...
26	-1.3	-1.3	-1.2	-1.3	-1.3	-1.3	-1.3	-1.4	-1.4	-1.4	-1.4	-1.3	-1.3	-1.3	-1.3	-1.2	-1.2	-1.2	-1.1	-1.0	-1.0	-1.0	-1.0	...
25	-1.3	-1.2	-1.1	-1.2	-1.2	-1.2	-1.2	-1.2	-1.3	-1.3	-1.2	-1.2	-1.2	-1.2	-1.2	-1.1	-1.1	-1.1	-1.0	-1.0	-1.0	-0.9	-0.9	...
24	-1.2	-1.1	-1.0	-1.1	-1.1	-1.1	-1.1	-1.1	-1.2	-1.2	-1.1	-1.1	-1.1	-1.1	-1.1	-1.1	-1.0	-1.0	-1.0	-0.9	-0.9	-0.9	-0.9	...
23	-1.1	-1.0	-1.0	-1.0	-1.0	-1.0	-1.0	-1.1	-1.1	-1.1	-1.1	-1.0	-1.0	-1.0	-1.0	-1.0	-0.9	-0.9	-0.9	-0.8	-0.8	-0.8	-0.8	...
22	-1.0	-0.9	-0.9	-0.9	-0.9	-0.9	-1.0	-1.0	-1.0	-1.0	-1.0	-1.0	-0.9	-0.9	-0.9	-0.9	-0.9	-0.8	-0.8	-0.8	-0.8	-0.8	-0.7	...
21	-0.9	-0.9	-0.8	-0.8	-0.8	-0.9	-0.9	-0.9	-0.9	-0.9	-0.9	-0.9	-0.9	-0.8	-0.8	-0.8	-0.8	-0.8	-0.8	-0.7	-0.7	-0.7	-0.7	...
20	-0.8	-0.8	-0.7	-0.7	-0.8	-0.8	-0.8	-0.8	-0.8	-0.8	-0.8	-0.8	-0.8	-0.8	-0.8	-0.7	-0.7	-0.7	-0.7	-0.7	-0.7	-0.7	-0.6	...
19	-0.8	-0.7	-0.7	-0.7	-0.7	-0.7	-0.7	-0.7	-0.7	-0.7	-0.7	-0.7	-0.7	-0.7	-0.7	-0.7	-0.7	-0.7	-0.6	-0.6	-0.6	-0.6	-0.6	...
18	-0.7	-0.7	-0.6	-0.6	-0.6	-0.6	-0.6	-0.6	-0.6	-0.6	-0.6	-0.6	-0.6	-0.6	-0.6	-0.6	-0.6	-0.6	-0.6	-0.6	-0.6	-0.6	-0.6	...
17	-0.6	-0.6	-0.5	-0.5	-0.5	-0.6	-0.6	-0.6	-0.6	-0.6	-0.6	-0.6	-0.6	-0.6	-0.6	-0.5	-0.5	-0.5	-0.5	-0.5	-0.5	-0.5	-0.5	...
16	-0.6	-0.5	-0.5	-0.4	-0.5	-0.5	-0.5	-0.5	-0.5	-0.5	-0.5	-0.5	-0.5	-0.5	-0.5	-0.5	-0.5	-0.5	-0.5	-0.5	-0.5	-0.5	-0.5	...
15	-0.5	-0.5	-0.4	-0.4	-0.4	-0.4	-0.5	-0.5	-0.5	-0.4	-0.4	-0.4	-0.4	-0.4	-0.4	-0.4	-0.4	-0.4	-0.4	-0.4	-0.4	-0.4	-0.4	...
14	-0.5	-0.4	-0.4	-0.3	-0.4	-0.4	-0.4	-0.4	-0.4	-0.4	-0.4	-0.4	-0.4	-0.4	-0.4	-0.4	-0.4	-0.4	-0.4	-0.4	-0.4	-0.4	-0.4	...
13	-0.4	-0.4	-0.3	-0.3	-0.3	-0.3	-0.3	-0.3	-0.3	-0.3	-0.3	-0.3	-0.3	-0.3	-0.3	-0.3	-0.3	-0.3	-0.3	-0.4	-0.3	-0.3	-0.3	...
12	-0.4	-0.3	-0.3	-0.3	-0.3	-0.3	-0.3	-0.3	-0.3	-0.3	-0.3	-0.3	-0.3	-0.3	-0.3	-0.3	-0.3	-0.3	-0.3	-0.3	-0.3	-0.3	-0.3	...
11	-0.4	-0.3	-0.3	-0.2	-0.2	-0.2	-0.2	-0.2	-0.2	-0.2	-0.2	-0.2	-0.2	-0.2	-0.2	-0.2	-0.2	-0.2	-0.2	-0.3	-0.3	-0.3	-0.3	...
...	...	...	...	...	...	...	...	...	...	...	...	...	...	...	...	...	...	...	...	...	...	...	...	...

FLAC results: Total deformation (lateral disp.) for Case 2- day 12

(mm)

I	12	13	14	15	16	17	18	19	20	21	22	23	24	25	26	27	28	29	30	31	32	33	34	...
J																								...
73																							-10.1	...
72																				-8.0	-7.9	-7.9	-10.9	...
71																	-14.7	-14.8	-12.2	-7.8	-7.3	-7.1	-11.2	...
70														-15.2	-15.3	-14.8	-14.2	-13.3	-12.9	-6.6	-6.6	-6.5	-11.8	...
69											-14.6	-15.6	-15.7	-15.1	-13.8	-13.2	-13.0	-12.6	-12.0	-5.8	-5.8	-5.8	-12.4	...
68								-12.7	-13.8	-14.0	-13.8	-13.1	-13.0	-13.1	-13.0	-12.9	-12.6	-12.2	-11.2	-5.2	-5.2	-5.2	-13.0	...
67					-10.5	-11.2	-11.8	-11.9	-11.4	-11.4	-11.7	-12.0	-12.3	-12.5	-12.6	-12.5	-12.2	-11.6	-10.4	-4.6	-4.7	-4.7	-13.3	...
66		-12.4	-11.5	-11.1	-9.5	-10.3	-10.4	-10.5	-10.6	-10.7	-11.0	-11.4	-11.7	-12.0	-12.2	-12.1	-11.7	-10.8	-9.6	-4.0	-4.2	-4.2	-13.4	...
65	-15.2	-13.0	-12.3	-11.7	-10.4	-10.1	-9.8	-9.8	-9.9	-10.1	-10.5	-10.8	-11.2	-11.5	-11.7	-11.5	-10.9	-10.0	-8.5	-3.4	-3.6	-3.6	-13.3	...
64	-14.9	-13.1	-12.5	-11.3	-10.4	-9.6	-9.3	-9.3	-9.5	-9.8	-10.1	-10.3	-10.6	-10.8	-11.0	-10.8	-10.1	-9.1	-7.6	-2.8	-3.0	-3.1	-13.0	...
63	-14.6	-13.0	-12.3	-10.6	-9.6	-9.0	-8.8	-8.9	-9.1	-9.3	-9.6	-9.8	-9.9	-10.0	-10.0	-9.8	-9.2	-8.1	-6.5	-2.3	-2.5	-2.6	-12.6	...
62	-14.4	-13.0	-12.1	-10.0	-9.2	-8.6	-8.5	-8.6	-8.8	-9.0	-9.1	-9.1	-9.1	-9.0	-8.8	-8.6	-8.2	-7.3	-5.6	-1.8	-2.0	-2.1	-12.2	...
61	-14.1	-12.9	-11.7	-9.6	-8.7	-8.3	-8.3	-8.3	-8.4	-8.4	-8.4	-8.3	-8.1	-7.9	-7.6	-7.2	-6.9	-6.4	-4.9	-1.4	-1.5	-1.6	-11.6	...
60	-14.1	-12.5	-11.4	-9.4	-8.8	-8.5	-8.3	-8.2	-8.0	-7.8	-7.6	-7.4	-7.2	-6.8	-6.4	-5.9	-5.5	-5.1	-4.2	-1.3	-1.3	-1.2	-11.0	...
59	-13.1	-12.3	-11.4	-10.4	-9.7	-8.9	-8.3	-7.9	-7.5	-7.1	-6.8	-6.5	-6.2	-5.8	-5.3	-4.7	-4.1	-3.3	-2.5	-1.6	-1.1	-0.9	-10.3	...
58	-13.7	-12.6	-11.7	-8.8	-8.1	-7.7	-7.2	-6.8	-6.5	-6.3	-6.1	-5.8	-5.5	-5.1	-4.8	-4.3	-3.7	-2.9	-2.4	-0.2	-0.4	-0.6	-9.7	...
57	-13.2	-12.5	-11.1	-7.7	-6.9	-6.5	-6.2	-6.0	-5.8	-5.6	-5.4	-5.1	-4.8	-4.5	-4.1	-3.8	-3.2	-2.6	-2.0	0.3	0.1	-0.2	-9.0	...
56	-13.0	-12.1	-10.4	-6.9	-6.2	-5.8	-5.6	-5.5	-5.3	-5.1	-4.8	-4.5	-4.2	-3.8	-3.5	-3.1	-2.8	-2.3	-1.6	0.5	0.4	0.1	-8.3	...
55	-12.8	-11.6	-9.5	-6.5	-5.9	-5.5	-5.3	-5.1	-4.8	-4.5	-4.2	-4.0	-3.6	-3.2	-2.8	-2.5	-2.2	-2.0	-1.3	0.7	0.6	0.3	-7.6	...
54	-12.8	-10.6	-8.9	-6.7	-6.3	-5.7	-5.3	-4.9	-4.5	-4.1	-3.8	-3.4	-3.1	-2.7	-2.3	-1.9	-1.6	-1.4	-0.9	0.7	0.7	0.4	-6.8	...
53	-11.0	-9.9	-8.9	-7.7	-6.8	-6.0	-5.3	-4.7	-4.2	-3.8	-3.4	-3.0	-2.6	-2.3	-1.9	-1.5	-1.1	-0.7	-0.2	0.4	0.6	0.4	-6.1	...
52	-11.4	-9.8	-8.6	-6.0	-5.6	-4.9	-4.3	-3.9	-3.5	-3.1	-2.7	-2.4	-2.1	-1.8	-1.6	-1.4	-1.0	-0.6	-0.1	1.0	0.9	0.5	-5.4	...
51	-10.6	-9.4	-7.8	-5.0	-4.6	-4.2	-3.8	-3.5	-3.1	-2.6	-2.2	-1.9	-1.6	-1.4	-1.3	-1.2	-0.9	-0.5	0.0	1.2	1.0	0.6	-4.7	...
50	-10.4	-8.9	-7.1	-4.4	-4.2	-3.9	-3.7	-3.2	-2.7	-2.2	-1.8	-1.5	-1.3	-1.2	-1.1	-0.9	-0.7	-0.4	0.1	1.1	1.0	0.6	-4.1	...
49	-9.7	-8.4	-6.5	-4.4	-4.3	-4.1	-3.6	-3.0	-2.4	-1.9	-1.5	-1.2	-1.0	-0.9	-0.8	-0.7	-0.5	-0.3	0.2	1.0	0.9	0.5	-3.5	...
48	-9.8	-7.9	-6.3	-4.6	-4.6	-4.1	-3.4	-2.7	-2.1	-1.7	-1.4	-1.1	-0.9	-0.7	-0.6	-0.5	-0.3	-0.1	0.3	0.9	0.7	0.4	-3.0	...
47	-8.9	-7.7	-6.5	-5.3	-4.5	-3.8	-3.1	-2.5	-2.0	-1.6	-1.3	-1.0	-0.8	-0.6	-0.4	-0.3	-0.1	0.1	0.4	0.6	0.4	0.2	-2.5	...
46	-8.5	-7.6	-6.2	-3.7	-3.4	-2.8	-2.3	-2.0	-1.6	-1.4	-1.1	-0.9	-0.7	-0.5	-0.3	-0.1	0.0	0.2	0.4	0.7	0.4	0.0	-2.1	...
45	-7.9	-7.3	-5.6	-2.6	-2.4	-2.2	-2.0	-1.8	-1.5	-1.3	-1.1	-0.8	-0.6	-0.4	-0.2	-0.1	0.1	0.3	0.4	0.6	0.2	-0.1	-1.9	...
44	-7.4	-6.8	-5.0	-2.1	-2.2	-2.1	-2.0	-1.8	-1.6	-1.3	-1.1	-0.9	-0.6	-0.4	-0.2	0.0	0.2	0.3	0.5	0.5	0.1	-0.2	-1.8	...
43	-6.5	-6.0	-4.5	-2.2	-2.2	-2.1	-2.0	-1.8	-1.6	-1.4	-1.1	-0.9	-0.7	-0.5	-0.2	0.0	0.1	0.3	0.4	0.4	0.0	-0.3	-1.9	...
42	-6.2	-5.3	-4.1	-2.4	-2.4	-2.2	-2.1	-1.8	-1.6	-1.4	-1.2	-1.0	-0.7	-0.5	-0.3	-0.1	0.0	0.2	0.3	0.3	-0.1	-0.4	-2.1	...
41	-5.6	-4.8	-4.0	-3.1	-2.6	-2.3	-2.1	-1.8	-1.6	-1.4	-1.2	-1.0	-0.8	-0.6	-0.4	-0.3	-0.1	0.0	0.0	0.0	-0.3	-0.5	-2.0	...
40	-5.1	-4.4	-3.6	-2.3	-2.3	-2.1	-1.9	-1.8	-1.6	-1.4	-1.2	-1.0	-0.9	-0.7	-0.5	-0.4	-0.2	-0.1	0.0	-0.1	-0.4	-0.6	-2.0	...
39	-4.5	-3.9	-3.3	-2.1	-2.0	-1.9	-1.8	-1.7	-1.6	-1.4	-1.3	-1.1	-0.9	-0.8	-0.6	-0.5	-0.4	-0.3	-0.2	-0.3	-0.5	-0.6	-1.9	...
38	-3.9	-3.5	-3.0	-2.1	-1.9	-1.8	-1.8	-1.7	-1.5	-1.4	-1.3	-1.2	-1.0	-0.9	-0.8	-0.7	-0.6	-0.5	-0.4	-0.4	-0.6	-0.6	-1.8	...
37	-3.4	-3.2	-2.9	-2.3	-2.0	-1.8	-1.7	-1.7	-1.6	-1.5	-1.4	-1.3	-1.1	-1.0	-0.9	-0.8	-0.8	-0.7	-0.6	-0.6	-0.6	-0.6	-1.7	...
36	-3.3	-3.0	-2.7	-2.5	-2.1	-2.0	-1.8	-1.8	-1.7	-1.6	-1.5	-1.4	-1.3	-1.2	-1.1	-1.0	-0.9	-0.8	-0.8	-0.7	-0.6	-0.6	-1.7	...
35	-3.1	-2.8	-2.6	-2.4	-2.3	-2.2	-2.1	-2.0	-1.9	-1.8	-1.7	-1.6	-1.4	-1.3	-1.2	-1.1	-1.0	-0.9	-0.7	-0.7	-0.6	-0.6	-1.6	...
34	-2.9	-2.7	-2.4	-2.1	-2.1	-2.0	-1.9	-1.9	-1.8	-1.7	-1.6	-1.5	-1.3	-1.2	-1.1	-1.0	-0.9	-0.8	-0.7	-0.6	-0.6	-0.6	-1.5	...
33	-2.7	-2.5	-2.3	-2.0	-1.9	-1.9	-1.8	-1.7	-1.7	-1.6	-1.5	-1.4	-1.3	-1.2	-1.1	-1.0	-0.9	-0.8	-0.7	-0.6	-0.6	-0.5	-1.4	...
32	-2.6	-2.4	-2.1	-1.9	-1.8	-1.8	-1.7	-1.6	-1.5	-1.5	-1.4	-1.3	-1.2	-1.1	-1.0	-0.9	-0.8	-0.7	-0.7	-0.6	-0.5	-0.5	-1.4	...
31	-2.4	-2.2	-2.0	-1.9	-1.7	-1.7	-1.6	-1.5	-1.4	-1.4	-1.3	-1.2	-1.1	-1.0	-0.9	-0.9	-0.8	-0.7	-0.6	-0.6	-0.5	-0.5	-1.3	...
30	-2.3	-2.1	-1.9	-1.6	-1.6	-1.5	-1.5	-1.4	-1.3	-1.3	-1.2	-1.1	-1.0	-1.0	-0.9	-0.8	-0.7	-0.7	-0.6	-0.5	-0.5	-0.5	-1.2	...
29	-2.1	-2.0	-1.8	-1.5	-1.5	-1.4	-1.4	-1.3	-1.3	-1.2	-1.1	-1.0	-1.0	-0.9	-0.8	-0.8	-0.7	-0.6	-0.6	-0.5	-0.5	-0.5	-1.2	...
28	-2.1	-1.9	-1.7	-1.4	-1.4	-1.3	-1.3	-1.2	-1.2	-1.1	-1.0	-1.0	-0.9	-0.8	-0.8	-0.7	-0.6	-0.6	-0.5	-0.5	-0.5	-0.4	-1.1	...
27	-1.9	-1.7	-1.6	-1.4	-1.3	-1.3	-1.2	-1.1	-1.1	-1.0	-1.0	-0.9	-0.8	-0.8	-0.7	-0.7	-0.6	-0.6	-0.5	-0.5	-0.4	-0.4	-1.0	...
26	-1.8	-1.6	-1.5	-1.2	-1.2	-1.1	-1.1	-1.0	-1.0	-0.9	-0.9	-0.8	-0.8	-0.7	-0.7	-0.6	-0.6	-0.5	-0.5	-0.4	-0.4	-0.4	-1.0	...
25	-1.6	-1.5	-1.3	-1.1	-1.1	-1.0	-1.0	-1.0	-0.9	-0.9	-0.8	-0.8	-0.7	-0.7	-0.6	-0.6	-0.5	-0.5	-0.4	-0.4	-0.4	-0.4	-0.9	...
24	-1.6	-1.4	-1.2	-1.0	-1.0	-1.0	-0.9	-0.9	-0.8	-0.8	-0.8	-0.7	-0.7	-0.6	-0.6	-0.5	-0.5	-0.5	-0.4	-0.4	-0.4	-0.3	-0.9	...
23	-1.4	-1.2	-1.1	-1.0	-0.9	-0.9	-0.9	-0.8	-0.8	-0.7	-0.7	-0.7	-0.6	-0.6	-0.5	-0.5	-0.5	-0.4	-0.4	-0.4	-0.3	-0.3	-0.8	...
22	-1.3	-1.1	-1.0	-0.8	-0.8	-0.8	-0.8	-0.7	-0.7	-0.7	-0.6	-0.6	-0.6	-0.5	-0.5	-0.5	-0.4	-0.4	-0.4	-0.3	-0.3	-0.3	-0.7	...
21	-1.1	-1.0	-0.9	-0.7	-0.7	-0.7	-0.7	-0.7	-0.6	-0.6	-0.6	-0.5	-0.5	-0.5	-0.4	-0.4	-0.4	-0.4	-0.3	-0.3	-0.3	-0.3	-0.7	...
20	-1.1	-0.9	-0.8	-0.7	-0.7	-0.6	-0.6	-0.6	-0.6	-0.5	-0.5	-0.5	-0.5	-0.4	-0.4	-0.4	-0.3	-0.3	-0.3	-0.3	-0.3	-0.3	-0.6	...
19	-0.9	-0.8	-0.7	-0.6	-0.6	-0.6	-0.6	-0.5	-0.5	-0.5	-0.5	-0.4	-0.4	-0.4	-0.4	-0.3	-0.3	-0.3	-0.3	-0.3	-0.2	-0.2	-0.6	...
18	-0.9	-0.7	-0.7	-0.5	-0.5	-0.5	-0.5	-0.5	-0.4	-0.4	-0.4	-0.4	-0.4	-0.3	-0.3	-0.3	-0.3	-0.3	-0.3	-0.2	-0.2	-0.2	-0.6	...
17	-0.7	-0.7	-0.6	-0.4	-0.4	-0.4	-0.4	-0.4	-0.4	-0.4	-0.4	-0.3	-0.3	-0.3	-0.3	-0.3	-0.3	-0.2	-0.2	-0.2	-0.2	-0.2	-0.5	...
16	-0.7	-0.5	-0.5	-0.4	-0.4	-0.4	-0.4	-0.3	-0.3	-0.3	-0.3	-0.3	-0.3	-0.3	-0.2	-0.2	-0.2	-0.2	-0.2	-0.2	-0.2	-0.2	-0.5	...
15	-0.5	-0.4	-0.4	-0.3	-0.3	-0.3	-0.3	-0.3	-0.3	-0.3	-0.3	-0.2	-0.2	-0.2	-0.2	-0.2	-0.2	-0.2	-0.2	-0.2	-0.2	-0.2	-0.4	...
14	-0.5	-0.4	-0.3	-0.2	-0.3	-0.3	-0.3	-0.2	-0.2	-0.2	-0.2	-0.2	-0.2	-0.2	-0.2	-0.2	-0.2	-0.2	-0.2	-0.2	-0.1	-0.1	-0.4	...
13	-0.4	-0.3	-0.2	-0.2	-0.2	-0.2	-0.2	-0.2	-0.2	-0.2	-0.2	-0.2	-0.2	-0.1	-0.1	-0.1	-0.1	-0.1	-0.1	-0.1	-0.1	-0.1	-0.3	...
12	-0.3	-0.2	-0.2	-0.2	-0.2	-0.2	-0.1	-0.1	-0.1	-0.1	-0.1	-0.1	-0.1	-0.1	-0.1	-0.1	-0.1	-0.1	-0.1	-0.1	-0.1	-0.1	-0.3	...
11	-0.2	-0.1	-0.1	-0.1	-0.1	-0.1	-0.1	-0.1	-0.1	-0.1	-0.1	-0.1	-0.1	-0.1	-0.1	-0.1	-0.1	-0.1	-0.1	-0.1	-0.1	-0.1	-0.3	...
...	...	...	...	...	...	...	...	...	...	...	...	...	...	...	...	...	...	...	...	...	...	...	...	...